DOCTOR OF PHILOSOPHY

Biochemical characterisation of the Parkinson's disease-associated kinase PINK1 Insights from the insect world

Woodroof, Helen I.

Award date:
2014

Biochemical characterisation of the Parkinson's disease-associated kinase PINK1: Insights from the insect world

Helen I. Woodroof

A thesis submitted for the degree of
Doctor of Philosophy
University of Dundee
November 2014

"We do not embrace reason at the expense of emotion.

We embrace it at the expense of self-deception"

-Herbert Muschamp-

I. Acknowledgements

First and foremost I would like to thank my supervisors, Dr. Miratul Muqit, Professor Daan van Aalten and Professor Dario Alessi, for giving me the opportunity to work in their respective laboratories. Belonging to and working in three different labs is an unusual situation, however it has been an experience from which I have learnt a huge amount. In particular, I would like to thank Miratul for his enthusiasm and dedication to the PINK1 field and for looking out for me. Daan I would like to thank for his crystallography knowledge and ability to approach a problem from a different angle. I thank Dario for his guidance and for providing a good example of the stringent standard to which all research should be held. I would also like to thank my thesis committee, Professor Frank Sargent and Professor Grahame Hardie, for their advice and support.

I wish to thank my collaborators for their contributions to this thesis: Joe Pogson and Dr. Alex Whitworth for their Drosophila complementation experiments, Dr. Mike Begley and Professor Lewis Cantley for the positional scanning library experiment, and Dr. Natasha Pirman and Dr. Jesse Rinehart for sharing the Sep technology with us. Thanks also to Professor Oliver Bandmann and his lab for giving me the opportunity to contribute to their exciting work.

I would like to thank all the DSTT staff, in particular James Hastie and Hilary McLauchlan for running the facility so well and Maria Deak and Mark Peggie for generating so many clones for my work, without which I wouldn't have got half as much done. In addition I would also like to thank Sam, Susan and Shabana of the insect cell team for their help when I first started out. Thanks to Axel Knebel and Clare Johnson for protein purification advice and providing proteins for my experiments. Thanks to David Campbell and Stella Ritorto for phosphopeptide mapping and MALDI analysis, respectively. Thanks go to all the divisional support staff, particularly Alison Hart, Allison Bridges and Judith Hare. Thanks to Charles Williams for help with the Sep expression technology, and to Satpal Virdee and Matthew Stanley for assistance with LC-MS analysis.

Belonging to so many labs means many people to thank, so firstly thanks to all MM, DVA and DRA lab members, past and present, for making each respective lab such a lovely place to work. From the DVA lab, particular thanks to Alex Snr and Jnr, who started me on my scientific journey, Laurie and Elton for useful advice, Helge for crystallography suggestions, Ritchie, Daniel and Riccardo for being fantastic office mates and breakfast companions, and Marianne for all her wisdom and assistance. From the DRA lab, thanks to Chandana for being my companion in PINK1-related struggles and such a great person, to Agne and Eeva for being wonderful friends, to Ning for suggestions and scientific discussion, to Youcef for being a fellow crystallographer, to Jinwei for the AlphaScreen assays, to Paul for being a goldmine of knowledge and advice on a multitude of subjects, and to Sourav for the potluck lunches. From the MM lab, thanks to Jevgenia, Tom and Yu-Chiang for all being such nice people to work with.

Outside the lab, thanks go to Chesca, Amy, Alex, Leah, Sato, Judith, Louise, Chloe, Dean, to Mimi, Karim, Ryan, Erin and Chris, to all of you for being wonderful people to know and at one time or another brightening up my time in Dundee (and elsewhere!) and for making the difficult times easier. Finally and most of all, thanks to my parents and the rest of my family for supporting me no matter what and for always wanting the best for me, and to Mehmet, for being with me, through the light and the dark.

II. Declarations

I hereby declare that the following thesis is based on the results of investigations conducted by myself, and that this thesis is of my own composition. Work other than my own is clearly indicated in the text by reference to the researchers or their publications. This thesis has not in whole or in part been previously presented for a higher degree.

Helen I. Woodroof

We certify that Helen Woodroof has spent the equivalent of at least nine terms in research work in the School of Life Sciences, University of Dundee and that she has fulfilled the conditions of the Ordinance General No. 14 of the University of Dundee and is qualified to submit the accompanying thesis in application for the degree of Doctor of Philosophy.

Dr. Miratul M. K. Muqit M.B. (Ch. B), PhD

Professor Daan M. F. van Aalten

Professor Dario Alessi, FRS, FRSE

III. List of Publications

The work described in this thesis has been published in the following articles:

Kazlauskaite A, Kelly V, Johnson C, Baillie C, Hastie CJ, Peggie M, Macartney T, Woodroof HI, Alessi DR, Pedrioli PG, Muqit MM (2014) Phosphorylation of Parkin at Serine65 is essential for activation: elaboration of a Miro1 substrate-based assay of Parkin E3 ligase activity. Open Biol. 4:130213.

Flinn LJ, Keatinge M, Bretaud S, Mortiboys H, Matsui H, De Felice E, Woodroof HI, Brown L, McTighe A, Soellner R, Allen CE, Heath PR, Milo M, Muqit MM, Reichert AS, Köster RW, Ingham PW, Bandmann O (2013) TigarB causes mitochondrial dysfunction and neuronal loss in PINK1 deficiency. Ann Neurol. 74(6):837-47.

Kondapalli C, Kazlauskaite A, Zhang N, Woodroof HI, Campbell DG, Gourlay R, Burchell L, Walden H, Macartney TJ, Deak M, Knebel A, Alessi DR, Muqit MM (2012) PINK1 is activated by mitochondrial membrane potential depolarization and stimulates Parkin E3 ligase activity by phosphorylating Serine 65. Open Biol. 2(5):120080

Woodroof HI, Pogson JH, Begley M, Cantley LC, Deak M, Campbell DG, van Aalten DM, Whitworth AJ, Alessi DR, Muqit MM (2011) Discovery of catalytically active orthologues of the Parkinson's disease kinase PINK1: analysis of substrate specificity and impact of mutations. Open Biol. 1(3):110012

IV. List of abbreviations

Å	Angstroms
A_{280}	Absorbance at 280 nm
ABC	DimethylAmine Borane Complex
ADP	Adenosine 5'-diphosphate
Amp	Ampicillin
AMP-PNP	Adenosine 5′-(β, γ-imido) triphosphate
aPK	atypical protein kinase
APS	Ammonium persulphate
ATP	Adenosine 5'-triphosphate
A.U.	Arbitrary units
BLAST	Basic Local Alignment Search Tool
BSA	Bovine serum albumin
°C	Degrees Celsius
CaMKI/II	Calcium/calmodulin-dependent kinase I/II
cAMP	cyclic adenosine monophosphate
CCCP	Carbonyl cyanide *m*-chlorophenyl hydrazone
Cdc	Cell division cycle
CDK	Cyclin-dependent kinase
CH	Compound heterozyous
CK1/2	Casein kinase 1/2
CLK	Cdc-like kinase
CNS	Central nervous system
cpm	counts per minute
CV	Column volume
Da	Daltons
ddH_2O	double distilled H_2O/MilliQ water
DmPINK1	*Drosophila melanogaster* PINK1
DMPK	Myotonic dystrophy protein kinase
DMSO	Dimethyl sulfoxide
DNA	Deoxyribonucleic acid
DTT	Dithiothreitol
DUB	Deubiquitinating enzyme
DYRK	Dual specificity tyrosine-phosphorylation-regulated kinase
ε	Extinction coefficient
ECL	Enhanced chemiluminescence
EDTA	Ethylenediaminetetraacetic acid
EF-Tu	Elongation factor-Tu
EGTA	Ethylene glycol tetraacetic acid
eIF-2α	eukaryotic initiation factor 2α
ePK	eukaryotic protein kinase
ERK	Extracellular signal regulated kinase
ETD	Electron transfer dissociation
g	Gram or gravity
Glc	Glucose
GSK3	Glycogen synthase kinase 3
GST	Glutathione-S-transferase
h	Hour
HECT	Homologous to the 6-AP Carboxyl Terminus
HEPES	4-(2-hydroxyethyl)-1-piperazineethanesulfonic acid

HOM	Homozygous
hPINK1	human PINK1
HRI	Heme-regulated eIF-2α kinase
HRP	Horseradish peroxidase
HtrA2/Omi	High temperature requirement protein A2
IBR	In-Between Ring
IGFR	Insulin-like growth factor receptor
IMS	Intermembrane space
IPTG	Isopropyl-β-D-1-thiogalactoside
JNK1/2	c-Jun N-terminal kinase
Kan	Kanamycin
kDa	kilo Dalton
KI	Kinase inactive
l	Litre
LB	Luria-Bertani media
LC-MS	Liquid chromatography-mass spectrometry
LKB1	Liver kinase B1
LRRK2	Leucine-rich repeat kinase 2
MALDI	Matrix-assisted laser desorption ionisation
MAPK	Mitogen-activated protein kinase
M	milli
M	Molar
µ	micro
MBP	Maltose binding protein
MEK1	Mitogen-activated ERK-activating kinase 1
min	Minute
mol	Mole
MO25α	Mouse protein 25 α
MPD	2-Methyl-2,4-pentanediol
MPP	Mitochondrial processing peptidase
MPTP	1-methyl-4-phenyl-1,2,3,6-tetrahydropyridine
mRNA	messenger RNA
mTOR	mammalian target of rapamycin
MTS	Mitochondrial targeting sequence
MUSCLE	MUltiple Sequence Comparison by Log- Expectation
MW	Molecular weight
MWCO	Molecular weight cut-off
n	nano
NEK4	Never in mitosis A-related kinase 4
Ni-NTA	Nickel-nitrilotriacetic acid resin
OD_{600}	Optical density at 600 nm
PAGE	Polyacrylamide gel electrophoresis
PARL	Presenilin-associated rhomboid-like protein
PD	Parkinson's disease
PDB	Protein Dat Bank
PDK1	Phosphoinositide-dependent kinase-1
PH	Pleckstrin homology domain
PhcPINK1	*Pediculus humanus corporis* PINK1
PINK1	PTEN-induced kinase 1
PIP_3	Phosphatidylinositol (3,4,5)-trisphosphate
PKA	cAMP-dependent protein kinase
PKB	Protein kinase B

PKC	Protein kinase C
PKG	cGMP-dependent protein kinase
PKR	Protein kinase RNA-activated
PMSF	Phenylmethanesulphonyl fluoride
PTEN	Phosphatase and tensin homologue
PTM	Post-translational modification
PVDF	Polyvinylidene difluoride
RBR	Ring-Between-Ring
REM	Rapid eye movement
REP	Regulatory element of Parkin
RF-1	Release factor-1
RING	Really Interesting New Gene
RNA	Ribonucleic acid
rpm	revolutions per minute
RT	Room temperature
ROS	Reactive oxygen species
SD	Standard deviation
SDS	Sodium dodecyl sulphate
sec	seconds
SENP1	Sentrin-specific protease 1
Sep	*O*-phospho-L-serine
Sf9	Spodoptera frugiperda 9 cells
SNCA	α-synuclein
SRPK	Serine/arginine-rich-protein kinase
STRADα	STE20-related kinase adapter protein
SUMO	Small ubiquitin-like modifier
TB	Terrific Broth
TCEP	Tris(2-carboxyethyl)phosphine
TcPINK1	*Tribolium castaneum* PINK1
TEMED	*N*,*N*,*N*′,*N*′-Tetramethylethane-1,2-diamine
TIMM	Translocate of the inner mitochondrial membrane
TOM	Translocase of the outer membrane
TRAP1	Tumor necrosis factor type 1 receptor-associated protein
Ubl	Ubiquitin-like
UV	Ultraviolet
V	Volts
VDAC	Voltage-dependent anion channel
v/v	Volume per volume
WT	Wild type
w/v	Weight per volume
ZfPINK1	Zebrafish PINK1

V. Amino acid codes

Amino acid	Three letter code	One letter code
Alanine	Ala	A
Arginine	Arg	R
Asparagine	Asn	N
Aspartic acid	Asp	D
Cysteine	Cys	C
Glutamine	Gln	Q
Glutamic acid	Glu	E
Glycine	Gly	G
Histidine	His	H
Isoleucine	Ile	I
Leucine	Leu	L
Lysine	Lys	K
Methionine	Met	M
Phenylalanine	Phe	F
Proline	Pro	P
Serine	Ser	S
Threonine	Thr	T
Tryptophan	Trp	W
Tyrosine	Tyr	Y
Valine	Val	V
Any amino acid	Xaa	X

VI. Summary

Parkinson's disease (PD) is the second most common neurodegenerative disorder, affecting approximately 1% of the population over the age of 65. Around 5% of these cases can be linked to mutations in known genes, one of which is the PINK1 gene, first linked to PD a decade ago. Since then, over 30 mutations in PINK have been described. The PINK1 gene encodes an unusual serine/threonine protein kinase; uniquely among protein kinases, PINK1 is anchored to the mitochondria and furthermore possesses three unusual insertions of unknown function in the N-lobe of its kinase domain. Recently, two important PINK1 substrates have been identified - the ubiquitin E3 ligase Parkin and ubiquitin itself. Phosphorylation of both of these substrates has further been shown to be necessary for the activation of Parkin E3 ligase activity. At the start of this project, little was known about the catalytic properties of PINK1 or the effects of the identified PD-linked mutations due to the lack of a robust *in vitro* assay for PINK1 activity. In addition, the mechanisms by which PINK1 phosphorylation activated Parkin were not understood. The work described in this thesis was carried out with the aim of overcoming these hurdles by using a PINK1 homologue from a more tractable species.

In Chapter III of this thesis, I describe the identification of a PINK1 homologue from the insect species *Tribolium castaneum* (TcPINK1) and its validation as a *bona fide* model for human PINK1. The activity assay established with TcPINK1 is used to show the PINK1 C-terminal domain is required for kinase activity and that TcPINK1 strongly prefers peptide substrates with a +1 proline. Interestingly, this requirement is absent when intact protein substrates are used. TcPINK1 is then used as a model to analyse the effects of PD-linked disease mutations, revealing that all the tested point and truncating mutations lead to a decrease in kinase activity. In most cases activity is completely abolished. In Chapter IV, progress towards the crystal structure of TcPINK1 is described. Several TcPINK1

constructs were expressed and purified to homogeneity and used for crystallisation trials. Crystals were obtained under multiple conditions and some progress was made towards improving their diffraction resolution, although this project did not reach a point at which data could be collected. Lastly, in Chapter V, preliminary data describing the molecular mechanism by which PINK1 phosphorylation of the Parkin Ubl domain at residue Ser65 leads to Parkin activation is presented. An AlphaScreen assay was used to produce data suggesting that PINK1 phosphorylation of the Parkin Ubl domain relieves autoinhibitory binding of the Ubl domain to Parkin.

Overall, this work provides the PINK1 field with a useful tool in the form of a robust and reproducible activity for PINK1 activity using TcPINK1, which has already been utilised several times to facilitate discoveries in both this lab and others. Significant progress has been made towards determination of the crystal structure of TcPINK1, which will provide insight into the molecular mechanisms of PD-linked mutations and may shed light onto PINK1 regulation and function. Finally, preliminary data suggests that PINK1-phosphorylation of the Parkin Ubl domain may activate Parkin via alterations of autoinhibitory intramolecular interactions.

VII. Table of Contents

X. List of figures

IX. List of tables

Chapter 1

1 General Introduction

1.1 Post-translational modification

Post-translational modification is a process that occurs in all living organisms, ranging from bacteria, fungi and unicellular eukaryotes through to plants and complex multicellular animals. It is defined as the modification of proteins by the cleavage or formation of covalent bonds and despite the name, the classification encompasses modification of amino acids before, during and after their incorporation into a mature protein (Farriol-Mathis et al, 2004). PTMs encompass a huge diversity of protein modifications, with one study on the relative abundance of PTMs in the human proteome analyzing a catalog of 431 distinct modifications (Khoury et al, 2011). Two types of modification, phosphorylation and ubiquitylation, will be discussed in greater detail in Section 1.2.1 and Section 1.5.1 respectively.

The general role of PTMs is to increase the complexity of the proteome, since a modified protein is chemically and often functionally distinct from its non-modified counterpart. In addition, the PTM status of a protein can vary independently of the level of expression of that protein, providing another layer of control above that of regulation of gene expression. It is estimated that from fewer than 25,000 human genes, around 1 million different protein molecules can be produced as a result of the diversity provided by PTMs in combination with alternative splicing (Farriol-Mathis et al, 2004). PTMs are known to influence or alter a number of aspects of protein biochemistry. They can control enzymatic activity; protein conformation and localization; and influence protein-protein interactions as well as controlling protein stability and targeting proteins for degradation.

PTMs can be added to a protein at any point during its life cycle and many, but not all PTMs, are reversible, with one enzyme carrying out the modification and another opposing enzyme undoing it. This reversibility of PTMs gives them a switch-like character and allows them to be dynamically regulated in response to a stimulus. This ability of PTMs to respond reversibly and rapidly to particular signals makes them a critical element of signal transduction cascades.

Signal transduction is the general term for the mechanism by which cells, both unicellular and multicellular organisms, detect and respond appropriately to extracellular environmental stimuli. The key components of a signal transduction cascade include an activating signal, a receptor, a response relay and an output event (Figure 1.1). The activating signal binds to a receptor that spans the cell membrane and thereby contacts both the extracellular and intracellular environments. A change in the status of this receptor, for example a change in enzymatic activity, leads to the propagation of a signal through the cell by the sequential activation of a number of consecutive components. The cell achieves signal amplification at this stage in several ways. Protein kinase cascades can generate signal amplification, since the kinase activated at each step can phosphorylate and activate multiple copies of its substrate kinase that makes up the next step of the cascade. The generation of a small molecule known as a second messenger is an effective amplification technique since these molecules can diffuse rapidly in the cell to spread the signal and can be generated in large quantities to switch on many copies of a downstream component. The relayed signal ultimately induces a response from the cell, for example a change in gene expression or exocytosis and secretion of a substance from the cell surface.

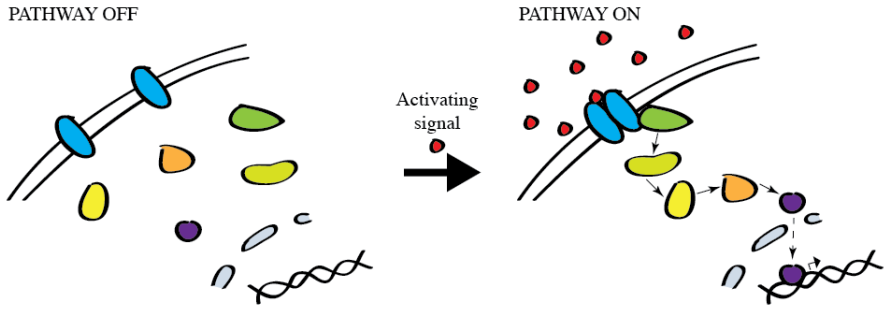

Figure 1.1: Schematic illustration of a general signal transduction pathway.

(L) The pathway is switched off and all components are dissociated. **(R)** The pathway is switched on by the binding of an extracellular signal (red) to the transmembrane receptors (blue). The signal propagates down the signal transduction cascade (green-orange), ending with the localization of an effector protein (purple) to the nucleus. This leads to a response from the cell, in this case the switching on of gene expression.

To ensure the proper switch-like nature and rapid response of a signal transduction pathway, it is important that the signal can be switched off and the system swiftly reset following transmission of a message. For this reason, post-translational modification, particularly in the form of protein phosphorylation, forms a key part of any signal transduction cascade. These modifications are added enzymatically in a rapid and highly specific fashion and can be removed just as quickly by the opposing enzyme, allowing the fast transmission of discrete signals within the cell. A classic example of post-translational modification acting as a core component of a signal transduction cascade is seen in the MAP kinase (mitogen activated protein kinase) pathways (Morrison, 2012). This family of kinases includes members such as the ERKs (extracellular signal-regulated kinases) and JNKs (Jun amino-terminal kinases), which respond to diverse extracellular stimuli and regulate processes such as cell proliferation, differentiation and survival. Their signaling cascades typically consisting of an extracellular stimulus and cognate receptor, followed by a series of three protein kinases that sequentially phosphorylate and activate one another. The final kinase in the cascade then phosphorylates a range of substrates to bring about the appropriate response.

1.2 Protein kinases and protein phosphorylation

1.2.1 Protein phosphorylation

Protein phosphorylation is the reversible modification of serine, threonine and tyrosine residues in a target protein by the addition of a phosphate group to the hydroxyl group of these amino acids, thus forming a phosphoester bond. Protein kinase activity was first observed in the 1950s with the identification of a liver enzyme that phosphorylated casein (Burnett & Kennedy, 1954) and subsequently with studies on glycogen metabolism that showed a phosphorylation/dephosphorylation cycle converted phosphorylase *a* to phosphorylase *b* and back again (Krebs & Fischer, 1956). Further historical discoveries in the field of protein phosphorylation are reviewed in (Cohen, 2002). It is now known that around 30% of the proteome is predicted to be subject to modification by protein phosphorylation, making this an important and ubiquitous method of regulating protein function (Kreegipuu et al, 1999).

Protein phosphorylation is catalyzed by a family of 518 enzymes known as protein kinases, which transfer a phosphate group from the donor substrate adenosine triphosphate (ATP) onto a target protein. The reverse reaction is catalyzed by the protein phosphatase family (Figure 1.2A). Phosphorylation of a target protein can have a number of effects, many of which are as a direct consequence of the phosphate group possessing a double negative charge. Addition of such a charged group to a protein can lead to the formation of new ionic or hydrogen bond interactions in addition to creating attracting or repulsive electrostatic interactions (Johnson & Lewis, 2001). In this way, protein phosphorylation can mediate a large number of diverse effects upon its target proteins, broadly including: changes in conformation and/or enzymatic activity such as that seen in protein kinase activation loop phosphorylation; changes in protein-protein interactions such as binding to

regulatory partners or binding of enzymes to substrates; and changes in localisation, for example nuclear localisation of proteins upon phosphorylation (Figure 1.2B).

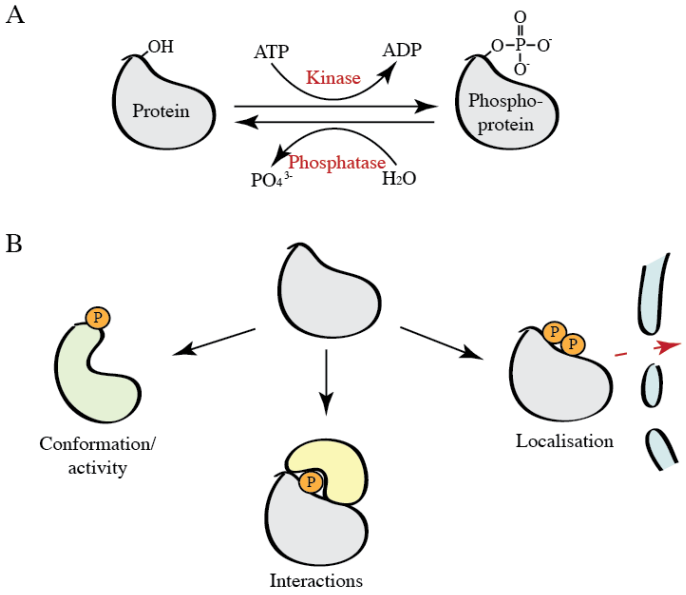

Figure 1.2: Schematic of mechanism and effects of protein phosphorylation

(A) The forward reaction is catalysed by a protein kinase and consumes ATP, yielding a phosphorylated substrate. The reverse dephosphorylation reaction is catalysed by a phosphatase and hydrolyses water. **(B)** Phosphorylation of a target protein can lead to changes in conformation and/or activity, changes in interactions, for example with substrates or regulatory partners, and changes in protein localization.

A landmark study in 2002 classified all protein kinases in the human genome, known as the human "kinome", according to their sequence similarity, firstly grouping them into either a superfamily of proteins containing a eukaryotic protein kinase (ePK) domain, or into a smaller superfamily of proteins containing an atypical protein kinase domain (aPK). These aPKs lack sequence similarity to the ePKs but are known to have protein kinase activity (Manning et al, 2002). The ePKs can mostly be further classified into one of seven subfamilies: TK (tyrosine kinase); TKL (tyrosine kinase-like); STE (containing the homologues of yeast Sterile 7, Sterile 11 and Sterile 20 kinases); CK1 (casein kinase 1); AGC (containing PKA, PKG and PKC families); CAMK (calcium/calmodulin-dependent protein kinases); and CMGC (containing the CDK, MAPK, GSK3 and CLK families). A phylogenetic tree of the ePK family was created to depict the evolutionary relationship

between the family members and to allow a visual representation of their grouping into the different subfamilies (Figure 1.3).

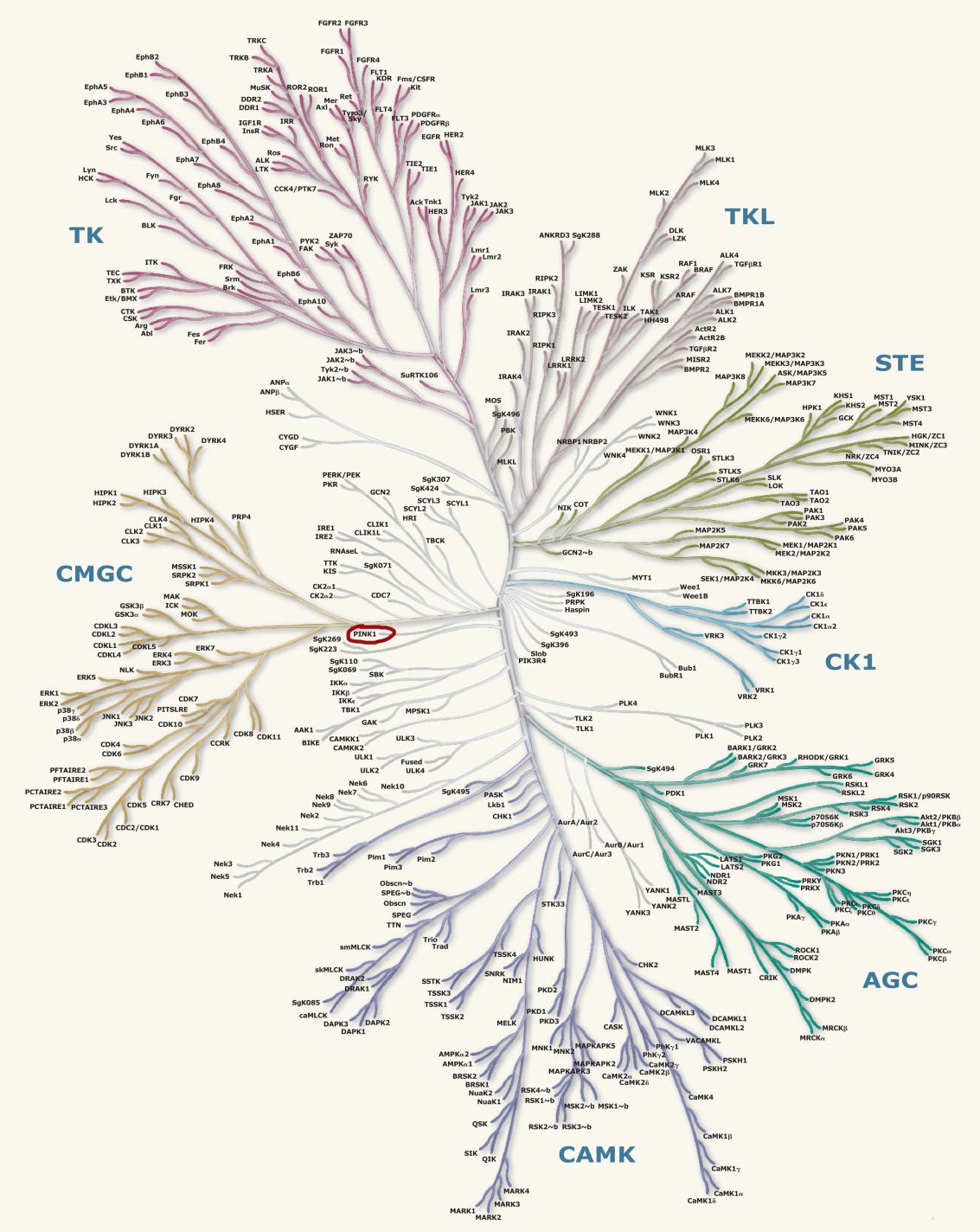

Figure 1.3: The human kinome

The ePKs can be classified into one of seven families: TK (tyrosine kinase); TKL (tyrosine kinase-like); STE (containing the homologues of yeast Sterile 7, Sterile 11 and Sterile 20 kinases); CK1 (casein kinase 1); AGC (containing PKA, PKG and PKC families); CAMK (calcium/calmodulin-dependent protein kinases); and CMGC (containing the CDK, MAPK, GSK3 and CLK families). The kinase PINK1, of relevance to this thesis, is highlighted in a red oval. Adapted from Manning et al, 2002.

1.2.2 The structural basis of protein kinase activity

The first structure of a protein kinase, that of cAMP-dependent protein kinase (PKA) revealed that the protein adopted a bilobal fold, with the smaller N-lobe consisting primarily of β-strands and the larger C-lobe mainly of α-helices. A flexible hinge region connected the two (Zheng et al, 1993). All protein kinases catalyse the same basic reaction, the transfer of a phosphoryl group onto a serine, threonine or tyrosine residue in a target protein (Adams, 2001). They also possess the same overall structural fold and a number of conserved amino acid motifs required for activity (Hanks & Hunter, 1995). These motifs are primarily involved in ATP binding and catalysis and are depicted in the schematic below along with a model of the crystal structure of PKA in the active state (Figure 1.4). PKA is one of the most well studied protein kinases and is used in this thesis as a model for the general protein kinase domain.

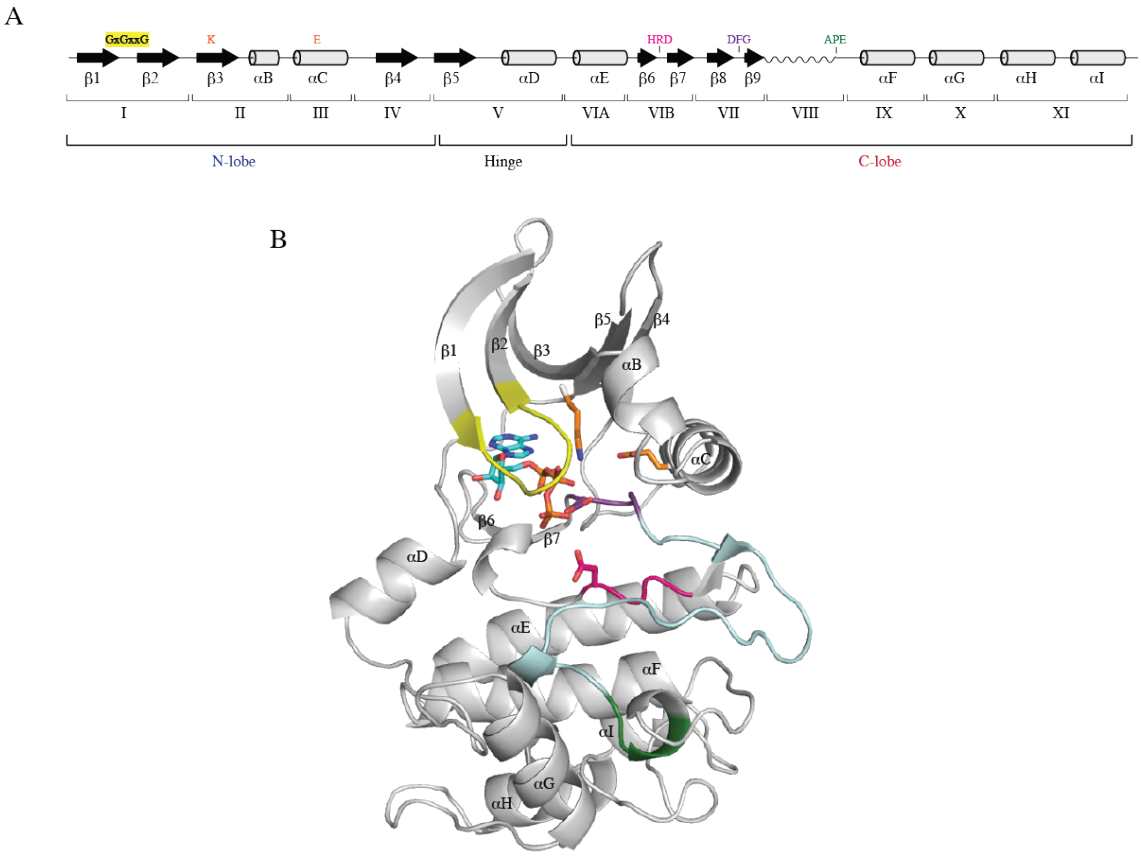

Figure 1.4: Conserved structural and sequence motifs of protein kinases

(A) Secondary structure of PKA (α-helices: barrels; β-strands: arrows) showing conserved amino acid motifs (top) and the boundaries of the conserved kinase subdomains as defined by Hanks & Hunter (bottom). The N- and C-lobes and hinge region are also shown. **(B)** Crystal structure of PKA in the active state showing motifs involved in catalysis. Yellow: glycine-rich loop; orange: β3-αC salt bridge; pink: HRD catalytic motif; purple: DFG motif/N-terminal activation segment anchor; pale blue: activation segment; green: APE motif/C-terminal activation segment anchor. ATP is shown as turquoise/orange sticks. PDB ID: 1ATP.

Protein kinases are dynamic enzymes, cycling between a fully active closed conformation and a fully inactive open conformation. Studies on the structure of PKA have revealed a number of discrete conformations in between these two opposing states, although it is uncertain if these intermediate structures represent partially active conformations that are steps on the way to full activation, or normal parts of the kinase catalytic cycle (Nolen et al, 2004). As mentioned above, there are a number of conserved features common to all kinases that play a role in kinase activity. These will be discussed in greater detail, moving from N- to C-terminus within the kinase domain. Numbering is given according to PKA.

The glycine-rich loop motif is found in Subdomain I, in the loop between strands β1 and β2, starting with Gly50. The small glycine residues allow the loop to approach the ATP molecule and form hydrogen bonds from its peptide backbone atoms to the β-phosphate of ATP (Huse & Kuriyan, 2002). Hydrophobic side chains in this subdomain also contribute to the hydrophobic adenine-binding portion of the ATP binding pocket (Hanks & Hunter, 1995).

An important ionic interaction occurs between a conserved lysine residue (Lys72) in the β3 strand (Subdomain II) and a glutamic acid (Glu91) in the αC helix (Subdomain III). Lys72 forms a stabilising ionic interaction with the α- and β-phosphates of ATP and when the kinase is in the active conformation, forms a salt bridge with Glu91 (Huse & Kuriyan, 2002). The conformation of αC relative to the rest of the kinase is flexible and often varies dependent on the activation state of the enzyme.

The hinge region, made up of the β5 strand and the αD helix, connects the two lobes of the kinase domain and comprises Subdomain V. This region of the protein is flexible to allow for the movement of the two lobes relative to one another that occurs as the kinase moves from the active to the inactive state. The loop between strands β6 and β7 is referred to as the catalytic loop and is found in Subdomain VIB. It contains the catalytic base, an aspartic acid (Asp 166) found within the HRD motif.

The activation segment spans Subdomains VII and VIII and is subdivided into several sections (Figure 1.5). The activation segment is a key structure for controlling the activation status of protein kinases, with many being regulated by an activating phosphorylation event within this region.

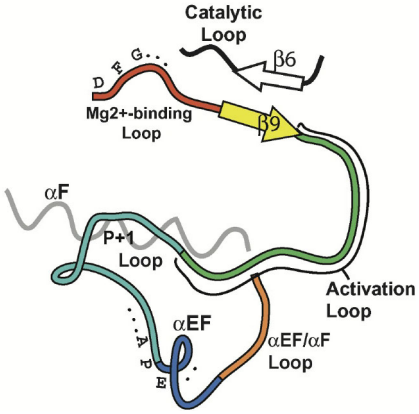

Figure 1.5: Schematic of the activation segment of protein kinases

The same nomenclature for the different components of the activation segment is used throughout this thesis. Adapted from Nolen et al, 2004.

The loop between strands β8 and β9 (Subdomain VII) is known as the magnesium-binding loop and contains the conserved DFG motif that defines the start of the activation segment. The structure of the DFG motif is highly similar in all kinases in the active state (Nolen et al, 2004). The DFG aspartic acid (Asp184) is involved in coordinating the magnesium ions that chelate the β- and γ-phosphates of ATP, helping to orient it correctly for catalysis (Adams, 2001). When the kinase is in the inactive state, Asp184 is positioned incorrectly and this interaction cannot take place. Furthermore, in PKA the DFG phenylalanine (F185) forms a hydrophobic interaction with the αC helix, disruption of which can perturb the conformation of this helix (Nolen et al, 2004).

Subdomain VIII contains the activation loop and the P+1 loop. The APE motif found here marks the end of the activation segment, and as with the DFG motif, seems to adopt a similar conformation in all active kinases. The APE glutamic acid (Glu208) is generally conserved and forms a stabilising ionic bond with an arginine residue (Arg280) in Subdomain XI (Yang et al, 2012). The activation loop itself is variable in both sequence and structure, which reflects the diverse methods of regulation that are used to control the activity of different kinases via their activation segments. Many proteins are activated by phosphorylation within the activation segment, either by an upstream kinase or by autophosphorylation. Regulation of kinase activity will be discussed in more depth in Section 1.2.3. The P+1 loop is known to be involved in dictating the sequence specificity

of protein kinases, particularly with regards to the amino acids C-terminal to the site of phosphorylation (Ubersax & Ferrell, 2007). The sequence and conformation of this region is therefore tailored according to the substrate specificity of each kinase.

Finally, although they are not discrete amino acid motifs or linear regions, two structures known as the R- and C-spines also play an important role in kinase activity (Kornev et al, 2006; Kornev et al, 2008). These spines were identified by computational studies and are made up of a number of amino acids spread throughout the primary sequence. They are separated in three-dimensional space in the inactive state, but come together and interact to form rigid structures that traverse the entire kinase domain upon entering the active conformation (Figure 1.6).

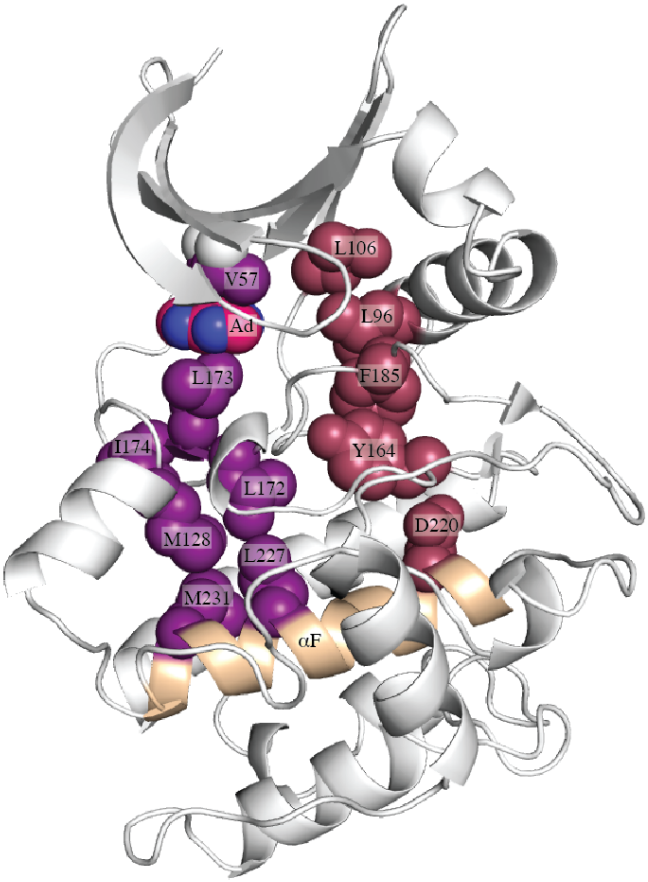

Figure 1.6: Crystal structure of active PKA showing R- and C-spines

Spines are shown in sphere representation to illustrate the space occupied and each component is labelled. R-spine: raspberry; C-spine: purple; adenine ring of ATP: pink; αF helix: cream. PDB ID: 1ATP.

The R-spine is made up of Leu96 from the αC helix, Leu106 from β4, Tyr 164 from the catalytic loop, Phe185 from the magnesium loop (DFG motif) and Asp220 from αF. Its assembly is linked to the conformation of the activation segment and with the αC helix (Kornev 2006). The C-spine consists of Leu227 and Met231 from the αF helix, Met128 from αD, Leu127, Leu173 and Ile174 from β7, Val57 from β2 and Ala70 from β3. Critically, the adenine ring of ATP also contributes to the formation of this spine and its assembly is therefore linked to the binding of ATP to the kinase. Since the completed C-spine extends throughout the kinase and traverses well into the N-lobe, binding of the

adenine moiety can be considered an important event that integrates the N-and C-lobes in preparation for catalysis.

It is interesting to note that both the R- and C-spines contain amino acids that are located in the αF helix, with the R-spine originating from the N-terminus of the helix and the C-spine from the C-terminus. In addition to providing support for these two structures, it has been shown that the αF helix forms a tight hydrophobic interaction with the αH helix that is presumed to aid in stabilising the hydrophobic core of the kinase. Furthermore, in PKA, interactions between the αF helix and the P+1 loop have been observed, along with more indirect interactions with the catalytic and activation loops. These are regions of the protein that play a key role in substrate recognition and are directly responsible for catalysis. The sum of these many interactions is that the αF helix is able to act as a central organising structure, coordinating separate inputs from activation segment and αC helix conformation, ATP binding, catalytic loop status and substrate binding. With this in mind, it becomes easy to understand how kinase activation can occur as an ordered multi-stage process where each step is sensitive to the occurrence of the others. This complex activation mechanism provides multiple levels of control to allow the precise activity of a given kinase to be finely tuned.

1.2.3 Regulation of protein kinase activity

Protein kinases play important roles in the regulation of almost every cellular process, including those such as cell division, survival, growth and metabolism and as a result it is not surprising that the presence of aberrant kinase activity has been linked to many human diseases (see Section 1.2.5 for more detail). The activity of protein kinases must therefore be kept tightly regulated both to avoid inappropriate activation and to ensure the enzyme responds only at the correct time to its physiological stimuli.

One of the most common regulatory mechanisms used to control the activity of many kinases is phosphorylation of the activation loop. This can be carried out either by a regulatory upstream kinase or as an activating autophosphorylation event. As a general rule, kinases with an arginine in the HRD motif, referred to as RD kinases, are regulated by activation loop phosphorylation and those without, referred to as non-RD kinases, are not. In RD kinases requiring phosphorylation, the arginine residue forms part of a basic pocket that captures the phosphorylated activation loop and holds it in the active conformation (Nolen et al, 2004). An example of this is seen in the structure of the Aurora-A spindle kinase in complex with a binding partner, in which Aurora-A is phosphorylated at residue Thr288 of the activation loop (Bayliss et al, 2003). This phosphorylated residue then forms an interaction with the HRD arginine (Arg255) and two other arginine residues, Arg180 and Arg286, which form a basic pocket. The overall structure of the activation loop in this structure is highly similar to that of PKA in its active conformation.

In RD kinases that are not phosphorylated, the basic pocket has been observed to bind anions, such as a sulphate ion in the case of GSK-3β (glycogen synthase kinase 3 beta), however this is not necessary for proper activation loop conformation (Bax et al, 2001), suggesting the activation loop is able to independently assume the conformation required for kinase activity. Other kinases, both RD and non-RD, make use of binding partners to position the activation loop. An example of this is the constitutively active CK2 (casein kinase 2), which uses interactions between its N-terminal extension and the activation loop to maintain the activation loop in the active conformation (Niefind et al, 1998).

Regulation of kinase activity by phosphorylation is not just confined to phosphorylation events within the activation loop, however. Phosphorylation of GSK3 at its N-terminus (Ser9 in GSK3β, Ser21 in GSK3-α) has been shown to inhibit GSK3 activity and decrease the phosphorylation of glycogen synthase (Cross et al, 1995). The mechanism for this

inhibition was not understood until much later. GSK3 phosphorylates previously phosphorylated, or primed, substrates that then bind to a basic pocket analogous to the one used to bind phosphorylated activation loop residues in other kinases (ter Haar et al, 2001). When the N-terminus of GSK3 is phosphorylated, it is able to occupy this basic substrate-binding site and prevent binding of the physiological substrate (Frame et al, 2001). In this way, the phosphorylated N-terminus acts as an inhibitory pseudosubstrate.

Another important mechanism for the regulation of kinase activity is by protein-protein interactions. These can occur either with another protein molecule, or with another segment of the same molecule such as a regulatory domain outside the kinase domain. A well-known example of regulation via a binding protein is the activation of the CDKs (cyclin-dependent kinases) by cyclin binding. In the inactive structure of human CDK2, the αC helix is rotated outwards and the salt bridge between this structure and the β3 strand is broken (De Bondt et al, 1993). However, upon cyclin binding (in this case Cyclin A) to the αC helix, it rotates inwards towards the ATP binding site. Lys33 from β3 and Glu51 from αC are then able to form an ionic interaction and Lys33 is correctly positioned to interact with and stabilise the ATP molecule. In addition, Cyclin A binds to the activation loop of CDK2, moving it away from where it was obscuring the peptide binding site and correctly positioning it for phosphorylation by its upstream kinase, which will in turn lead to maximal kinase activity (Jeffrey et al, 1995). The activation mechanism of CDK2 also provides an example of how several events required for kinase activation, in this case activation segment and αC helix conformation, can be linked and interdependent.

A further interesting example of kinase regulation by binding partners is the regulation of the LKB1 kinase by the pseudokinase STRADα (Ste20-related adapter) and the scaffold protein MO25α (mouse protein-25) (Zeqiraj et al, 2009). Despite STRADα being a

pseudokinase, it is able to bind ATP and upon MO25α binding, adopt the canonical "active" kinase conformation. Interactions between MO25α and the LKB1 activation loop, αC and αI helices, along with interactions between STRADα and both the N- and C-lobes of LKB1, position LKB1 in the active conformation.

CaMKII (Ca^{2+}/calmodulin-dependent protein kinase II) is negatively regulated by a region C-terminal to its kinase domain. The structure of inactive CaMKII reveals that the regulatory segment, which contains the calmodulin-binding site, acts by blocking substrate binding. Interestingly, the activation loop is in an active conformation, although the N-lobe is rotated in an open conformation relative to the C-lobe (Rosenberg et al, 2005). This conformational change leads to a concomitant decrease in ATP binding affinity, mainly due to the loss of an interaction between residues in the αD helix and the ribose ring of ATP. Furthermore, interactions between the αF helix and the regulatory segment masks an autophosphorylation site within the regulatory segment that activates the enzyme in the absence of Ca^{2+} or calmodulin (Rosenberg et al, 2005). In this way, binding of the regulatory segment to CaMKII keeps multiple different checks upon its activity and ensures activation only occurs in the presence of the required stimulus.

1.2.4 Mechanisms of substrate recognition in protein kinases

Once a kinase has become activated, it needs to be able to discriminate between huge numbers of potential protein substrates. As previously mentioned, the basic reaction catalysed by a kinase is the phosphorylation of serine, threonine or tyrosine. It has been estimated that within a typical eukaryotic cell this provides a pool of around 700,000 potentially phosphorylatable residues (Ubersax & Ferrell, 2007). Therefore it is imperative that additional mechanisms of specificity be employed to ensure that each kinase is only

able to phosphorylate these amino acids within the correct physiological target, with many kinases employing several different methods to ensure specificity.

Protein kinases can generally be separated into those that phosphorylate serine and threonine residues and those that phosphorylate tyrosine residues. There are some exceptions, such as the DYRKs (dual-specificity tyrosine-regulated kinases), that are able to phosphorylate both serine/threonine and tyrosine residues (Aranda et al, 2011), although this is not common. To allow discrimination between serine/threonine and tyrosine residues, tyrosine kinases typically have a deeper catalytic cleft. In this case, only tyrosine is large enough to reach close to the γ-phosphate of ATP and become phosphorylated (Ubersax & Ferrell, 2007). In addition, a conserved residue within the P+1 loop of the activation segment aids in dictating serine/threonine versus tyrosine specificity. In S/T kinases, this residue is often a serine or threonine that forms a hydrogen bond to the catalytic loop, whereas in tyrosine kinases, it is usually a proline that is able to form a stacking interaction with the tyrosine side chain and position it correctly (Nolen et al, 2004).

Important interactions for dictating substrate specificity occur between the substrate, typically around four amino acids on either side of the phosphorylation site, and the active site groove of the protein kinase. In some cases, a particular protein kinase will have a well-defined consensus sequence for the residues surrounding the phosphorylation site that can even be used to predict its likely substrates. A well-known example of such a consensus motif is seen in PKB (protein kinase B), which phosphorylates substrates with the consensus sequence R-X-R-X-X-S/T-φ, where X is any amino acid and φ is a bulky hydrophobic residue (Alessi et al, 1996). PKB is part of the AGC family of protein kinases, which are known to display a general preference for basic substrates. For example, the

consensus sequence for PKA, another AGC family member, is R-R/K-X-S/T (Kemp et al, 1977). Since AGC kinases display similar substrate preferences, they often phosphorylate the same substrate proteins, such as GSK3, which is phosphorylated by multiple AGC family members (Frame & Cohen, 2001). This illustrates that although interactions around the active site can contribute significantly to kinase substrate specificity, they are limited in the degree of complexity of recognition they can confer.

An additional level of substrate specificity can be conferred by interactions away from the active site, known as distal docking sites. These interactions can often increase the affinity of a kinase for its substrate and as a result make phosphorylation more efficient. The MAPKs (mitogen-activated protein kinases) provide a good example of the use of docking domains to provide substrate specificity. JNK2 possesses a small region near the active site that is responsible for binding to its substrate, c-Jun. In contrast, JNK1 does not possess this docking site and as a result phosphorylates c-Jun much less efficiently (Kallunki et al, 1994).

Finally, controlling the localisation of the kinase can control the phosphorylation of target proteins. PDK1 (phosphoinositide-dependent kinase 1) is a constitutively active kinase that is localised to the inner plasma membrane via binding of its PH (pleckstrin homology) domain to the second messenger PIP_3 (Anderson et al, 1998). One of its substrates, PKB, also possesses a PH domain and is localised to the membrane by the same signal. Co-localisation of these proteins on the membrane appears to be a key step for enabling the activation loop phosphorylation of PKB at Thr308 by PDK1 (Scheid et al, 2002). This co-localisation was originally thought to be the main contributing factor to PKB activation, however it is now understood that prior phosphorylation of PKB at Ser473 by mTORC2

and the subsequent binding of this phosphorylated motif to the PIF pocket of PDK1 also plays a role (Najafov et al, 2012).

1.2.5 Protein phosphorylation and human disease

Aberrant protein phosphorylation is responsible for a large number of human diseases including cancer, autoimmune diseases and neurodegenerative disorders. In particular, inherited or sporadic mutations in protein kinases that lead to inactivation or inappropriate activation of the enzyme are a common cause of disease. A table of selected kinases and the disorder caused by their malfunction is presented below (Table 1.1). Much work has gone into understanding the pathways and mechanisms that lead to these diseases and as such, protein kinases are now a popular drug target. Extensive effort has gone towards developing potent and specific inhibitors against a plethora of different protein kinases. The first success with this approach came with the development of the inhibitor Imatinib (Gleevec), which targets the tyrosine kinase Bcr-Abl, a constitutively active fusion protein that causes the development of chronic myeloid leukaemia (Capdeville et al, 2002). Kinase inhibitors are now used to treat many other forms of cancer (Zhang et al, 2009) and have also been used with a moderate degree of success to treat autoimmune and inflammatory diseases, for example the JAK inhibitor tofacitinib, which has been approved in the United States for the treatment of rheumatoid arthritis (Patterson et al, 2014).

Kinase	Full Name	Disorder
Abl	Abelson murine leukemia viral oncogene homolog 1	Chronic myeloid leukaemia
Akt1	RAC-alpha serine/threonine-protein kinase	Proteus syndrome
AMPK	5'-AMP-activated protein kinase	Wolff-Parkinson-White syndrome
ATM	Ataxia telangiectasia mutated	Ataxia telangiectasia
BTK	B-cell progenitor kinase	X-linked agammaglobulinemia
CDK4	Cyclin-dependent kinase 4	Melanoma, sporadic cancers
CHK2	Checkpoint kinase 2	Li-Fraumeni syndrome, sporadic cancers
DMPK	Myotonic dystrophy protein kinase	Myotonic dystrophy
EGFR	Epidermal growth factor receptor	Non-small cell lung cancers
INSR	Insulin receptor	Insulin resistance
Lck	Leukocyte C-terminal Src kinase	Leukaemia
LKB1	Liver kinase B1	Peutz-Jeghers symdrome, sporadic cancers
LRRK2	Leucine-rich repeat serine/threonine-protein kinase 2	Parkinson's disease
MLCK2	Myosin light chain kinase 2	Cardiomyopathy
PDGFRβ	Platelet-derived growth factor receptor beta	Chronic myelogenous leukaemia
PINK1	PTEN-induced kinase 1	Early-onset Parkinson's disease
TTBK2	Tau-tubulin kinase 2	Spinocerebellar ataxia type 11
WNK1/4	Protein kinase with no lysine 1/4	Pseudohypoaldosteronism type 2
Zap70	70 kDa zeta-chain associated protein	Severe combined immunodeficiency

Table 1.1: Protein kinases mutated in human disease

The symbol and full name of each kinase is listed along with the disease or disorder caused by mutations in each kinase. Adapted from Alessi & Zeqiraj, 2007.

1.3 Parkinson's disease

Parkinson's disease (PD) is the second most common neurodegenerative disorder. Its prevalence increases with age and it occurs in 1% of the population over the age of 60 (de Lau & Breteler, 2006). The overwhelming majority of cases (~95%) are idiopathic, however in a small number of cases (~5%), the disease can be traced to mutations in one of several known genes. These cases are referred to as familial PD to distinguish them from the more common idiopathic form. Diagnosis of PD is currently based upon the presence of clinical symptoms and signs and it is not possible to test for biomarkers prior to the development of the disease to give an indication of likelihood of future development (Jankovic, 2008). The only available therapies manage the symptoms of the disease and do not alter or prevent disease progression. Once the disease process has begun, it is currently irreversible (Rascol et al, 2003).

1.3.1 Historical and landmark discoveries

Parkinson's disease was first formally described in 1817 by James Parkinson in his work "Essay on the Shaking Palsy", where he described the subjects he observed as follows (Parkinson, 1817):

"Involuntary tremulous motion, with lessened muscular power, in parts not in action and even when supported; with a propensity to bend the trunk forward, and to pass from a walking to a running pace: the senses and intellects being uninjured"

Further studies carried out by Charcot in 1872 refined the description of the disease, introducing the concept of bradykinesia as slowness in executing movement and being distinct from weakness caused by the tremor or rigidity also observed (Charcot, 1872). Charcot also re-named the disease Parkinson's disease at this point, in recognition of its

original description. In 1912, Lewy discovered neuronal inclusions in the brains of Parkinson's patients (Lewy, 1912), which later became known as Lewy bodies and are now a defining feature of Parkinson's disease. The primary component of Lewy bodies was much later shown to be the protein α-synuclein, now known to be mutated in familial PD (Spillantini et al, 1998). Around the same time as Lewy, it was discovered that the substantia nigra was a major site of damage in PD, which was validated by a thorough pathological analysis of the lesions seen in the PD brain (Greenfield & Bosanquet, 1953). Loss of dopamine in the striatum of post-mortem PD brains was first observed in 1960 (Ehringer & Hornykiewicz, 1960) and shortly after, administration of its precursor, L-DOPA, was demonstrated to be an effective therapy for relief of the symptoms of PD (Cotzias et al, 1967).

1.3.2 Clinical symptoms and pathology of Parkinson's disease

The clinical symptoms displayed by patients suffering from PD fall into two classes: motor and non-motor symptoms - with the motor symptoms of the disease being the most well known amongst laypersons, despite the non-motor symptoms being equally if not more debilitating. It is estimated that motor symptoms only start to manifest once 50-60% of dopaminergic neurons in the substantia nigra have been lost (Riederer & Wuketich, 1976), whereas certain non-motor symptoms can appear years before motor symptoms are detectable (Beitz, 2014).

The major motor symptoms of PD include a resting tremor that often begins on one side of the body and progresses to the other side over time. This is the most common motor symptom, and has been found to occur in approximately 75% of PD patients (Hughes et al, 1993). Bradykinesia is also seen in many patients and is slowness of movement, including slowness of initiation, long gaps between successive elements of a movement and

difficulty performing two movements simultaneously (Berardelli et al, 2001). Patients also display rigidity, postural instability and freezing (Jankovic, 2008).

The non-motor symptoms of PD can be broadly divided into cognitive and neurobehavioural symptoms, autonomic dysfunction and sleep and sensory dysfunction. Cognitive and neurobehavioural symptoms primarily include depression, anxiety, apathy and hallucinations. These disorders are thought to be present in up to 90% of PD patients (Aarsland et al, 2007). Autonomic dysfunctions seen in PD patients can include orthostatic hypotension (low blood pressure upon standing up), constipation, urinary difficulties, incontinence, sexual dysfunction, sialorrhea (excessive salivation), dysphagia (difficulty in swallowing) and sweating dysfunction (Jankovic, 2008). The sleep dysfunction seen in PD patients includes insomnia, excessive daytime sleepiness and REM sleep behavior disorder. REM sleep behavior disorder occurs in approximately one-third of PD patients and is known to be a risk factor for the development of PD (Postuma et al, 2013). Sensory dysfunctions include painful sensory symptoms and olfactory dysfunction, which is believed to be an early marker of the development of PD and is associated with an increased risk of developing the disease (Ponsen et al, 2004).

The most pronounced pathological feature of PD is the loss of dopaminergic neurons within the substantia nigra pars compacta (Bernheimer et al, 1973), which subsequently leads to loss of dopamine in the striatum, a region of the brain that receives input from the substantia nigra. Both of these regions of the brain form part of a larger structure called the basal ganglia (Bergman & Deuschl, 2002). Examination of post-mortem PD patient brains reveals that surviving dopaminergic neurons commonly contain Lewy bodies (Spillantini et al, 1998). The mapping of the basal ganglia circuitry has provided some mechanistic understanding of how loss of dopaminergic neurons and the subsequent reduction in

striatal dopamine levels leads to the motor symptoms of PD, but the neural basis of the non-motor symptoms is still not well understood (Wichmann et al, 2011).

1.3.3 Current therapies for Parkinson's disease

There are three main classes of treatment for patients suffering from PD, namely surgical interventions (Duker & Espay, 2013) and rehabilitation (Hindle et al, 2013), which will not be discussed further, and finally pharmacological treatments.

There are several classes of drugs that provide symptomatic relief for PD patients by increasing the levels of dopamine in the brain through various mechanisms, including promotion of dopamine synthesis, activation of neurotransmitter receptors in the brain, prolonging availability of dopamine in the brain, or prolonging the ability of other therapeutic drugs (Rascol et al, 2002). Treatment with the dopamine precursor L-DOPA remains one of the most potent forms of therapy for PD patients. L-DOPA, unlike dopamine itself, can cross the blood-brain barrier and once inside the brain is metabolised by DOPA decarboxylase to form dopamine. Unwanted metabolism of L-DOPA in the peripheral nervous system is blocked by taking a DOPA decarboxylase inhibitor in conjunction with L-DOPA. This restricts the conversion of L-DOPA and subsequently increases dopamine levels in the CNS (Katzenschlager & Lees, 2002). It should be noted that the existing therapies for PD focus on the motor symptoms of the disease and provide little relief for the non-motor symptoms, with few effective therapies being available for treatment of the latter set of symptoms (Rascol et al, 2002).

1.3.4 Genetics of Parkinson's disease

Although Parkinson's disease is primarily a sporadic disorder, approximately 5% of PD cases have been shown to have a known genetic cause and it has also been hypothesized that the presence of certain genetic variations may contribute towards or confer susceptibility to development of the sporadic form of the disease (de Lau & Breteler, 2006). To date, eighteen chromosomal regions, or loci, have been suggested to have a link to PD through methods such as linkage analysis and genome-wide association studies. So far, only five of these regions have been unequivocally linked to monogenic forms of canonical PD with multiple mutations described in independent families (Klein & Westenberger, 2012); these genes are described in greater detail below. The situation with the remainder is more ambiguous. For some regions, the association between the locus and PD has not been replicated and is therefore unconfirmed. For others, the causative gene within the locus has not yet been identified, and for others, variations in the gene are risk factors and only confer susceptibility to PD (Klein & Westenberger, 2012). Each of these 18 loci and their status with regards to confirmation, causative gene (if known), inheritance and clinical features is listed below (Table 1.2).

Symbol	Locus	Gene	Confirmed?	Inheritance	Disorder
PARK1	4q21-22	SNCA	Confirmed	AD	Aggressive PD with early cognitive decline
PARK2	6q25.2–q27	Parkin	Confirmed	AR	EOPD
PARK3	2p13	Unknown	Unconfirmed	AD	Classical PD
PARK4	4q21–q23	SNCA	Erroneous locus, same as PARK1	AD	Aggressive PD with early cognitive decline
PARK5	4p13	UCHL1	Unconfirmed	AD	Classical PD
PARK6	1p35–p36	PINK1	Confirmed	AR	EOPD
PARK7	1p36	DJ-1	Confirmed	AR	EOPD
PARK8	12q12	LRRK2	Confirmed	AD	Classical PD
PARK9	1p36	ATP13A2	Confirmed	AR	Atypical PD with dementia + additional symptoms
PARK10	1p32	Unknown	Confirmed	Risk factor	Classical PD
PARK11	2q36-27	Unknown	Unconfirmed	AD	LOPD
PARK12	Xq21–q25	Unknown	Confirmed	Risk factor	Classical PD
PARK13	2p12	HTRA2	Unconfirmed	AD/Risk factor	Classical PD
PARK14	22q13.1	PLA2G6	Confirmed	AR	EO dystonia-parkinsonism
PARK15	22q12–q13	FBX07	Confirmed	AR	EO parkinson-pyramidal syndrome
PARK16	1q32	Unknown	Confirmed	Risk factor	Classical PD
PARK17	16q11.2	VPS35	Confirmed	AD	Classical PD
PARK18	3q27.1	EIF4G1	Unconfirmed	AD	Classical PD

Table 1.2: Genetic loci implicated in familial Parkinson's disease

The symbol of each locus is listed along with its location and whether or not the link between that locus and PD has been definitively confirmed. For each locus, the relevant gene (if known), mode of inheritance and details of the disorder caused is listed. Two genes of relevance to this thesis, PINK1 and Parkin, are highlighted. Adapted from Klein & Westenberger, 2012.

LRRK2 (PARK8) mutations are the most common cause of autosomal dominant Parkinsonism (Paisan-Ruiz et al, 2004; Zimprich et al, 2004). The LRRK2 (Leucine-Rich Repeat Kinase 2) gene encodes for a large protein containing both a kinase domain and a GTPase domain in addition to multiple domains predicted to be involved in protein-protein interactions. Many mutations in LRRK2 have been reported, with the most prevalent and well-studied being the G2019S mutation that increases kinase activity relative

to the wild-type protein (Jaleel et al, 2007; West et al, 2005). Little is known about the physiological function of LRRK2.

The SNCA gene (PARK1/4) was the first gene to be linked to PD and encodes the protein α-synuclein (Polymeropoulos et al, 1997). Endogenous α-synuclein exists as a tetramer, with the monomers having a largely α-helical structure (Bartels et al, 2011). Aggregated α-synuclein forms the primary component of the Lewy bodies that are observed in the surviving neurons of patients with PD (Spillantini et al, 1997). Several point mutations in the SNCA gene have been reported, some of which increase the aggregation propensity of the protein (Bussell & Eliezer, 2001) More frequently reported are gene duplications and triplications, which have a gene dosage effect (Wales et al, 2013).

Mutations in the Parkin gene (PARK2), first identified in 1998 (Kitada et al, 1998), are the most common cause of early-onset autosomal recessive Parkinsonism, with age of onset typically being between 30-40 years of age, but sometimes younger than 21 (referred to as juvenile PD). Over 100 mutations in Parkin have been reported (Klein & Westenberger, 2012). The Parkin protein is a 465 amino acid ubiquitin E3 ligase belonging to the RBR family (Wenzel et al, 2011). The regulation, substrates and function of Parkin will be discussed in greater detail in Section 1.5.

The PINK1 gene (PARK6) encodes a protein kinase (PTEN (phosphatase and tensin homologue)-induced kinase 1) of 581 amino acids. Mutations in the PINK1 gene were first identified in 2004 (Valente et al, 2004), and since then approximately 30 pathogenic mutations have been reported along with many more heterozygous variants of uncertain pathogenic significance (Appendix 1). Both point and truncating mutations have been

identified. PINK1, its substrates, regulation and function will be discussed in more detail in Section 1.4.

Finally, mutations in the DJ-1 gene (PARK7) were first identified in 2003 (Bonifati et al, 2003) and to date several additional point mutations have been identified. The L166P mutation is known to destabilize the protein, although the effect of the other mutations is less clear (Kahle et al, 2009). The DJ-1 protein is believed to act as an oxidative chaperone and is ubiquitously expressed.

1.4 PINK1 (PTEN-induced kinase 1)

The gene encoding PINK1 (PTEN (phosphatase and tensin homologue)-induced kinase 1) was first identified in 2001 after it was discovered that its transcription was upregulated as a response to PTEN overexpression in endometrial cancer cells (Unoki & Nakamura, 2001). It was not until 2004 that PINK1 was linked to Parkinson's disease, when homozygous mutations in PINK1 were found in patients with autosomal recessive early-onset Parkinson's disease (Valente et al, 2004). A full list of PINK1 point mutations is provided in Appendix 1.

The PINK1 gene is around 1.8 kb in length, consists of 8 exons and is found on Chromosome 1. The PINK1 protein is 581 amino acids in length. Initial Northern blot analysis of mRNA levels revealed that PINK1 is expressed ubiquitously in humans and is particularly abundant in the heart, skeletal muscle and testis (Unoki & Nakamura, 2001). A more detailed analysis of expression levels within the human brain revealed that PINK1 is expressed in neuronal cells, with higher levels seen in the substantia nigra, among other areas. In the same study it was shown that in brains from PD patients, PINK mRNA levels remained the same within the cerebellum and did not decrease in neurons of the substantia nigra (Blackinton et al, 2007).

Patients harbouring PINK1 mutations generally have a strong and long-lasting response to Levodopa (L-DOPA) and have a lower prevalence of non-motor symptoms than sporadic PD patients (Puschmann, 2013). They may, however show psychiatric symptoms in addition to rigidity, lower limb dystonia (involuntary contractions) and hyperreflexia (over-responsive reflexes). There is only a single report of a post-mortem brain from a PINK1 patient showing Lewy body pathology (Samaranch et al, 2010).

1.4.1 Domain architecture of PINK1

PINK1 is an unusual member of the protein kinase family; it does not fall into any of the known groupings in the human kinome tree and is found on a branch by itself, meaning there are no closely related or homologous kinases. The most closely related protein kinase is DMPK (myotonin-protein kinase), which shares only 31% sequence identity with PINK1. This lack of similarity to other kinases is due to a number of unusual features seen in this enzyme (Figure 1.7). At the N-terminus there is a mitochondrial targeting sequence and transmembrane domain - features not seen in any other member of the human kinome. This is followed by a moderately conserved stretch of amino acids that are predicted to form a disordered region. The kinase domain, found towards the C-terminus of the protein, contains three unusual insertions in its N-lobe (Cardona et al, 2011; Mills et al, 2008). The first, most N-terminal insertion is the longest and least conserved between species, the second and third are shorter and more highly conserved. Immediately following the kinase domain is a small, 68 amino acid domain that is predicted to be α-helical in structure. The function of the N-lobe insertions and the C-terminal domain remains unclear, and it is these unique features that explain the lack of similarity between PINK1 and other protein kinases.

A

B

```
PINK1   150 G--FRLEEYLIGQSIGKGCSAAVYEATMPTLPQNLEVTKSTGLLPGRGPGTSAPGEGQERAPGA--PAFPLAIKMMWNISAGSSSEAILNTMSQELVP 243
PKA      39 ---AHLDQFERIKTLGTGSFGRVMLVKH----------------------------------KETGNHYAMKILDKQKVVKLKQIEHTLNEKRILQ  97
CaMKI    12 QAEDIRDIYDFRDVLGTGAFSEVILAED----------------------------------KRTQKLVAIKCI----AKEALEGKEGSMENEIAV  69
CaMKII   10 ---FT-DDYQLFEELGKGAFSVVRRCVK---------- Insertion 1 ----------KTSTQEYAAKII-------NTKKLSARDHQKLER  60
NEK4      3 -----LAAYCYLRVVGKGSYGEVTLVKH----------------------------------RRDGKQYVIKKL-NLRNASSRERRAAEQEAQLLS  58
DMPK     73 EVRLQRDDFEILKVIGRGAFSEVAVVKM----------------------------------KQTGQVYAMKIMNKWDMLKRGEVSCFREERDVLV 134

PINK1   244 ASRVALAGEYGAVTYRKSKRGPKQLAPHPNIIRVLRAFTSSVPLLPGALVDYPDVLPSRLHPEGLGHGRTLFLVMKNYPCT--LRQYLC-VNTPSPR- 337
PKA      98 AVNF----------------------PFLVKLEFSFKD----------------------NSNLYMVMEYVPGGEMFSHLRR-IGRFSEP- 142
CaMKI    70 LHKI----------------------KHPNIVALDDIYES----------------------GGHLYLIMQLVSGGELFDRIVE-KGFYTER- 116
CaMKII   61 EARIC------ Insertion 2 ------RLLKHPNIVRLHDSISE---------- Insertion 3 ----------EGFHYLVFDLVTGGELFEDIVA-REYYSEA- 111
NEK4     59 QLK----------------------HPNIVTYKESWE----------------------GGDGLLYIVMGFCEGGDLYRKLKEQKGQLLPEN 106
DMPK    135 NGDR----------------------RWITQLHFAFQD----------------------ENYLYLVMEYYVGGDLLTLLSK-FGERIPAE 180

PINK1   338 LAAMMLLQLLEGVDHLVQQGIAHRDLKSDNILVELDPDGCPWLVIADFGCCLADESIGLQLPFSSWYVDRGGNGCLMAPEVSTARPGPRAVIDYSKA- 434
PKA     143 HARFYAAQIVLTFEYLHSLDLIYRDLKPENLLI----DQQGYIQVTDFGFAKRVK--G-----RTWTLC--GTPEYLAPEIILSKG-------YNKAV 220
CaMKI   117 DASRLIFQVLDAVKYLHDLGIVHRDLKPENLLYYSL-DEDSKIMISDFGLS-KMEDPGSVLSTAC------GTPGYVAPEVLAQKP-------YSKAV 199
CaMKII  112 DASHCIHQILESVNHIHQHDIVHRDLKPENLLLASKCKGAA-VKLADFGLAIEVQGEQ-----QAWFGFA-GTPGYLSPEVLRKDP-------YGKPV 195
NEK4    107 QVVEWFVQIAMALQYLHEKHILHRDLKTQNVFL----TRTNIIKVGDLGIARVLENHCDMASTLI------GTPYYMSPELFSNKP-------YNYKS 187
DMPK    181 MARFYLAEIVMAIDSVHRLGYVHRDIKPDNILL----DRCGHIRLADFGSCLKLRADGTVRSLVAV-----GTPDYLSPEILQAVGGGPGTGSYGPEC 269

PINK1   435 DAWAVGAIAYEIFGLVNPFYGQGKAHLESRS--YQEA---QLPALPESVPPDVRQLVRALLQREASKRPSA-RVAANVL--HLSLWG          513
PKA     221 DWWALGVLIYEMAAGYPPFFADQPIQIYEKI--VSGK-----VRFPSHFSSDLKDLLRNLLQVDLTKRFGNLKNGVNDIKNHKWF--          298
CaMKI   200 DCWSIGVIAYILLCGYPPFYDENDAKLFEQI--LKAEYEFDSPYW-DDISDSAKDFIRHLMEKDPEKRFTC-EQALQ----HPWIAG          278
CaMKII  196 DIWACGVILYILLVGYPPFWDEDQHKLYQQI--KAGAYDFPSPEW-DTVTPEAKNLINQMLTINPAKRITA-DQALK----HPWVCQ          274
NEK4    188 DVWALGCCVYEMATLKHAFNAKDMNSLVYRI--IEG----KLPPMPRDYSPELAELIRTMLSKRPEERPSV-RSILR----QPYIKR          263
DMPK    270 DWWALGVFAYEMFYGQTPFYADSTAETYGKIVHYKEH--LSLPLVDEGVPEEARDFIQRLLCPPETRLGRG-GAGDFRT--HPFFFG          351
```

Figure 1.7: Domain architecture and multiple sequence alignment of PINK1

(A) Domain structure of PINK1. MTS: mitochondrial targeting sequence; TM: transmemrane helix; Ins1-3; insertions in PINK1 kinase domain; CTD: C-terminal domain. **(B)** Multiple sequence alignment of PINK1 kinase domain against kinase domains of PKA, CaMKIα, CaMKIIγ, NEK4 and DMPK. Yellow: glycine-rich loop; orange: αC helix lysine; red: HRD catalytic motif; purple: DFG motif/N-terminal activation segment anchor; green: APE motif/C-terminal activation segment anchor. PINK1 kinase domain insertions are highlighted in dashed pink boxes and labelled.

As previously discussed (Section 1.2.2), all active protein kinases possess several amino acid motifs required for catalysis and substrate binding, and are therefore a critical indicator of protein kinase function (Hanks & Hunter, 1995). To analyse the kinase domain of PINK1 in more detail, a multiple sequence alignment of the human PINK1 kinase domain against the kinase domains of various other protein kinases was performed. Calcium/calmodulin-dependent protein kinase 1 alpha subunit (CAMKIα, Uniprot ID: Q14012), Calcium/calmodulin-dependent protein kinase 2 gamma subunit (CAMKIIγ, Uniprot ID: Q13555), Never in mitosis A-related kinase 4 (NEK4, Uniprot ID: P51957) and Myotonin-protein kinase (DMPK, Uniprot ID: Q09013) were identified as being the most similar to human PINK1 by BLAST search. In addition, cAMP-dependent protein kinase alpha subunit (PKAα, Uniprot ID: P17612) was included in the alignment since it is an extremely well studied kinase and much information relating its structure to its function is available. Alignment of the selected sequences was performed with MUSCLE (Edgar, 2004a; Edgar, 2004b) and the resulting alignment was analysed and annotated using Jalview (Waterhouse et al, 2009).

Inspection of this alignment reveals that all of the motifs that have been identified as critical for catalysis are conserved in PINK1 (Figure 1.7). Within the N-lobe these are the glycine-rich loop and the residues forming the conserved Arg-Glu salt bridge between β3 and αC. Within the C-lobe, the HRD motif in the catalytic loop and the DFG and APE motifs that form the N- and C-terminal anchors of the activation segment respectively are

also conserved. Further analysis of this alignment confirms the three insertions in the N-lobe of the PINK1 kinase domain are not observed in any of the other kinases analysed. The first of these insertions falls between the β2 and β3 strands, the second between the αC helix and the β4 strand, and the third and final one between the β4 and β5 strands. They are all similar in length, ranging from 23 to 28 amino acids long. Several other protein kinases contain insertions such as these, and they are often involved in regulation of kinase activity. HRI (heme-regulated α-subunit of eukaryotic initiation factor-2α (eIF-2α) kinase) contains an insertion in its N-lobe responsible for binding heme and downregulating its kinase activity (Rafie-Kolpin et al, 2000). A further interesting example of the function of insertions in protein kinases is seen in the CLKs (Cdc-like kinases). These function along with SRPK (SR (serine/arginine-rich) protein kinase) to phosphorylate the SR proteins that are involved in mRNA splicing. An insertion seen in the C-lobe of the CLKs blocks an interaction site in the αG helix that helps to determine substrate specificity in SRPK, thereby conferring a distinct and less rigid substrate specificity on the CLKs (Bullock et al, 2009).

1.4.2 Mitochondrial import and processing of PINK1

PINK1 possesses a mitochondrial targeting sequence (MTS) and a transmembrane helix at its N-terminus and it was quickly confirmed after its discovery that PINK1 does indeed localise to the mitochondria (Valente et al, 2004). Mitochondria are double membrane-bound organelles and possess both an inner and outer mitochondrial membrane, with the space in between the two being referred to as the intermembrane space (IMS) and the compartment contained inside the inner membrane as the matrix. Therefore, there are several possible orientations PINK1 could assume: bound to the inner membrane with the kinase domain facing the matrix; bound to the inner membrane and facing the IMS; bound to the outer membrane and facing the IMS; and finally bound to the outer membrane and

facing the cytoplasm. It is also possible that at different points in its lifespan, PINK1 could adopt one or more of these different orientations. Various reports have suggested PINK1 localises to the inner membrane with the kinase domain facing the IMS (Muqit et al, 2006; Plun-Favreau et al, 2007; Pridgeon et al, 2007; Silvestri et al, 2005) although the most convincing data suggests that it is found on the outer membrane and faces the cytoplasm (Becker et al, 2012; Zhou et al, 2008).

PINK1 is imported into the mitochondria via the TOM40/TIMM23 complexes in a manner dependent on the electrochemical potential across the inner mitochondrial membrane, or mitochondrial membrane potential (Greene et al, 2012). It appears that following import, PINK1 is initially cleaved by MPP (mitochondrial processing peptidase), which normally acts to remove the MTS from imported proteins (Greene et al, 2012), followed by further cleavage by the protease PARL (presenilin-associated rhomboid-like protein (Deas et al, 2011; Jin et al, 2010). The site of this cleavage has been mapped and occurs between Ala103 and Phe104, which are predicted to be near the middle of the transmembrane helix (Deas et al, 2011; Kondapalli et al, 2012). Once PINK1 has been cleaved, it is rapidly degraded by the N-end rule pathway (Yamano & Youle, 2013), whereby it becomes ubiquitylated and then degraded by the 26S proteasome (Lin & Kang, 2008; Muqit et al, 2006).

A critical discovery in the field was the finding that, in contrast to basal conditions, where PINK1 is constitutively imported, cleaved and degraded, under conditions where the mitochondrial membrane potential is lost, PINK1 is imported and then accumulates on the mitochondria (Lin & Kang, 2008). The compound CCCP (carbonyl cyanide m-chlorophenyl hydrazone) acts as an ionophore and abolishes the proton gradient across the mitochondrial inner membrane. Treatment of cells with CCCP leads to mitochondrial

depolarisation and the subsequent stabilisation of PINK1 on the mitochondria (Matsuda et al, 2010; Narendra et al, 2010). This stabilisation is due to PINK1 cleavage by PARL being dependent on the presence of the mitochondrial membrane potential (Jin et al, 2010; Narendra et al, 2010). When mitochondria become depolarized, PARL cleavage is blocked and PINK1 subsequently accumulates on the mitochondrial outer membrane.

1.4.3 PINK1 activity and function

The link between PD and mitochondrial dysfunction was first established when it was discovered that the neurotoxin and mitochondrial Complex I inhibitor MPTP (1-methyl-4-phenyl-1,2,3,6-tetrahydropyridine), found in a contaminated batch of heroin, led to a Parkinsonian syndrome indistinguishable from idiopathic PD in the affected drug users (Langston et al, 1983). Studies on the post-mortem brains of PD patients have also shown a decrease in Complex I activity (Schapira et al, 1989). Mitochondria also play an important role in the regulation of Ca^{2+} homeostasis, with dysregulation of Ca^{2+} levels being implicated in several neurodegenerative disorders, including PD (Mattson, 2007). Since PINK1 is targetted to the mitochondria, it is not surprising that its biological role involves regulation of mitochondrial function.

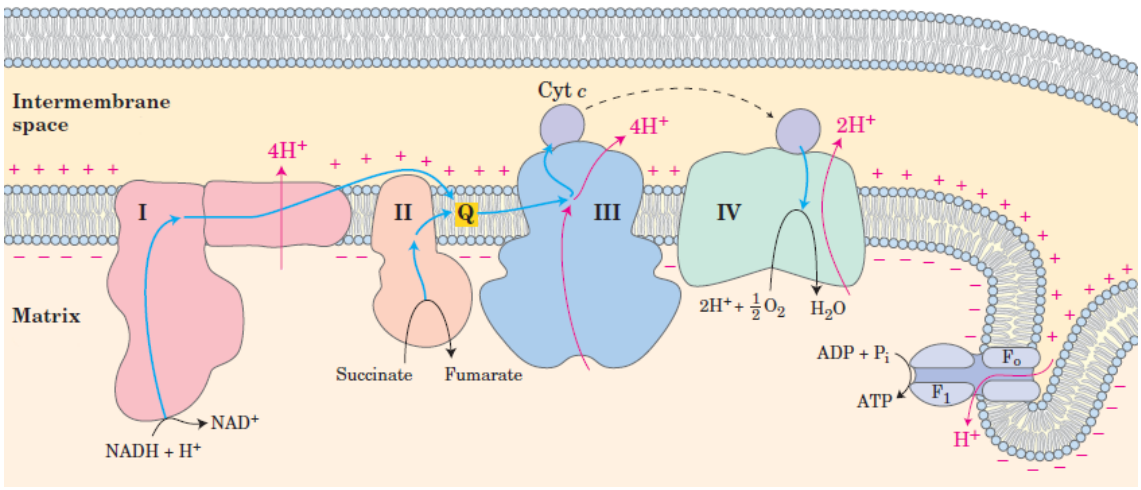

Figure 1.8: Schematic of the mitochondrial electron transport chain

I-IV: Complexes I-IV; Q: ubiquinone; Cyt c: cytochrome c. Blue lines show the flow of electrons, pink lines show the passage of protons. The relative charge (+/-) on either side of the inner membrane is also depicted. Adapted from Lehninger et al, 2008.

It has been shown on a general level that PINK1 appears to be neuroprotective, with overexpression of PINK1 in neuronal cells leading to decreased susceptibility to apoptosis (Petit et al, 2005; Valente et al, 2004). Studies in PINK1 knockout mice and *Drosophila* have shown that loss of PINK1 impairs mitochondrial function, specifically mitochondrial respiration via a reduction in the activity of Complex I and subsequently reduced mitochondrial membrane potential (Gautier et al, 2008; Morais et al, 2009). Further work has shown that loss of PINK1 leads to loss of a phosphorylation site in the Complex I subunit NdufA10 that is required for the ubiquinone reductase activity of Complex I (Morais et al, 2014). This is corroborated by the discovery that in *Drosophila*, administration of Vitamin K_2, which acts as an electron transporter and can substitute for ubiquinone, is able to rescue the phenotype of PINK1 null flies, presumably by bypassing the requirement for ubiquinone in the electron transport chain (Figure 1.8) (Vos et al, 2012). Studies in cell lines and neuronal cells have also shown that PINK1 regulates mitochondrial Ca^{2+}/Na^{+} exchange and as a result, PINK1-deficient neurons have impaired Ca^{2+} handling ability, showing an elevated level of mitochondrial Ca^{2+} and are susceptible to mitochondrial Ca^{2+} overload after a rise in cytosolic Ca^{2+} (Gandhi et al, 2009). An increase in the level of

cellular reactive oxygen species (ROS) was observed in the same study. Similar data regarding the loss of mitochondrial membrane potential, increased ROS levels, defects in the electron transport chain and altered Ca^{2+} handling has been obtained from studies in fibroblasts of PD patients harbouring PINK1 mutations (Abramov et al, 2011). Interestingly, a study showing PINK1 is required for maintaining normal heart function also identified the same mitochondrial defects (Billia et al, 2011).

Although it became apparent when the PINK1 gene was discovered that PINK1 was likely to possess protein kinase activity, it proved difficult to reliably detect and characterise this activity. Several studies describing the kinase activity of PINK1 emerged following its discovery, however they often reported conflicting data. Several studies claimed PD-linked point mutations decreased activity against a variety of substrates (Beilina et al, 2005; Pridgeon et al, 2007; Sim et al, 2006), however another study claimed they had no effect on activity (Silvestri et al, 2005). The same studies also claimed that C-terminal truncation of PINK1 either increased (Silvestri et al, 2005), decreased (Sim et al, 2006) or had no effect on kinase activity (Pridgeon et al, 2007). It was not possible to reproduce any of these findings in our own laboratory and furthermore, in our hands mammalian PINK1 did not exhibit detectable kinase activity. The lack of a suitable *in vitro* assay for PINK1 activity was a major obstacle in the field and severely hampered further understanding of the biochemical properties and function of PINK1.

1.5 PINK1 and Parkin

1.5.1 Parkin

The Parkin gene was first identified in 1998 after the mapping of partial deletions of the gene in patients with autosomal recessive early-onset PD (Kitada et al, 1998). Mutations in Parkin are the primary cause of autosomal recessive early onset PD where the age of onset is under 40, with Parkin mutations being responsible for around 50% of these cases (Lucking et al, 2000). The Parkin protein is 465 amino acids long with a molecular weight of 51 kDa and belongs to the ubiquitin E3 ligase family, which catalyse the final step in the ubiquitylation of substrate proteins.

Ubiquitin is a small, 76 amino acid protein of 8.5 kDa and its attachment to target proteins is a reversible and highly complex form of post-translational modification. The ubiquitylation cycle is depicted below (Figure 1.9) and proceeds as follows: firstly, an E1 ubiquitin-activating enzyme activates the ubiquitin molecule in an ATP-dependent step, followed by transfer to the catalytic cysteine of an E2 ubiquitin conjugating-enzyme. This step is referred to as "charging" of the E2 (Komander, 2009). Next, an E3 ligase mediates the transfer of ubiquitin from the E2 onto the substrate protein. The majority of E3 ligases belong one of two classes. The RING family, which act as adaptors, simply bring the E2 and substrate into close proximity so ubiquitin transfer can occur. HECT E3 ligases on the other hand have a catalytic cysteine and accept ubiquitin from the E2, forming a thioester intermediate before conjugating it to the substrate (Metzger et al, 2012). Ubiquitylation of a protein is reversed by the action of deubiquitylating enzymes, or DUBs (Reyes-Turcu et al, 2009).

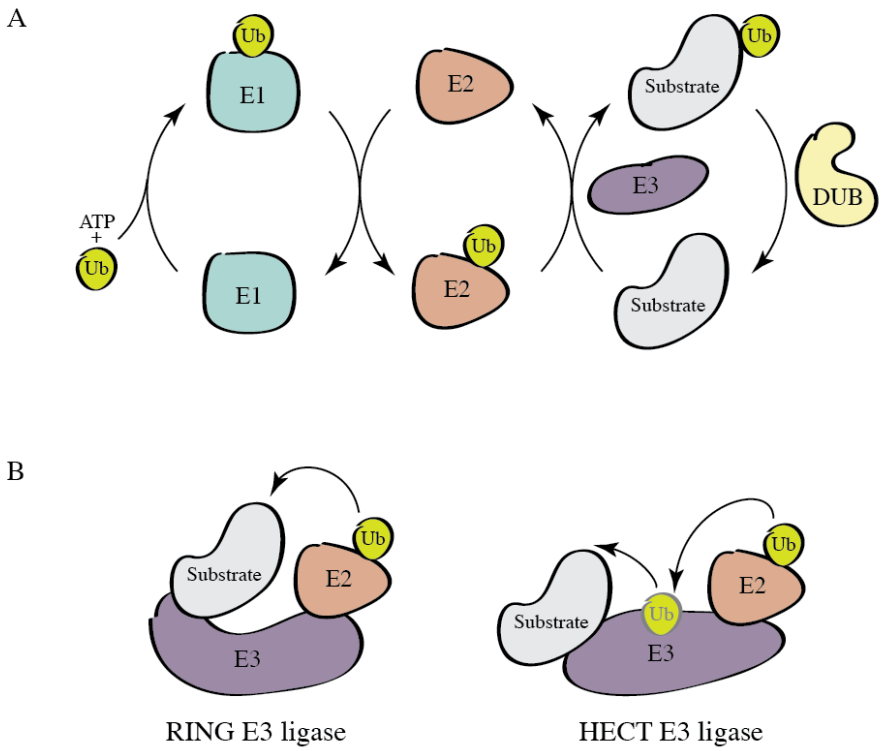

Figure 1.9: The ubiquitylation cycle and mechanisms of ubiquitin E3 ligases

(A) Ubiquitin is activated by an E1 enzyme in an ATP-dependent manner and is then passed on to an E2 enzyme. From here an E3 ligase mediates the transfer of the ubiquitin molecule to the substrate. Ubiquitin is removed from proteins by the action of DUBs (deubiquitylating enzymes). **(B)** *(L)* Mechanism of RING E3 ligases. These act as scaffolds, bringing the charged E2 and substrate into close proximity. Ubiquitin is then directly transferred from the E2 to the substrate. *(R)* Mechanism of HECT E3 ligases. These have a catalytic cysteine and accept ubiquitin from the E2 before transferring it on to the substrate.

Ubiquitin is attached via its C-terminal glycine to lysine residues within the target protein. In addition to monoubiquitylation and multi-monoubiquitylation of substrates, polyubiquitin chains can be formed. Ubiquitin itself contains seven lysine residues and an N-terminal methionine to which additional ubiquitin molecules can be attached (Figure 1.10). Depending on which lysine the ubiquitin is conjugated to, different chain topologies can be formed. Homotypic chains are the best studied and contain only one type of linkage (Lys6, Lys11, Lys27, Lys29, Lys33, Lys48, Lys63-linked or linear (Met1) chains), whereas mixed, branched or forked ubiquitin chains are much less well understood (Komander, 2009; Komander & Rape, 2012). It is apparent that with so many linkage combinations

available, a great number of different chain types could be generated and as such, ubiquitylation is an ideal system for specifying many diverse cellular signals. Ubiquitylation has been shown to play a role in many important cellular processes, but perhaps the most well-characterised example is the tagging of proteins for degradation by the proteasome using Lys48-linked ubiquitin chains (Finley, 2009). As with protein phosphorylation, defects in the ubiquitin system have been implicated in many human diseases (Popovic et al, 2014).

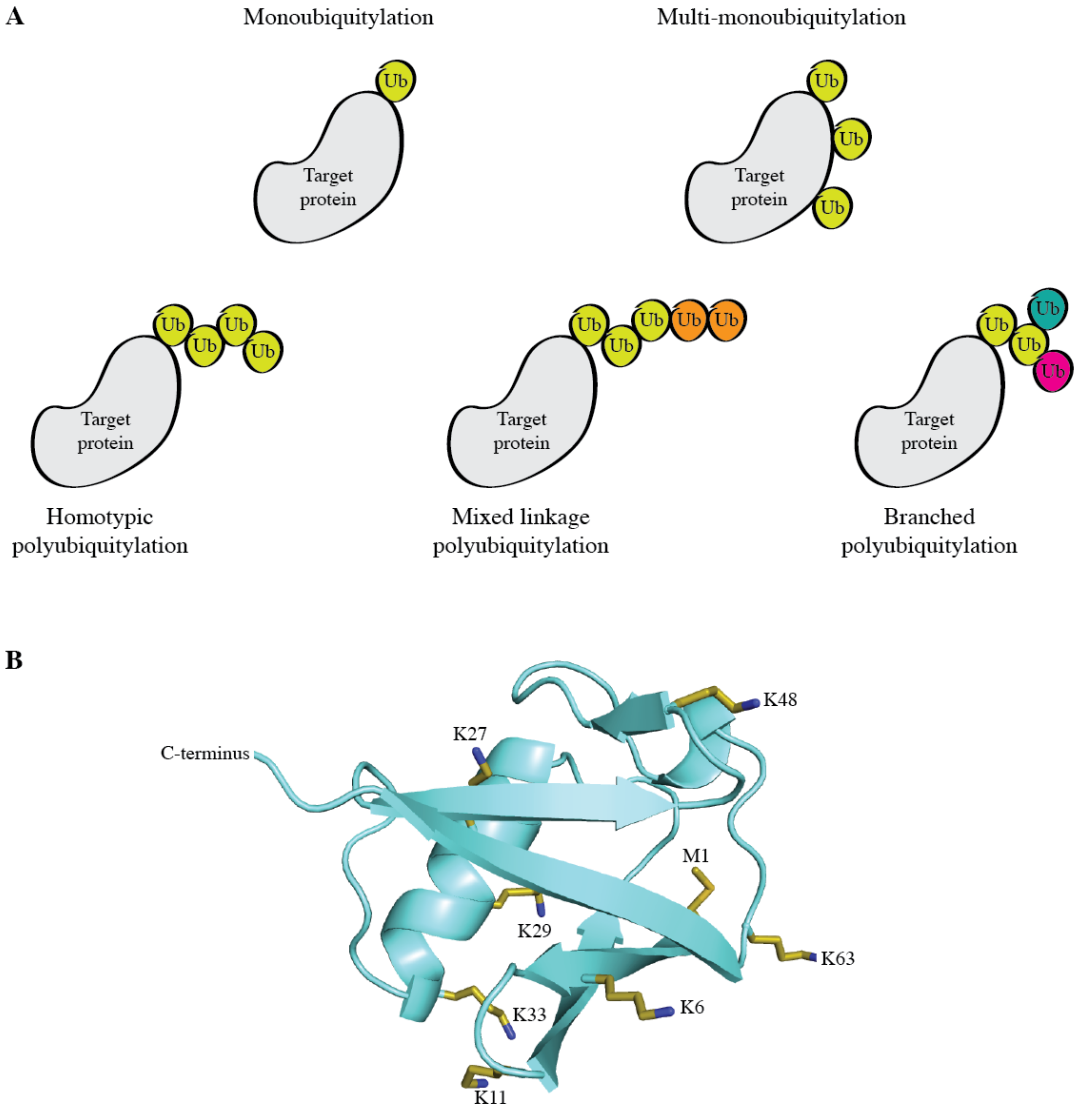

Figure 1.10: Different forms of ubiquitylation

(A) Ubiquitin can be attached to proteins in several different ways. Monoubiquitylation is the attachment of a single ubiquitin that is not extended into a chain. Multi-mono ubiquitylation is the attachment of several ubiquitin molecules that are not extended. Homotypic polyubiquitylation is the attachment of a chain with a single linkage type. Mixed chains and branched chains contain more than one linkage type. **(B)** Structure of ubiquitin showing lysine residues and N-terminal methionine that can act as linkage points for the formation of different polyubiquitin chains. PDB ID: 1UBQ.

Parkin is a multidomain protein containing an N-terminal Ubl (ubiquitin-like) domain, a RING0 domain followed by two RING (really interesting new gene) domains (RING1 and RING2) separated by an IBR domain (Figure 1.11). It is a member of the RBR (RING-In Between-RING) family of E3 ligases that act as RING-HECT hybrids (Wenzel et al, 2011).

This means that although Parkin contains RING domains, its mode of action is similar to that of a HECT E3 ligase. A key discovery in the understanding of Parkin's biological function was the finding that Parkin exists in an autoinhibited conformation, similar to other RBR family members. This autoinhibition can be disrupted by the addition of an N-terminal affinity tag. On the basis of this, it was proposed that the N-terminal Ubl domain was responsible for Parkin autoinhibition (Burchell et al, 2012; Chaugule et al, 2011).

Further weight was added to this hypothesis when various crystal structures of Parkin, including a low-resolution structure of the full-length protein, were determined (Riley et al, 2013; Spratt et al, 2013; Trempe et al, 2013; Wauer & Komander, 2013). In addition to an expected interaction with the Ubl domain, several other autoinhibitory interactions were revealed. The catalytic cysteine (Cys431), found in RING2, was occluded by an interaction with the RING0 domain and an interaction between the RING1 domain, the Ubl domain and a novel structural element designated the REP (regulatory element of Parkin) helix blocked what is predicted to be the E2 binding site.

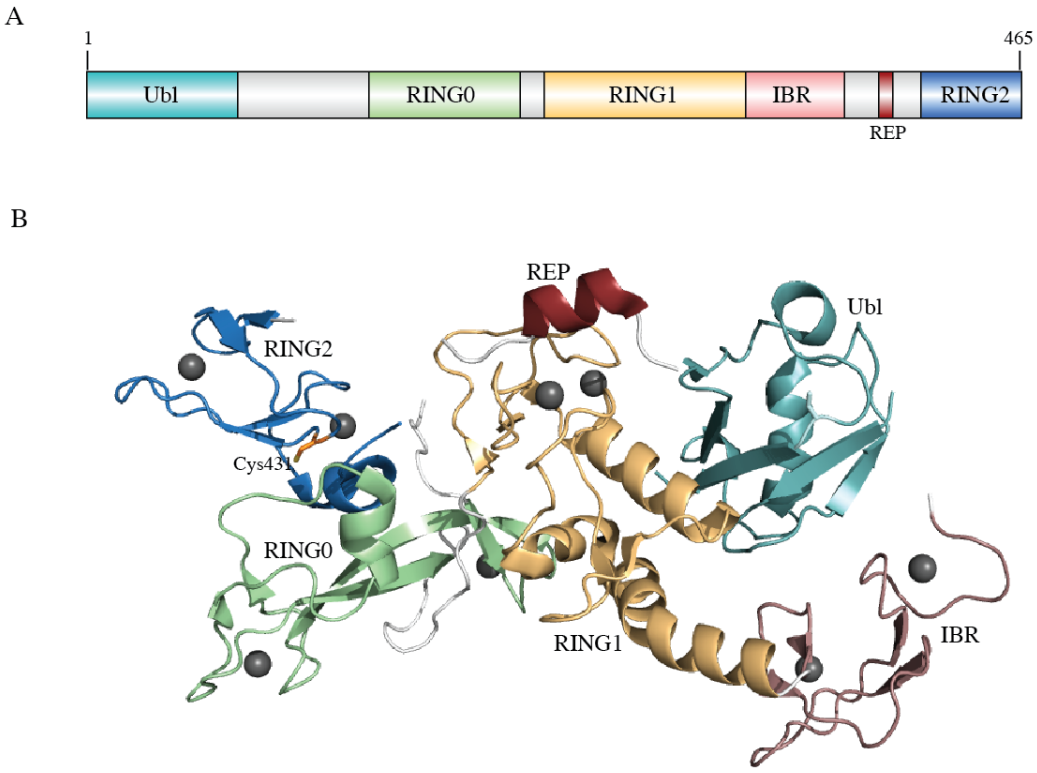

Figure 1.11: Domain architecture and crystal structure of autoinhibited Parkin

(A) Domain architecture of Parkin. Ubl: Ubiquitin-like domain; RING0: RING0 domain; RING1: Really Interesting New Gene domain 1; IBR: In-Between RING domain; REP: Regulatory Element of Parkin helix; RING2: Really Interesting New Gene domain 2. **(B)** Crystal structure of full-length Parkin. Colouring is the same as in (A). PDB ID: 4K95.

1.5.2 The link between PINK1 and Parkin

Several lines of evidence have suggested that PINK1 and Parkin may have a functional link. Patients with mutations in either PINK1 or Parkin tend to display a similar phenotype (Puschmann, 2013). Further substantiation for this idea came from genetic studies in *Drosophila*. The *Drosophila* PINK1 null mutant shows male sterility, a shortened lifespan and reduced ATP levels, poor climbing and flying ability, various muscle phenotypes including an altered wing posture, a crushed or indented thorax and degeneration of the indirect flight muscles and finally swollen and impaired mitochondria (Clark et al, 2006; Park et al, 2006). These phenotypes are very similar to that of the Parkin null fly (Greene et al, 2003). It was demonstrated that PINK1 acts upstream of Parkin genetically since Parkin overexpression is able to rescue the PINK1 null phenotype, but not vice versa. In addition,

double knockout of the PINK1 and Parkin genes has a non-additive effect, due to epistatic interaction. This suggests the two genes act in the same genetic pathway, as opposed to acting in parallel pathways (Clark et al, 2006; Park et al, 2006).

It was later shown that in addition to mitochondrial depolarisation leading to accumulation of PINK1, it also led to the recruitment of the normally cytosolic Parkin to the mitochondria. This recruitment of Parkin is dependent on the presence of PINK1 in the cell and overexpression of a non-cleavable form of PINK1 leads to recruitment of Parkin to the mitochondria in the absence of membrane depolarisation, suggesting PINK1 is both necessary and sufficient to recruit Parkin (Narendra et al, 2010). In addition, the kinase activity of PINK1 is required for this recruitment, with both PD-linked and artificial mutations in PINK1 blocking the translocation of Parkin to the mitochondria, but not affecting accumulation of PINK1 on the mitochondria (Matsuda et al, 2010).

The mechanism by which PINK1 recruits Parkin from the cytosol to the mitochondria is not yet clear, although it has been suggested that PINK1 autophosphorylation might play a role. PINK1 has been shown to autophosphorylate at Thr257 (Kondapalli et al, 2012) and further sites have been identified at Ser228 and Ser402 (Okatsu et al, 2012), although these sites were not identified conclusively. Alanine mutations of these two sites prevented recruitment of Parkin to the mitochondria after membrane depolarisation, however this finding has yet to be reproduced by independent laboratories.

1.5.3 Regulation of Parkin by PINK1

It has now been shown that PINK1 directly phosphorylates Parkin, confirming that PINK1 plays a key role in Parkin regulation. The PINK1 phosphorylation site in Parkin was mapped to residue Ser65, which is found in the N-terminal Ubl domain (Kondapalli et

al, 2012). As mentioned previously, this domain was believed to be responsible for Parkin autoinhibition and so an obvious hypothesis was that PINK1 phosphorylation would relieve this inhibition. This suggestion turned out to be correct; phosphorylation of PINK1 leads to a marked increase the activity of the normally inactive Parkin (Kazlauskaite et al, 2014a; Kondapalli et al, 2012). The mechanism by which Ser65 phosphorylation activates Parkin was not clear however, since examination of the full-length low-resolution structure of Parkin shows that Ser65 most likely not located at the interface between the RING1 domain and the Ubl domain (Trempe et al, 2013). Parkin phosphorylation is also detectable in cells and occurs only 5 minutes after mitochondrial depolarisation takes place. This is in contrast to PINK1 autophosphorylation on Thr257, which only occurs around 40 minutes after the membrane potential is lost (Kondapalli et al, 2012). However, it appears that mutation of this phosphorylation site to alanine only partially prevents the translocation of Parkin to the mitochondria (Okatsu et al, 2012), suggesting that other factors may be regulating this process.

It was later discovered that in addition to phosphorylating the Ubl domain of Parkin, PINK1 is also able to phosphorylate ubiquitin, also at Ser65, which is conserved between the Ubl domain and ubiquitin (Kane et al, 2014; Kazlauskaite et al, 2014b; Koyano et al, 2014). This phosphorylation also occurs in cells in a manner dependent on depolarisation of the mitochondrial membrane potential (Kazlauskaite et al, 2014b). It appears that both Ubl domain and ubiquitin phosphorylation are required for Parkin activity, since each of them can activate Parkin to some degree but not to the same extent as both of them in combination. Likewise, only mutation of both proteins to alanine at Ser65 is able to completely abolish Parkin activation by PINK1 (Kazlauskaite et al, 2014b). However, the molecular mechanisms by which Parkin and ubiquitin phosphorylation activate the E3 ligase activity of Parkin still remain unclear.

1.5.4 Function of the PINK1/Parkin pathway

An accumulating body of evidence suggests that the PINK1/Parkin pathway plays a central role in mitochondrial quality control, specifically in the regulation of a process known as mitophagy. This is the selective destruction of damaged mitochondria by the process of autophagy. Before anything was known about PINK1 directly regulating Parkin, it was discovered that Parkin is selectively recruited to impaired mitochondria that have lost their membrane potential. Subsequently, these damaged mitochondria would be cleared from the cell by mitophagy (Narendra et al, 2008). Once it became clear that the trigger for Parkin recruitment was the accumulation of PINK1 on these damaged mitochondria, it was suggested that PINK1 acts as a sensor for mitochondrial impairment. The constitutive degradation of PINK1 ensures this signal is only present when the mitochondrial membrane potential is compromised; only under these circumstances can it accumulate and mark the mitochondria for Parkin-mediated destruction (Matsuda et al, 2010; Narendra et al, 2010; Ziviani et al, 2010).

Once Parkin has been recruited to impaired mitochondria, a ubiquitylation signal can be observed (Matsuda et al, 2010). Different studies have shown conflicting results regarding the types of chains generated by mitochondrially-localised Parkin. One study reported Lys63 and Lys27-linked polyubiquitin chains (Geisler et al, 2010), whereas another reported Lys48, Lys63, Lys6 and Lys11-linked chains (Ordureau et al, 2014). In *Drosophila*, Parkin has been shown to ubiquitylate the protein Mitofusin, which promotes mitochondrial fusion (Poole et al, 2010; Ziviani et al, 2010). This Parkin substrate has also been detected in human cell lines, along with the ubiquitylation of Miro1, a mitochondrial GTPase implicated in mitochondrial trafficking (Sarraf et al, 2013). Miro1 is also a well-characterised *in vitro* Parkin substrate (Kazlauskaite et al, 2014a). Many other candidate substrates have been proposed for Parkin, however the majority of these have not been

well characterised (Walden & Martinez-Torres, 2012). Furthermore, the mechanism by which the autophagy machinery is recruited to damaged mitochondria by the PINK1/Parkin pathway and the mechanism of mitochondrial clearance still remain unresolved.

In addition to the role played in the removal of damaged mitochondria, it has also been suggested that the PINK1/Parkin pathway plays a role in the process of mitochondrial remodelling. Mitochondria are dynamic organelles that are transported within the cell and undergo fusion and fission events to increase or decrease the size of the mitochondria and to alter the structure of the mitochondrial network. Imbalances in mitochondrial dynamics have been linked to neurodegenerative diseases and the process appears to be essential for the health of the individual mitochondria themselves (Chan, 2006). Studies in *Drosophila* have shown that three proteins involved in mitochondrial remodelling, Drp1, OPA1 and Mfn2, interact genetically with PINK1 and Parkin. Specifically, an increase in Drp1 levels (GTPase, fission promoting) or a decrease in the levels of either OPA1 (dynamin-related GTPase, controls inner membrane fusion) or Mfn2 (transmembrane GTPase, controls outer membrane fusion) led to rescue of the PINK1 and Parkin null fly phenotypes (Park et al, 2009; Poole et al, 2008). However, in human cell lines the situation is reversed, with a decrease in Drp1 or an increase in OPA1 or Mfn2 rescuing PINK1 and Parkin loss of function. In the same study, knockdown of Parkin was also shown to lead to an increase in mitochondrial fission (Lutz et al, 2009). The precise roles played by PINK1 and Parkin in regulating mitochondrial morphology therefore remains unclear, and more work is necessary to dissect this pathway.

1.6 Project aims

Although PINK1 was first discovered almost 15 years ago (Unoki & Nakamura, 2001) and was linked to Parkinson's disease 10 years ago (Valente et al, 2004), at the start of this project (October 2010), little was known about the kinase PINK1 aside from the fact that its mutation leads to the development of early-onset PD. No well-validated substrates of PINK1 had been identified and there was a lack of a robust kinase assay for assessing its *in vitro* activity. The effects of PD-linked mutations on kinase activity and at a structural level were therefore unknown. In addition, it was known that PINK1 has several unusual features that make it distinct from other protein kinases, including three insertions in the N-lobe of the kinase domain and a small C-terminal domain, but the function of these features was not understood. Several years later it was discovered that PINK1 phosphorylates another PD-linked protein, the ubiquitin E3 ligase Parkin. This phosphorylation, in combination with the phosphorylation of ubiquitin by PINK1, leads to an activation of Parkin E3 ligase activity. The mechanism by which this activation occurs, however, is still to be determined.

The primary aim of this thesis was to utilise a more tractable PINK1 homologue from the insect species *Tribolium castaneum* (TcPINK1) and employ a joint structural and biochemical approach in order to gain insight into some of the following questions regarding PINK1 that were unsolved at the time:

- What is the substrate specificity of PINK1 and what factors dictate this?
- What is the function and requirement for the C-terminal domain and kinase domain insertions?
- What are the biochemical and structural effects of Parkinson's disease-linked PINK1 mutations?

- What are the molecular mechanisms by which the dual PINK1 phosphorylation of the Parkin Ubl domain and ubiquitin lead to activation of Parkin?

Chapter 2

2 Materials and methods

2.1 Reagents

2.1.1 Bacterial strains

The following bacterial strains were used in this thesis: BL21 (DE3) RIL CodonPlus from Stratagene (La Jolla, CA) for recombinant protein expression and EcAR7, kindly provided by Dr. Natasha Pirman and Dr. Jesse Rinehart (Yale University) for production of phosphorylated proteins.

2.1.2 Cloning and DNA constructs

All mutagenesis was carried out using the QuikChange site-directed-mutagenesis method (Stratagene, Santa Clara, CA) with KOD polymerase (Novagen, Merck, Whitehouse Station, NJ). All DNA constructs were verified by DNA sequencing, which was performed by The Sequencing Service (School of Life Sciences, University of Dundee) using DYEnamic ET terminator chemistry (Amersham Biosciences, GE Healthcare, Little Chalfont, UK) on Applied Biosystems automated DNA sequencers (Foster City, CA). cDNA for *Tribolium castaneum* PINK1 and *Pediculus humanus corporis* PINK1 were synthesized by GenScript USA (Piscataway, NJ).

Bacterial expression vectors used in this thesis were: pMal4c with a PreScission cleavage site after the MBP affinity tag; pGEX-6P-1, with a PreScission protease site following the GST tag; and pET6His-SUMO with a SENP1 cleavage site following the 6-His-SUMO affinity tag. Table 2.1 lists all DNA constructs used in this thesis. All constructs were generated by Dr. Mark Peggie and Dr. Maria Deak, with the exception of GST-Parkin 1-76, generated by Dr. Thomas Macartney, and His-SUMO-Parkin 1-465, generated by Dr. Rachel Toth.

Construct	Tag	Vector	DU No.
TcPINK1 1-570	MBP	pMal4c	34701
TcPINK1 1-570 D359A	MBP	pMal4c	34832
PhcPINK1 1-575	MBP	pMal4c	34699
PhcPINK1 1-575 D357A	MBP	pMal4c	34825
DmPINK1 1-721	MBP	pMal4c	37735
DmPINK1 1-721 D501A	MBP	pMal4c	37791
TcPINK1 128-570	MBP	pMal4c	34759
TcPINK1 128-570 D359A	MBP	pMal4c	34817
TcPINK1 155-570	MBP	pMal4c	34718
TcPINK1 155-570 D359A	MBP	pMal4c	34816
TcPINK1 155-486	MBP	pMal4c	34709
TcPINK1 155-486 D359A	MBP	pMal4c	34934
TcPINK1 1-570 S205A	MBP	pMal4c	38190
TcPINK1 1-570 S207A	MBP	pMal4c	38191
TcPINK1 1-570 S205 S207/AA	MBP	pMal4c	38192
TcPINK1 1-570 Y375F	MBP	pMal4c	38193
TcPINK1 1-570 T376A	MBP	pMal4c	38194
TcPINK1 1-570 Y378F	MBP	pMal4c	38195
TcPINK1 1-570 S402A	MBP	pMal4c	38196
TcPINK1 1-570 Y406F	MBP	pMal4c	38197
TcPINK1 1-570 S407A	MBP	pMal4c	38198
TcPINK1 1-570 Y439F	MBP	pMal4c	38199
TcPINK1 1-570 C130G (C125G)	MBP	pMal4c	34999
TcPINK1 1-570 A194D (A217D)	MBP	pMal4c	38002
TcPINK1 1-570 E217K (E240K)	MBP	pMal4c	38003
TcPINK1 1-570 G285D (G309D)	MBP	pMal4c	38006
TcPINK1 1-570 L322P (L347P)	MBP	pMal4c	38009
TcPINK1 1-570 L341P (L369P)	MBP	pMal4c	38010
TcPINK1 1-570 G361A (G386A)	MBP	pMal4c	38011
TcPINK1 1-570 C363R (C388R)	MBP	pMal4c	38012
TcPINK1 1-570 G384V (G409V)	MBP	pMal4c	38013
TcPINK1 1-570 P391R (P416R)	MBP	pMal4c	38014
TcPINK1 1-570 E392G (E417G)	MBP	pMal4c	38015
TcPINK1 1-570 G415E (G440E)	MBP	pMal4c	38017
TcPINK1 1-570 L462P (L489P)	MBP	pMal4c	38201

Construct	Tag	Vector	DU No.
TcPINK1 1-412 (W437X)	MBP	pMal4c	37722
TcPINK1 1-431 (Q456X)	MBP	pMal4c	37705
TcPINK1 1-465 (R492X)	MBP	pMal4c	37723
hPINK1 123-581	MBP	pMal4c	34758
hPINK1 123-581 D384A	MBP	pMal4c	34945
hPINK1 123-581 Δ184-212	MBP	pMal4c	34894
hPINK1 123-581 Δ184-212 D384A	MBP	pMal4c	34948
TcPINK1 128-570 D359A	His-SUMO	pET6His-SUMO	38895
TcPINK1 138-570 D359A	His-SUMO	pET6His-SUMO	38896
TcPINK1 147-570 D359A	His-SUMO	pET6His-SUMO	43665
TcPINK1 148-570 D359A	His-SUMO	pET6His-SUMO	38897
TcPINK1 149-570 D359A	His-SUMO	pET6His-SUMO	43666
TcPINK1 150-570 D359A	His-SUMO	pET6His-SUMO	43126
TcPINK1 151-570 D359A	His-SUMO	pET6His-SUMO	43667
TcPINK1 152-570 D359A	His-SUMO	pET6His-SUMO	43669
TcPINK1 153-570 D359A	His-SUMO	pET6His-SUMO	43133
TcPINK1 155-570 D359A	His-SUMO	pET6His-SUMO	38898
TcPINK1 155-570	His-SUMO	pET6His-SUMO	43060
TcPINK1 156-570 D359A	His-SUMO	pET6His-SUMO	43134
TcPINK1 157-570 D359A	His-SUMO	pET6His-SUMO	43137
TcPINK1 160-570 D359A	His-SUMO	pET6His-SUMO	43114
TcPINK1 165-570 D359A	His-SUMO	pET6His-SUMO	38899
Parkin 1-76	GST	pGEX-6P-1	37369
Parkin 1-76 S65 TAG	GST	pGEX-6P-1	43028
Parkin 1-465	His-SUMO	pET6His-SUMO	40847
Parkin 80-465	His-SUMO	pET6His-SUMO	39813
Parkin 1-76	His-SUMO	pET6His-SUMO	39607

Table 2.1: DNA constructs used in this thesis.

2.1.3 Protein expression and purification

Isopropyl-β-D-1-thiogalactoside (IPTG, dioxane free), ampicillin sodium (Amp), kanamycin monosulphate (Kan), 4-(2-hydroxyethyl)-1-piperazineethanesulfonic acid

(HEPES) and dithiothreitol (DTT) were from ForMedium (Norfolk, UK). Tris base, glycerol, D-(+)-sucrose and sodium chloride were from VWR (Radnor, PA). D-(+)-maltose monohydrate, β-mercaptoethanol, ethylene diamine tetraacetic acid (EDTA), ethylene glycol tetraacetic acid (EGTA), *O*-phospho-L-serine (SEP), D-(+)-glucose, imidazole, Triton™ X-100, phenylmethanesulphonyl fluoride (PMSF), benzamidine, and lysozyme from chicken egg white were from Sigma-Aldrich (Poole, UK). Brij® 35 was from Merck Millipore (Billerica, MA). Amylose resin was from New England Biolabs (Ipwitch, MA). Nickel resin and GST resin were provided by the DSTT (University of Dundee). cOmplete protease inhibitor cocktail tablets were from Roche (Lewes, UK). VivaSpin centrifuge concentrators of all sizes were from Sartorius Stedim (Gottingen, Germany), Slide-A-Lyzer dialysis cassettes and SnakeSkin dialysis tubing of all sizes and Tris (2-carboxyethyl)phosphine hydrochloride (TCEP) were from Thermo Scientific (Essex, UK). EconoPac disposable columns were from BioRad (Herts, UK). GST- and MBP-PreScission protease and His-SENP1 were produced by the DSTT (University of Dundee).

2.1.4 Protein analysis

40% (w/v) 29:1 Acrylamide: Bis-Acrylamide solution was from Flowgen Bioscience (Nottingham, UK). Ammonium persulphate (APS), *N*,*N*,*N*′,*N*′-Tetramethylethane-1,2-diamine (TEMED), sodium dodecyl sulphate (SDS), bovine serum albumin (BSA) and Immobilon PVDF membrane (pore size 0.45μm) were from Sigma-Aldrich (Poole, UK). Precision Plus Protein unstained standards were from BioRad (Herts, UK). Coomassie (Bradford) protein assay kits were from Thermo Scientific (Essex, UK). InstantBlue Coomassie stain was from Expedeon (San Diego, CA). 3MM paper was from Whatman (Maidstone, UK). Photographic developer (LX24) and liquid fixer (FX40) were from Kodak (Liverpool, UK). X-ray films were from Konica Corporation (Japan). Enhanced chemiluminescence (ECL) kit was from GE Healthcare (Piscataway, NJ).

2.1.5 Antibodies

Sheep polyclonal antibodies (Table 2.2) were produced in-house by the Division of Signal Transduction Therapy (DSTT, University of Dundee). Antisera were raised in sheep by Diagnostics Scotland (Lanarkshire, UK). All in-house antibodies were affinity purified on CH-Sepharose covalently coupled to the corresponding antigen. The commercial anti-phosphotyrosine 4G10 antibody was from Merck Millipore (Billerica, MA).

Antibody	Antigen	Sheep No.
Human Parkin	GST-Parkin 1-108	S229D
Parkin phospho serine 65	RDLDQQS*IVHIVQR (residues 60-72 of human Parkin)	S210D

Table 2.2: Antibodies used in this thesis

2.1.6 Lysine methylation

Borane dimethylamine complex (ABC) and 37% formaldehyde solution were from Sigma-Aldrich (Poole, UK).

2.1.7 Protein crystallisation

The Crystal Screen 1 and 2, Natrix, MembFac, Index 1 and 2, PEG/Ion, Salt Rx and Additive screens were from Hampton Research (Aliso Viejo, CA). The ProPlex 1 and 2, JCSG, PACT Premier, Morpheus, MemStart, MemSys and MemPlus screens were from Molecular Dimensions (Suffolk, UK). The Protein Complex screen, adenosine 5'-triphosphate disodium salt hydrate (ATP), adenosine 5'-diphosphate (ADP), adenosine 5′-(β, γ-imido) triphosphate lithium salt hydrate (AMP-PNP), magnesium chloride and 2-methyl-2,4-pentanediol/hexylene glycol (MPD) were from Sigma-Aldrich (Poole, UK).

2.1.8 Kinase assays

[γ-^{32}P] ATP was from PerkinElmer (Waltham, MA) P81 paper was from Whatman (Maidstone, UK), bovine myelin basic protein and casein were from Sigma (St. Louis, MO). Bovine histone H1 was from Abcam (Cambridge, UK). PINKtide and its derivatives were synthesized by GL Biochem (Shanghai, China). Other substrate peptides were provided by the DSTT (University of Dundee).

2.2 Equipment

Bacterial incubators were from Infors (Reigate, UK). All centrifuges, rotors and centrifuge tubes were from Beckmann Coulter (Brea, CA). The digital sonicator was from Branson (Danbury, CT). AKTA protein purification systems, Superdex 200 26/60, Mono Q 5/50 GL and 5 ml Hi-Trap columns were from GE Healthcare (Piscataway, NJ). The pH meters and electrodes were from Horiba (Kyoto, Japan). Power packs for electrophoresis, Trans-Blot cells, Model 583 vacuum gel drier and GelAir Dryer were from BioRad (Herts, UK). Mini gel tank electrophoresis systems were from Atto (Tokyo, Japan). The LiCOR Odyssey infrared imaging system was from LiCOR biosciences (Cambridge, UK). X-omat autoradiography cassettes with intensifying screens were from Kodak (Liverpool, UK). The Konica automatic film processor was from Konica Corporation (Tokyo, Japan). The scintillation counter (Tri-Carb 2800 TR) was from Perkin- Elmer (Waltham, MA). The 96-well Versamax plate reader was from Molecular Devices (Wokingham, UK). The NanoDrop was from Thermo Scientific (Essex, UK). The BioPhotometer spectrophotometer and Thermomixer IP shakers were from Eppendorf (Hamburg, Germany). The Mosquito crystallography robot and consumables were from TTP Lab Tech (Herts, UK). MRC 96 well crystallisation plates were from Molecular Dimensions (Suffolk, UK). The in-house X-ray generator was from Rigaku (Tokyo, Japan). The LC-MS machine was from the Agilent 1200 Infinity series (Santa Clara, CA).

2.3 General buffers & solutions

2.3.1 Bacterial growth media

Luria Bertani (LB) media and plates and Terrific broth (TB) and SOC media were kindly supplied by the Media Kitchen (University of Dundee).

LB media: 10.0 g bacto-tryptone, 5.0 g bacto-yeast extract, 10.0 g NaCl, 950 ml ddH_2O and was adjusted to pH 7.0 with NaOH. The media was adjusted to 1 L using ddH_2O after autoclaving for 20 minutes at 2 bar.

TB media: 12.0 g bacto-tryptone, 24.0 g bacto-yeast extract, 4.0 ml glycerol and 900 ml ddH_20. One hundred ml of a sterile 0.17M KH2PO4 and 0.72M K2HPO4 solution was added after autoclaving for 20 minutes at 2 bar.

SOC media: contained 2.0 g bacto-tryptone, 0.5 g bacto-yeast extract, 0.2 ml of 5 M NaCl, 0.25 ml of 1 M KCl, 1.0 ml of 1 M $MgCl_2$, 1.0 ml of 1 M $MgSO_4$, 2.0 ml of 1 M glucose, 90 ml ddH_20. The media was adjusted to 100 ml using ddH_2O after autoclaving for 20 minutes at 2 bar.

The following extra components were added as necessary: the antibiotics ampicillin (Amp) to a final concentration of 50 μg/ml from a 100 mg/ml stock and kanamycin (Kan) to 25μg/ml from a 50 mg/ml stock, glucose (Glu) to 0.08% (w/v) from a 20% (w/v) stock, and *O*-phospho-L-serine (SEP) to 2 mM from an 125 mM, pH 6.8 stock.

2.3.2 Buffers for preparation of competent EcAR7 cells

Prepared buffers were sterile filtered and stored and used at 4°C.

TFB1 buffer: 100 mM RbCl, 50 mM $MnCl_2$, 30 mM potassium acetate, 10 mM $CaCl_2$, 15% (v/v) glycerol, adjusted to pH 5.8 with dilute acetic acid

TFB2 buffer: 10 mM MOPS, 10 mM RbCl, 75 mM $CaCl_2$, 15% (v/v) glycerol, adjusted to pH 6.8

2.3.3 SDS-PAGE stock solutions

The following stock solutions were used for preparation of SDS-polyacrylamide gels: 1.5 M Tris-HCl (pH 8.6), 2 M Tris-HCl (pH 6.8), 10% (w/v) SDS, a 40% acrylamide solution containing bis-acrylamide at 29:1, TEMED solution and a 10% (w/v) APS solution stored at -20°C.

Tris-Glycine running buffer: 25 mM Tris-HCl (pH 8.3), 192 mM glycine, 0.1% (w/v) SDS.

5X sample buffer: 250 mM Tris-HCl (pH 6.8), 5% SDS, 5% (v/v) β-mercaptoethanol, 32.5% (v/v) glycerol, 0.05% bromophenol blue.

2.3.4 Buffers for Western blotting

Tris-Glycine transfer buffer: 48 mM Tris-HCl (pH 8.3), 39 mM glycine, 20% (v/v) methanol.

TBST buffer: 50 mM Tris-HCl (pH 7.5), 0.15 M NaCl and 0.1% (v/v) Tween-20.

2.4 Gel pouring

SDS-PAGE was used to separate proteins for analysis according to their molecular weight. Gels were prepared with varying concentrations of acrylamide as necessary. Recipes for one gel at various concentrations are provided below (Table 2.3).

Stock solution	Acrylamide concentration						Stacking gel
	6%	8%	10%	12%	15%	18%	
40% acrylamide	1.1 ml	1.4 ml	1.8 ml	2.1 ml	2.6 ml	3.15 ml	284 µl
1.5 M Tris-HCl pH 8.6 (** 2 M Tris-HCl pH 6.8 for stacking gel)	1.8 ml	1.8 ml	1.8 ml	1.8 ml	1.8 ml	1.8 ml	186 µl **
ddH_20	4.1 ml	3.8 ml	3.4 ml	3.1 ml	2.5 ml	1.95 ml	2 ml
10% SDS	70 µl	70 µl	70 µl	70 µl	70 µl	70 µl	30 µl
TEMED	6 µl	6 µl	6 µl	6 µl	6 µl	6 µl	3 µl
10% APS	24 µl	24 µl	24 µl	24 µl	24 µl	24 µl	26 µl
Total volume	**7 ml**	**7 ml**	**7 ml**	**7 ml**	**7 ml**	**7 ml**	**3 ml**

Table 2.3: Recipes for a single SDS-PAGE gel at various acrylamide percentages

The components of the separating gel were first mixed thoroughly, poured into assembled glass plates and covered with a thin layer of isopropanol. The gels were left to polymerise at RT for 15 min. The isopropanol layer was then removed and the top surface of the gel washed with water. The stacking gel components were mixed and poured on top of the separating gel, followed by insertion of a 12-well comb. The stacking gel was left to polymerise for 20 min at RT, and completed gels were used immediately or stored at 4°C.

2.5 Buffers for protein purification

2.5.1 Buffers for purification of MBP-TcPINK1 (kinase assays)

Lysis buffer: 50 mM Tris-HCl pH 7.5, 150 mM NaCl, 1 mM EDTA, 1 mM EGTA, 5%(v/v) glycerol, 1%(v/v) Triton X-100, 0.1% (v/ v) β-mercaptoethanol, 1 mM benzamidine, 0.1 mM PMSF.

High salt wash buffer: 50 mM Tris-HCl pH 7.5, 500 mM NaCl, 0.1 mM EGTA, 5% (v/v) glycerol, 0.03% (v/v) Brij-35, 0.1% (v/v) β-mercaptoethanol, 1 mM benzamidine, 0.1 mM PMSF.

Equilibration buffer: 50 mM Tris-HCl pH 7.5, 150 mM NaCl, 0.1 mM EGTA, 5% (v/v) glycerol, 0.03% (v/v) Brij-35, 0.1% (v/v) β-mercaptoethanol, 1 mM benzamidine, 0.1 mM PMSF.

Elution buffer: 50 mM Tris-HCl pH 7.5, 150 mM NaCl, 0.1 mM EGTA, 5% (v/v) glycerol, 0.03% (v/v) Brij-35, 0.1% (v/v) β-mercaptoethanol, 1 mM benzamidine, 0.1 mM PMSF, 12 mM maltose.

Storage buffer: 50 mM Tris pH 7.5, 150 mM NaCl, 0.27 M sucrose, 0.03% (v/v) Brij-35, 0.1% (v/v) β-mercaptoethanol

2.5.2 Buffers for purification of His-SUMO TcPINK1 (crystallization)

Lysis buffer: 50 mM Tris-HCl pH 9.0, 350 mM NaCl, 20 mM imidazole, 5% (v/v) glycerol, 0.1% (v/v) β-mercaptoethanol, 0.1 mM PMSF, 1 mM benzamidine.

High salt wash buffer: 50 mM Tris-HCl pH 9.0, 500 mM NaCl, 20 mM imidazole, 5% (v/v) glycerol, 0.1% (v/v) β-mercaptoethanol

Elution buffer: 50 mM Tris-HCl pH 9.0, 350 mM NaCl, 200 mM imidazole, 5% (v/v) glycerol, 0.1% (v/v) β-mercaptoethanol

Ion exchange buffer A: 50 mM Tris-HCl pH 9.0, 5% (v/v) glycerol, 0.1% (v/v) β-mercaptoethanol, filtered using a 0.2 μm filter, then degassed.

Ion exchange buffer B: 50 mM Tris-HCl pH 9.0, 1 M NaCl, 5% (v/v) glycerol, 0.1% (v/v) β-mercaptoethanol filtered using a 0.2 μm filter, then degassed.

Tag cleavage buffer: 50 mM Tris-HCl pH 9.0, 350 mM NaCl, 5% (v/v) glycerol, 0.1% (v/v) β-mercaptoethanol

Gel filtration buffer: 50 mM Tris-HCl pH 9.0, 350 mM NaCl, 5% (v/v) glycerol, 10 mM DTT, filtered using a 0.2 μm filter, then degassed.

2.5.3 Buffers for purification of the His-SUMO-Ubl domain

Lysis buffer: 50 mM Tris pH 7.5, 500 mM NaCl, 25 mM imidazole, 5% (v/v) glycerol, 0.1% (v/v) β-mercaptoethanol, 0.1 mM PMSF, 1 mM benzamidine

Wash buffer: 50 mM Tris pH 7.5, 500 mM NaCl, 25 mM imidazole, 5% (v/v) glycerol, 0.1% (v/v) β-mercaptoethanol

Elution buffer: 50 mM Tris pH 7.5, 200 mM NaCl, 5% (v/v) glycerol, 200 mM imidazole, 0.1% (v/v) β-mercaptoethanol

Dialysis buffer: 50 mM Tris pH 7.5, 200 mM NaCl, 5% (v/v) glycerol, 0.1% (v/v) β-mercaptoethanol

Ion exchange buffer A (cation and anion exchange): 50 mM HEPES pH 7.0, 5% (v/v) glycerol, 0.1% (v/v) β-mercaptoethanol, filtered using a 0.2 μm filter, then degassed

Ion exchange buffer B (cation and anion exchange): 50 mM HEPES pH 7.0, 1M NaCl, 5% (v/v) glycerol, 0.1% (v/v) β-mercaptoethanol, filtered using a 0.2 μm filter, then degassed

2.5.4 Buffers for purification of the GST-pS65-Ubl domain

Lysis buffer: 50 mM Tris pH 7.5, 500 mM NaCl, 0.5 mM EDTA, 0.5 mM EGTA, 10% (v/v) glycerol, 5 mM DTT, 1 mg/ml lysozyme, 50 mM NaF, 1 mM $NaVO_4$, 1x 50 ml Roche Protease inhibitor tablet

Wash Buffer: 50 mM Tris pH 7.5, 500 mM NaCl, 0.5 mM EDTA, 0.5 mM EGTA, 10% (v/v) glycerol, 5 mM DTT, 50 mM NaF, 1 mM $NaVO_4$

2.6 Molecular biology methods

2.6.1 Preparation of competent EcAR7 cells

Competent EcAR7 cells were provided by Charles Williams and Dr. Natasha Pirman (Yale University). A 30 ml culture of LB + glucose was inoculated with EcAR7 cells and grown overnight at 30°C, 230 rpm. The next day, the culture was diluted to 500 ml with LB + glucose and grown at 30°C, 230 rpm until OD_{600} = 0.6. The cells were then spun down at 4000 rpm, 10 min, 4 °C and the pellet re-suspended in 150 ml TFB1 buffer and incubated on ice for 15 min. The cells were then spun down again as before, the pellet re-suspended in 15 ml TFB2 buffer and then incubated on ice for 30 min. The cells were then aliquoted and stored at -80°C.

2.6.2 Bacterial transformation

Competent BL21 CodonPlus *E. coli* cells were provided by the Division of Signal Transduction Therapy (University of Dundee). For each transformation, 100 µl of bacteria were incubated with approximately 10 ng of plasmid DNA and incubated on ice for 10 min. Cells were then heat shocked at 42°C for 1 min, incubated on ice for a further 15 min, then plated onto LB agar plates containing the appropriate antibiotic for selection. The plates were then incubated overnight at 37°C.

Competent EcAR7 *E.coli* cells were provided by either Dr. Natasha Pirman (Yale University) or Charles Williams (University of Dundee). For each transformation, 200-300 ng of both the required plasmid and the OTS plasmid were added to 100 µl of cells. The cells were incubated on ice for 30 min, heat shocked for 40 sec at 42 °C, then incubated on

ice for 2 min. 700 µl of SOC media was added and the cells incubated at 30 °C, 230 rpm for at least 2 h. 10 µl and 100 µl of recovered cells were plated onto LB + Glc, 2x Amp, Kan plates. The remaining cell mixture was spun down at 4000 g, 2 min, and all but 100 µl of the supernatant was removed. This remaining 100 µl was also plated onto the same plates. All three plates were then incubated for 2 days at 30°.

2.6.3 Preparation of glycerol stocks

For BL21 CodonPlus cells, single colonies transformed with the required plasmid were picked from an agar plate and used to inoculate 5 ml of LB + Amp. The culture was grown overnight at 37°C with shaking, and the next day 500 µl of culture was added to 500 µl of autoclaved sterile glycerol and thoroughly mixed. The resulting glycerol stocks were then stored at -80°C.

2.7 Expression and purification of recombinant proteins

2.7.1 Expression of TcPINK1 in BL21 CodonPlus E. coli strain

All forms of MBP and His-SUMO tagged TcPINK1, including all mutants and truncations, were expressed as N-terminal fusions in *E. coli* BL21 CodonPlus cells. For each litre of expression culture, a 10 ml starter culture of TB + Amp was inoculated with a single transformed colony or cells from a glycerol stock and grown overnight at 37°C with shaking. The next day, TB + Amp expression media was inoculated 1:100 (v/v) with starter culture, then grown at 37 °C, 180 rpm. When OD_{600} = 0.3 was reached the cells were cooled to 16 °C, 180 rpm, then induced with 250 µM IPTG at OD_{600} = 0.5 and grown for a further 16-18 h.

2.7.2 Expression of His-SUMO-Ubl in BL21 CodonPlus *E. coli* strain

For each litre of expression culture, a 10 ml starter culture of LB + Amp was inoculated with a single transformed colony or cells from a glycerol stock and grown overnight at 37°C with shaking. The next day, LB + Amp expression media was inoculated 1:100 (v/v) with the starter culture, then grown at 37 °C, 180 rpm. When OD_{600} = 0.3 was reached they were cooled to 15 °C, 180 rpm, then induced with 25 μM IPTG at OD_{600} = 0.5 and grown for a further 16-18 h.

2.7.3 Expression of GST Sep65-Ubl in EcAR7 *E. coli* strain

In the morning, for each 500 ml of final expression culture, 10 ml of LB + Glc, 2x Amp, Kan starter pre-culture was inoculated with 5 colonies from an agar plate and grown at 30°C, 230 rpm. In the evening, this starter pre-culture was diluted into 100 ml of LB + Glc, 2x Amp, Kan to form a larger starter culture, which was then grown overnight at 30°C, 230 rpm. The next day, the OD_{600} of the starter culture was measured and it was used to inoculate 500 ml of LB + Glc, 2x Amp, Kan, SEP to an OD_{600} of 0.15. The cells were then grown at 30°, 200 rpm until OD_{600} reached 0.8, at which point they were induced with 1 mM IPTG, and the temperature reduced to 20°C. The cells were then grown overnight.

2.7.4 Purification of MBP TcPINK1

Cells were harvested by centrifugation at 3290 g, 15 min, 4 °C and the pellet re-suspended in Lysis buffer to a volume of 40 ml per cell pellet. The cell suspension was lysed by sonication (14x 10 s pulses alternating with 10 s cooling time, with amplitude of 45%) and the resulting lysate centrifuged at 30,000 g, 30 min, 4 °C. The clarified lysate was incubated for 1.5 h at 4 °C in a 50 ml Falcon tube on a rotating platform, with amylose resin (2 ml 50:50 slurry per litre of culture) pre-washed with Lysis buffer. The resin in each tube was then washed with 5x 50 ml Wash buffer and 1x 40 ml Equilibration buffer. All resin was

then pooled by washing into an Econo-Pac disposable column using more Equilibration buffer. Elution buffer was then added and protein was collected in 1 ml fractions. Protein purity and quantity were assessed by SDS-PAGE analysis and Bradford assay respectively. Proteins were dialysed into Storage buffer and frozen at -80 °C for later use.

2.7.5 Purification of His-SUMO TcPINK1

Cells were harvested by centrifugation at 3290 g, 15 min, 4 °C and the pellet re-suspended in Lysis buffer to a volume of 40 ml per cell pellet. The cell suspension was lysed by sonication (14x 10 s pulses alternating with 10 s cooling time, with amplitude of 45%) and the lysate centrifuged at 30,000 g, 30 min, 4 °C. The clarified lysate was then incubated for 1.5 h at 4 °C in a 50 ml Falcon tube on a rotating platform with Ni-NTA resin (1 ml 50:50 slurry per litre of culture) pre-washed with Lysis buffer. The resin was centrifuged and the supernatant poured off, and then all resin was pooled in an Econo-Pac disposable column and washed with Wash buffer until flow-through A_{280} <0.05. Elution buffer was then added and protein was collected in 5 ml fractions. Purity and quantity of eluted protein was analysed by SDS-PAGE and Bradford assay respectively.

Protein-containing fractions were pooled and diluted 3.5-fold in Ion exchange buffer A to lower the salt concentration. Diluted protein was loaded manually with a syringe onto a pre-washed 5 ml Hi-Trap Q FF anion exchange column at a rate of 5 ml/min. The column was then attached to an AKTA Purifier and washed in Buffer A for 10 column volumes (CV) to remove unbound protein. Bound protein was eluted by increasing the concentration of Ion exchange buffer B, producing a gradient of increasing salt concentration from 0-500 mM over 10 CV, followed by a step to 1M NaCl for 6 CV. Eluted protein was collected in 1.5 ml fractions, and peak fractions analysed by SDS-PAGE.

Peak fractions were pooled together and then diluted to 0.25 mg/ml in Tag cleavage buffer. SENP1 protease was then added in a 1:25 (w/w) ratio to cleave off the His-SUMO tag, and the mixture was incubated for 16-18 h on a rolling platform at 4 °C. The cleaved mixture was then incubated twice with Ni-NTA resin (100 µl 50:50 slurry per mg of uncleaved protein), pre-washed with Tag cleavage buffer. Incubations were for 1 h at 4 °C.

The resulting TcPINK1 solution was concentrated to 5 ml using a spin concentrator, centrifuged at 14,000 g, 15 min, 4 °C and filtered through a 0.2 µm filter to remove aggregates. The protein was loaded through a 5ml loop onto a Superdex 200 26/60 column attached to an AKTA Prime and pre-equilibrated in Gel filtration buffer. Protein was eluted with Gel filtration buffer at 2 ml/min and 3 ml fractions were collected. Protein purity was analysed by SDS-PAGE.

2.7.6 Purification of His-SUMO Ubl domain

Cells were harvested by centrifugation at 3290 g, 15 min, 4 °C and each cell pellet re-suspended in Lysis buffer to 15 ml. The cell suspension was lysed by sonication (14x 10 s pulses alternating with 10 s cooling time, with amplitude of 45%) and the lysate centrifuged at 30,000 g, 30 min, 4 °C. Clarified lysate was then incubated for 45 min at 4 °C in a 50 ml Falcon tube on a rotating platform with Ni-NTA resin (0.6 ml 50:50 slurry per litre of culture) pre-washed with lysis buffer. The resin was centrifuged and the supernatant discarded, then transferred into an Econo-Pac disposable column and washed with Wash buffer until flow-through A_{280} <0.05. Elution buffer was added and protein was collected in 5 ml fractions. Protein purity and quantity was analysed by SDS-PAGE and Bradford assay respectively.

Protein-containing fractions were pooled and cleaved overnight at 4°C with 1:10 SENP1 whilst dialysing into Dialysis buffer. The cleaved mixture was then incubated with Ni-NTA

resin pre-washed with Tag cleavage buffer (for 12 L culture, twice with 2 ml 50:50 slurry, once with 1 ml 50:50 slurry). Incubations were for 45 min at 4 °C. The resulting protein solution was dialysed overnight at 4°C into Ion exchange buffer A.

Dialysed protein was manually loaded with a syringe onto a 5 ml Hi-Trap CM FF cation exchange column at a rate of 5 ml/min. The column was attached to an AKTA Purifier and the column washed in Buffer A for 10 column volumes (CV) to remove unbound protein. Bound protein was eluted by increasing the concentration of Ion exchange buffer B, producing a gradient of increasing salt concentration from 0-500 mM over 10 CV, followed by a step to 1M NaCl for 6 CV. Eluted protein was collected in 1.5 ml fractions.

2.7.7 Phosphorylation of Ubl domain with TcPINK1 and purification of Ser65-phospho Ubl domain

After purification by cation exchange, the Ubl phosphorylation reaction was set up as follows in a final volume of 500 µl: MBP-TcPINK1 128-570 and Ubl domain were at 0.2 mg/ml, ATP at 0.1 mM, and $MgCl_2$ at 10 mM in 50 mM Tris-HCl pH 7.5, 0.1 mM EGTA, 1 mM DTT. Reactions were incubated in a ThermoMixer at 16°C for 2h. The reaction was terminated by passing the mixture through a 30 kDa molecular weight cutoff (MWCO) spin concentrator to separate TcPINK1 from the Ubl domain. The Ubl domain was collected from the flow-through, buffer exchanged into Ion exchange buffer A and then concentrated to 4 ml using a 3 kDa MWCO spin concentrator.

The protein was loaded using a 4 ml loop onto a pre-washed 1 ml Mono Q 5/50 GL column attached to an AKTA Explorer. The column was then washed with Ion exchange buffer A until the UV baseline returned to zero to remove unbound protein. Bound protein was then eluted with a gradient of Ion exchange buffer B to 50% over 40 CV. One

ml fractions were collected throughout the run and subsequently analysed by SDS-PAGE and Western blotting to assess the presence of phosphorylated protein.

2.7.8 Purification of GST Sep65-Ubl

Cells were harvested by centrifugation at 4000 g, 20 min, 4°C. The resulting cell pellet was re-suspended in 30 ml of the used media and centrifuged again. This pellet was frozen at -80°C to be stored for later use or defrosted immediately to aid with cell lysis. Cell pellets to be thawed were incubated in a water bath at 37°C for around 30 s and then placed on ice. Thawed pellets were re-suspended in 10 ml of Lysis buffer and incubated on ice for 30 min to allow the lysozyme to digest the cell wall. Cells were lysed by sonication with 20 cycles at 55 Amps, with 5 s on time and 40 s off time for each cycle.

Lysates were centrifuged at 20,000 g, 15, min, 4 °C and the resulting supernatant was incubated with glutathione resin prewashed in lysis buffer (400 µl 50:50 slurry per 500 ml culture) for 1 h at 4°C. The resin was then centrifuged at 500 g, 5 min and the supernatant removed, followed by washing with Wash buffer until the A_{280} <0.05. GST-Prescission protease was then added and the resin incubated overnight at 4°C. The next day, the supernatant was collected and remaining cleaved Sep65-Ubl was washed from the resin using Wash buffer.

2.8 Lysine methylation of protein preparations

Lysine methylation of TcPINK1 was carried out according to (Walter et al, 2006), with slight modifications. TcPINK1 purified by anion exchange and with the His-SUMO tag cleaved off was diluted to below 0.1 mg/ml in Tag cleavage buffer. Twenty microlitres of freshly prepared 1 M dimethylamine-borane complex (ABC) and 40 µl of 1 M formaldehyde were added per 1 ml of protein solution, which was then incubated at 4°C

on a platform roller for 2 h. Then, another 20 µl ABC and 40 µl formaldehyde per 1 ml of solution was added and incubated for a further 2 h. Following a final addition of 10 µl ABC per 1 ml of solution, the reaction was then incubated overnight at 4°C. The methylated protein solution was centrifuged at 4000 rpm, 15 min, 4°C to remove any aggregated protein before gel filtration as described in Section 2.7.5.

2.9 Analysis and of protein preparations

2.9.1 SDS-PAGE analysis

Protein samples were prepared in 1X SDS sample buffer and heated to 90 °C for 2 min. Gels were loaded into an Atto tank filled with running buffer and 20 µl of each sample was loaded onto the gel along with Precision Plus protein standard, which contains markers with the following apparent molecular weights: 250, 150, 100, 75, 50, 37, 25, 20, 15 and 10 kDa. Electrophoresis was carried out at 180 V for 90 min, after which gels were either Coomassie stained with InstantBlue stain for 1 h followed by de-staining with water or used for Western blotting.

2.9.2 Determination of protein concentration

For rough estimation of protein concentration, for example prior to SDS-PAGE analysis, the Bradford assay was employed (Bradford, 1976). Ten microlitres of protein sample was mixed with 200 µl of Bradford reagent in a 96-well plate. BSA standards at concentrations of 0.1, 0.25, 0.5 and 1.0 mg/ml were used to produce a standard curve and water was used as a blank. The absorbance at 595 nm was measured using a plate reader and the standard curve was used to determine sample concentration. Samples were measured in duplicate and highly concentrated samples were diluted in water before measurement.

For accurate determination of the concentration of highly pure protein samples, the absorbance at 280 nm was measured (A_{280}). The theoretical extinction coefficients (ε) were calculated using the ExPASY ProtParam tool (http://web.expasy.org/protparam/) and are listed below in Table 2.4. Samples were diluted as required in either buffer or water in a cuvette with a 1 cm path length and either buffer or water was used as a blank. The concentration of the protein sample was determined using the following formula:

$$\text{Concentration (mg/ml)} = (A_{280}/\varepsilon) \times \text{MW (Da)} \times \text{Dilution factor}$$

Protein	Extinction coefficient, ε (M^{-1} cm^{-1})
TcPINK1 (155-470 & 150-570)	62340
Parkin full-length (1-465)	58900
ΔUbl Parkin (80-465)	47900
Ubl domain (1-76)	11000
Ubiquitin (1-76)	1490

Table 2.4: Extinction coefficients used for accurately calculating concentrations of proteins in this thesis

To accurately determine the concentration of less pure proteins, the Li-Cor Odyssey system was used. Approximately 1 μg of protein sample, and 1μl of BSA standards at 0.125, 0.25, 0.5 and 1.0 mg/ml were run on an SDS-PAGE gel, and the de-stained gel was scanned by the Li-Cor scanner at 700 nm. The intensity of each band was quantified using the Odyssey software, allowing measurement of the intensity of only the band of interest in a less pure protein sample. A standard curve was constructed using the BSA standards and the concentration of the protein of interest could then be determined.

2.9.3 Immunoblotting

After separation of proteins by SDS-PAGE, gels were assembled into BioRad transfer apparatus. Prior to assembly, the nylon sponge pads and Whatman 3mm filter papers were soaked in transfer buffer, and the PVDF membrane was activated by soaking in methanol. The completed transfer assembly was then loaded into a BioRad Mini Trans-blot electrophoretic transfer tank, which was then filled with transfer buffer and an ice pack. Proteins were transferred from the gel to the membrane at 100 V for 1.5 h.

Membranes were blocked for 30 min in TBST buffer containing 5 % (w/v) BSA and incubated overnight at 4°C with the appropriate primary antibody. Membranes were then washed 3 times for 5 min with TBST, incubated with horseradish peroxidase (HRP)-conjugated secondary antibodies for 1 h at RT and washed another 3 times with TBST. In-house primary antibodies were used at 1 μg/ml in 5% BSA in TBST with the addition of 10 μg/ml of dephospho peptide for phospho-specific antibodies. Secondary antibodies were used at a 1:2500 dilution in 5% BSA in TBST.

Finally, membranes were incubated with enhanced chemiluminescence reagent (ECL) and exposed to X-ray film for the required length of time. Films were developed using a Konica automatic developer.

2.9.4 MALDI-TOF analysis

Matrix-assisted laser desorption/ionisation and time of flight (MALDI-TOF) analysis of lysine methylated TcPINK1 and Ser65-phosphorylated Ubl domain was performed by Dr. Stella Ritorto (University of Dundee).

2.10 Protein crystallography

2.10.1 Crystallisation theory and experimental setup

A full discussion of the theory behind protein crystallography will not be presented here, however the reader is directed to the following book for further information: "Crystallography Made Crystal Clear" (Rhodes, 2006).

All crystallisation experiments described in this thesis were carried out in the sitting drop format (Figure 2.1). This consists of a reservoir solution and a platform, on which sits a drop of protein solution mixed with a small quantity of the reservoir solution (typically in a 1:1 ratio) and additive solutions, if required. The setup is sealed and equilibration occurs between the reservoir solution and the crystal drop. As this occurs, the concentration of components in the drop increases until supersaturation occurs. In the ideal situation, at this stage, nucleation occurs and crystals begin to grow. As more protein molecules enter the growing crystals, the overall concentration of components in the drop decreases and nucleation ceases. The crystals will continue to grow, increasing in size but not number. Many less desirable variations on this situation are possible, including too many nucleation events occurring and too many small crystals forming, crystals growing that are twinned or stuck together, or the protein precipitating, or crystals failing to grow entirely.

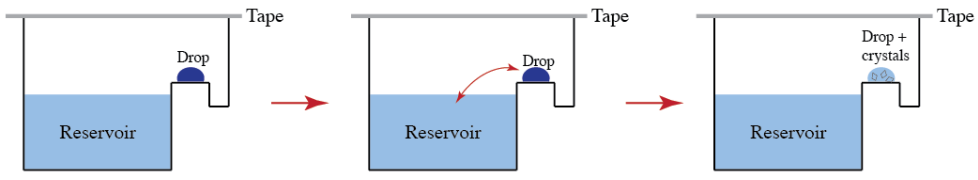

Figure 2.1: Schematic showing setup used for crystallization screening

A drop of protein solution is mixed with reservoir solution and the setup is sealed. Equilibration occurs between the drop and the reservoir solution, leading to an increase in the concentration of the drop and crystal growth.

2.10.2 Sample preparation

Protein solutions after gel filtration were concentrated to between 1 and 5 mg/ml, depending on the construct using Vivaspin 500 centrifugal concentrators, with centrifugation at 13,000 g, 4°C until the required concentration was obtained. Following concentration, proteins were prepared for crystallisation trials by centrifugation at 14,000 g, 15 min, 4°C to pellet any aggregated or insoluble material. If required, the protein was then incubated in the presence of a ligand. ADP, ATP and AMP-PNP (plus $MgCl_2$) were added at a 5-fold molar excess and the protein solution then incubated on ice for 30 min.

2.10.3 Setting up of crystal trays

Crystallisation screens were set up in sitting drop format (Figure 2.1) using 96-well MRC plates, either manually or with a Mosquito crystallisation robot. The reservoir volume for all screens was 50 µl. For screens set up manually, the drop size was 2 µl (1 µl protein + 1 µl reservoir solution). For screens set up with the Mosquito, the drop size was 1 µl (0.5 µl protein + 0.5 µl reservoir solution). During setup, the protein solution was either kept on ice (manual setup) or in a chilled reservoir (Mosquito) to avoid precipitation of the concentrated protein. For all screens, 1 µl β-mercaptoethanol was added to the reservoir as a final step to help improve crystal size and growth. For additive screening, additives were added at 1:10 of the final drop volume, so 0.1 µl for manual screens and 0.05 µl for those set up with the Mosquito. Finished trays were sealed with Crystal Clear tape, incubated in a temperature controlled room set at 18°C and checked regularly for crystal growth.

2.10.4 Crystal handling and diffraction experiments

Protein crystals were harvested from the mother liquor prior to a diffraction experiment using CryoLoops of the appropriate size. Crystals were submerged in a cryoprotectant solution, typically the mother liquor + 20% MPD, for a few seconds before freezing in

liquid nitrogen. Cryoprotectants were tested before use to ensure that a high enough concentration to prevent ice formation had been selected. Frozen crystals were either transferred to the storage dewar on the home X-ray generator or into a travel dewar for transport. Diffraction experiments were carried out at the European Synchrotron Radiation Facility (ESRF) in Grenoble, France, at the Diamond Light Source in Oxfordshire, UK and on the Rigaku generator at Dundee University.

2.11 Kinase assays

2.11.1 Assays with phosphorylation measured by autoradiography

For assays using recombinant proteins where phosphorylation was detected by autoradiography, the following method was used. Reactions were set up in a final volume of 40 µl, using 1 µg of enzyme, either 2 µg or 2 µM of the appropriate substrate and [γ-^{32}P] ATP at 0.1 mM in 50 mM Tris-HCl pH 7.5, 0.1 mM EGTA, 10 mM $MgCl_2$, and 2 mM DTT. Assays were incubated at 30°C, 1200 rpm for the indicated time, usually 30 min, followed by termination by the addition of SDS sample buffer. Reactions were then resolved by SDS-PAGE. The de-stained gel was then either dried in a GelAir Dryer or a Model 583 vacuum gel dryer. The dried gel was then exposed to ultra sensitive X-ray film for several hours or until an appropriate level of signal had developed. Where necessary, for further quantification the appropriate bands were cut out of the dried gel and the incorporation of [γ-^{32}P] into each band was measured by Cerenkov counting.

2.11.2 Assays with phosphorylation measured by scintillation counting

For assays where phosphorylation was detected by scintillation counting, reactions were set up in a final volume of 50 µl, with 1 µg of enzyme, 5 µg of substrate for protein substrates and 1mM of peptide substrates (unless otherwise indicated) and 0.1 mM [γ-^{32}P] ATP, also in 50 mM Tris-HCl pH 7.5, 0.1 mM EGTA, 10 mM $MgCl_2$, and 2 mM DTT. Assays were

normally incubated at 30°C, 1200 rpm for the required time and then terminated by spotting onto P81 paper squares and washing in 50 mM phosphoric acid. Assays set up in 96-well format (PINKtide kinetics analysis) were incubated at 30°C with no shaking and terminated by addition of 20 µl 0.1 M EDTA, followed by spotting of 50 µl of this solution onto P81 paper and washing in 50 mM orthophosphoric acid. P81 papers were washed twice in fresh orthophosphoric acid for 30 min before being thoroughly dried. Incorporation of radioactivity into the substrate was then detected by Cerenkov counting. One unit of TcPINK1 activity was defined as the amount of enzyme that catalysed the incorporation of 1 nmol of ATP into a given substrate. K_m and V_{max} values were determined by analysing the phosphorylation of PINKtide and its variants at various concentrations. K_m and V_{max} values were calculated using the GraphPad Prism program.

2.12 AlphaScreen assays

AlphaScreen assays were set up in 384-well plates with a final reaction volume of 20 µl. GST-Ubl (1-76) was added at 0.3 µM and ΔUbl Parkin-biotin was added at 0.1 µM. Plates were sealed with an adhesive seal and incubated at RT for 60 min to allow protein binding to occur. Acceptor (glutathione-coated) and donor (streptavidin-coated) beads were added to a final concentration of 20 µg/ml each. Plates were then centrifuged at 500 g for 5 min, followed by horizontal shaking at 100 rpm for 5 min and incubation for 60 min at RT in the dark. As before, plates were sealed during this period with an adhesive seal to prevent evaporation. After incubation, plates were read with an EnVision Multilabel plate reader and data was collected.

Chapter 3

3 Analysis of the biochemical properties of an active PINK1 orthologue from the species *Tribolium castaneum*:

3.1 Introduction:

The link between the PINK1 (PTEN (phosphatase and tensin homologue)-induced kinase) gene and Parkinson's disease (PD) was first reported in 2004 after two families with autosomal recessive PD were found to harbour PINK1 mutations (Valente et al, 2004). Since then, many additional PINK1 mutations have been described in patients with familial PD. Whilst these mutations occur throughout the entire coding sequence of the PINK1 gene, the majority are found within the region encoding the kinase domain (Mills et al, 2008). There has therefore been a strong motivation to understand the biological function of PINK1 and how it is disrupted by PD-linked mutations. However, despite nearly a decade of research, relatively little progress has been made, in large part due to difficulties in assessing the enzymatic activity of PINK1 *in vitro*. In our laboratory and many others, it has been found that human PINK1 exhibits very low *in vitro* kinase activity and therefore no robust, reliable assay for its activity has been developed. This in turn has hampered efforts to identify genuine PINK1 substrates and regulators and to understand how its function may be altered by PD-linked mutations.

It has been suggested that PINK1 may be an inactive pseudokinase with a function not dependent on catalytic activity, however bioinformatics analysis of the sequence of human PINK1 reveals that PINK1 contains all of the conserved amino acid motifs found in active protein kinases that are necessary for catalysis (Hanks & Hunter, 1995), (Sim et al, 2012). In addition, this hypothesis conflicts with data showing that *Drosophila melanogaster* PINK1 null mutants have a severe phenotype that can be rescued by re-introduction of wild-type

but not kinase-inactive PINK1 (Kim et al, 2008). This provides an indication that, at least in *Drosophila*, the kinase activity of PINK1 is important for its biological function.

In order to overcome these difficulties in studying the catalytic properties of human PINK1 *in vitro*, I sought to identify orthologues of PINK1 in non-mammalian species that might display detectable *in vitro* activity and subsequently to characterise them as a potential surrogate model for the kinase activity of human PINK1. Such a model could subsequently be used to further understand its biological function and how it might be impacted by PD-linked mutations. Bioinformatics analysis in the form of a BLAST search and analysis of multiple sequence alignments suggested PINK1 orthologues from the species *Tribolium castaneum* (TcPINK1) and *Pediculus humanus corporis* (PhcPINK1) as potential candidates for further investigation. Both of these PINK1 orthologues also appear to be more tractable candidates than human PINK1 with regards to crystallisation screening, which will aid in future work determining the crystal structure of PINK1.

3.2 Identification and validation of TcPINK1 and PhcPINK1 as bona fide PINK1 orthologues

3.2.1 Bioinformatics identification of two insect PINK1 orthologues, *Tribolium castaneum* PINK1 and *Pediculus humanus corporis* PINK1, lacking the non-conserved first kinase domain insertion:

To identify putative non-mammalian PINK1 orthologues that might possess detectable *in vitro* activity, a BLAST search was performed using the full amino acid sequence of human PINK1. Orthologous protein sequences from a diverse range of species were selected and used as the input for a multiple sequence alignment, performed with MUSCLE (Edgar, 2004a; Edgar, 2004b). The resulting alignment was viewed, edited and annotated using Jalview (Waterhouse et al, 2009). Incomplete sequences were removed from the alignment, leaving a total of PINK1 sequences from 18 different species including human in the final version (Figure 3.1). The criteria for identification of potential candidates for enzymatic characterisation was to look for orthologues with variations in the N-lobe insertions, since similar insertions have been shown to act as regulatory features in other protein kinases. Inspection of the alignment revealed that PINK1 orthologues from the species *Tribolium castaneum* (red flour beetle) and *Pediculus humanus corporis* (human body louse) completely lacked the first, longest insertion in the kinase domain. These two proteins were chosen as potential candidates for further analysis. Interestingly, this insertion is highly variable in both length and conservation between different species, whereas the second and third insertions are far less variable (Figure 3.1).

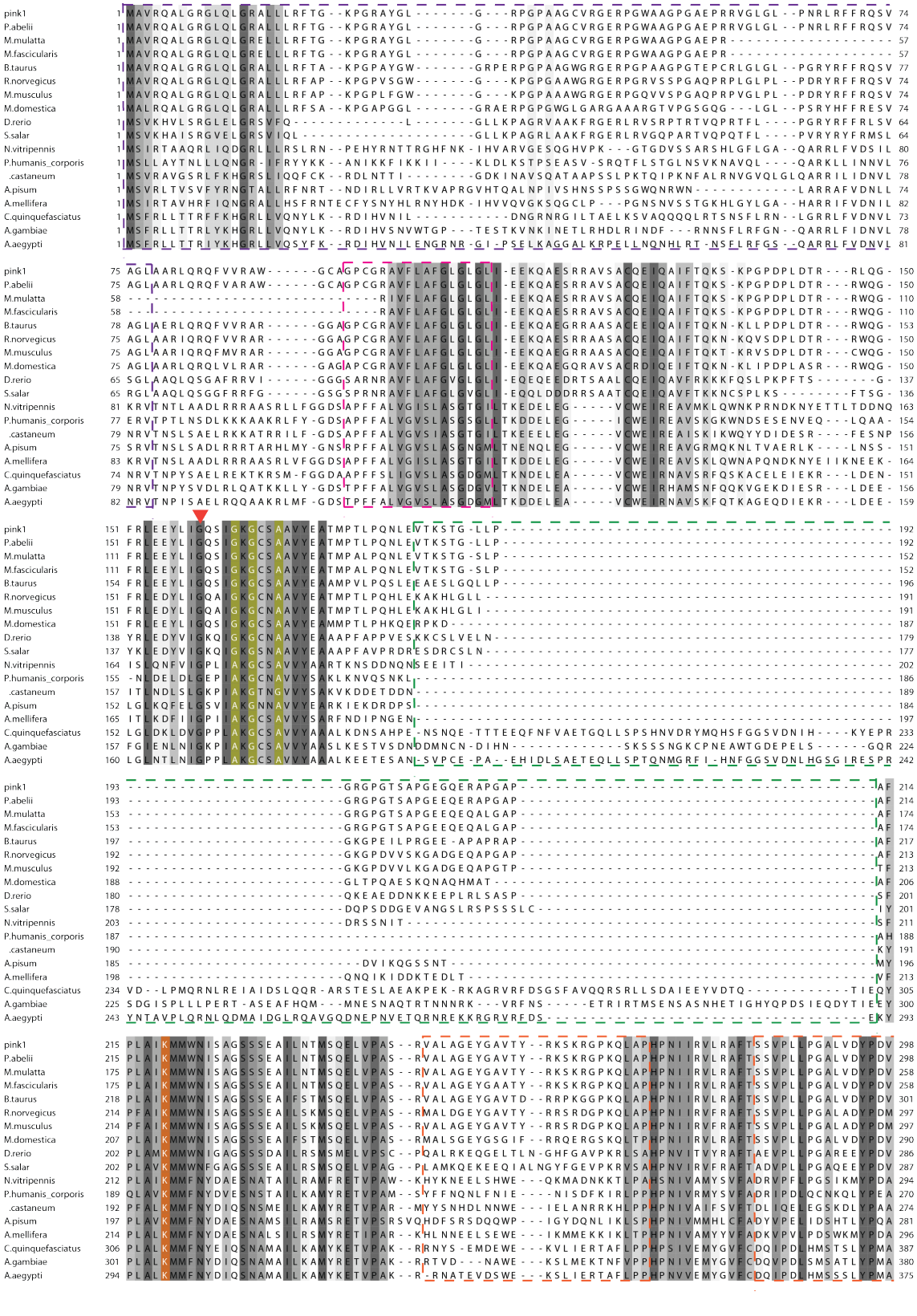
pink1
P.abelii
M.mulatta
M.fascicularis
B.taurus
R.norvegicus
M.musculus
M.domestica
D.rerio
S.salar
N.vitripennis
P.humanis_corporis
.castaneum
A.pisum
A.mellifera
C.quinquefasciatus
A.gambiae
A.aegypti

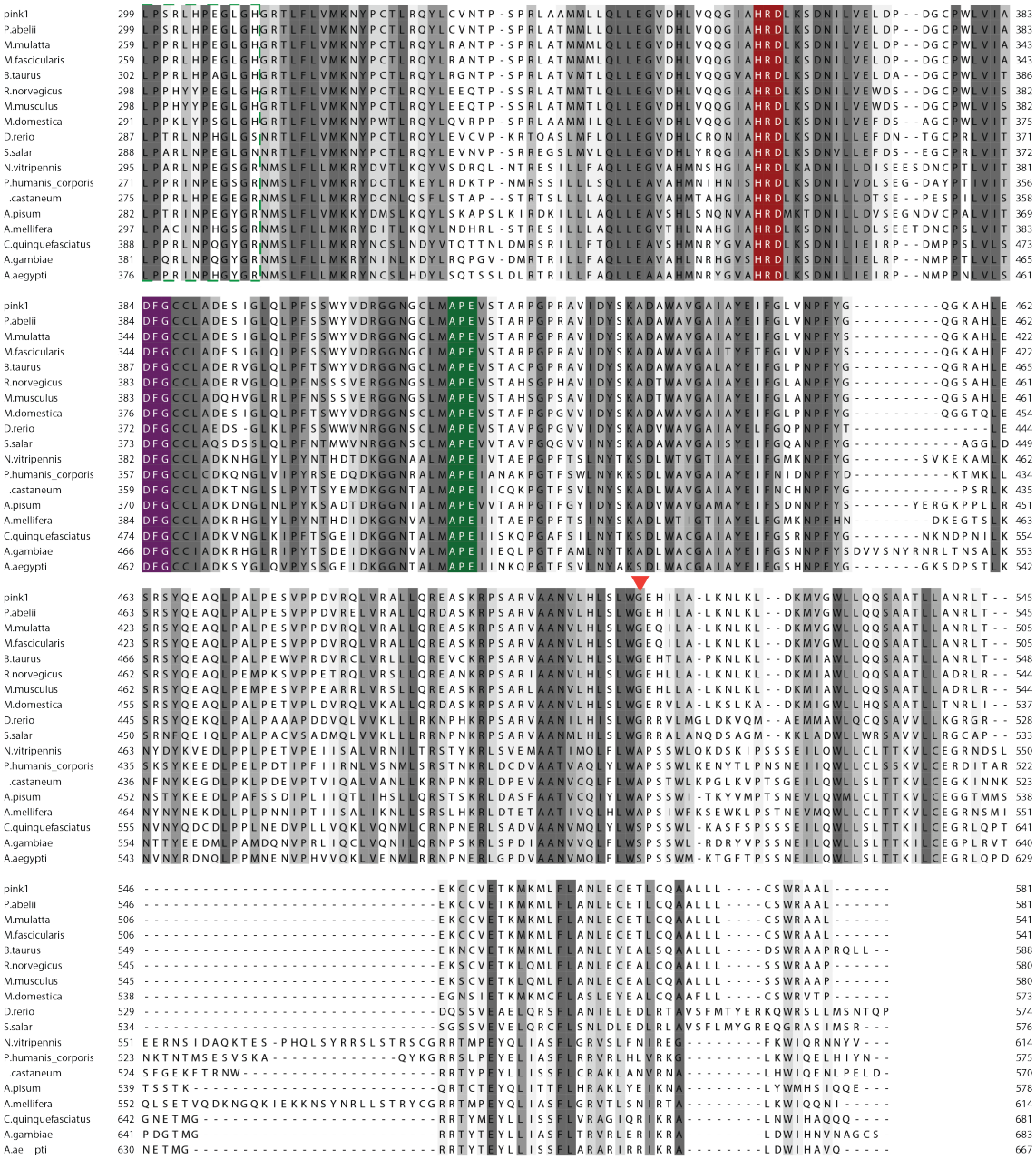

Figure 3.1: Multiple sequence alignment of PINK1

Full-length human PINK1 was aligned against PINK1 orthologues from other species identified by BLAST search. Alignment performed with MUSCLE and annotated with Jalview. The mitochondrial targeting sequence is highlighted inside a purple dashed box and the transmembrane helix inside a pink dashed box. The start and finish of the kinase domain are highlighted with red arrows. Within the kinase domain, the first variable insertion is highlighted in a green dashed box, and second and third insertions are highlighted inside orange dashed boxes. Amino acid motifs critical for catalysis are highlighted as follows – yellow: glycine rich loop; orange: LAIK motif lysine; dark red: HRD catalytic motif; purple: DFG motif/N-terminal activation loop anchor; green: APE motif/C-terminal activation loop anchor.

3.2.2 Complementation of PINK1 null Drosophila melanogaster phenotypes with Tribolium castaneum PINK1 and Pediculus humanus corporis PINK1

Subsequently it was critical to address whether or not the two proteins identified in the bioinformatics search, *Tribolium castaneum* PINK1 (TcPINK1) and *Pediculus humanus corporis* PINK1 (PhcPINK1) were genuine PINK1 orthologues, since the only information available at the time was their amino acid sequence. This was done in collaboration with Joe Pogson & Professor Alex Whitworth (University of Sheffield), who determined whether TcPINK1 and PhcPINK1 were able rescue the phenotype of a PINK1 null *Drosophila* model. PINK1 null flies display several quantifiable phenotypes (Clark et al, 2006; Park et al, 2006) and for this experiment locomotion defects, namely flight and climbing ability and the presence of thoracic indentations were assessed. Multiple transgenic lines bearing TcPINK1 or PhcPINK1 under the control of the inducible GAL4/UAS system were generated and then combined into a *PINK1* mutant background and found to rescue the flight and climbing defects as well as the appearance of thoracic indentations that are attributed to loss of PINK1. Each of these phenotypes was rescued to wild type levels by expression of both TcPINK1 and PhcPINK1, indicating that both of these proteins are likely to be genuine, functional orthologues of human PINK1 (Figure 3.2).

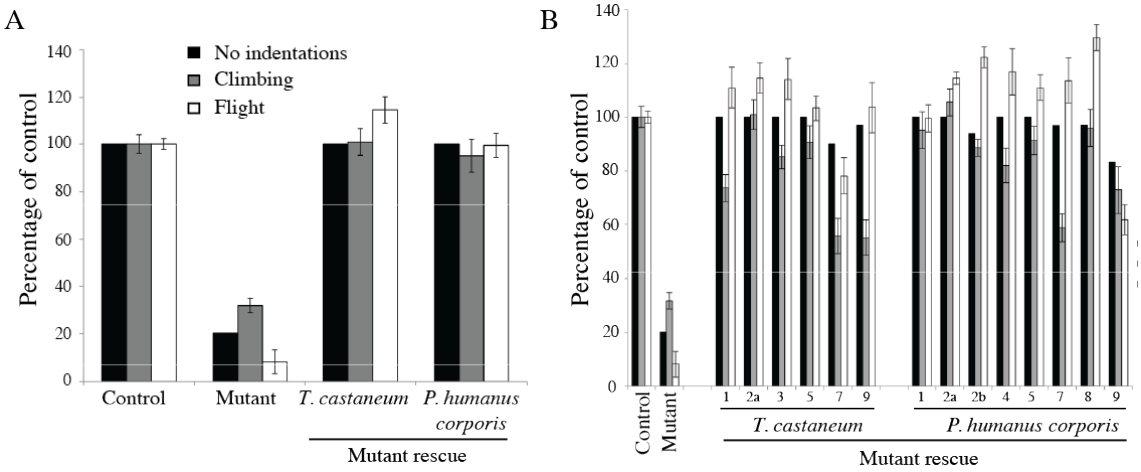

Figure 3.2: Analysis of *T. castaneum* and *P. humanus corporis* PINK1 function *in vivo*

Performed by Joe Pogson & Alex Whitworth. **(A)** Averaged data of PINK1 null *Drosophila* phenotype rescued by overexpression of *Tribolium castaneum* PINK1 (TcPINK1) or *Pediculus humanus corporis* PINK1 (PhcPINK1). Flight and climbing ability, and presence of thoracic indentations were quantified. Genotypes are - control: PINK1B9/+, mutant: PINK1B9/Y; da-GAL4/+, mutant rescue: PINK1B9/Y; da-GAL4/+, UAS-Tb.PINK12a/+ or PINK1B9/Y; da-GAL4/+, UAS- Phc.PINK11/+. Data are presented as mean ± SEM. **(B)** Raw data for each of the five fly lines analysed with TcPINK1 overexpression and each of the 8 lines analysed with PhcPINK1 overexpression. Analysis and genotypes are same as in (A).

3.3 Comparison of *in vitro* activity of insect PINK1 homologues and human PINK1

3.3.1 *In vitro* kinase activity of *Tribolium castaneum* PINK1 and *Pediculus humanus corporis* PINK1 against generic kinase substrates

After validating that TcPINK1 and PhcPINK1 were genuine orthologues of human PINK1, it was next necessary to assess whether they possessed detectable *in vitro* kinase activity. To do this, MBP-tagged full-length wild type and kinase inactive forms of TcPINK1 (aa 1-570) and PhcPINK1 (aa 1-575) were recombinantly expressed in *Escherichia coli*. Kinase inactive mutations used as controls were D359A and D357A for TcPINK1 and PhcPINK1 respectively. Proteins were incubated in the presence of [γ^{32}P] ATP and one of three generic kinase substrates: myelin basic protein, histone H1 or casein. Assays were resolved by SDS-PAGE and incorporation of [γ^{32}P] ATP into substrates was detected by autoradiography. This revealed that both TcPINK1 and PhcPINK1 displayed detectable *in vitro* kinase activity, with a preference for myelin basic protein as a substrate (Figure 3.3). Histone H1 was phosphorylated to a lesser extent and casein was only phosphorylated in trace amounts. TcPINK1 appeared to be significantly more active than PhcPINK1, and interestingly, a band corresponding to autophosphorylation was observed with both kinases and was absent in the kinase inactive controls (Figure 3.3).

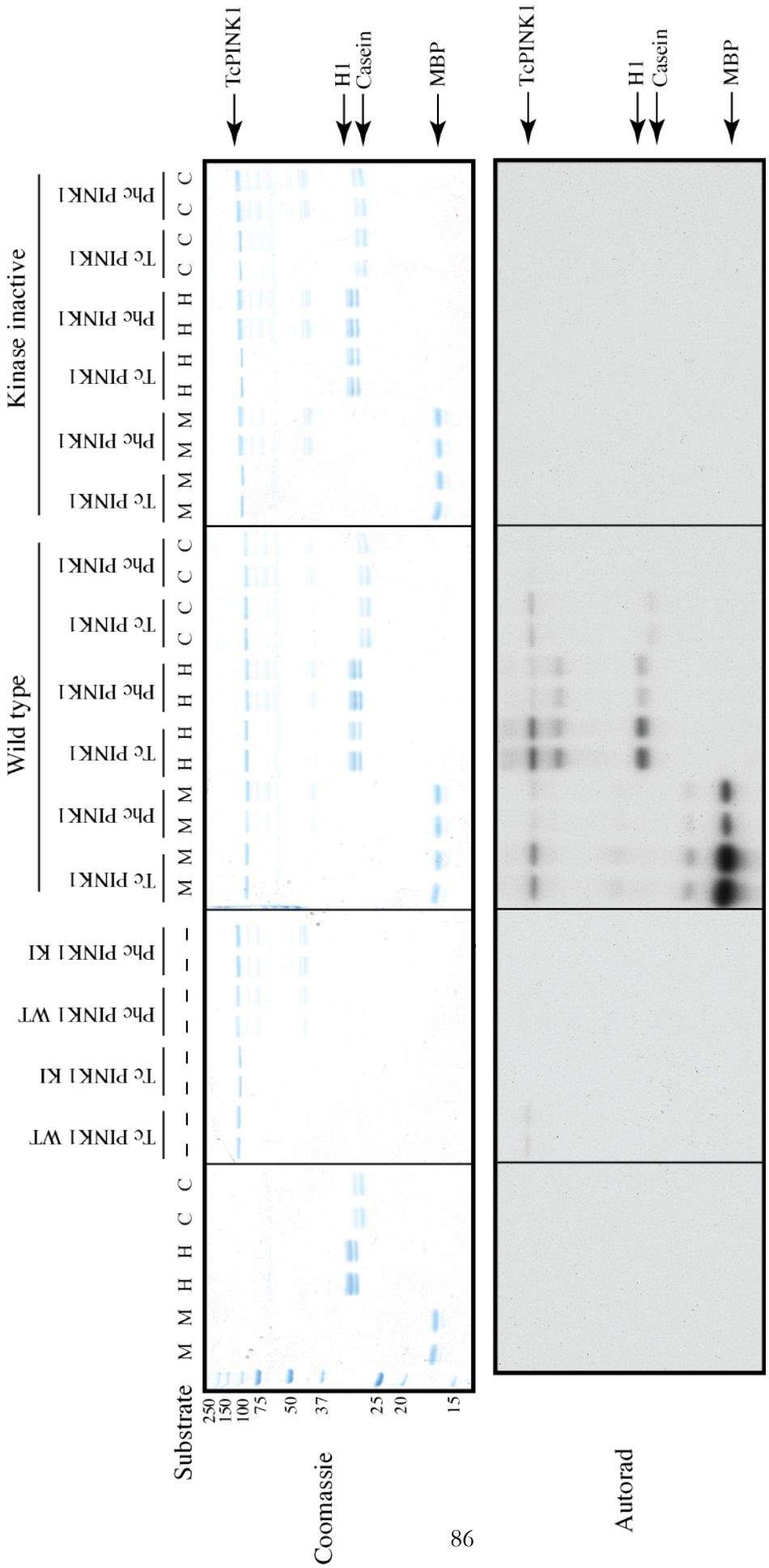
TcPINK1
H1
Casein
MBP
Coomassie
Autorad
Substrate
250
150
100
75
50
37
25
20
15
Wild type
Kinase inactive
Tc PINK1 WT
Tc PINK1 KI
Phe PINK1 WT
Phe PINK1 KI
Tc PINK1
Phe PINK1
M
H
C

Figure 3.3: Activity of TcPINK1 and PhcPINK1 against generic kinase substrates

Full-length wild type TcPINK1 (1-570), kinase inactive TcPINK1 (D359A), wild type PhcPINK1 (1-575) and kinase inactive (D357A) were tested against myelin basic protein, histone H1 and casein. The indicated enzymes (1 μg) were incubated in the presence of the indicated substrate (2 μM) and [γ^{32}P] ATP for 30 min. Assays were terminated by addition of loading buffer and separated by SDS-PAGE. Proteins were detected by Coomassie staining (upper panel) and incorporation of [γ^{32}P] ATP was detected by autoradiography (lower panel). Similar results were obtained in two experiments carried out in duplicate. Fine dividing lines indicate that reactions were resolved on separate gels and grouped in the final figure. Abbreviations: M/MBP, myelin basic protein; H/H1, histone H1; C, casein.

3.3.2 Insect PINK1 orthologues display detectable *in vitro* activity against generic substrates in comparison to human PINK1

Subsequently, the activity of the newly identified active insect orthologues was compared to that of human PINK1 (hPINK1), expressed in both *E. coli* and *Sf9* cells. Although we were unable to detect hPINK1 kinase activity in our lab, there were several reports in the literature showing activity of hPINK1 both towards substrates (Kim et al, 2008; Pridgeon et al, 2007), by measuring autophosphorylation (Beilina et al, 2005; Silvestri et al, 2005) and when expressed in *Sf9* cells (Sim et al, 2006). TcPINK1 and PhcPINK1 had been initially selected for analysis since they lacked the first insertion in the kinase domain. In contrast, the PINK1 orthologue from another insect species, *Drosophila melanogaster* PINK1 (DmPINK1), possesses a very long first insertion of approximately 90 amino acids, compared to around 30 in hPINK1. We therefore chose to include DmPINK1 in this experiment to provide further information on the role of the first insertion in regulation of PINK1 kinase activity.

Full-length MBP-tagged forms of TcPINK1 (1-570), PhcPINK1 (1-575) and DmPINK1 (1-721), both wild type and kinase inactive (D359A, D357A and D501A respectively) were compared to N-terminally truncated hPINK1, since it was not possible to express full-length hPINK1 in *E. coli*. Wild type and kinase inactive (D384A) MBP-tagged hPINK1 was

expressed in *E. coli* (aa 123-581) and *Sf9* cells (aa 125-581). These enzymes were incubated in the presence of myelin basic protein, the preferred substrate for TcPINK1 and PhcPINK1, and [γ^{32}P] ATP, and phosphorylation of myelin basic protein was detected by scintillation counting. This revealed that hPINK1 expressed in either *E. coli* or *Sf9* cells displayed no detectable kinase activity, in contrast to previous reports in the literature, and DmPINK1 displayed activity against myelin basic protein, albeit considerably weaker than the most active kinase, TcPINK1 (Figure 3.4).

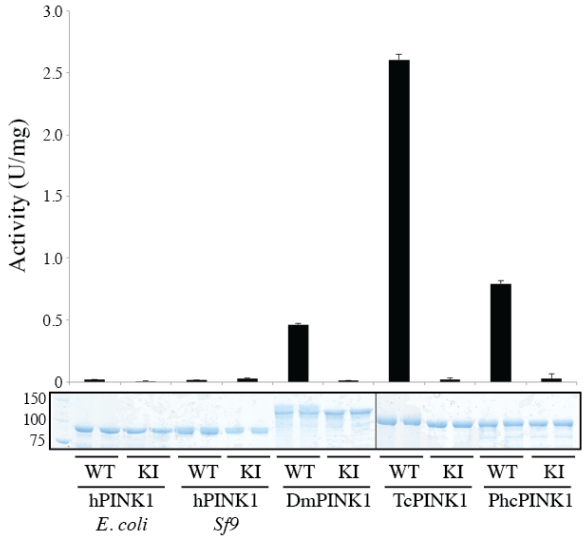

Figure 3.4: Activity of insect PINK1 homologues and human PINK1 against myelin basic protein

Wild type N-terminally truncated human PINK1 (125-581) expressed in *E. coli* and *Sf9* cells, full-length *D. melanogaster* PINK1 (DmPINK1, 1-721), *T. castaneum* PINK1 (TcPINK1, 1-570) and *P. humanus corporis* PINK1 (PhcPINK1, 1-575) and corresponding kinase inactive mutants (HsPINK1-D384A, DmPINK1-D501A, TcPINK1-D359A, PhcPINK1-D357A) were tested against myelin basic protein. The indicated enzymes (1 μg) were incubated in the presence of 5 μg myelin basic protein and [γ^{32}P] ATP for 30 min. Reactions were terminated by spotting on P81 paper, washing in phosphoric acid and quantifying phosphorylation of myelin basic protein. The results are presented as ± SD for a representative experiment undertaken in duplicate (upper panel). In the lower panel representative Coomassie stained gels showing the relative amounts of PINK1 enzyme used for each assay are shown. Fine dividing lines indicate that reactions were resolved on separate gels and grouped in the final figure.

To ensure that the lack of detectable hPINK1 activity was not due to myelin basic protein being a poor substrate for this enzyme, *E. coli* and *Sf9*-expressed hPINK1 was again assayed in parallel with TcPINK1 and PhcPINK1 against histone H1 and casein in addition to myelin basic protein. Full-length MBP-tagged forms of TcPINK1 (1-570) and PhcPINK1 (1-575), both wild type and kinase inactive (D359A and D357A respectively) were used along with N-terminally truncated MBP-tagged hPINK1 expressed in *E. coli* (aa 123-581) and *Sf9* cells (aa 125-581), both wild type and kinase inactive (D384A) forms. These proteins were incubated with the indicated substrates in the presence of [γ^{32}P] ATP, and incorporation of [γ^{32}P] was detected by autoradiography. In this case, hPINK1, expressed in both *E. coli* and *Sf9* cells again did not display detectable *in vitro* activity against any of the substrates utilized, suggesting the lack of kinase activity is not dependent on the substrate used (Figure 3.5).

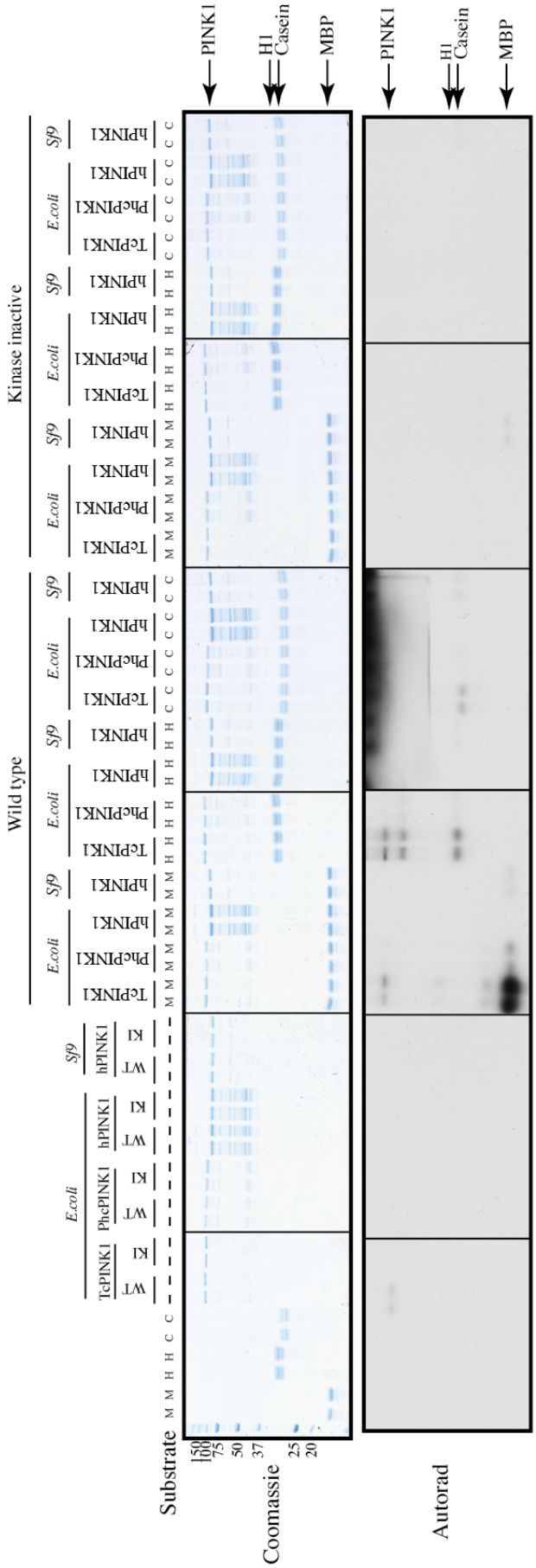
PINK1
H1
Casein
MBP
Substrate
Coomassie
Autorad
Wild type
Kinase inactive
E.coli
Sf9
TcPINK1
PhcPINK1
hPINK1
WT
KI
M
H
C
150
100
75
50
37
25
20

Figure 3.5: Activity of insect PINK1 orthologues and human PINK1 against generic kinase substrates

Comparison of activity of full length TcPINK1 (1-570) and PhcPINK1 (1-575) with N-terminal truncations of hPINK1 expressed in both *E. coli* (aa 123-581) and *Sf9* cells (aa 125-581). The indicated enzymes (1 μg) were incubated in the presence of the indicated substrate (2 μM) and [γ^{32}P] ATP for 30 min. Assays were terminated by addition of loading buffer and separated by SDS-PAGE. Proteins were detected by Coomassie staining (upper panel) and incorporation of [γ^{32}P] ATP was detected by autoradiography (lower panel). Similar results were obtained in two experiments carried out in duplicate. Fine dividing lines indicate that reactions were resolved on separate gels and grouped in the final figure. Abbreviations: M/MBP, myelin basic protein; H/H1, histone H1; C, casein.

3.3.3 Deletion of the non-conserved insertion 1 in human PINK1 does not impart *in vitro* kinase activity

Since a major difference at the primary sequence level between the active TcPINK1 and the inactive hPINK1 was the first kinase domain insertion, we hypothesized that this insertion, which is present in hPINK1 and absent in TcPINK1, might play an autoinhibitory role, thus regulating PINK1 catalytic activity. To test this idea, an artificial deletion of the first insertion (aa 184-212) in hPINK1 was designed. This protein was expressed in *E. coli* and tested for catalytic activity against myelin basic protein. Incorporation of [γ^{32}P] ATP was measured by scintillation counting. The results clearly show that deletion of the first insertion of hPINK1 is not sufficient to impart *in vitro* kinase activity, since this protein, like wild type hPINK1, displays no detectable phosphorylation of myelin basic protein (Figure 3.6).

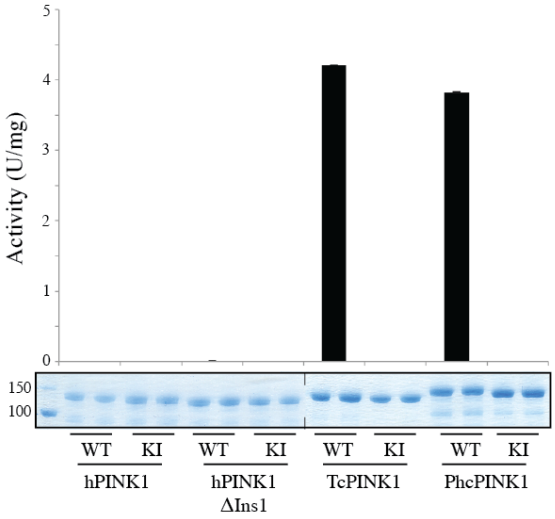

Figure 3.6: Analysis of the effect of first kinase domain insertion on human PINK1 activity

(A) Activity of wild type and kinase inactive (D384A) hPINK1 (123-581) was compared to ΔIns1 hPINK1 (123-581 Δ184-212) wild type and kinase inactive, *Tribolium castaneum* PINK1 (TcPINK1) wild type and kinase inactive (D359A), and *Pediculus humanus corporis* PINK1 (PhcPINK1) wild type and kinase inactive (D357A). Enzymes (1 μg) were incubated with myelin basic protein (5 μg) and [γ^{32}P] ATP for 30 min. Assays were terminated by spotting on P81 paper and phosphorylation was quantified by scintillation counting. Results are presented as ± SD for a representative experiment undertaken in triplicate (upper panel). Coomassie stained gels showing the relative amounts of PINK1 enzyme used for each assay are shown (lower panel). Fine dividing lines indicate that reactions were resolved on separate gels and grouped in the final figure. **(B)** Schematic of the protein constructs used in (A).

3.4 Deletion of the PINK1 C-terminal domain leads to a loss of kinase activity

To further probe the factors necessary for the catalytic activity of PINK1, the contribution of each domain of the protein to the catalytic activity of TcPINK1 was analysed. From this point, all further studies were carried out with TcPINK1, since it was the most active of the identified insect orthologues. PINK1 contains several major regions: the N-terminal region of the protein, comprising the mitochondrial targeting sequence and transmembrane helix, followed by the disordered region, the kinase domain and finally the small C-terminal domain (Figure 3.7A). Constructs were designed comprising truncations of each of these regions: construct aa 128-570 lacked the mitochondrial targeting sequence and transmembrane helix; construct aa 155-570 lacked all regions N-terminal to the kinase domain; and construct aa 155-486 lacked all N-terminal regions and the C-terminal domain (Figure 3.7A). These proteins were expressed in *E. coli* and their activity was assessed by incubation with myelin basic protein and [γ^{32}P] ATP. Incorporation of [γ^{32}P] into the substrate was detected by autoradiography. This experiment demonstrated that all regions of the protein N-terminal to the kinase domain were dispensable for kinase activity, since both the truncations from aa 128 and 155 were still active, although a slight loss of activity was seen when the entire N-terminal region, from aa 155, was deleted (Figure 3.7B). In contrast, the isolated kinase domain (aa 155-486) exhibited a complete loss of myelin basic protein phosphorylation, suggesting that the C-terminal domain is essential for kinase activity. Interestingly, all active constructs still displayed a detectable level of autophosphorylation, which was reduced in a fashion mirroring substrate phosphorylation in the less active N-terminal truncations (Figure 3.7B).

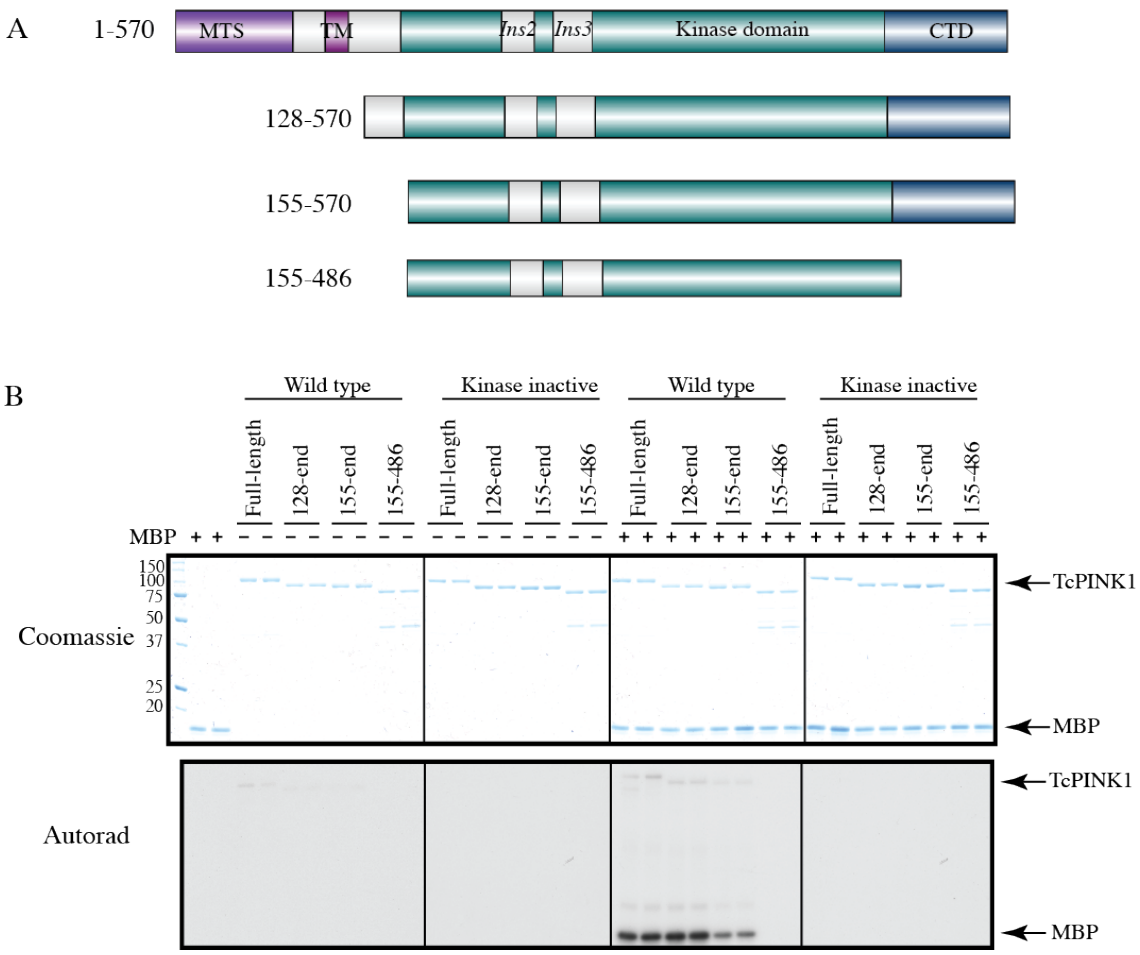

Figure 3.7: Analysis of requirement for each domain of TcPINK1 for kinase activity

(A) Schematic of protein constructs utilised in this experiment. **(B)** Assessment of kinase activity of wild type or kinase inactive (D359A) full-length (1-570), N-terminal truncation (128-570 & 155-570) and N- & C-terminal truncation mutants (155-486) of TcPINK1. The indicated forms of TcPINK1 (1 µg) were incubated in the presence (+) or absence (-) of myelin basic protein (2 µM) and [γ^{32}P] ATP for 30 min. Reactions were terminated by the addition of SDS sample buffer and separated by SDS- PAGE. Gels were analysed by Coomassie staining (upper panel) and incorporation of [γ^{32}P] ATP was detected by autoradiography (lower panel). Fine dividing lines indicate that reactions were resolved on separate gels and grouped in the final figure.

3.5 Analysis of TcPINK1 autophosphorylation

3.5.1 *Tribolium castaneum* PINK1 is able to autophosphorylate on both serine/threonine and tyrosine residues within the kinase domain

Autophosphorylation is a widespread mechanism of both kinase activation and regulation of kinase activity, and since PINK1 autophosphorylation had been observed in several prior experiments, autophosphorylation sites in TcPINK1 were mapped and it was determined whether any of them were required for kinase activity. To do this, full-length wild type TcPINK1 was analysed using a Thermo-Electron LTQ-Orbitrap mass spectrometer (performed by Dr. David Campbell). This analysis revealed multiple putative autophosphorylation sites. TcPINK1 appears to autophosphorylate on serine and threonine residues, but also strikingly on some tyrosine residues, which is unexpected since PINK1 belongs to the serine/threonine kinase family. For the majority of the identified phosphopeptides it was not possible to distinguish the exact phosphorylation site, since there were several adjacent or nearby residues that could potentially be phosphorylated (Table 3.1). Tyr439 and Thr 186 were identified unambiguously, but the other peptides contained clusters of several residues that could become phosphorylated. Each of the putative sites was assessed for conservation between TcPINK1 and hPINK1. Many of the identified sites are not conserved between TcPINK1 and hPINK1, and so were not considered for further analysis. Ten possible sites, found in four distinct peptides, are conserved between TcPINK1 and hPINK1 and these are highlighted in Table 3.1.

Peptide sequence	Phosphorylated residue	Conservation in hPINK1	Observed mass (m/z)	Theoretical mass (m)
SFGEKFTR	S524/T530	✖/✖	1130.41	566.21
AMYRETVPAR	Y215/T218	✖/✖	677.27	1352.53
NFNYKEGDLPK	Y439	✔	702.81	1403.61
WQYYDIDESR	Y144/Y145	✖/✖	727.78	1453.55
INNKSFGEKFTR	S524/T530	✖/✖	800.85	1599.68
TNGLSLPYTSYEMDK	Y375/T376/S377/Y378	✖/~/✔/✖	899.88	1797.75
VKDDETDDNKYPFALK	T186	✖	989.44	1976.87
MMFNYDIQSNSMEILK	S205/S207	✔/✔	1022.43	2042.85
RYDCNLQSFLSTAPSTR	S303/S306/T307	✖/✖/✖	1048.47	2094.91
MYYSNHDLNNWEIELANR	Y224/Y225/S226	✖/✖/✖	788.00	2360.98
GGNTALMAPEIICQKPGTFSVLNYSK	S402/Y406/S407	✖/✔/✔	959.46	2875.36
WQYYDIDESRFESNPITLNDLSLGK	S150/S154	✖/✖	1028.47	3082.39
SDNLLLDTSEPESPILVISDFGCCLADK	T347/S348/S352/S358	✖/✖/✖/✖	1063.48	3187.43

Table 3.1: Putative autophosphorylation sites identified in TcPINK1

Phospho-site mapping performed by Dr. David Campbell. The sequence of each identified phosphopeptide is shown with potential phosphorylation sites highlighted in red and the residue numbers of potential phospho-sites are listed. The conservation of the identified sites between TcPINK1 and hPINK1 is depicted as follows: ✔, residue conserved in hPINK1; ✖, residue not conserved in hPINK1; ~, residue substituted with another phosphorylatable amino acid in hPINK1. The theoretical (m) and observed (m/z) masses of each peptide are also listed.

To assess the relative importance of the identified potential sites, non-phosphorylatable alanine and phenylalanine mutants in full-length MBP-tagged TcPINK1 were designed for each of the serine/threonine and tyrosine sites respectively, including a double alanine mutant for residues Ser205 and Ser207 (Figure 3.8A). Ser205 is the only fully conserved residue that is not a tyrosine, and was therefore considered likely to be significant for potential regulation of PINK1 kinase activity. These mutants were expressed in *E. coli* and their ability to phosphorylate myelin basic protein in the presence of [γ^{32}P] ATP was assessed by autoradiography. No strong effect on kinase activity was seen with mutation of

any residue, with the exception of the S205A and S205/S207A single and double mutants, which led to an approximately 75% reduction in kinase activity relative to the wild type protein (Figure 3.8B). This suggests that Ser205 is most likely to be the phosphorylation site on this peptide, and may be important for regulating the kinase activity of PINK1. However, further mass spectrometry analysis using additional techniques such as ETD (Electron Transfer Dissociation) would be required to confirm that Ser205 is indeed phosphorylated and that the observed loss of activity is not due to an alternative explanation, such as destabilization of the protein due to the introduction of an alanine mutation.

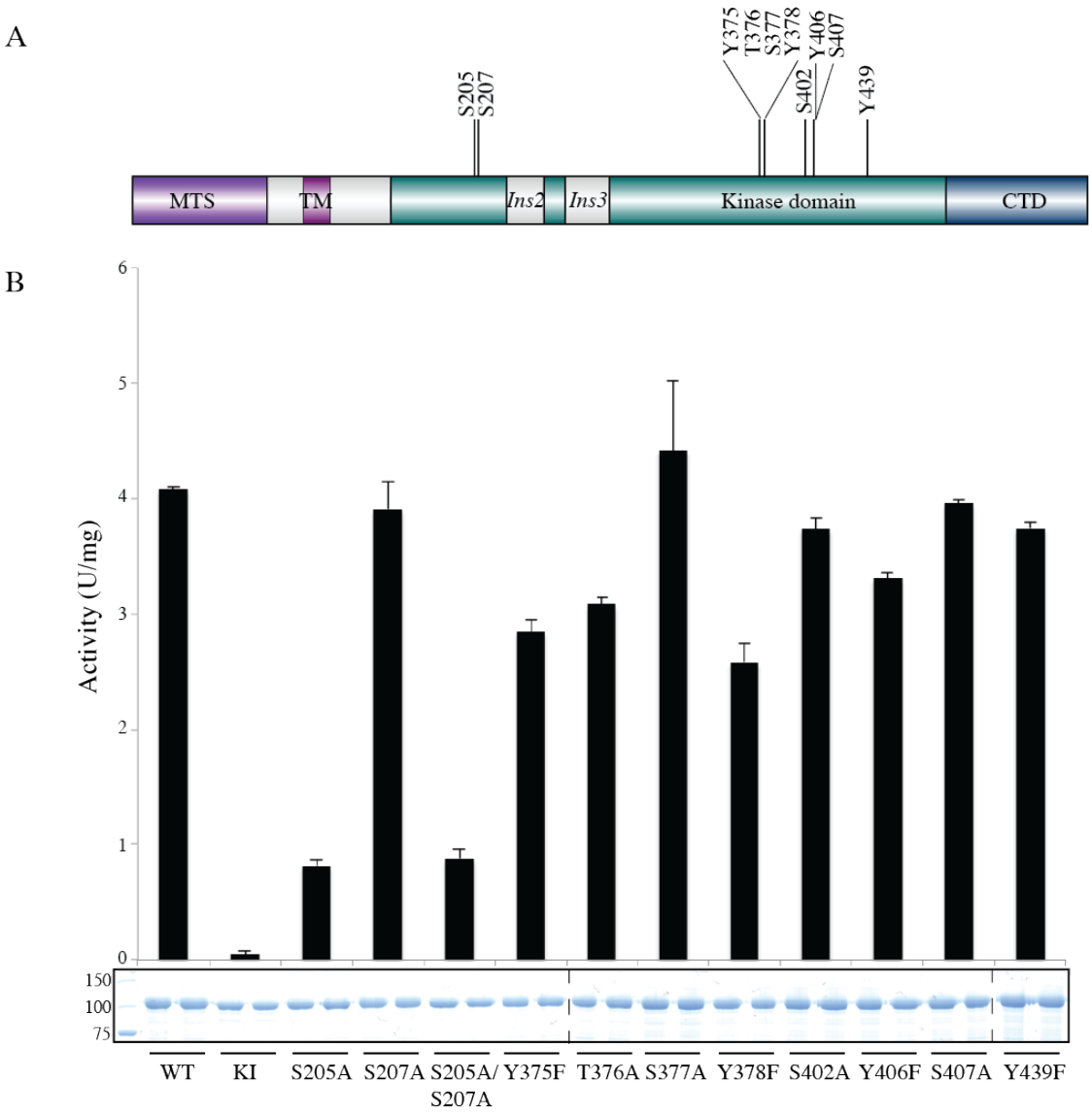

Figure 3.8: Effect of autophosphorylation site mutants on TcPINK1 kinase activity

(A) Schematic of location of autophosphorylation sites in TcPINK1. **(B)** The indicated mutants (1 μg) of full-length TcPINK1 (1-570) were incubated with myelin basic protein (5 μg) in the presence of [γ^{32}P] ATP for 30 min. Reactions were terminated by spotting on P81 paper and incorporation of [γ^{32}P] was detected by scintillation counting. Results are presented as ± SD for a representative experiment undertaken in triplicate (upper panel). Coomassie stained gels showing the relative amounts of PINK1 enzyme used for each assay are shown (lower panel).

3.5.2 *Tribolium castaneum* PINK1 can tyrosine phosphorylate itself but not the substrate myelin basic protein

Although PINK1 belongs to the serine/threonine kinase family, several potential tyrosine autophosphorylation sites were identified in the phosphopeptide mapping experiment. To

further investigate this unexpected finding, and to determine whether TcPINK1 was additionally capable of tyrosine phosphorylating substrates other than itself, the tyrosine kinase activity of full-length wild type and kinase inactive (D359A) TcPINK1 against both itself and myelin basic protein was tested (performed by Dr. Miratul Muqit). Incorporation of [γ^{32}P] ATP was measured by autoradiography and phosphorylation of tyrosine residues by immunoblotting with an anti-phosphotyrosine antibody (4G10) (Figure 3.9). This revealed that PINK1 is able to tyrosine autophosphorylate itself but is unable to phosphorylate tyrosine residues on the substrate myelin basic protein. Further experiments would be necessary to determine the exact residues modified, and it is unclear whether tyrosine autophosphorylation is a unique feature of TcPINK1 under *in vitro* conditions or whether it has broader relevance to PINK1 in general.

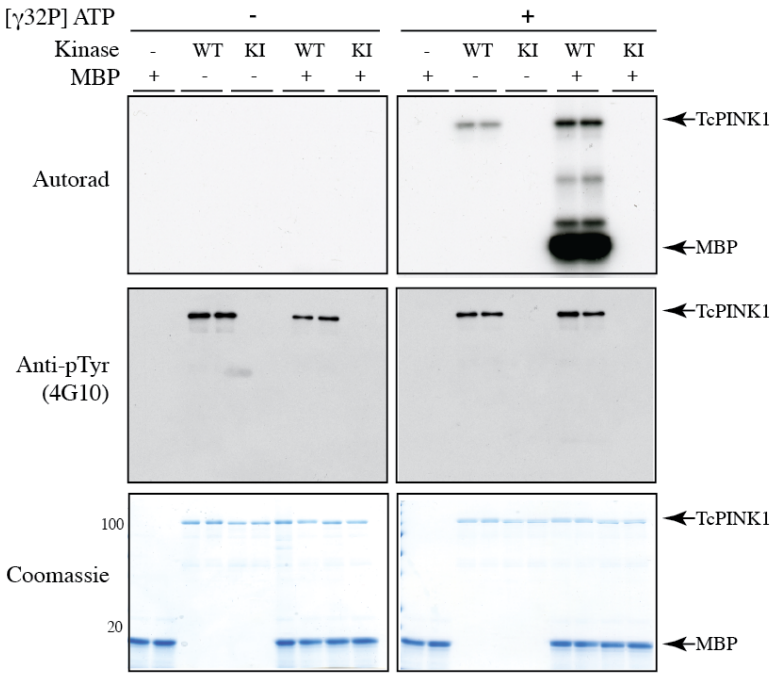

Figure 3.9: Analysis of tyrosine autophosphorylation of TcPINK1

Performed by Dr. Miratul Muqit. Full-length wild type and kinase-inactive (D359A) TcPINK1 (1 μg) was incubated with myelin basic protein (MBP, 5 μg) in the presence or absence of [γ-^{32}P] ATP. Reactions were terminated by addition of SDS sample buffer and analysed by SDS-PAGE (lower panel). Incorporation of [γ-^{32}P] was assessed by autoradiography (top panel). Tyrosine autophosphorylation of enzymes and substrates was detected by blotting with an anti-phospho tyrosine antibody (4G10, middle panel).

3.6 Substrate specificity of TcPINK1

3.6.1 Determination of the optimal peptide substrate, PINKtide, for *Tribolium castaneum* PINK1 using a positional scanning peptide library

One of the major mechanisms by which protein kinases identify and interact with their correct physiological substrates is through recognition of a consensus amino acid sequence surrounding the site of phosphorylation. Since it has previously not been possible to detect the *in vitro* kinase activity of PINK1, there was nothing known about its potential modes of substrate recognition and whether it displays a preference for a particular amino acid consensus sequence. To address this lack of information, it was decided to carry out a positional scanning peptide library assay - a technique for assessing kinase substrate specificity (Hutti et al, 2004). This approach utilises libraries of degenerate peptides with a central serine/threonine amino acid as the phospho-acceptor, a single fixed amino acid at an additional position and randomized amino acids at each other position from -5 to +4 surrounding the phosphorylation site. The phosphorylation of each of these library mixtures by the kinase of interest is assessed, and the strength of phosphorylation reveals the effect of each amino acid at each position in the peptide upon phosphorylation. Using this technique, it is possible to assess the enzymes preference for each amino acid, including phospho-threonine and phospho-tyrosine at each position surrounding the phosphorylation site in an unbiased fashion.

Screening of TcPINK1 against the peptide libraries was carried out as follows (performed by Dr. Mike Begley and Professor Lewis Cantley, Harvard Medical School). Wild type and kinase inactive (D359A) TcPINK1 was incubated with these peptide libraries in the presence of [γ^{32}P] ATP. The relative phosphorylation of each peptide was measured by spotting the biotin-coupled peptides onto a streptavidin membrane, and incorporation of

[γ^{32}P] was detected by phosphoimaging. This experiment revealed that TcPINK1 has a preference for tryptophan at the -5 position, followed by isoleucine at -4, then a strong preference for phospho-tyrosine at -3, and a weak preference for arginine at -2 and -1. The strongest preference was for proline at the +1 position, then again followed by a weak preference for arginine at positions +2 to +4 (Figure 3.10). In total this suggests the optimal peptide substrate for PINK1 would be WIpYRR**S/T**PRRR, where the phospho-acceptor is indicated in bold. Key determinants of TcPINK1 substrate specificity at the peptide level might be the -5 tryptophan, -3 phosphotyrosine and +1 proline in combination with a general preference for a basic peptide (Figure 3.10). The discovery of this sequence allowed the design of an optimal peptide substrate for PINK1, which was designated PINKtide. Its sequence is as follows, with the addition of N-terminal lysine residues to aid solubility: KKWIpYRRSPRRR.

A weighted matrix based on the intensity of phosphorylation at each position in the peptide scanning library (Figure 3.10) was also generated (Appendix 2). This matrix can be used to search the Scansite database (scansite.mit.edu) to return a list of proteins containing the input phosphorylation consensus sequence and that are ranked in order of how closely they conform to the consensus. Searching the database with this matrix did not find any proteins that precisely conformed to the PINKtide sequence, and returned mostly serine and arginine rich proteins such as splicing factors (Appendix 2).

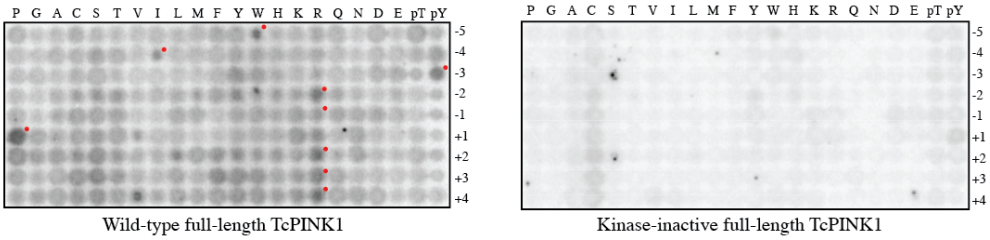

Figure 3.10: Determination of optimal peptide substrate sequence for TcPINK1

Performed by Dr. Mike Begley and Professor Lewis Cantley (Harvard Medical School). Full-length (1-570) wild type (left panel) and kinase inactive (D359A, right panel) TcPINK1 was used to screen a positional scanning peptide library of 198 sets of biotinylated peptides. Reaction products were bound to a streptavidin-coated membrane, washed and visualised by phosphoimaging. Small red dots indicate the residues selected for the PINKtide peptide sequence.

3.6.2 Kinetics analysis of PINKtide mutants reveals a +1 proline is essential for phosphorylation by *Tribolium castaneum* PINK1

After the elaboration of the PINKtide sequence, it was next important to assess which features of the peptide were critical for its phosphorylation by TcPINK1. Three residues were selected as being most likely to contribute to PINK1 specificity towards PINKtide: the -5 tryptophan, -3 phospho-tyrosine and +1 proline. Peptides varying at each of these positions were designed. The -5 position was varied to another large and two small hydrophobic residues (F, L and A) and a positive and negatively charged residue (K and E). The -3 phospho-tyrosine was changed to tyrosine and phenylalanine, phospho- and dephospho-serine and threonine, plus lysine and glutamic acid. Finally, the +1 proline was changed to the same five residues as the -5 position. This choice of alternative residues covers the spectrum of large and small hydrophobic residues, charged residues and in the case of the -3 position, alternative phospho and de-phospho amino acids. Additionally, a version of PINKtide containing tyrosine at the phosphorylation site was included, giving a total of 20 peptides including the original PINKtide.

The ability of full-length MBP-tagged wild type TcPINK1 to phosphorylate each of these new peptides was tested and compared to the phosphorylation of the original PINKtide sequence. This analysis revealed that there was no strong effect upon activity due to variation of residues at the -5 and -3 position, as assessed by variation in the K_m and V_{max} values. However, variation of the +1 proline to any other amino acid tested led to a complete loss of the ability of TcPINK1 to phosphorylate the peptide (Figure 3.11). This demonstrates that the +1 proline is an essential determinant of selectivity for TcPINK1 and suggests that this kinase may possess strong +1 proline-directed activity. In agreement with previous data (Figure 3.9), TcPINK1 was not able to phosphorylate PINKtide with a central tyrosine residue, confirming that it does not possess the ability to carry out tyrosine phosphorylation of non-self substrates.

A

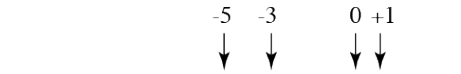

B

Position	Peptide sequence	Km (μM)	Vmax (U/mg)
PINKtide	KKWIpYRRSPRRR	493	8
0	KKWIpYRR**T**PRRR	756	8
0	KKWIpYRR**Y**PRRR	ND	ND
-5	KK**F**IpYRRSPRRR	163	3
-5	KK**K**IpYRRSPRRR	165	2
-5	KK**L**IpYRRSPRRR	381	5
-5	KK**E**IpYRRSPRRR	192	6
-5	KK**A**IpYRRSPRRR	435	8
-3	KKW**I**YRRSPRRR	30	3
-3	KKW**I**FRRSPRRR	63	2
-3	KKW**I**TRRSPRRR	278	3
-3	KKW**I**pTRRSPRRR	970	8
-3	KKW**I**SRRSPRRR	81	3
-3	KKW**I**pSRRSPRRR	117	3
-3	KKW**I**ERRSPRRR	36	2
-3	KKW**I**KRRSPRRR	50	1
+1	KKWIpYRRS**F**RRR	ND	ND
+1	KKWIpYRRS**L**RRR	ND	ND
+1	KKWIpYRRS**A**RRR	ND	ND
+1	KKWIpYRRS**K**RRR	ND	ND
+1	KKWIpYRRS**E**RRR	ND	ND

C

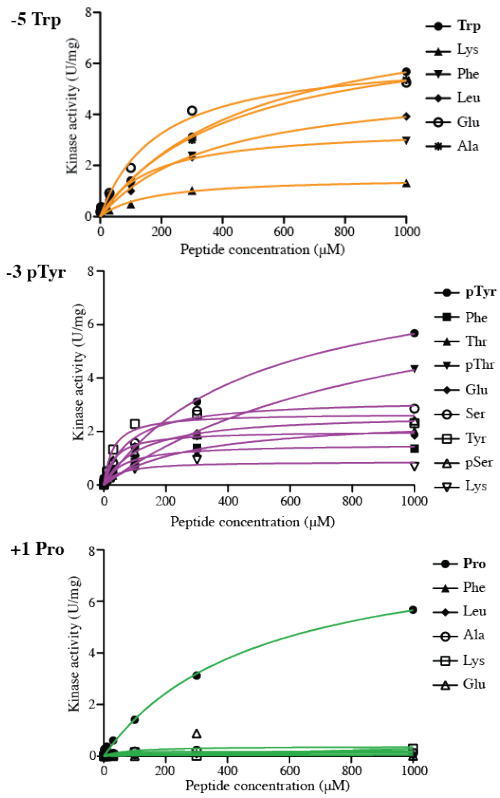

Figure 3.11: Analysis of kinetics of PINKtide phosphorylation

(A) Schematic of PINKtide sequence with -5 (orange), -3 (purple) and +1 (green) positions depicted. **(B)** Kinetic values of phosphorylation of PINKtide and indicated variants by full length (1-570) TcPINK1. Residues that were changed relative to PINKtide are indicated in bold. K_m and V_{max} values were derived by nonlinear regression analysis as described in Materials and methods. ND denotes that a particular peptide was phosphorylated poorly and kinetic values were not determinable. Similar results were obtained in at least 2 experiments. **(C)** Kinetics of phosphorylation of mutants of PINKtide at the 0, +1, -3 and -5 positions by full-length TcPINK1 (1-570). Enzyme was at 1 μg, peptides were at 1μM, 3μM, 10 μM, 30 μM, 100 μM, 300 μM and 1 mM. Reactions were incubated for 30 min in the presence of [γ-^{32}P] ATP. Graphs are colour-coded to match the illustrated PINKtide sequence in (A).

3.6.3 *Tribolium castaneum* PINK1 is not able to phosphorylate the peptide substrates of a diverse array of other protein kinases

To further confirm that PINKtide was a specific substrate for PINK1, we decided to test the ability of TcPINK1 to phosphorylate a diverse selection of peptide substrates that had been previously described for other protein kinases. The substrate peptides selected corresponded to kinases from all families of the kinome except the STE family, ensuring

that the selected peptides represented the preferred substrates of a wide range of kinases. Full-length MBP-tagged TcPINK1 was used to phosphorylate each of these peptides in parallel with PINKtide and incorporation of [γ^{32}P] ATP was detected by scintillation counting. None of the substrate peptides were phosphorylated to a significant extent compared to PINKtide, with weak phosphorylation of the NEK2a and PKB peptide substrates observed (Figure 3.12). This data confirms that PINKtide is the optimal and strongly preferred substrate of TcPINK1.

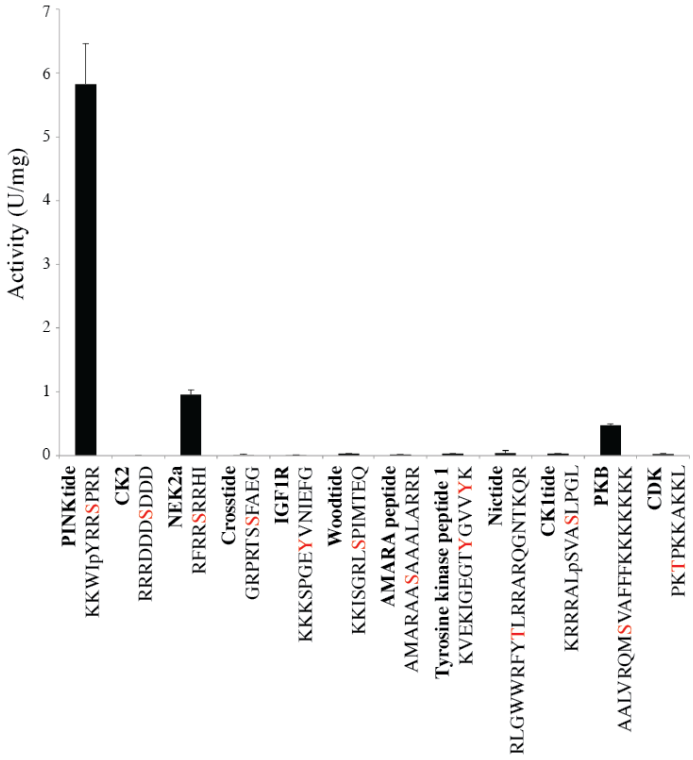

Figure 3.12: Analysis of specificity of TcPINK1 for PINKtide

Full-length TcPINK1 (1-570, 1 µg) was incubated with the indicated substrate peptides (1 mM) for 30 min. Reactions were terminated by spotting onto P81 paper and incorporation of [γ^{32}P] ATP was quantified by scintillation counting. Similar results were obtained in two separate experiments carried out in duplicate; data is presented as average values ± SD. Names of peptides or the kinases for which they are a substrate are indicated, the site of phosphorylation is coloured red in each sequence.

3.6.4 PINKtide is an optimal substrate for *Tribolium castaneum* PINK1 only

In addition to demonstrating that PINKtide is a highly specific and optimal substrate for TcPINK1, it would be interesting to test whether it is a general substrate for other insect PINK1 orthologues, and further to this, whether it is a substrate for human PINK1. The activity of TcPINK1 against PINKtide was measured in parallel with the activity of PhcPINK1, DmPINK1 and hPINK1, expressed in both *Sf9* cells and *E. coli*. Incorporation of [γ^{32}P] ATP was measured by scintillation counting. This experiment demonstrated that TcPINK1 strongly phosphorylated PINKtide, but in contrast, both PhcPINK1 and DmPINK1 phosphorylated PINKtide at a much lower level (Figure 3.13). This suggests that PINKtide is an optimized substrate for TcPINK1 only, as opposed to all insect PINK orthologues. hPINK1 expressed in both *Sf9* cells and *E. coli* did not show any activity against PINKtide (Figure 3.13).

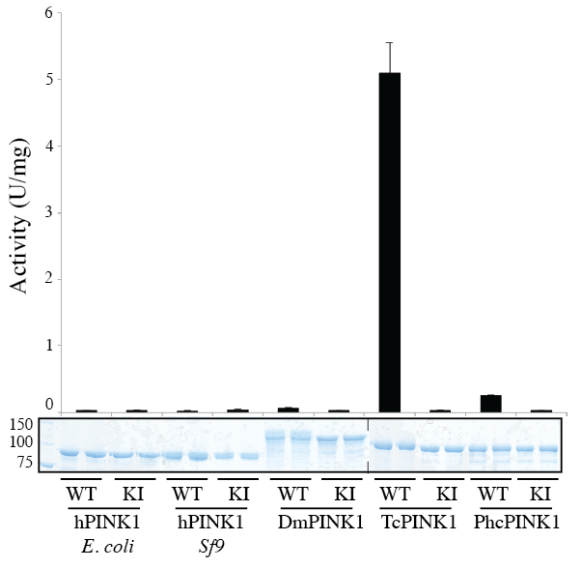

Figure 3.13: Phosphorylation of PINKtide by different PINK1 species

1 µg of wild type N-terminally truncated human PINK1 (125-581) expressed in *E. coli* and *Sf9* cells, full-length *Drosophila* PINK1 (dPINK1, 1-721), *T. castaneum* PINK1 (TcPINK1, 1-570) and *P. humanus corporis* PINK1 (PhcPINK1, 1-575) and corresponding kinase inactive mutants (HsPINK1-D384A, dPINK1-D501A, TcPINK1-D359A, PhcPINK1-D357A), were incubated as indicated with PINKtide (1 mM) and [γ-32P] ATP for 30 min. Reactions were terminated by spotting onto P81 paper and incorporation of [γ^{32}P] ATP was quantified by scintillation counting (upper panel). Amounts of proteins used in the assay

are depicted in the lower panel. Fine dividing lines indicate that proteins were resolved on separate gels and grouped in the final figure.

3.6.5 *Tribolium castaneum* PINK1 cannot phosphorylate putative PINK1 substrates previously described in the literature

Several putative PINK1 substrates have been described in the literature, however previous work in our lab to try and reproduce this data has been unsuccessful due to the lack of detectable *in vitro* activity displayed by human PINK1. Now that an active model of PINK1 is available, it was possible to revisit these findings. The reported substrates chosen for analysis were: TRAP1, a mitochondrial chaperone protein that has been suggested as an interacting partner and direct substrate of PINK1 (Pridgeon et al, 2007); and Omi/HtrA2, a mitochondrial serine protease that was reported to be phosphorylated in a PINK1-dependent manner (Plun-Favreau et al, 2007). Each of these proteins was incubated in the presence of [γ^{32}P] ATP with full-length wild type or kinase inactive (D359A) TcPINK1, PhcPINK1 (kinase inactive: D357A), DmPINK1 (kinase inactive: D501A) and human PINK1 expressed in either *E. coli* (aa 123-581) or *Sf9* cells (aa 125-581), (kinase inactive: D384A). Substrate phosphorylation was detected by autoradiography. No phosphorylation of any substrate by any of the tested kinases was detected, suggesting that may not be genuine PINK1 substrates (Figure 3.14).

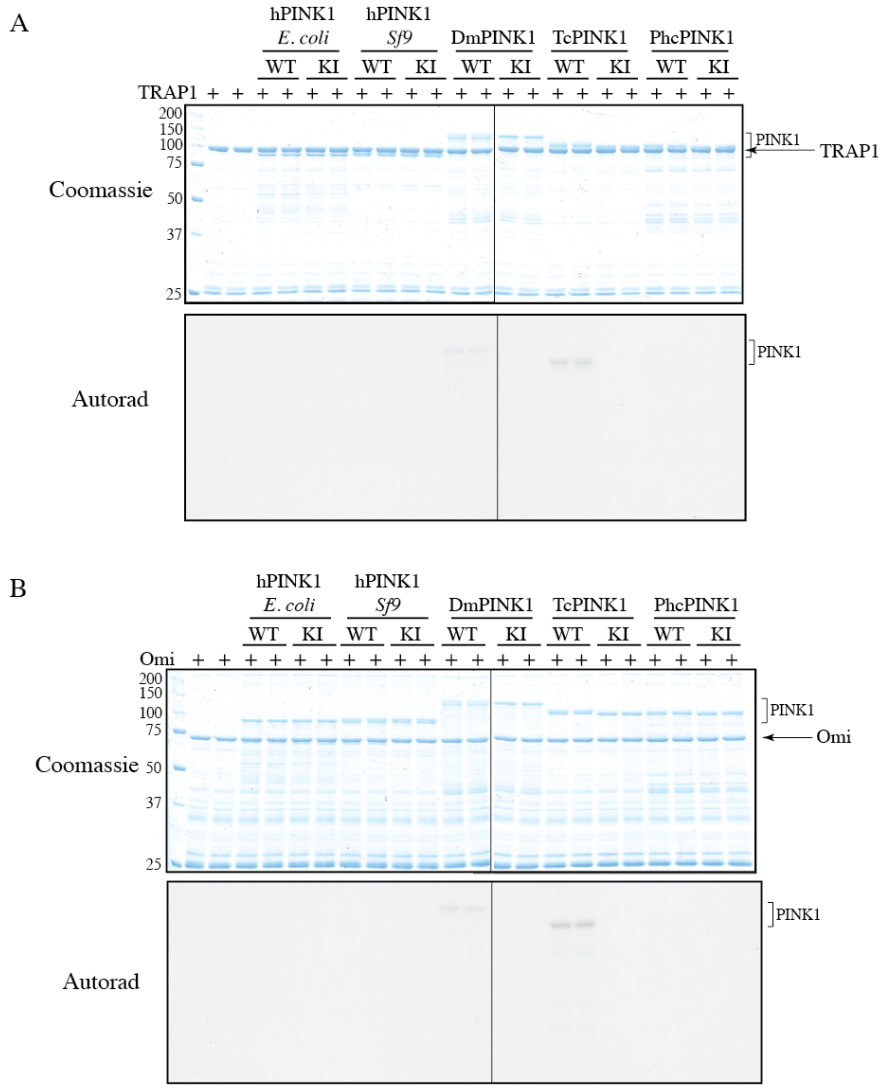

Figure 3.14: Phosphorylation of putative PINK1 substrates/interactors reported in the literature

1 µg of wild type N-terminally truncated human PINK1 (125-581) expressed in *E. coli* and *Sf9* cells, full-length *Drosophila* PINK1 (dPINK1, 1-721), *T. castaneum* PINK1 (TcPINK1, 1-570) and *P. humanus corporis* PINK1 (PhcPINK1, 1-575) and corresponding kinase inactive mutants (HsPINK1-D384A, dPINK1-D501A, TcPINK1-D359A, PhcPINK1-D357A), were incubated as indicated with GST- TRAP1 or GST-Omi (2 µg) and [γ^{32}P] ATP for 30 min. Assays were terminated by addition of loading buffer and separated by SDS-PAGE. Proteins were detected by Coomassie staining (upper panel) and incorporation of [γ^{32}P] ATP was detected by autoradiography (lower panel). Fine dividing lines indicate that reactions were resolved on separate gels and grouped in the final figure.

3.6.6 *Tribolium castaneum* PINK1 can phosphorylate Parkin but not a peptide containing the Parkin phosphorylation site

Further work in our lab utilizing TcPINK1 revealed that the ubiquitin E3 ligase Parkin, also linked genetically to Parkinson's disease, is a substrate for PINK1 (Kondapalli et al, 2012). The mapping of the PINK1 phosphorylation site in Parkin to residue Ser65 revealed an amino acid sequence of surrounding residues quite different to the previously established consensus sequence for TcPINK1 as seen in PINKtide. This raised the question as to whether TcPINK1 would be able to phosphorylate a peptide comprising the phosphorylation site in Parkin. To address this, a peptide was designed with the sequence RDLDQQ**S**IVHIVQR (phospho-acceptor site is highlighted and in bold) and its ability to be phosphorylated by TcPINK1 was examined. This experiment revealed that the Parkin peptide could not be phosphorylated at all by TcPINK1, in comparison to PINKtide, which was robustly phosphorylated (Figure 3.15). This suggests that the interactions that govern Parkin phosphorylation by PINK1 are not mediated solely through the canonical kinase substrate-binding groove, and instead may include interactions distal from the active site.

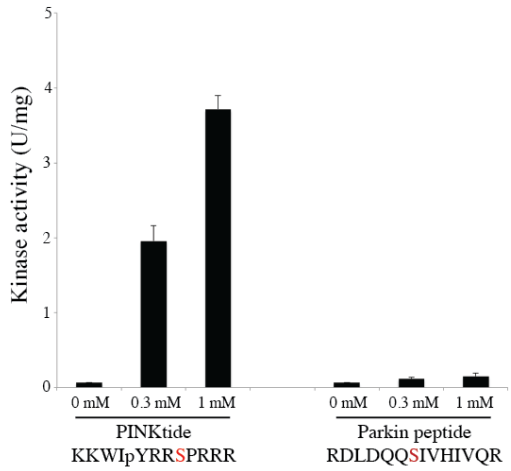

Figure 3.15: Phosphorylation of PINKtide and Parkin serine 65 peptide by TcPINK1

Full-length MBP-tagged TcPINK1 (1 μg) was incubated in the presence of PINKtide or Parkin peptide at the indicated concentrations and [γ^{32}P] ATP for 30 min. Reactions were terminated by spotting onto P81 paper, and quantified by scintillation counting.

3.7 Application of TcPINK1 activity assay to characterise PD-linked mutations and a novel *in vivo* PINK1 knockout model

3.7.1 Parkinson's disease-linked mutations in PINK1 lead to a loss of catalytic activity of *Tribolium castaneum* PINK1

Since 2004, when the first PD-linked missense mutation in PINK1 was described, many other mutations have been identified (Appendix 1). However, due to the lack of a suitable *in vitro* assay for PINK1 activity it has not been possible to test the effect of these mutations on the kinase activity of PINK1. We therefore chose to use the active TcPINK1 as a model to analyse for the first time the effects of PD-linked mutations on PINK1 kinase activity. A subset of the disease mutants comprising only those described as homozygous or compound heterozygous point mutations in patients were selected (Table 3.2). Due to the recessive nature of PINK1 mutations, these were likely to be genuine disease-causing mutations, as opposed to the heterozygous variants whose pathogenicity is less certain. From this list, only the mutations where the original, wild type residue was conserved between human PINK1 and TcPINK1 were selected, resulting in a final total of fourteen missense mutations to be analysed. In addition, three C-terminally truncating nonsense mutations were selected for analysis (Table 3.2).

Mutation	State in patient	Conservation in TcPINK1	Location in TcPINK1
C125G	CH	✔ (C130)	N-terminal non-catalytic region
A217D	HOM	✔ (A194)	Kinase domain (β3)
E240K	CH	✔ (E217)	Kinase domain (αC)
H271Q	HOM	✔ (H247)	Kinase domain (Ins2)
G309D	HOM	✔ (G285)	Kinase domain (Ins3)
L347P	HOM	✔ (L322)	Kinase domain (αE)
L369P	CH	✔ (L344)	Kinase domain (β6)
G386A	HOM	✔ (G361)	Kinase domain (DFG motif)
C388R	HOM	✔ (C363)	Kinase domain
G409V	HOM	✔ (G384)	Kinase domain
P416R	HOM	✔ (P391)	Kinase domain (APE motif)
E417G	HOM	✔ (E392)	Kinase domain (APE motif)
G440E	HOM	✔ (G415)	Kinase domain (αF)
L489P	CH	✔ (L462)	Kinase domain (αH)
W437X	HOM	✔ (W412)	Kinase domain
Q456X	HOM	-	Kinase domain
R492X	CH	✔ (R465)	Kinase domain

Table 3.2: PD-linked PINK1 mutations conserved in TcPINK1

The genotype of the patient in which each mutation was identified is listed as follows: HOM, homozygous; CH, compound heterozygous. The conservation and equivalent residue in TcPINK1 is listed, followed by the location of each mutated residue in TcPINK1. For mutations within the kinase domain, the secondary structure element or conserved motif in which each mutation is found is noted.

Each of the missense mutants were expressed in *E. coli* as full-length MBP-tagged proteins, and their ability to phosphorylate PINKtide in the presence of [γ^{32}P] ATP was determined by scintillation counting. All of the point mutations falling within the kinase domain led to a complete loss of kinase activity, with the exception of the G309D mutation that reduced

activity by about 90% when assessing activity using PINKtide. One mutation tested that fell outside the kinase domain, C125G, led to a more modest reduction in activity, reducing it to about 40% of the wild type levels (Figure 3.16). A similar trend was seen when using myelin basic protein as a substrate although the impact of C125G on phosphorylation was more modest (Appendix 3).

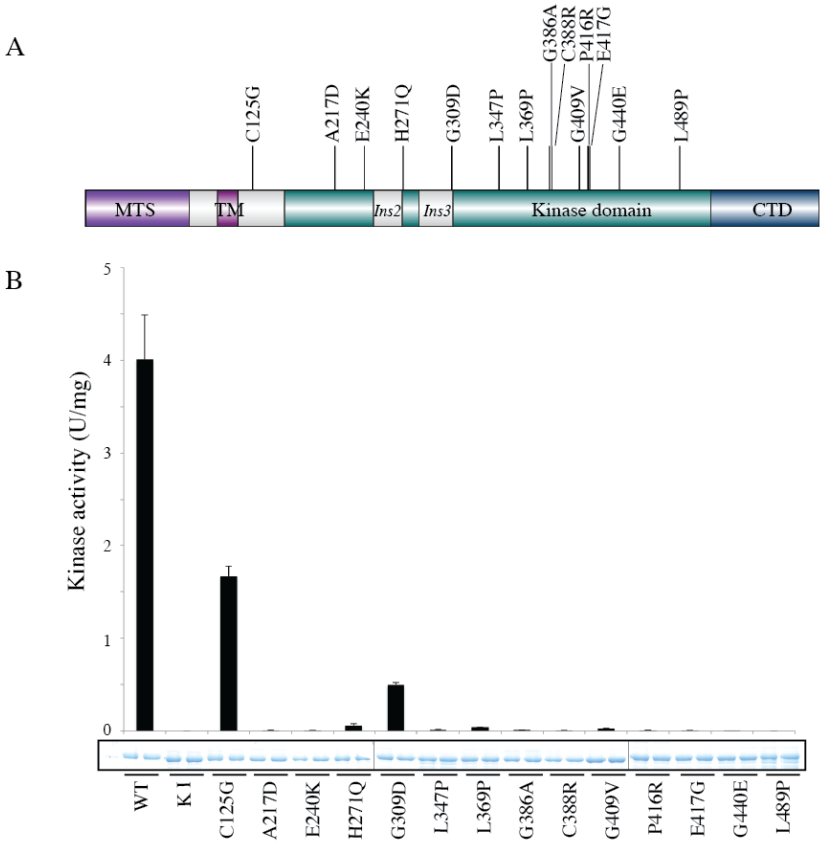

Figure 3.16: Effect of PD-linked missense mutations on TcPINK1 kinase activity

(A) Schematic showing location of point mutations in TcPINK1. Numbering is according to residue numbers in human PINK1. **(B)** Full-length MBP-tagged TcPINK1 enzymes containing point mutations (1 μg) were incubated in presence of PINKtide (1 mM) and [γ^{32}P] ATP for 30 min. Reactions were terminated by spotting onto P81 paper, and quantified by scintillation counting. The results are presented as ± SD for three experiments undertaken in duplicate (upper panel). In the lower panel, representative Coomassie stained gels showing the relative amounts of PINK1 enzyme used for each assay are shown.

Each of the C-terminally truncating mutants were also expressed in *E. coli* as MBP fusion proteins and their activity against PINKtide was tested. All of the truncating nonsense mutations tested led to a total loss of kinase activity (Figure 3.17), which is in agreement

with the previous experiment showing that removal of the C-terminal domain of the protein leads to abrogation of kinase activity (Section **Error! Reference source not found.**). A similar result was observed when the activity of these mutants was tested against myelin basic protein (Appendix 3). The fact that all of the tested mutations led to at least some decrease in kinase activity and in most cases led to a dramatic loss of activity is also in accordance with the genetic information regarding the mode of action of PINK1 mutations.

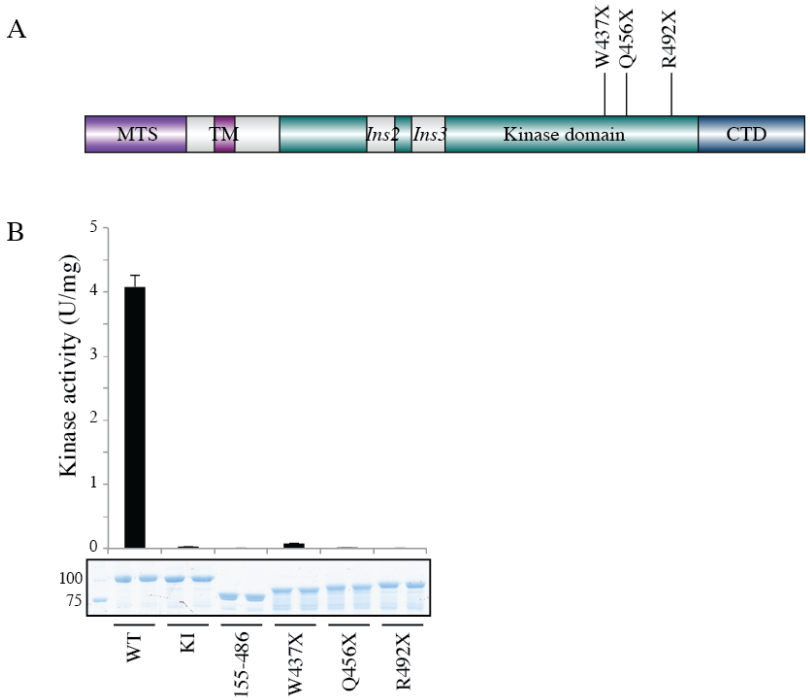

Figure 3.17: Effect of PD-linked nonsense mutations on TcPINK1 kinase activity

(A) Schematic showing location of mutations in TcPINK1. Numbering is according to residue numbers in human PINK1. **(B)** Full-length MBP-tagged TcPINK1 enzymes containing point mutations (1 μg) were incubated in presence of PINKtide (1 mM) and [γ^{32}P] ATP for 30 min. Reactions were terminated by spotting onto P81 paper, and quantified by scintillation counting. The results are presented as ± SD for three experiments undertaken in duplicate (upper panel). In the lower panel, representative Coomassie stained gels showing the relative amounts of PINK1 enzyme used for each assay are shown.

3.7.2 Analysis of a novel Zebrafish PINK1 knockout using TcPINK1 as a model for PINK1 activity

Several well-characterised models for the loss of PINK1 seen in familial PD patients have been previously described, including the PINK1 knockout mouse and the PINK1 null *Drosophila*, and these have both provided insight into the biological functions of PINK1. However, these model systems are not without their limitations. The PINK1 knockout mouse does not show the loss of dopaminergic neurons or the decrease in striatal dopamine levels that are seen in PD patients (Kitada et al, 2007). Although the PINK1 null fly shows loss of dopaminergic neurons, mitochondrial dysfunction and muscular defects (Clark et al, 2006; Park et al, 2006), *Drosophila* are invertebrates and they are evolutionarily distant from humans, meaning studies carried out with fly models may not be relevant to human PD. There is therefore significant interest in the development of novel *in vivo* PINK1 models. *Danio rerio* (Zebrafish) is an ideal intermediate between the fly and the mouse, since Zebrafish are vertebrates and the PINK1 knockout Zebrafish shows a neurodegenerative and mitochondrial phenotype.

Genetic studies in Zebrafish are commonly carried out using morpholino knockout technology, however this has the disadvantage of only inducing a very short-term knockdown, meaning it is not possible to conduct studies in the adult organism. Morpholinos may also produce off-target effects and their use in the PINK1 field has generated conflicting data. Studies in the Bandmann laboratory (University of Sheffield) had generated by mutagenesis a stable Zebrafish line carrying a premature stop codon in the pink1 gene, leading to truncation of the protein at amino acid 431. In order to use this line as a genetic model for studying the effects of loss of PINK1 function, it was necessary to demonstrate that the identified truncating mutation led to a loss of kinase activity. To do this, full-length wild-type Zebrafish PINK1 (ZfPINK1) and the Y431X mutant were

expressed as MBP fusions in *E. coli*. The ability of wild type ZfPINK1 and the Y431X mutant to phosphorylate myelin basic protein in the presence of [γ^{32}P] ATP was assessed. Incorporation of [γ^{32}P] was detected by autoradiography and quantified by scintillation counting (Figure 3.18). This revealed that wild type ZfPINK1 does not display detectable *in vitro* kinase activity against myelin basic protein. A similar result was obtained when the Ubl domain of Parkin was used as a substrate (Appendix 4).

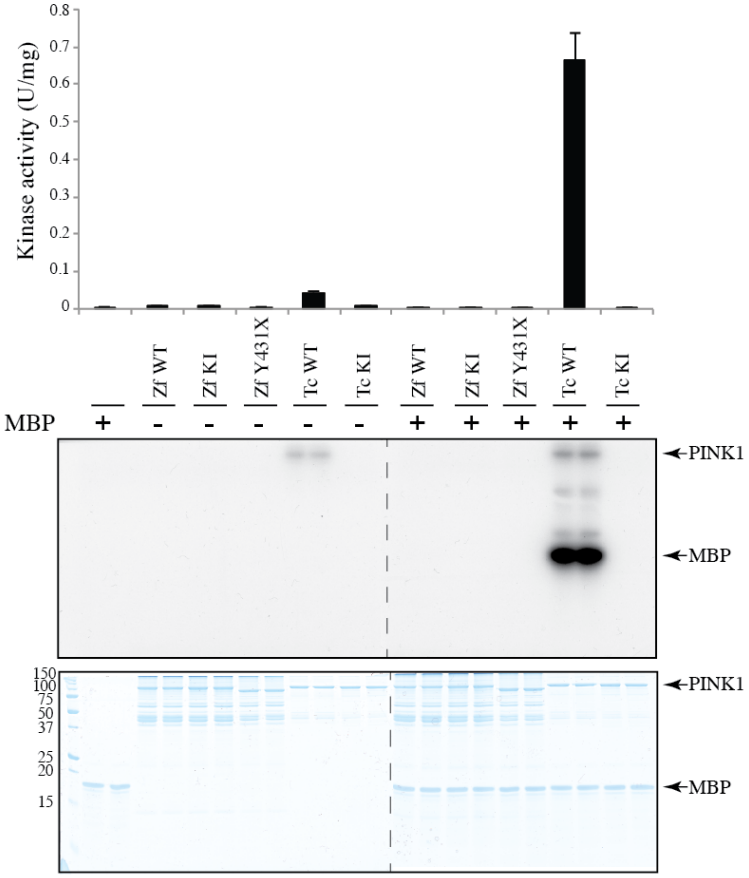

Figure 3.18: *In vitro* activity of Zebrafish PINK1

Full-length MBP-tagged wild type, kinase inactive (D372A) ZfPINK1, Y431X mutant and TcPINK1 wild type and kinase inactive (D359A) (1µg) were incubated in the presence of [γ^{32}P] ATP and MBP (2 µM) for 30 min at 30°C. Assays were terminated by addition of loading buffer and separated by SDS-PAGE. Proteins were detected by Coomassie staining (upper panel) and incorporation of [γ^{32}P] ATP was detected by autoradiography (lower panel). Fine dividing lines indicate that reactions were resolved on separate gels and grouped in the final figure. Phosphorylation was quantified by scintillation counting of excised gel bands.

It was therefore necessary to assess the effect of the Y431X mutation of PINK1 kinase activity by another method, since ZfPINK1 was not active *in vitro*. The equivalent mutation to Y431X in TcPINK1 (Y419X) was therefore introduced and expressed as an MBP fusion protein in *E. coli*. The activity of this mutant against myelin basic protein was then compared to that of full-length wild type TcPINK1. Incorporation of [γ^{32}P] into the substrate was measured by autoradiography and quantified by scintillation counting. This showed that, compared to the wild type protein, the Y419X mutation completely abolished the kinase activity of TcPINK1 against myelin basic protein (Figure 3.19). A similar result was obtained when the Ubl domain of Parkin was used as a substrate (Appendix 4). It is therefore possible to conclude that the Y431X mutation of PINK1 seen in the newly characterised Zebrafish model leads to a loss of kinase activity and that this provides a genuine model of PINK1 deficiency *in vivo*.

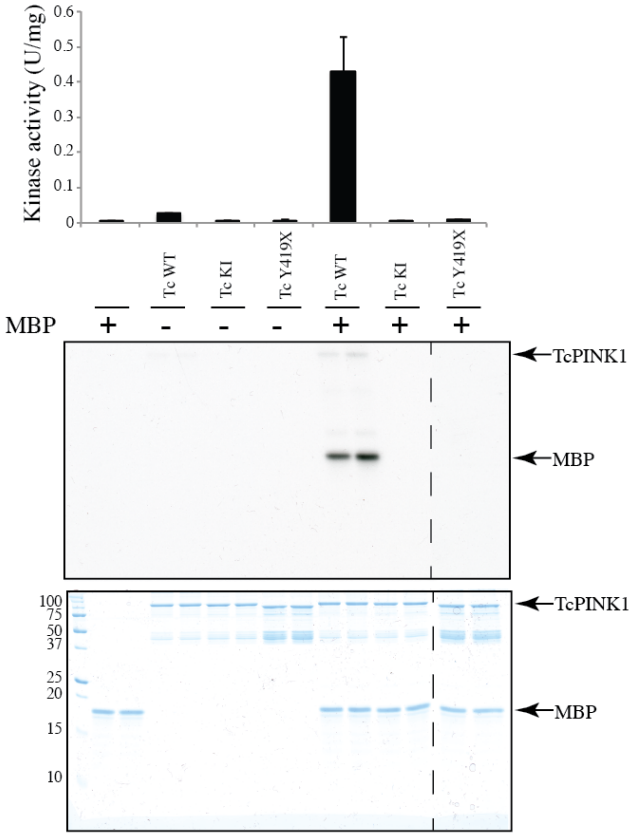

Figure 3.19: Effect of Y419X mutation on TcPINK1 activity

Full-length MBP-tagged wild type and kinase inactive (D359A) TcPINK1 and Y419X mutant (1µg) were incubated in the presence of [γ^{32}P] ATP and MBP (2 µM) for 30 min at 30°C. Assays were terminated by addition of loading buffer and separated by SDS-PAGE. Proteins were detected by Coomassie staining (upper panel) and incorporation of [γ^{32}P] ATP was detected by autoradiography (lower panel). Fine dividing lines indicate that reactions were resolved on separate gels and grouped in the final figure. Phosphorylation was quantified by scintillation counting of excised gel bands.

3.8 Discussion

Although the gene encoding PINK1 was first linked to early-onset Parkinson's disease in 2004, little progress in terms of biochemical understanding had been made in the field since then, in large part due to the lack of a suitable and robust *in vitro* assay for mammalian PINK1 kinase activity. Several human PINK1 assays based on autophosphorylation (Beilina et al, 2005; Silvestri et al, 2005) and a number of putative substrates and interacting partners had been reported over the years, namely the mitochondrial chaperone TRAP1 (Pridgeon et al, 2007) and the serine protease Omi/HtrA2 (Plun-Favreau et al, 2007), but this work has not been reproducible in our lab. The inability to study the catalytic activity of this enzyme led to a dearth of information on its potential substrates, mechanisms of regulation, and innate catalytic properties. To address this problem, I developed a novel assay for PINK1 activity by utilizing the PINK1 orthologue from the species *Tribolium castaneum* (TcPINK1). This approach has been validated by demonstrating that when TcPINK1 is overexpressed in PINK1 null *Drosophila*, the phenotype of these flies is fully rescued to the same levels as observed in a wild type fly (Figure 3.2). This system had previously been used to demonstrate a genetic interaction between PINK1 and Parkin (Clark et al, 2006; Park et al, 2006). In addition, only wild type and not kinase inactive PINK1 can rescue this phenotype (Kim et al, 2008), showing the importance of PINK1 kinase activity for its function. The *Drosophila* system is therefore a robust and well-validated system for assessing PINK1 function *in vivo*.

3.8.1 Why do insect PINK1 orthologues display detectable *in vitro* activity when human PINK1 does not?

Initially, the kinase activity of two insect PINK1 orthologues, TcPINK1 and PhcPINK1 was tested against a panel of generic kinase substrates, revealing both possessed detectable

kinase activity and a preference for the substrate myelin basic protein (Figure 3.3). An immediate question raised by these experiments is why are insect PINK1 orthologues active *in vitro* when hPINK1 is not?

It is possible that hPINK1 requires chaperones not found in *E. coli* to fold correctly and hence be active, whereas TcPINK1 is able to fold correctly in the absence of additional chaperones. In addition, hPINK1 may require post-translational modifications that are not conserved in TcPINK1 for activation of its kinase activity that may not be possible in the *E. coli* cell. To try and address these issues, *Sf9* cells were utilised. These insect expression cells have a chaperone system more closely related to that found in humans and may possess necessary upstream kinases for expressing active enzymes. In spite of this, hPINK1 expressed in *Sf9* cells did not display detectable kinase activity (Figure 3.4 & Figure 3.5). So far, no upstream enzymes carrying out post-translational modifications of PINK1 have been identified despite extensive searching, so it is unlikely this is the reason for the lack of hPINK1 activity.

PINK1 in cells is anchored in the mitochondrial outer membrane by its transmembrane helix. Since transmembrane proteins are often not stable when removed from their membrane environment, hPINK1 may not be stable when it is not anchored to the mitochondria. It is not possible to express full-length hPINK1 in *E. coli*, so instead a truncated construct (aa 123-581) was used. Since this construct does not possess the mitochondrial targeting sequence (MTS) and transmembrane helix, it is possible that this construct is stable even in the absence of mitochondrial localization. In addition, multiple constructs of TcPINK1, including the full-length protein containing both the predicted MTS and transmembrane helix, are stable on overexpression and display detectable kinase

activity (Figure 3.7), suggesting that lack of mitochondrial localization and any subsequent stabilizing effect may not be the cause of the lack of detectable hPINK1 activity.

An immediately obvious difference at the sequence level between the active TcPINK1 and the inactive hPINK1 is the presence or absence of the first kinase domain insertion. If this were acting as an autoinhibitory feature of hPINK1 and was not conserved in TcPINK1 and PhcPINK1, this might explain why TcPINK1 and PhcPINK1 are constitutively active whereas hPINK1 is not. However, we were unable to validate this hypothesis, since deletion of the first insertion in hPINK1 does not restore its kinase activity (Figure 3.6). In addition, testing of the activity of DmPINK1, which has a significantly longer first insertion than hPINK1, showed that this orthologue is also active *in vitro* (Figure 3.4), clearly demonstrating there is no correlation between the presence or absence of this insertion and kinase activity.

A critical factor determining whether or not an enzymatic activity can be assessed *in vitro* is the presence of a specific substrate. There are examples of protein kinases that can only phosphorylate a single substrate, for example the kinase PKR and its substrate eIF2α (Dar et al, 2005), illustrating the importance of using the correct substrate when attempting to measure kinase activity. TcPINK1 displays detectable kinase activity against a variety of generic substrates (Figure 3.3) and more specific substrates such as PINKtide (Figure 3.13), whereas hPINK1 did not appear to display *in vitro* kinase activity against any of these substrates (Figure 3.4, Figure 3.5 & Figure 3.13). However, once a specific substrate, the E3 ligase Parkin, was identified, very low-level *in vitro* activity of immunoprecipitated hPINK1 could be detected (Kondapalli et al, 2012). This activity is considerably weaker than that displayed by TcPINK1, and it now raises the question as to why this is the case.

One important difference that has been observed between TcPINK1 and hPINK1 is in their responsiveness to CCCP-induced depolarization of the mitochondrial membrane. TcPINK1, which shows strong *in vitro* activity, has been found in our lab to be constitutively active when overexpressed in mammalian cells and this activity is not altered by CCCP stimulation (Hazel Rooney, unpublished data). hPINK1, on the other hand, under overexpression conditions shows only very weak *in vitro* activity after CCCP stimulation (Kondapalli et al, 2012). Under basal conditions, hPINK1 is constitutively degraded, but when cells are treated with CCCP, the mitochondrial proton gradient is abolished and the mitochondria becomes depolarized, subsequently leading to the stabilization of PINK1 on the mitochondria (Matsuda et al, 2010).

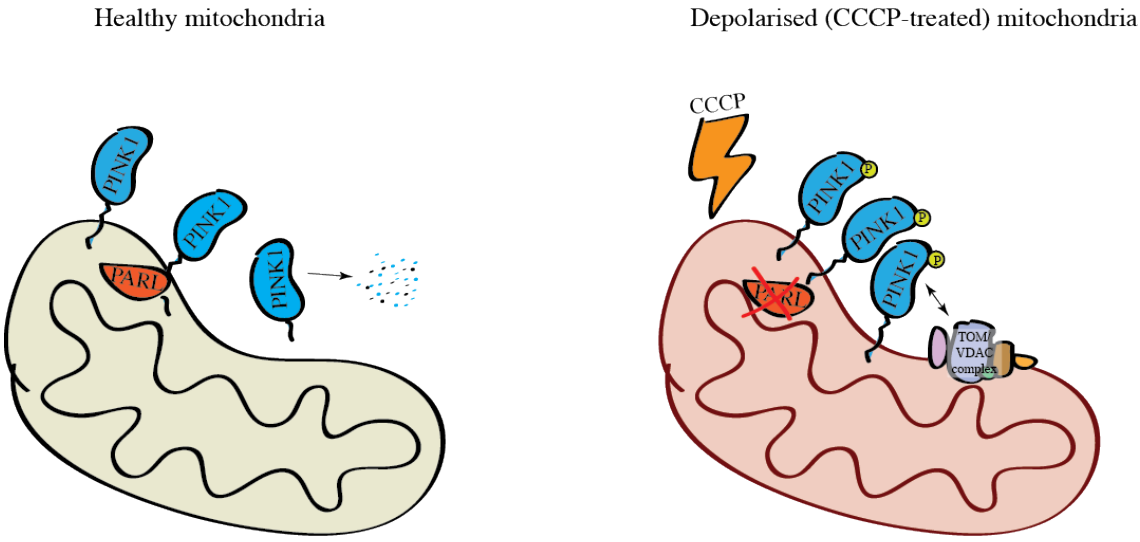

Figure 3.20: Schematic of PINK1 activation by mitochondrial depolarization

(L) In healthy mitochondria, PINK1 is imported then subsequently cleaved by the mitochondrial integral membrane protease PARL then subsequently degraded by the proteasome. **(R)** Upon mitochondrial depolarization, for example with the ionophore CCCP, PARL activity is lost and PINK1 is able to accumulate on the mitochondrial surface. It also then autophosphorylates and forms a complex with proteins such as VDAC and the TOM complex.

After CCCP stimulation, hPINK1 has been shown to form a complex on the outer mitochondrial membrane with a number of other outer mitochondrial membrane (OMM)

proteins, namely the TOM (translocase of the outer membrane) complex (Lazarou et al, 2012) and VDAC2 (voltage-dependent anion-selective channel protein 2) (Chandana Kondapalli, unpublished data). It is not known whether this complex is conserved in *Tribolium castaneum* and whether TcPINK1 forms the same interactions. However, it is clear that when hPINK1 is expressed in *E. coli*, no mitochondria are present and in *Sf9* cells this complex may either not be conserved or will not form due a lack of mitochondrial depolarization. Therefore hPINK1 is unable to interact with these potentially stabilising interacting partners when overexpressed in these two systems. In contrast, these CCCP-dependent interactions do not seem necessary for the activity of TcPINK1.

A further change induced by CCCP stimulation and following mitochondrial depolarization is the appearance of autophosphorylation sites on hPINK1 (Kondapalli et al, 2012; Okatsu et al, 2012). The role of these autophosphorylation events is currently not clear, and the best-characterised site, Thr257, is not detectable until a considerable time after substrate phosphorylation is detected, as judged by Parkin Ser65 phosphorylation (Kondapalli et al, 2012). This suggests that autophosphorylation is not essential for initial activation of PINK1 kinase activity, and may instead be involved in maintenance of activity or reaching maximal activation. TcPINK1, on the other hand, is able to autophosphorylate *in vitro*, in the absence of CCCP stimulation (Table 3.1 & Figure 3.8).

It seems most likely that hPINK1 displays a very low level of basal activity directed towards specific substrates and therefore appeared inactive *in vitro* until the correct substrate was identified. *In vivo,* its activity is facilitated and maintained by a number of factors, such as interacting partners and autophosphorylation, that only occur upon CCCP stimulation and will therefore not be present in recombinant overexpression systems such as *E. coli* and *Sf9* cells. TcPINK1 and the other insect kinases on the other hand, do not

appear to be subject to such complex regulation, presumably due to evolutionary differences between humans and insects, and as such display robust *in vitro* activity that is not modulated by the effects of CCCP.

3.8.2 Requirement of the C-terminal domain for kinase activity

Using the newly established assay for PINK1 activity, it was possible to analyse the requirement of each domain of the protein for kinase activity. This experiment revealed that only truncation of the C-terminal domain had any effect on TcPINK1 kinase activity, abolishing it completely (Figure 3.7). This suggests that the MTS and transmembrane helix are dispensable for the activity of PINK1, at least *in vitro,* where localization will not affect access to substrates. In contrast, the C-terminal domain appears to be essential.

It is common for protein kinases to have regions outside the kinase domain that have an impact on kinase activity, for example CaMKI, which has an autoinhibitory C-terminal domain (Goldberg et al, 1996), and PKA, whose C-terminal extension is important for maintaining the kinase in its active conformation (Batkin et al, 2000). Very little is known about the PINK1 C-terminal domain except that is it predicted to be α-helical in nature. Inspection of the sequence of PINK1 (Figure 3.1) shows that there appears to be no linker region between the end of the kinase domain C-lobe and the start of the C-terminal domain. This, combined with the C-terminal domain's hydrophobicity and probable α-helical nature, suggests that it may form an extension of the primarily α-helical C-lobe and that its removal may destabilize the protein by exposing the hydrophobic core, leading to a loss of kinase activity. Knowledge of the structure of PINK1 would confirm whether or not this hypothesis is correct and may shed light on whether or not this domain plays a role in regulation of kinase activity.

3.8.3 Mechanisms and significance of TcPINK1 tyrosine autophosphorylation

It was observed that TcPINK1 appears to undergo autophosphorylation (Figure 3.3, Figure 3.5 & Figure 3.7). To analyse this, autophosphorylation sites in the protein were mapped. The only site that could be conclusively pinpointed was residue Tyr439 (Table 3.1). This was unexpected as PINK1 is predicted to belong to the serine/threonine kinase family. Anti-phosphotyrosine Western blotting confirmed that TcPINK1 is able to tyrosine autophosphorylate, but cannot tyrosine phosphorylate the substrate myelin basic protein (Figure 3.9).

An example of a protein kinase family that can both tyrosine autophosphorylate and phosphorylate substrates on serine/threonine residues is the DYRK (dual specificity tyrosine-phosphorylation regulated kinase) family. These proteins have been shown to tyrosine autophosphorylate co-translationally and after translation as a mature protein (Walte et al, 2013). The data regarding overexpressed TcPINK1 suggests that it becomes tyrosine autophosphorylated whilst it is inside the *E. coli* cell, since this autophosphorylation is visible by Western blotting before further incubation with ATP (Figure 3.9). However, further experiments would need to be done to determine whether or not this is a co-translational event. Furthermore, it is unclear whether this tyrosine autophosphorylation is relevant to hPINK1, since no tyrosine autophosphorylation sites have been observed on the human protein (Chandana Kondapalli and Miratul Muqit, unpublished data).

With regards to the mechanism by which TcPINK1 undergoes tyrosine autophosphorylation, a key determinant of specificity for serine/threonine versus tyrosine kinases is a single amino acid in a region of the activation segment known as the P+1 loop (Nolen et al, 2004). In serine/threonine kinases, this residue is a serine or a threonine, and

in tyrosine kinases, it is a proline essential for interacting with the phospho-acceptor tyrosine residue. In dual-specificity kinases, for example in the DYRKs, it is a serine (Aranda et al, 2011). In TcPINK1, and in PINK1 from all other species, this amino acid is a conserved asparagine (Figure 3.1). The significance of this for PINK1 substrate selectivity is not clear, and further experiments would be necessary to define how this amino acid contributes to substrate selectivity, for example mutagenesis to either serine/threonine or proline and analysis of the effect on tyrosine/serine/threonine autophosphorylation. In addition, the crystal structure of TcPINK1 in complex with its substrates might aid in defining the contribution of this region to serine/threonine versus tyrosine substrate selectivity.

3.8.4 Autophosphorylation in TcPINK1 and hPINK1

Several putative autophosphorylation sites were identified on each peptide found in the site-mapping experiment with the exception of the peptide containing Tyr439. A mutagenesis study revealed that only mutation of Ser205 to alanine and a double mutation of Ser205 and Ser207 led to any disruption of kinase activity, in both cases reducing it to about ¼ of the wild-type activity (Figure 3.8). Based on these findings, it is most likely that Ser205, located in the loop between the β3 sheet and the αC helix, is a relevant autophosphorylation site and that it may play a role in regulating PINK1 activity. However, further studies leading to more conclusive mapping of potential site would be needed in future.

The equivalent residue in hPINK1, Ser228, was identified by mass spectrometry and mutagenesis as being autophosphorylated in a manner dependent on mitochondrial depolarization (Okatsu et al, 2012). The authors suggest that this site is necessary for

recruitment of the PINK1 substrate Parkin to the mitochondria and did not examine the effect of mutating this residue on PINK1 activity. In addition, the authors identified another site by mutagenesis, Ser402, located in the activation loop of human PINK1. They propose a structural model of hPINK1 and suggest that the two sites, Ser228 and Ser402, are located very close together (Okatsu et al, 2012). However, our lab has never observed any evidence of Ser402 phosphorylation despite conducting multiple experiments searching specifically for activation loop phosphorylation (Miratul Muqit, unpublished data). The best-characterised PINK1 autophosphorylation site is Thr257 (Kondapalli et al, 2012), substituted to a glutamic acid in TcPINK1. Since this site is not required for activation of human PINK1, it indicates that there is a discrepancy between the autophosphorylation observed in hPINK1 and TcPINK1.

3.8.5 Mechanisms of substrate specificity

Since at the time of this work there was a lack of information on substrates of PINK1 and it was not possible to reproduce any of the reported substrates in the literature (Figure 3.14), we sought to investigate the substrate specificity of PINK1 at the peptide level. There are well known examples of protein kinases that have a strict amino acid consensus sequence for phosphorylation, for example PKB and PKA (Pearce et al, 2010), where it is possible to predict their potential substrates by searching for this amino acid motif in other proteins. Although this approach will not allow identification of all substrates and may result in false positives, having such knowledge for PINK1 would aid greatly in the search for its substrates.

To this end, we carried out a positional scanning peptide library assay to determine the optimal peptide substrate for TcPINK1, resulting in the design of the peptide

KKWIpYRRSPRRR, designated PINKtide (Figure 3.10). Kinetics analysis of variants of PINKtide revealed that in agreement with previous data (Figure 3.9), TcPINK1 was not able to phosphorylate a peptide with tyrosine at the phospho-acceptor site and was able to phosphorylate serine and threonine equally well. Otherwise, with regards to levels of phosphorylation, only variation of the +1 position (proline) position had a strong effect; mutation of this residue led to a complete loss of phosphorylation of the peptide (Figure 3.11).

Several other protein kinase families are well known to demonstrate +1 proline-directed activity, including the CDKs (Brown et al, 1999) and MAPKs (Pelech, 1995). The structure of CDK2 in complex with a peptide substrate has been determined (Brown et al, 1999), which reveals the mechanism of +1 proline-directed specificity in this enzyme. Part of the activation loop adopts an unusual conformation that results in the lack of a hydrogen bond acceptor at this site, thus blocking the binding of any amino acid but proline, which is not able to form this hydrogen bond and can bind comfortably. Without knowledge of the crystal structure of PINK1, it is not possible to say if a similar mechanism exists or to speculate on which residues in the protein may be determining its specificity for peptides with a +1 proline.

Finally, to confirm that PINKtide is truly a specific substrate for TcPINK1, we tested the ability of TcPINK1 to phosphorylate a panel of different peptide substrates for kinases from a wide range of different kinome families. As expected, TcPINK1 was not able to phosphorylate any other peptide to a significant degree, confirming its specificity for PINKtide (Figure 3.12). Included in the peptide panel was the substrate for the DYRK kinases, Woodtide, which also contains a +1 proline (Woods et al, 2001). Interestingly, despite TcPINK1 displaying a marked preference for substrates with a +1 proline, it was

not able to phosphorylate Woodtide, indicating that a +1 proline is necessary but not sufficient for TcPINK1 phosphorylation (Figure 3.12). Attempts to use the PINKtide sequence to search for putative PINK1 substrates using a weighted matrix to search the Scansite database were not successful and did not return any promising candidate substrates (Appendix 2).

3.8.6 Substrate specificity at the peptide versus the protein level

The discovery of TcPINK1 also allowed the subsequent discovery of the first well-validated PINK1 substrate, the ubiquitin E3 ligase Parkin (Kondapalli et al, 2012). This facilitated detailed studies into how Parkin is activated by PINK1 phosphorylation (Kazlauskaite et al, 2014a) and played a part in the later discovery of another PINK1 substrate and Parkin activator, ubiquitin (Kane et al, 2014; Kazlauskaite et al, 2014b; Koyano et al, 2014). Upon discovery of the PINK1 phosphorylation site in Parkin, it became apparent that the amino acid sequence surrounding the site of modification (RDLDQQ**S**IVHIVQR) in no way resembled the PINKtide sequence previously described as being the optimal substrate for TcPINK1 (KKWIpYRR**S**PRRR). The +1 proline that had been shown to be critical for PINK1 phosphorylation was absent, and the peptide was slightly acidic. The ability of TcPINK1 to phosphorylate this peptide was tested, and no phosphorylation was detected (Figure 3.15). Since TcPINK1 is able to phosphorylate the intact Ubl domain, this strongly suggests that TcPINK1 is able to phosphorylate protein substrates on a residue with a flanking sequence strongly different from that of its optimal peptide substrate.

Recognition of substrates in the region directly surrounding the site of phosphorylation is mediated by the amino acids forming the active site groove of a protein kinase. However,

this is not the only method used by kinases to identify their substrates. Many protein kinases form additional interactions with the substrate using regions of the protein away from the active site cleft (reviewed in (Ubersax & Ferrell, 2007)), An example of such a distal interaction is the DEF sites on MAP kinases. This family of kinases has an overlapping substrate specificity at the peptide level, but unique specificities for binding partners at their DEF sites allows them to phosphorylate only their precise targets (Sheridan et al, 2008). In addition, binding of a substrate at the DEF site increases their affinity for the substrate dramatically when compared to an isolated peptide, allowing for more efficient phosphorylation.

A further instance of distal sites contributing to kinase specificity is provided by protein kinase B (PKB). PKB possesses a strong consensus sequence including a preference for a -5 arginine, which is absent in one of its substrates, ATP citrate lyase (Berwick et al, 2002). Despite this, PKB is still able to efficiently phosphorylate this protein *in vivo*. In addition, the kinase DYRK1A is able to phosphorylate substrates that conform precisely, partially or not at all to its optimal peptide consensus sequence (Soundararajan et al, 2013), giving another illustration of the flexibility of substrate recognition by protein kinases. Examples such as this suggest a mechanism for how TcPINK1 may be able to display highly differing substrate preferences at the peptide and whole protein level. Further studies would be necessary to identify regions on TcPINK1 that may required for binding and efficient phosphorylation of Parkin and ubiquitin. Furthemore, knowledge of the three-dimensional structure of TcPINK1 would shed light on the interactions formed in the peptide binding groove and how this region might contribute to substrate specificity.

3.8.7 Effects of Parkinson's disease-linked mutations on kinase activity

Finally, the effect of Parkinson's disease (PD) linked mutations on PINK1 kinase activity was tested. To date there has been no thorough analysis of the effect of disease mutations on PINK1 catalytic activity and so this was an important question to address. A panel of mutations that were present as homozygous or compound heterozygous mutations in patients and where the wild type residue was conserved between hPINK1 and TcPINK1 was selected (Table 3.2). These mutations were introduced into full-length TcPINK1 and the kinase activity of the resulting mutant enzymes was tested. In addition, the effects of three C-terminally truncating mutations were tested. More truncating mutations have been described, but these truncate the protein within the kinase domain and so would clearly lead to a loss of activity.

The results of these experiments showed that all point mutations falling inside the kinase domain completely abolished or severely reduced kinase activity (Figure 3.16). The most active mutant within the kinase domain is G309D, which displayed around 10% of the wild-type activity against PINKtide. Interestingly, the sole mutation outside of the kinase domain, C125G, only reduced kinase activity against PINKtide to just under half of wild type levels. This suggests that this mutation affects PINK1 function in a way distinct from directly interfering with catalysis. It has been shown in single-pass transmembrane proteins that the region of the protein close to the membrane on the cytoplasmic side, know as the juxtamembrane region, is often a disordered region that is enriched for protein-protein interaction motifs (Stavropoulos et al, 2012). The region of PINK1 between the transmembrane helix and kinase domain, where Cys125 is located, is predicted to be disordered and may be a binding site for interacting partners. If this is the case, mutation of this residue could well lead to a loss of interactions with a regulatory partner or substrate and the subsequent manifestation of PD. Alternatively, since this site is close to the

transmembrane helix, mutations could lead to defective mitochondrial import or processing, since PINK1 is known to undergo several proteolytic cleavage events upon mitochondrial import, notably by the proteases PARL (Deas et al, 2011) and MPP (Greene et al, 2012).

Each of the C-terminally truncating mutations tested also led to a complete loss of kinase activity relative to the wild-type protein (Figure 3.17), which is in agreement with previous data (Figure 3.7) showing that a construct lacking the C-terminal domain has no *in vitro* kinase activity. All of the data regarding point mutations and truncating mutations leading to a general decrease in kinase activity is supported by the genetic evidence linking PINK1 to PD, which shows that both copies of the *pink1* gene must be mutated before the patient develops a disease phenotype, suggesting mutations are loss-of-function mutations.

Various other studies have analysed the effect of PD-linked PINK1 mutations on several different parameters and have led to findings that are in agreement with our results. A study on PINK1 autophosphorylation (Okatsu et al, 2012) examined the effect of mutations upon PINK1 autophosphorylation and found that mutations outside the kinase domain did not affect autophosphorylation, whereas mutations inside the kinase domain led to a loss of autophosphorylation, with the exception of the G309D mutation that only reduced it slightly. An additional study on PINK1 activators also confirmed that the G309D mutation displays reduced but still detectable activity (Hertz et al, 2013). Studies in *Drosophila* provided further evidence for the effect of PINK1 mutations in the kinase domain, demonstrating that PINK1 mutants cannot rescue the PINK1 null phenotype (Song et al, 2013). These studies provide further evidence to consolidate our findings.

3.9 Conclusion

To conclude, the discovery of TcPINK1 has provided the PINK1 field with a valuable tool. It has facilitated the identification of several PINK1 substrates, greater understanding of PINK1 autophosphorylation, and regulation of its substrate the E3 ligase Parkin, and has generally advanced understanding of PINK1 biology. In addition, it has provided insight into its basic catalytic properties, most importantly the effect of Parkinson's disease-linked mutations on PINK1 kinase activity.

Chapter 4

4 Crystallisation of a PINK1 orthologue from the insect species *Tribolium castaneum*

4.1 Introduction

At the start of this project, there was no crystal structure available for PINK1. Although the crystal structures of multiple members of the protein kinase family have been determined over the years, revealing a highly conserved general architecture of the protein kinase fold, PINK1 possesses a number of unusual features which make its structure of particular interest. The domain architecture of PINK1 is depicted below (Figure 4.1). PINK1 is the only kinase to be targeted to the mitochondria via a mitochondrial targeting sequence (MTS) and anchored there by a transmembrane domain. The transmembrane domain is predicted to be α-helical and to extend from residues 94-110. Within the kinase domain itself, PINK1 possesses three insertions in its N-lobe between the conserved secondary structure elements that make up the protein kinase fold. The first is between the β2 and β3 strands, the second between the αC helix and the β4 strand, and the third falls between the β4 and β5 strands. The function and orientation of these insertions with respect to the rest of the kinase domain is unknown. Finally, PINK1 has a C-terminal domain, again of unknown function, but which has been shown to be essential for kinase activity (Section **Error! Reference source not found.**). This domain consists of approximately 70 amino acids and is predicted to be α-helical in nature. Knowledge of the crystal structure of PINK1 might shed light on the nature of some of these features and might hint towards their potential roles in PINK1 function.

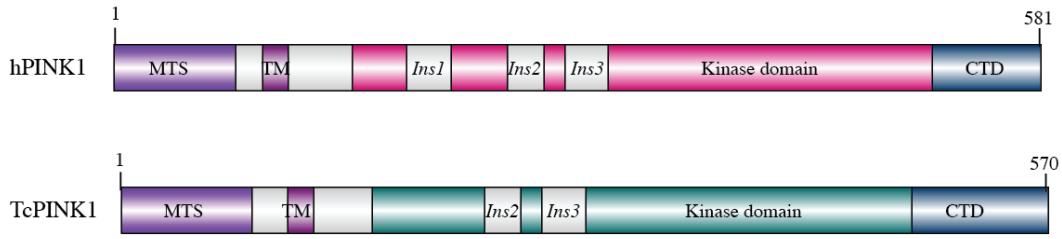

Figure 4.1: Schematic of human PINK1 and TcPINK1 domain architecture.

MTS: mitochondrial targeting sequence; TM: transmembrane helix; Ins1-3: kinase domain insertions 1-3; CTD: C-terminal domain.

Furthermore, due to the lack of a PINK1 structure, there is no molecular explanation for the effects of Parkinson's disease-linked mutations upon PINK1. Confirmed disease-causing homozygous and compound heterozygous mutations have been found throughout the protein but mainly fall within the kinase domain. Several studies have attempted to categorise PD-linked mutations based upon their likely effect on protein stability and activity (Cardona et al, 2011; Sim et al, 2012), however without knowledge of the PINK1 crystal structure, it is not possible to offer a definitive explanation for the observed effects on kinase activity (Section 3.7.1).

In order to address these questions, I undertook the structural characterisation, by macromolecular crystallography, of a more tractable homologue of human PINK (hPINK1) from the species *Tribolium castaneum* (TcPINK1). TcPINK1 was chosen for this purpose since it expresses readily in *E. coli* and with a higher yield and purity than human PINK1. Previous work has demonstrated that TcPINK1 is a functional orthologue of hPINK1 (Section 3.2) and therefore any findings made from the crystal structure of TcPINK1 ought to be possible to translate to hPINK1.

4.2 Optimisation of purification conditions for TcPINK1

4.2.1 Selection of the optimal affinity tag for purification of TcPINK1

Previous work with TcPINK1 (Chapter 3) had been carried out using a maltose binding protein (MBP) tag, since it can help to solubilise unstable proteins. It was decided to test the expression of a construct comprising the kinase domain, C-terminal domain and N-terminal region of TcPINK1 with alternative affinity tags to determine which tag and purification system gave the best yield and purity for crystallography purposes. Wild type and kinase inactive (D359A) TcPINK1 128-570 were expressed on a small scale in *E. coli* BL21-CodonPlus cells with either a 6-His, GST or MBP affinity tag. The resulting recombinant proteins were affinity purified with their respective affinity resins (6-His: Ni-NTA resin; GST: glutathione resin; MBP: amylose resin) and the results were analysed by SDS-PAGE (Figure 4.2). This showed that His-tagged TcPINK1 appeared to express to a high level and purity compared to the GST and MBP tags. In addition, the His-tag has the advantage that it is a small tag and so it may not be essential to remove it before beginning crystallisation trials. Furthermore, the nickel affinity purification system is very versatile and can easily yield protein of high purity.

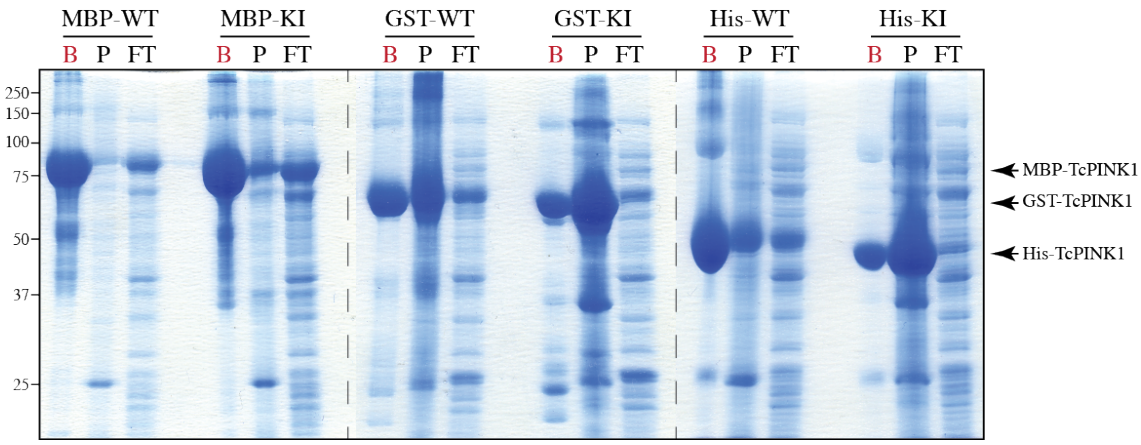

Figure 4.2: Comparison of TcPINK1 expression with different affinity tags

MBP: maltose binding protein; GST-glutathione-S-transferase; His: hexahistidine. B: recombinant protein bound to affinity beads; P: insoluble pellet fraction; FT: flow-through not bound to affinity resin.

4.2.2 Large-scale expression of His-tagged TcPINK1 128-570 (D359A)

Expression of kinase inactive His-TcPINK1 128-570 (D359A) was carried out on a large scale in *E. coli* BL21 CodonPlus cells and the resulting protein was affinity purified using nickel resin. The protein was then subjected to anion exchange purification. The chromatogram showed a very poor UV_{280} profile with a single extremely broad and low peak (Figure 4.3A). SDS-PAGE analysis showed that TcPINK1 was present throughout the peak and the contaminants present in the input sample had not been removed (Figure 4.3B). This suggests that the protein may not be stable under the low salt conditions required for binding of the protein to the ion exchange column.

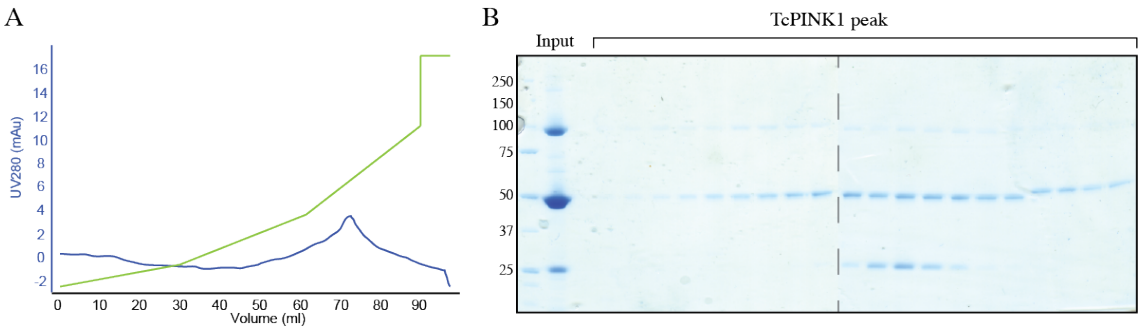

Figure 4.3: His-TcPINK1 128-570 (D359A) expression and purification

(A) Chromatogram of SourceQ anion exchange chromatography. Blue trace: UV_{280} absorbance; green trace: Buffer B gradient. **(B)** SDS-PAGE analysis of anion exchange chromatography. Input: protein before purification.

4.2.3 Optimisation of the buffer conditions used for purification of His-tagged TcPINK1

Since His-tagged TcPINK1 had performed poorly in previous purification attempts, it was decided to try and optimise the buffer conditions used for nickel affinity chromatography to promote protein stability and purity. A single large culture was split and used for multiple nickel affinity purifications carried out at a range of pH values, from pH 5.0 to 10.0. All buffers utilised throughout the protocol were adjusted to the required pH. SDS-PAGE analysis of the protein eluted from the nickel resin revealed that recombinant

protein was only obtained at pH values above 7.0 and that the yield decreased above pH 9.0 (Figure 4.4A). Separate analysis of the eluted protein showed that the purity was highest at pH 9.0 (Figure 4.4B). In addition, the salt concentration of the buffers used was optimised. As before, multiple nickel affinity purifications were carried out in which the salt concentration of the buffers was varied from 75 mM to 750 mM. The eluted protein was subjected to centrifugal concentration and the maximum concentration reached before the protein began to precipitate was measured (Figure 4.4C). This showed that the highest TcPINK1 concentration was obtained using buffers containing 350 mM NaCl. As a result the composition of the buffers used to purify TcPINK1 were changed where necessary to pH 9.0 and 350 mM NaCl.

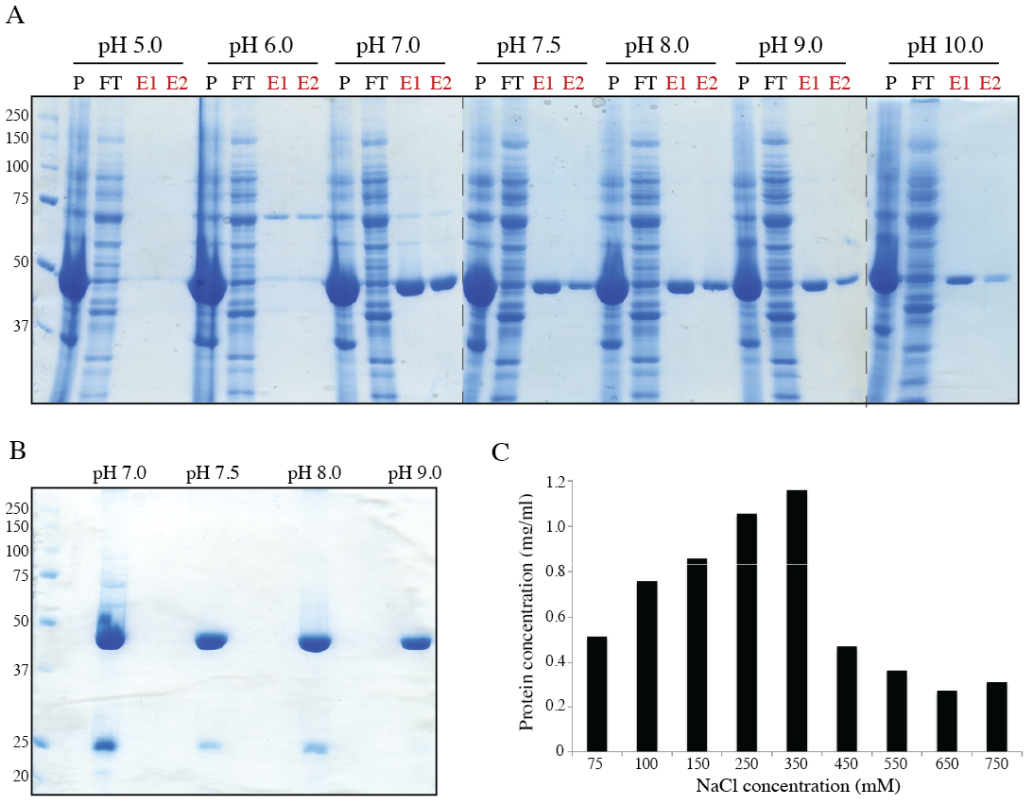

Figure 4.4: Optimisation of nickel affinity purification protocol to maximise His-TcPINK1 purity and stability

(A) SDS-PAGE analysis of nickel affinity purification from pH 5.0-10.0. P: insoluble pellet fraction; FT: flow-through not bound to nickel resin; E1-2: eluted recombinant His-TcPINK1. **(B)** SDS-PAGE analysis of concentrated eluted TcPINK1 purified at pH 7.0-9.0. **(C)** Graph showing maximal protein concentration (mg/ml) obtained while concentrating eluted TcPINK1 at salt concentrations from 75 to 750 mM.

4.2.4 Optimised large-scale purification of His-tagged TcPINK1 128-570 (D359A)

His-TcPINK1 128-570 (D359A) was overexpressed on a large scale in *E. coli* BL21-CodonPlus cells and the resulting protein was purified using buffers with the previously determined optimal pH and salt concentration. The eluted protein was then further purified by anion exchange. The chromatogram showed a large asymmetrical peak (Figure 4.5A) and SDS-PAGE showed that the entire peak contained TcPINK1 with visible contaminants (Figure 4.5B). This suggested that despite optimisation of the buffers used for the purification, the protein is still not stable.

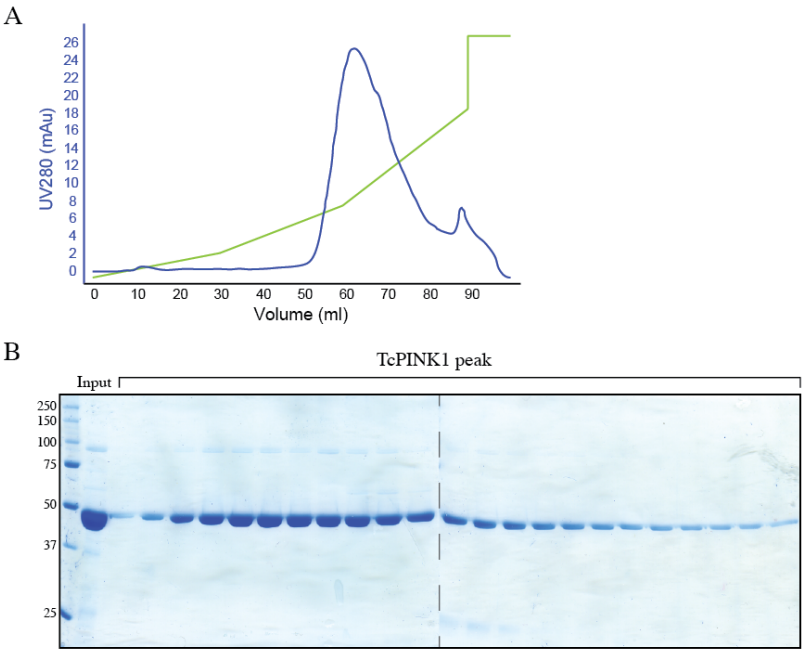

Figure 4.5: Purification of His-TcPINK1 128-570 (D359A) using optimised purification protocol

(A) Chromatogram of SourceQ anion exchange purification of TcPINK1. Blue trace: UV_{280} absorbance; green trace: Buffer B gradient. **(B)** SDS-PAGE analysis of TcPINK1 eluted from anion exchange column. Input: protein sample before anion exchange.

4.3 Purification and crystallisation trials of TcPINK1

4.3.1 Test expressions of TcPINK1 with the His-SUMO tag system: Constructs with N-terminal boundaries between residues 128 and 165

Since attempts to express and purify TcPINK1 using a His-tag had been unsuccessful due to protein instability, it was decided to utilise the His-SUMO tag system, which comprises the small ubiquitin-like protein SUMO with an N-terminal 6-His tag (Lee et al, 2008). This enables purification using the nickel affinity chromatography method and provides the benefits of a solubilising tag through the SUMO moiety. Furthermore, the tag can easily be removed in a sequence-independent manner by cleavage with the highly efficient protease SENP1, which recognises the three-dimensional structure of SUMO and cleaves immediately after the C-terminus of the SUMO molecule. Since both the cleaved SUMO tag and the protease have a His-tag, they can easily be removed after cleavage by incubation with nickel resin (Figure 4.6).

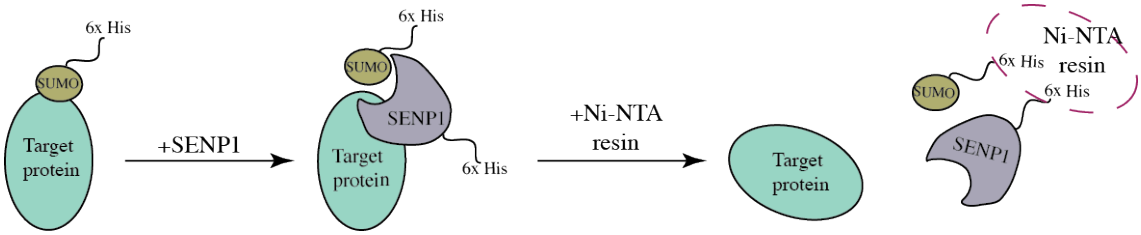

Figure 4.6: Schematic of His-SUMO tag cleavage by the SENP1 protease

The His-SUMO tag is fused directly to the target protein with no protease recognition sequence necessary. SENP1 recognises the three-dimensional structure of the SUMO moiety and cleaves directly C-terminal to it. The His-tagged SENP and the His-SUMO moiety can then be removed by incubation with nickel resin, leaving the target protein in the supernatant.

In addition, a range of new kinase inactive constructs was designed for expression with the His-SUMO tag. The N-terminal start sites of the constructs ranged from aa 128 to aa 165, (Figure 4.7A). A test expression of these constructs was carried out in *E. coli* BL21 CodonPlus cells. The protein was purified by nickel affinity chromatography and the

results were analysed by SDS-PAGE (Figure 4.7B & C). From the initial test expression it appeared that each of the constructs expressed to similar levels and with a similar purity. It was decided not to do any further work on the 128-570 construct, since previous studies with this construct and other tags had not been successful (Section 4.2). Large-scale expressions and purifications were carried out systematically for the remaining construct. Based on the results of these purifications (Appendix 5), no further work was done on the constructs starting at amino acids 138, 148 or 165. The 155-570 was chosen for further optimisation.

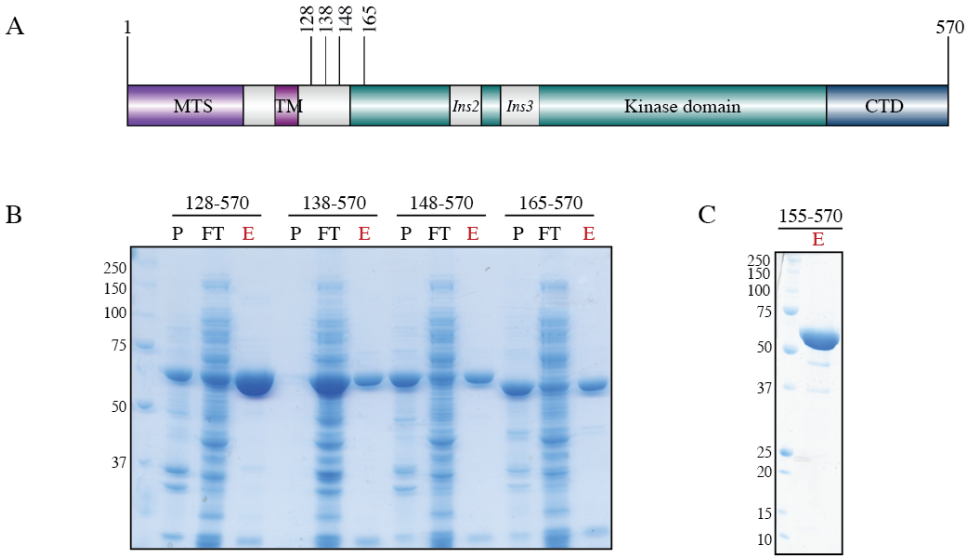

Figure 4.7: Test expression of TcPINK1 (D359A) constructs with His-SUMO tag

(A) Schematic of TcPINK1 domain architecture showing the domain boundaries of the new constructs. MTS: mitochondrial targeting sequence; TM: transmembrane helix; Ins2/3: kinase domain insertions; CTD: C-terminal domain. **(B)** SDS-PAGE analysis of His-SUMO TcPINK1 test expressions. P: insoluble pellet fraction; FT: flow-through not bound to nickel resin; E: eluted recombinant His-SUMO TcPINK1. **(C)** Test expression of His-SUMO TcPINK1 155-570. E: eluted protein.

4.3.2 Large-scale expression of His-SUMO TcPINK1 155-570 (D359A)

Large-scale expressions of His-SUMO-TcPINK1 155-570 (D359A) were carried out in *E. coli* BL21-CodonPlus cells and recombinant protein was purified by nickel affinity chromatography. Further purification was carried out using anion exchange

chromatography. The chromatogram showed a sharp symmetrical peak (Figure 4.8A) and SDS-PAGE analysis showed this peak contains TcPINK1 with some minor contaminants present (Figure 4.8B). Peak fractions were pooled and the His-SUMO tag was cleaved off. As a final purification step, the cleaved protein was subjected to gel filtration. The resulting chromatogram shows a single sharp peak with a small preceding shoulder (Figure 4.8C). SDS-PAGE analysis showed that both the main peak and the shoulder contained TcPINK1 of very high purity (Figure 4.8D). Peak fractions were pooled, avoiding fractions containing protein from the shoulder.

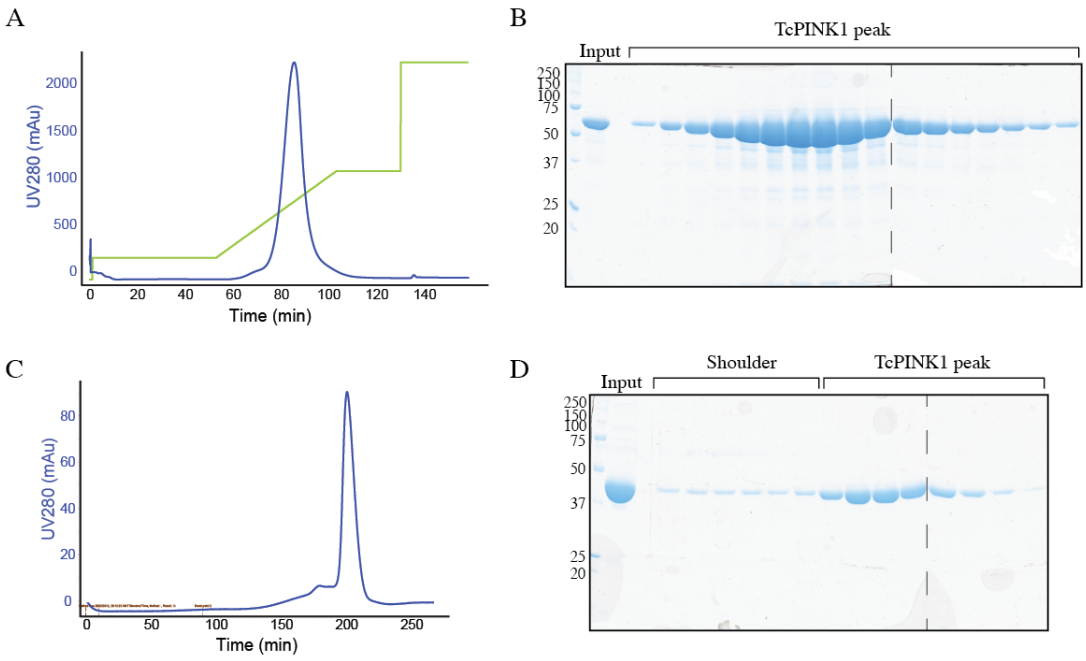

Figure 4.8: Purification of His-SUMO TcPINK1 155-570 (D359A)

(A) Chromatogram of HiTrap Q FF column anion exchange purification of His-SUMO-TcPINK1. Blue trace: UV_{280} absorbance; green trace: Buffer B gradient. **(B)** SDS-PAGE analysis of anion exchange peak fractions. **(C)** Chromatogram of S-200 gel filtration purification. Blue trace: UV_{280} absorbance. **(D)** SDS-PAGE analysis of gel filtration peak fractions.

4.3.3 Crystallisation screening of TcPINK1 155-570 (D359A)

Protein was prepared for crystallisation trials and used at concentrations between 1 and 5 mg/ml. Trays were set up with both the native protein and protein pre-incubated with one

of the following ligands: ATP, ADP or AMP-PNP, all with the counter-ion Mg^{2+}. Initial crystallisation trials of TcPINK1 155-570 (D359A) identified tiny crystals that grew within 3 days of setting up screens. Further screening led to the identification of multiple conditions in which tiny crystals formed in a manner generally not affected by the presence of absence of ligands (Figure 4.9A). Optimisation of all these hits using both grid and additive screening led to an improvement in the size of the crystals obtained in some cases. In other cases the original hit could not be reproduced or improved upon and so was not pursued further. Additional modifications to the screening protocol, including the inclusion of a high concentration of reducing agent (10 mM DTT) in the gel filtration buffer and the addition of the reducing agent β-mercaptoethanol to the reservoir solution generally led to a further increase in size and decrease in crystal number per drop. It should be noted that once a condition was found in which crystals grew, the presence and number of crystals was not very sensitive to variation of the crystallisation condition, with crystals usually being seen in most wells of a grid or additive screen for any given condition. For a full list of crystallisation screens set up with this construct, please refer to Appendix 6. The diffraction of crystals grown in a number of different conditions was tested and the diffraction limit of each of them was around 15-20 Å (Figure 4.9B&C). Extensive further screening was carried out to try and identify new hits and to improve on those already found, however it was not possible to improve the diffraction resolution to anything above ~15-20 Å.

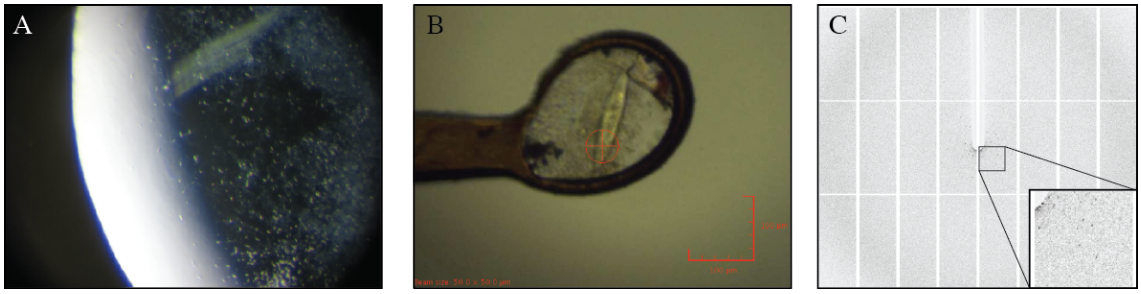

Figure 4.9: Crystals and diffraction pattern of TcPINK1 155-570 (D359A)

(A) Representative initial crystals of TcPINK1 before optimisation. **(B)** Representative crystal of TcPINK1 after optimisation to improve size and diffraction. **(C)** Representative diffraction pattern of TcPINK1 155-570 crystals showing weak diffraction.

4.3.4 Lysine methylation of TcPINK1 155-570 (D359A)

An additional technique that can be employed in the event that well-diffracting crystals cannot be grown is di-methylation of surface exposed lysine residues on the target protein (Walter et al, 2006). This method reduces the surface charge of the protein by modifying positively charged lysine residues with two neutral methyl groups. This may in turn allow the protein molecules to pack more tightly together and form a better-ordered crystal. TcPINK1 155-570 (D359A) was purified by nickel affinity chromatography and anion exchange and the His-SUMO tag removed. The protein was then diluted and subjected to the methylation protocol. Following this reaction, the methylated protein was purified by gel filtration to remove any excess of methylation reagents or aggregated protein. The resulting chromatogram showed a large shoulder preceding the main peak (Figure 4.10A) and SDS-PAGE analysis showed that both the peak and shoulder contained TcPINK1 (Figure 4.10B). Protein from the second half of the main peak was pooled to avoid contamination with the protein found in the shoulder. A sample of this protein was compared to the unmodified protein, and no degradation of the methylated sample was visible (Figure 4.10C). To determine the number of lysine residues modified in the course of the reaction, the methylated protein was analysed by MALDI mass spectrometry

(performed by Dr. Stella Ritorto). This revealed that 23 out of 27 lysine residues on TcPINK1 had become di-methylated (Figure 4.10D).

The methylated protein was prepared for crystallisation and initial screens were set up at a concentration of 1.60 mg/ml both in the presence and absence of ADP and Mg^{2+}. For a list of crystallisation screens set up with the methylated protein, please refer to Appendix 7. None of these screens produced any crystallisation hits, and since the gel filtration peak profile of the methylated protein was quite poor, this method was not pursued further.

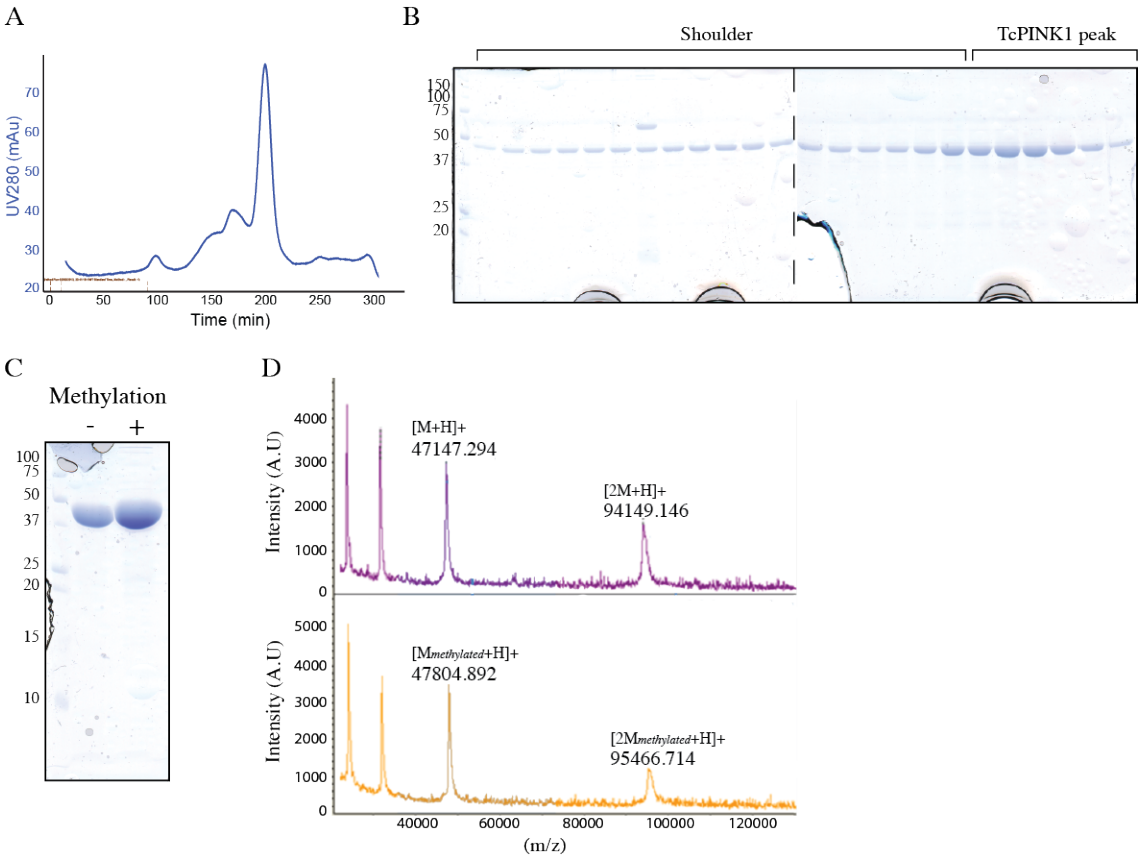

Figure 4.10: Purification of lysine methylated TcPINK1 155-570 (D359A)

(A) Chromatogram of S-200 purification of methylated TcPINK1. Blue trace: UV_{280} absorbance. **(B)** SDS-PAGE analysis of gel filtration fractions containing TcPINK1. **(C)** SDS-PAGE comparison of TcPINK1 before (-) and after (+) methylation reaction. **(D)** Performed by Dr. Stella Ritorto. MALDI mass spectra of unmethylated (top) and methylated (bottom) TcPINK1 showing the masses of the singly and doubly charged ions. An increase in molecular weight is visible in the methylated sample.

4.3.5 Large scale expression of His-SUMO TcPINK1 155-570

A further strategy to try and obtain well-diffracting crystals of TcPINK1 was to try and purify wild type His-SUMO TcPINK1 155-570. Use of the wild type protein had previously been avoided since heterogeneous autophosphorylation might interfere with crystal formation. However, previous data had suggested that at least one autophosphorylation site might be important for maximal kinase activity (Figure 3.8). It was therefore decided to use the wild type protein in case a lack of autophosphorylation led to a loss of protein stability.

Large-scale overexpression of His-SUMO TcPINK1 155-570 was performed in *E. coli* BL21-CodonPlus cells and the recombinant protein was purified by nickel affinity chromatography. The protein was further purified by anion exchange chromatography. The protein eluted at a higher salt concentration and showed a broader peak profile than seen for the kinase inactive protein (Figure 4.11A&B). Peak fractions were pooled and the His-SUMO tag was cleaved off. Finally, the cleaved protein was subjected to gel filtration. The resulting chromatogram shows a single peak with a large preceding shoulder not seen with the kinase inactive protein. SDS-PAGE analysis showed that both the main peak and the shoulder contained TcPINK1 (Figure 4.11C&D). Due to the poor gel filtration peak profile when compared to the kinase inactive protein, no further work was done with the wild type protein.

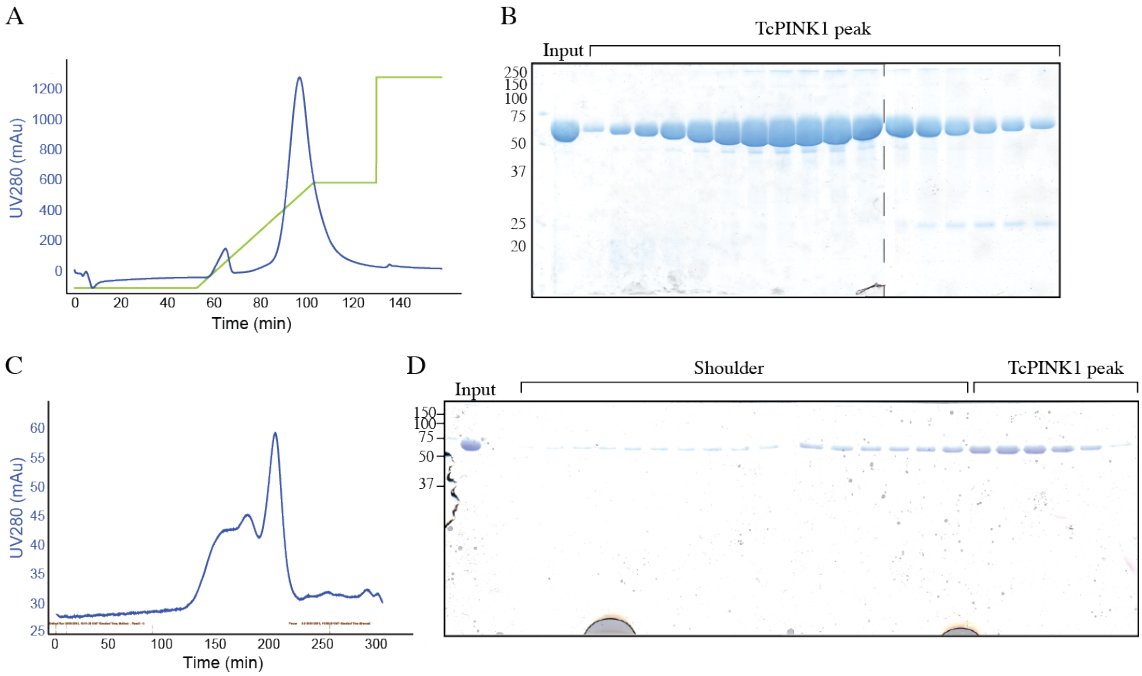

Figure 4.11: Purification of His-SUMO TcPINK1 155-570

(A) Chromatogram of HiTrap Q FF column anion exchange purification of His-SUMO-TcPINK1. Blue trace: UV_{280} absorbance; green trace: Buffer B gradient. **(B)** SDS-PAGE analysis of anion exchange peak fractions. **(C)** Chromatogram of S-200 gel filtration purification. Blue trace: UV_{280} absorbance. **(D)** SDS-PAGE analysis of gel filtration fractions containing TcPINK1.

4.3.6 Test expressions of TcPINK1 with the His-SUMO tag system: constructs with N-terminal boundaries between residues 150 and 165

Since work on the construct aa 155-570 had not yielded well-diffracting crystals, it was decided to design a range of new constructs to test. The N-terminal boundary of these 8 new constructs ranged from aa 150 to 163, which surround the start of the kinase domain at aa 155 (Figure 4.12A). A small-scale test expression of each of these constructs was performed in *E. coli* BL21-CodonPlus cells. The resulting protein was purified with nickel affinity chromatography and analysed by SDS-PAGE (Figure 4.12B). As with the previous test expressions, the yield and purity of each construct was very similar. A large-scale expression and purification of each new construct was carried out. Based on the results of their purification (Appendix 5), no further work was done on the constructs beginning with

amino acids 153, 156, 157, 160 or 163. Construct 150-570 was selected for further optimisation.

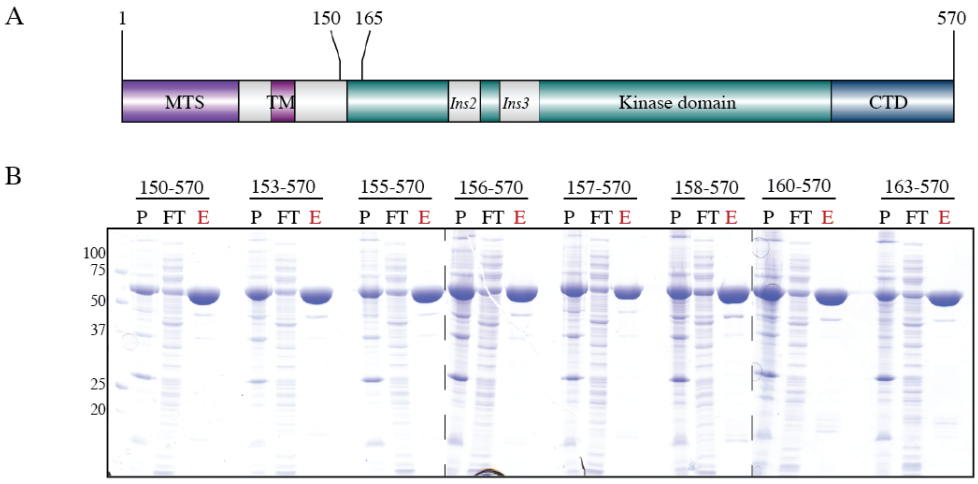

Figure 4.12: Test expression of His-SUMO-TcPINK1 (D359A) constructs

(A) Schematic of TcPINK1 showing region containing N-terminal start sites of new constructs. MTS: mitochondrial targeting sequence; TM: transmembrane helix; Ins2/3: kinase domain insertions; CTD: C-terminal domain. **(B)** SDS-PAGE analysis of His-SUMO-TcPINK1 test expressions. P: insoluble pellet fraction; FT: flow-through not bound to nickel resin; E: eluted recombinant His-SUMO-TcPINK1.

4.3.7 Large-scale expression of His-SUMO TcPINK1 150-570 (D359A)

A large-scale expression of His-SUMO-TcPINK1 150-570 (D359A) was carried out in *E. coli* BL21-CodonPlus cells and recombinant protein was purified by nickel affinity chromatography. Further purification was carried out using anion exchange chromatography. The chromatogram showed a sharp peak with a small shoulder after. SDS-PAGE analysis showed the peak contains TcPINK1 with some contaminants present (Figure 4.13A&B). Peak fractions were pooled and the His-SUMO tag was cleaved off. As a final purification step, the cleaved protein was subjected to gel filtration. The resulting chromatogram shows a single sharp peak with a small preceding shoulder (Figure 4.13C). SDS-PAGE analysis showed that both the main peak and shoulder contained TcPINK1 of

high purity (Figure 4.13D). Peak fractions were pooled, avoiding the fractions from the shoulder.

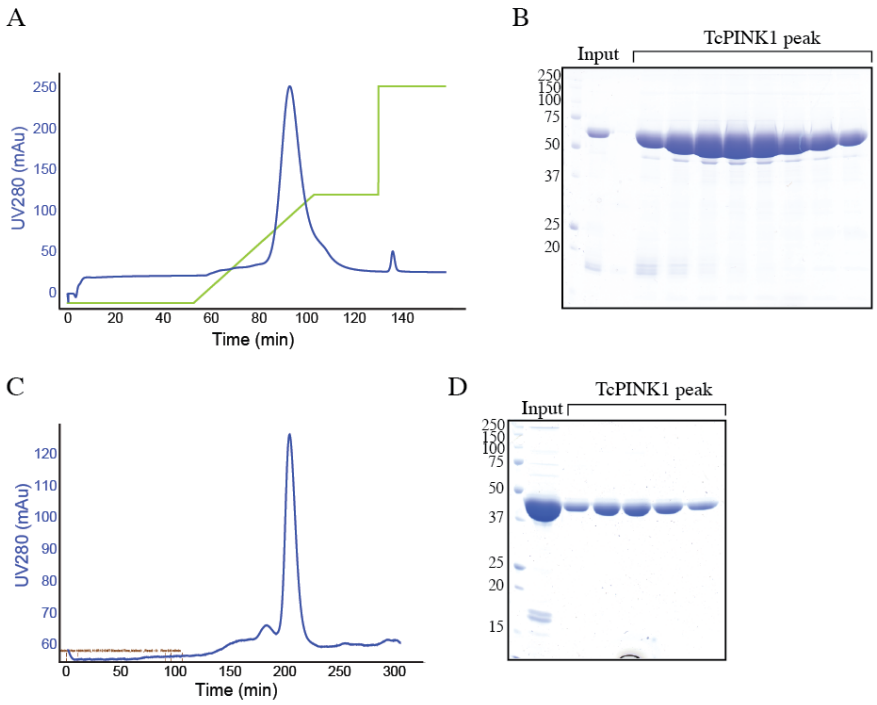

Figure 4.13: Purification of His-SUMO TcPINK1 150-570 (D359A)

(A) Chromatogram of HiTrap Q FF column anion exchange purification of His-SUMO-TcPINK1. Blue trace: UV_{280} absorbance; green trace: Buffer B gradient. **(B)** SDS-PAGE analysis of anion exchange peak fractions. **(C)** Chromatogram of S-200 gel filtration purification. Blue trace: UV_{280} absorbance. **(D)** SDS-PAGE analysis of gel filtration fractions containing TcPINK1.

4.3.8 Crystallisation screening of TcPINK1 150-570 (D359A)

Pooled protein after gel filtration was concentrated to between 1.5 and 4.5 mg/ml.

Trays were set up with both the native protein and protein pre-incubated with one of the following ligands: ATP, ADP or AMP-PNP, all with the counter-ion Mg^{2+}. Since it had been previously noted that addition of 10 mM DTT to the gel filtration buffer and β-mercaptoethanol to the crystallisation reservoir solution led to an increase in crystal size (Section 4.3.3), these were present for all crystal screening with TcPINK1 150-570 (D359A). Initial crystallisation trials of TcPINK1 150-570 (D359A) identified small crystals that grew within 2-3 days of setting up screens (Figure 4.14). In general, optimisation of

these hits using both grid and additive screening led to a modest improvement in the size of the crystals obtained. As with crystals of the 155-570 (D359A) construct, it was noted that the presence and number of crystals was not very sensitive to variation of the crystallisation conditions, with crystals usually being seen in most wells of a grid or additive screen for any given condition. For a list of crystallisation screens set up with this construct, please refer to Appendix 8. The diffraction of crystals grown in a number of different conditions was tested and the diffraction limit of each of them was improved compared to crystals of the 155-570 construct, typically being around 10 Å (Figure 4.14) Further optimisation was carried out but this did not lead to an improvement in diffraction resolution.

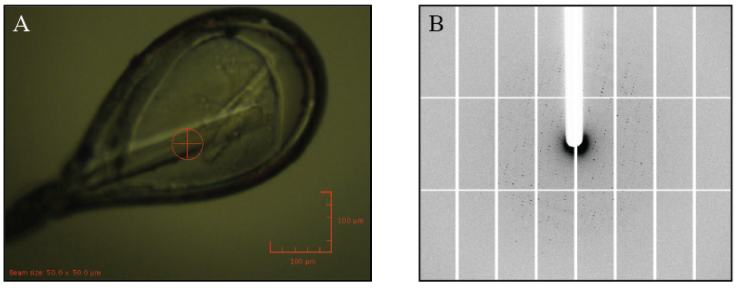

Figure 4.14: Crystals and diffraction pattern of TcPINK1 150-570 (D359A)

(A) Representative crystal of TcPINK1 150-570 (D359A). **(B)** Representative diffraction pattern of TcPINK1 150-570 (D359A) crystals.

4.3.9 Testing of alternative cryoprotectants for TcPINK1 150-570 (D359A) crystals

A critical stage in the preparation of crystals for data collection is the cryoprotection step, which allows the crystal to remain intact during freezing to prevent x-ray damage. Incorrect cryoprotection can cause an otherwise well-diffracting crystal to diffract poorly. Therefore, a number of different cryoprotectants were tested for TcPINK1 150-570 (D359A) crystals to see if the diffraction of these crystals was being affected by the use of an incorrect cryoprotectant. A diverse range of cryoprotectants was selected and the required concentration of each to ensure the crystallisation mother liquor froze as a clear drop, free

of ice, was determined. Several crystals were frozen in each cryoprotectant and their diffraction was then tested and compared to the diffraction of crystals frozen in the original cryoprotectant, 20% 2-methyl-2, 4-pentanediol (MPD). This showed that changing the cryoprotectant did not make any dramatic difference to the diffraction limit of TcPINK1 crystals (Figure 4.15), since all the crystals tested still only diffracted to around 10 Å or less.

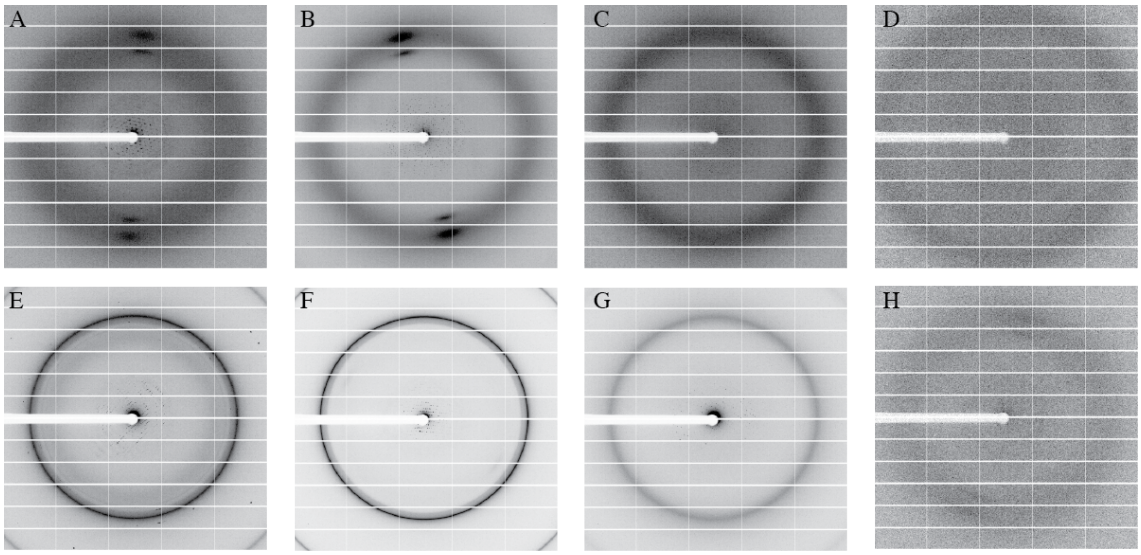

Figure 4.15: Analysis of the effect of different cryoprotectants on TcPINK1 150-570 (D359A) crystal diffraction

(A) Cryoprotection with 20% 2-methyl-2, 4-pentanediol (MPD), **(B)** 25% dimethyl sulfoxide (DMSO), **(C)** 25% glycerol, **(D)** saturated Li_2SO_4, **(E)** paraffin oil, **(F)** 35% propan-2-ol, **(G)** 35% sucrose, **(H)** 35% xylitol.

4.3.10 Lysine methylation of TcPINK1 150-570 (D359A)

As an additional attempt to improve the diffraction of the crystals obtained, the protein was modified by lysine di-methylation, as described in Section 4.3.4. The methylated protein was purified by gel filtration to remove aggregates and excess methylation reagents, resulting in a sharp peak with a small shoulder (Figure 4.16A). SDS-PAGE analysis showed the peak and shoulder contained TcPINK1 (Figure 4.16B). Peak fractions were pooled, avoiding contamination with fractions from the shoulder. A sample of methylated protein was compared to the unmodified protein. The methylated protein appears to run at a

higher molecular weight than the unmodified protein due to the increase in mass caused by the addition of methyl groups. No degradation of the methylated sample is visible (Figure 4.16C). To assess the number of lysine residues modified, a sample was analysed by MALDI mass spectrometry (performed by Dr .Stella Ritorto), which confirmed that 26 out of 27 lysine residues in TcPINK1 were modified (Figure 4.16D).

The methylated protein was prepared for crystallisation and initial screens were set up at a concentration of 1.6 mg/ml in the presence or absence of ADP + Mg^{2+}. Tiny crystals grew in several conditions after 2-3 days, but disappeared again after about 1 week, and attempts to reproduce these crystals or to find other growth conditions were not successful. For a list of crystallisation screens set up with this construct, please refer to Appendix 9.

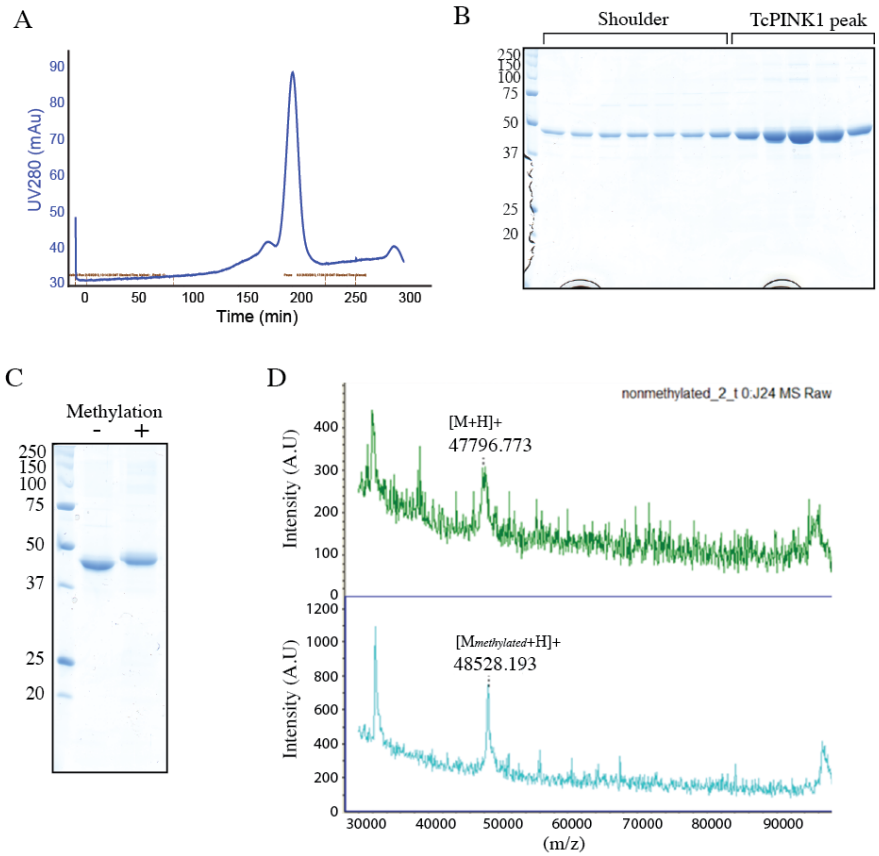

Figure 4.16: Purification of lysine methylated TcPINK1 150-570 (D359A)

(A) Chromatogram of S-200 purification of methylated TcPINK1. Blue trace: UV_{280} absorbance. **(B)** SDS-PAGE analysis of gel filtration fractions containing TcPINK1. **(C)** SDS-PAGE comparison of TcPINK1 before (-) and after (+) methylation reaction. **(D)** Performed by Dr. Stella Ritorto. MALDI mass spectra of unmethylated (top) and methylated (bottom) TcPINK1 showing the masses of the singly charged ions. An increase in molecular weight is visible in the methylated sample.

4.3.11 Test expressions of TcPINK1 with the His-SUMO tag system: Constructs with N-terminal boundaries between residues 145 and 154

Since work on TcPINK1 150-570 (D359A) had not led to well diffracting crystals and none of the other constructs tested had yielded high-quality protein, more constructs were designed and tested. These 7 constructs were designed with N-terminal starting residues surrounding aa 150, ranging from aa 145 to 154 (Figure 4.17A). Each of these new constructs was expressed on a small scale in *E. coli* BL21-CodonPlus cells and recombinant

protein was purified by nickel affinity chromatography. The yield and purity of each construct was judged by SDS-PAGE analysis, showing that each construct expressed to a similar level and purity (Figure 4.17B). A large-scale expression and purification of these constructs was carried out. Based on the results of this (Appendix 5), no further work was done on constructs 147-570 or 152-570. Constructs beginning with amino acids 145, 146 and 154 were not tested due to a lack of time. Constructs 149-570 and 151-570 were chosen for further optimization.

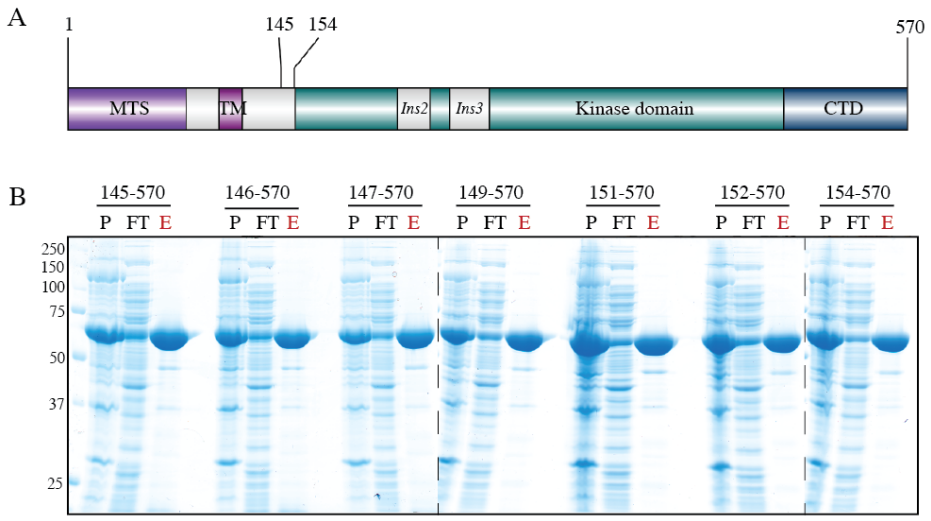

Figure 4.17: Test expression of His-SUMO-TcPINK1 (D359A) constructs

(A) Schematic of TcPINK1 showing region containing N-terminal start sites of new constructs. MTS: mitochondrial targeting sequence; TM: transmembrane helix; Ins2/3: kinase domain insertions; CTD: C-terminal domain. **(B)** SDS-PAGE analysis of His-SUMO-TcPINK1 test expressions. P: insoluble pellet fraction; FT: flow-through not bound to nickel resin; E: eluted recombinant His-SUMO-TcPINK1.

4.3.12 Large-scale expression of His-SUMO TcPINK1 149-570 (D359A) and preliminary crystallisation screening

A large-scale expression of His-SUMO-TcPINK1 149-570 (D359A) was carried out in *E. coli* BL21-CodonPlus cells and recombinant protein was purified by nickel affinity chromatography. Further purification was carried out using anion exchange

chromatography. The chromatogram showed a single peak that tailed towards the end, and SDS-PAGE analysis showed the peak contained TcPINK1 with some minor contaminants still present (Figure 4.18A&B). Peak fractions were pooled and the His-SUMO tag cleaved off. The protein was then further purified by gel filtration, and the resulting chromatogram showed a sharp peak with a preceding shoulder (Figure 4.18C). SDS-PAGE analysis showed that both the main peak and shoulder contained TcPINK1 of very high purity (Figure 4.18D). Peak fractions were pooled, avoiding contamination with fractions from the shoulder. Protein was prepared for crystallisation and initial screens were set up at a concentration of 1.7 mg/ml in the presence or absence of ADP and Mg^{2+}. For a list of crystallisation screens set up with this construct, please refer to Appendix 10. Small crystals grew in several conditions after a few days, however further optimization was not carried out due to a lack of time.

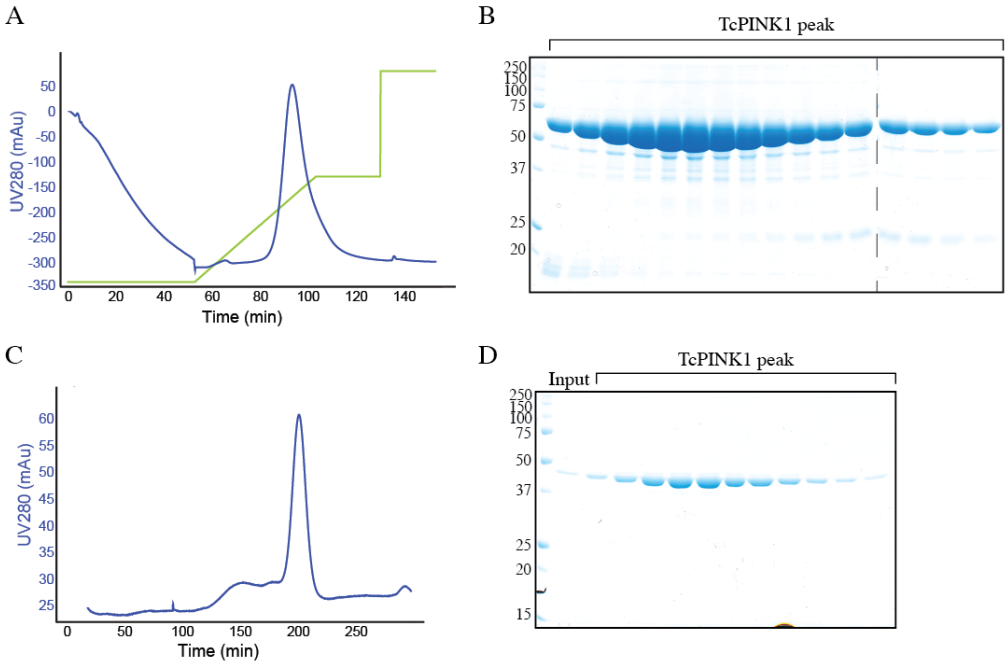

Figure 4.18: Purification of His-SUMO TcPINK1 149-570 (D359A)

(A) Chromatogram of HiTrap Q FF column anion exchange purification of His-SUMO-TcPINK1. Blue trace: UV_{280} absorbance; green trace: Buffer B gradient. **(B)** SDS-PAGE analysis of anion exchange peak fractions. **(C)** Chromatogram of S-200 gel filtration purification. Blue trace: UV_{280} absorbance. **(D)** SDS-PAGE analysis of gel filtration fractions containing TcPINK1.

4.3.13 Large-scale expression of His-SUMO TcPINK1 151-570 (D359A) and preliminary crystallisation screening

A large-scale expression of His-SUMO-TcPINK1 151-570 (D359A) was carried out in *E. coli* BL21-CodonPlus cells and recombinant protein was purified by nickel affinity chromatography. Further purification was carried out using anion exchange chromatography. The chromatogram showed a single peak with a shoulder towards the end (Figure 4.19A). SDS-PAGE analysis showed the peak contained TcPINK1 with some minor contaminants still present (Figure 4.19B). Peak fractions were pooled, avoiding the shoulder and the His-SUMO tag was cleaved off. The protein was then further purified by gel filtration. The resulting chromatogram shows a sharp peak and SDS-PAGE analysis showed the peak contained TcPINK1 of high purity (Figure 4.19C&D). Protein was prepared for crystallisation and initial screens were set up at a concentration of 1.7 mg/ml in the presence or absence of ADP and Mg^{2+}. For a list of crystallisation screens set up with this construct, please refer to Appendix 11. Small crystals grew in several conditions after a few days, however a lack of time prevented further optimization of these hits.

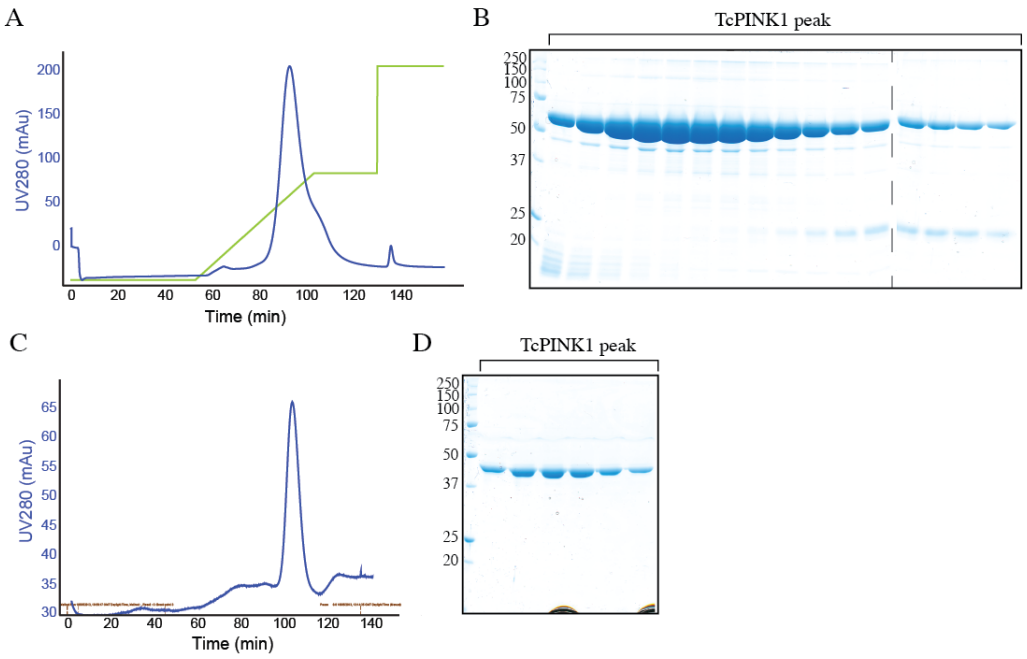

Figure 4.19: Purification of His-SUMO TcPINK1 151-570 (D359A)

(A) Chromatogram of HiTrap Q FF column anion exchange purification of His-SUMO-TcPINK1. Blue trace: UV_{280} absorbance; green trace: Buffer B gradient. **(B)** SDS-PAGE analysis of anion exchange peak fractions. **(C)** Chromatogram of S-200 gel filtration purification. Blue trace: UV_{280} absorbance. **(D)** SDS-PAGE analysis of gel filtration fractions containing TcPINK1.

4.4 Discussion:

Several constructs of PINK1 from the species *Tribolium castaneum* (TcPINK1) were expressed in *E. coli* with a His-SUMO tag and were purified by nickel affinity purification, anion exchange and gel filtration to yield protein of a suitable quality for crystallisation trials. Many conditions were discovered in which small crystals of TcPINK1 grew. This is, to my knowledge, the first successful attempt to obtain PINK1 crystals. However, despite extensive optimisation it was not possible to improve the resolution of the TcPINK1 crystals above ~10 Å and therefore it was not possible to determine the crystal structure of TcPINK1.

4.4.1 Why was it not possible to obtain well-diffracting crystals of TcPINK1?

The key factor for determining how well a crystal diffracts is the uniform or tight packing of the protein molecules that form the three-dimensional lattice of the crystal. In practice, crystals of macromolecules like proteins or nucleic acids contain irregularities. The molecules in protein crystals are held together by weak hydrogen bonding, which gives rise to these irregularities in the lattice structure of the crystal. In theory, the lesser this irregularity and the more tightly packed the molecules in the crystal, the better a crystal will diffract. However, in reality it is often not possible to know why a particular protein fails to produce well-diffracting crystals.

Heterogeneity in the protein sample to be used for crystallisation, for example caused by post-translational modification (PTMs), oxidation or degradation, can prevent crystal growth or lead to poor quality crystals forming. Since it is known that TcPINK1 is able to autophosphorylate (Section 3.5), in most cases a kinase inactive mutant that is incapable of autophosphorylation was used. When the wild type enzyme was purified, a large shoulder

was present on the gel filtration chromatogram that may indicate the presence of protein complexes or aggregates in the sample (Figure 4.11). To minimise degradation or oxidation, the purification protocol was performed in such a way to minimize the time between cell lysis and setting up of crystal trays and in addition, reducing agent was present throughout the purification with a higher concentration being used in the gel filtration buffer in which the protein was crystallised.

Conformational flexibility of the protein molecules can also interfere with the formation of a well-diffracting crystal. TcPINK1 belongs to the protein kinase family, which is well known to undergo a dramatic conformational change upon moving from the active to the inactive conformation (reviewed in (Huse & Kuriyan, 2002)). The existence of multiple protein conformations in a crystallisation sample is likely to be detrimental to the chances of obtaining a high quality crystal. To counteract this potential problem, a ligand such as a substrate or cofactor, can be included in the crystallisation screen. Binding of such a molecule to the protein might lock it into a single conformation and subsequently aid the formation of a well-diffracting crystal. All crystallisation screens for TcPINK1 were performed both in the presence and absence of a ligand (ADP, ATP and the non-hydrolysable ATP analog AMP-PNP along with the counter ion Mg^{2+}). Crystal formation and diffraction did not seem to be in any way influenced by the presence of these ligands. In addition, flexibility or disorder in specific regions of the protein, such as flexible loops, can also lead to a poorly diffracting crystal since they can impede tight crystal packing. TcPINK1 was selected for crystallisation studies due to its lack of the first insertion in the kinase domain and was truncated to remove regions prior to the kinase domain that might be disordered. However, it is possible that the remaining second and third insertions might be flexible enough to interfere with crystal formation.

Charged regions on the surface of the protein molecules cause electrostatic repulsion between the protein molecules, preventing them from coming together to form a well-ordered lattice. One method for circumventing this issue is to modify or remove charged surface residues from the target protein, for example by methylation of surface-exposed lysine residues, which neutralises their positive charge (Walter et al, 2006). This method was applied to TcPINK1 (Figure 4.10 & Figure 4.16) with the majority of lysine residues becoming successfully modified, although screening with these modified proteins did not yield any crystals. There is a possibility that the reduced surface charge will lead to reduced protein solubility and stability. For both the TcPINK1 constructs modified by methylation, a shoulder was present on the gel filtration chromatogram (Figure 4.10A & Figure 4.16A) that may indicate the presence of aggregated protein.

Finally, an otherwise high quality crystal can end up diffracting poorly due to the way it is prepared for a diffraction experiment. It is usual to cool crystals to a very low temperature using a liquid nitrogen cryostream during the course of a diffraction experiment to protect the crystal from radiation damage. To avoid the water molecules in the mother liquor in which the crystal is contained from freezing and destroying the crystal, it is common practice to cryoprotect the crystal before freezing (Hope, 1988; Vera & Stura, 2013). During cryoprotection, the water molecules surrounding the crystal are partially replaced with molecules such as sugars, certain salts or organic compounds that prevent the formation of ice and maintains the native structure of the protein molecules in the crystal. The crystal can then safely be frozen and placed in the cryostream to keep it cold throughout the experiment. Initially, 20% MPD was utilised as a cryoprotectant for TcPINK1 crystals, since this compound is present in several of the conditions in which TcPINK1 crystals grow. Subsequently, a variety of alternate cryoprotectants were tested, however none of these different cryoprotectants led to any improvement in the diffraction

of the TcPINK1 crystals (Figure 4.15). This suggests either that crystals of TcPINK1 are of low quality, or that they cannot withstand freezing with any of the tested cryoprotectants. To determine which is the case, it would be necessary to carry out a diffraction experiment at room temperature using unfrozen crystals. If the crystals diffracted well at room temperature, then the freezing protocol would need further optimisation. If not, then a higher quality crystal form would be required.

4.4.2 What could be done to obtain higher quality TcPINK1 crystals?

In future, it would be important to try alternate methods to improve the resolution of diffraction that are not solely focused on modification of the crystallisation condition itself. Mutagenesis of charged residues, in particular lysine and glutamic acid, which are predicted to be surface exposed can reduce the entropy of crystal formation and can permit the formation of crystal contacts that help hold molecules in the crystal together (Derewenda, 2004). This approach has been shown to yield well-diffracting crystals of otherwise difficult proteins and a web server, SERp, is available to aid in the design of such mutations for a given target protein (Goldschmidt et al, 2007). Dehydration of existing crystals has also been shown to dramatically improve their diffraction in certain cases. Dehydration of the crystal reduces the solvent content and leads to tighter packing of the protein molecules in the crystal, which can in turn increase the resolution of diffraction. This dehydration is often achieved in a controlled fashion by equilibration of previously grown crystals in a small drop against a larger reservoir of a dehydrating solution. This leads to transfer of water from the small drop to the reservoir and if performed in incremental steps over a sufficiently long period of time can lead to dehydration of the crystal without damage (Hagelueken et al, 2012; Heras et al, 2003). An alternative, more hi-tech approach is the use of a humidity-controlled beamline at a synchrotron facility, which allows alteration of the

humidity of the gas surrounding a mounted crystal (Russi et al, 2011). In short, incremental changes in humidity can be made and the diffraction of the crystal (or crystals, since these experiments often require multiple crystals) can be assessed at each stage. If a positive change is observed, a higher-resolution dataset can then be collected at the required relative humidity.

Many constructs were tested in the course of identifying those that yielded protein of a sufficient quality to begin crystallisation trials. The identification of the optimal construct is not always straightforward, as in this case where many of the constructs initially tested expressed to the same level and purity and could only be assessed properly after further purification attempts. The two most successful constructs, 150-570 and 155-570 both have their N-terminal start sites around the beginning of the TcPINK1 kinase domain. Two further constructs were tested briefly, 149-570 and 151-470 and appear to behave very similarly to the 150-570 construct (Figure 4.18 & Figure 4.19). Nevertheless, in future it would be important not only to continue work with these constructs, but to also continue testing additional new constructs since the difference between success and failure can be in the presence or absence of only one or two extra amino acids. It would also be possible to continue exploiting the approach of using PINK1 orthologues from different species in order to increase the chances of obtaining well-diffracting PINK1 crystals. TcPINK1 was selected for this study due to its lack of the variable first insertion within the kinase domain, however other criteria could be used to select potential targets for crystallization. PINK1 is present in many other organisms that are more closely related to humans, such as fish or mammals, as well as those that are more distantly related, such as the nematode worm *Caenorhabditis elegans*. Selecting PINK1 orthologues from a range of different branches of the animal kingdom might maximize the chances of success.

4.4.3 What are the predicted structural effects of Parkinson's disease-linked PINK1 mutations?

Although it was not possible to determine the crystal structure of TcPINK1, it is still possible to rationalize the likely structural effects of Parkinson's disease-linked mutations found within the protein kinase domain. The protein kinase fold is highly conserved amongst all members of the family, with invariant secondary structure elements being present in all but the most atypical kinases (Hanks & Hunter, 1995). In addition, multiple structures of protein kinases have been determined and extensive studies on the functional role of many conserved motifs and features had been carried out. There is therefore a wealth of information on how kinase structure informs function and activity. Therefore by comparing the primary amino acid sequence of PINK1 to one of the most well-characterised protein kinases, PKA (cAMP-dependent protein kinase) it is possible to speculate how mutations within the PINK1 kinase domain might disrupt its function. Almost 100 sequence variants of PINK1 have been described (Appendix 1), however only those that are found in Parkinson's patients in either the homozygous or compound heterozygous state can be unequivocally linked to Parkinson's disease. Only the likely structural effects of selected PINK1 heterozygous or compound homozygous PINK1 mutations will be discussed further.

To use the available knowledge relating to PKA to understand the potential effect of PD-linked mutations on PINK1, it is necessary to be able to directly compare the sequences of PKA and hPINK1. To this end, an alignment of the kinase domains of PINK1 and PKA was prepared (Figure 4.20), showing the locations of each of the PINK1 disease mutations. In addition, conserved kinase motifs, the secondary structure of PKA (based on PDB ID: 1ATP (Zheng et al, 1993)) and kinase subdomain boundaries are annotated to allow easy comparison between the two proteins.

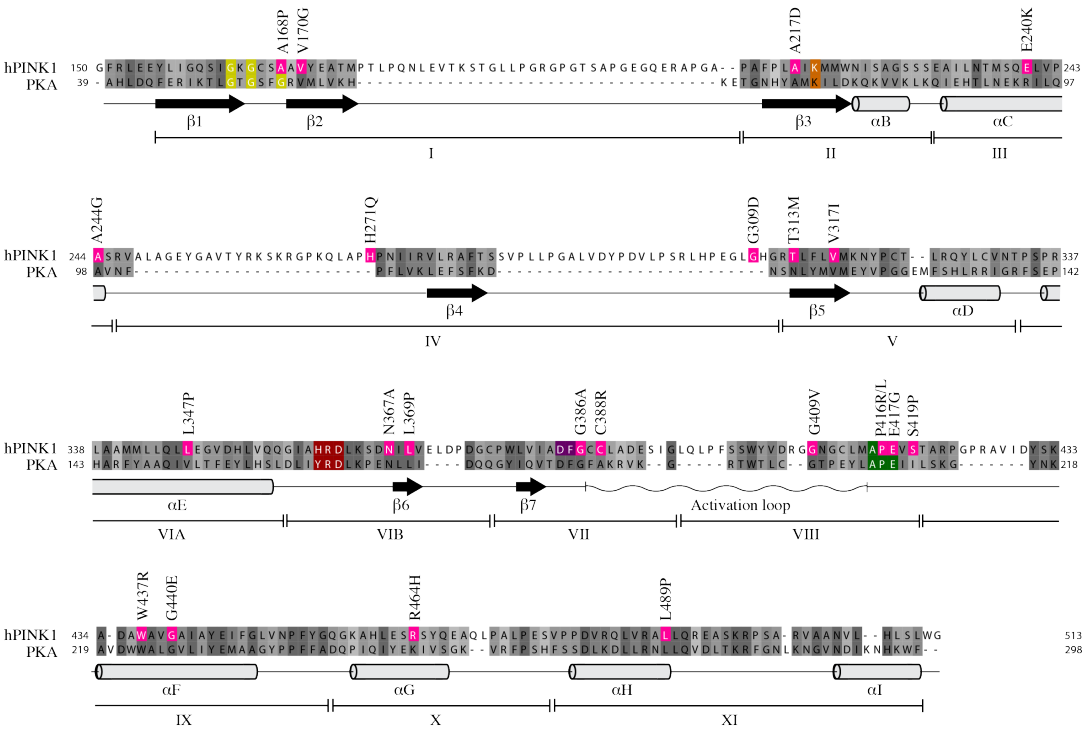

Figure 4.20: Sequence alignment of the kinase domains of PKA and human PINK1

Conserved kinase motifs are coloured as follows: Gly-rich loop: yellow; ATP-binding lysine: orange; HRD catalytic motif: red; DFG activation loop anchor: purple; APE activation loop anchor: green. PINK1 disease mutations are highlighted in pink and labelled (numbering according to hPINK1), residues conserved between hPINK1 and PKA are indicated with an asterisk. The secondary structure of PKA and the conserved kinase subdomains are shown underneath. Black arrows: β-strands; grey cylinders: α-helices. PDB ID: 1ATP

Two residues mutated in PD, Val170 (V170G) and Ala217 (A217D), contribute to the hydrophobic portion of the ATP binding pocket that accommodates the adenine moiety (Hanks & Hunter). In addition, they form part of a conserved network of hydrophobic residues stretching throughout the protein kinase. It begins at the C-terminus of the αF helix, traverses both the N- and C-lobes, and is known as the catalytic, or C-spine (Kornev et al, 2008). Val170 and Ala217 are the most N-terminal of these C-spine residues and form the topmost part of the C-spine together with the adenine moiety of ATP (Figure 4.21A). In this way, assembly of this stabilising structure and therefore the switching of the kinase to the active conformation is directly linked to binding of ATP (Kornev et al, 2008). Val170 was identified as being mutated to glycine in PD, which is a polar and highly

flexible residue, suggesting that this mutation might reduce the hydrophobicity of the adenine pocket and/or prevent formation of a rigid C-spine structure. However, the effect of this mutation on *in vitro* kinase activity is not known. Ala217 is mutated to aspartic acid in PD, which is a change from a small hydrophobic to a larger and negatively charged residue. This would most likely prevent binding of ATP in the ATP binding pocket, and would also be disruptive to the formation of the C-spine, explaining why this mutation leads to a loss of TcPINK1 kinase activity.

Residue Glu240 (E240K) forms an important ionic interaction that stabilises the N-lobe in the ATP-bound conformation (Hanks & Hunter, 1995). It is located in the αC helix and forms a salt bridge with another highly conserved N-lobe residue, K219, found in β3, which interacts with the α- and β-phosphates of the ATP molecule, orientating it properly for catalysis (Figure 4.21B). The formation of this bond is critical for kinase activity and so it is not surprising that the PD-linked mutation of Glu240 to lysine, which has the opposite charge, leads to a complete loss of kinase activity.

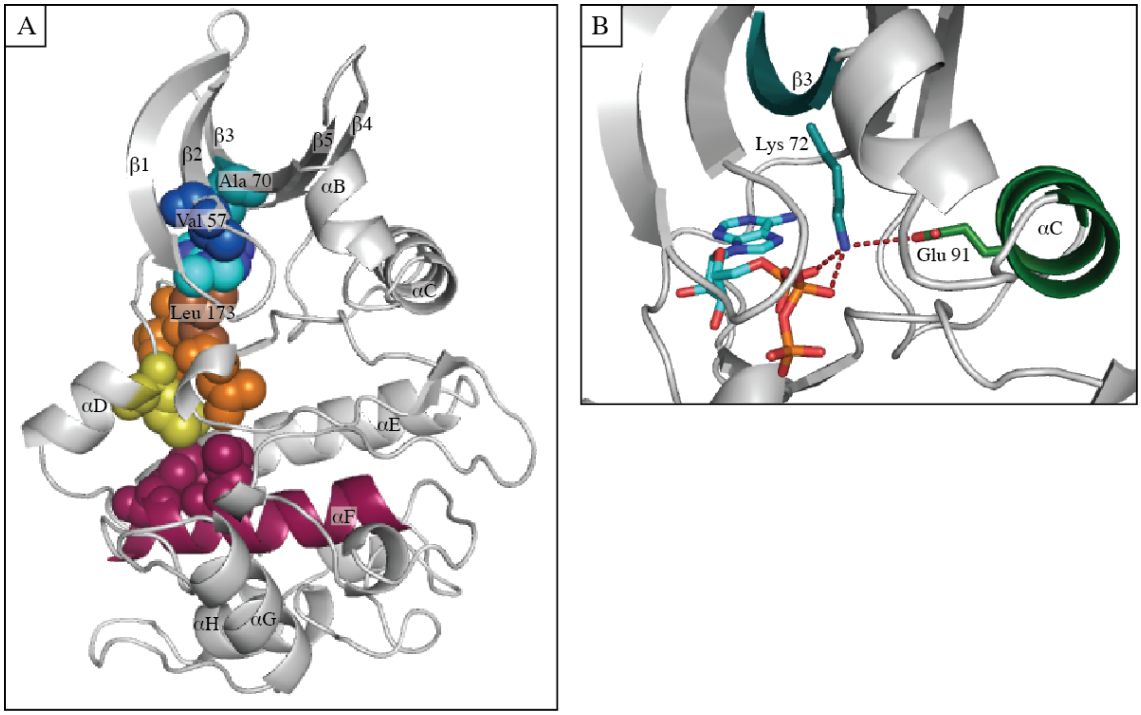

Figure 4.21: Depiction of the structure of PKA in the active conformation showing selected residues and motifs homologous to PD-mutated residues in PINK1

(A) Structure of PKA depicting the catalytic spine (C-spine). Residues that make up the C-spine are shown as spheres and are coloured according to the secondary structure element they reside in – blue: β2 strand; teal: β3 strand; orange: β6 strand; yellow: αD helix; raspberry: αF helix. The adenine moiety of ATP that completes the C-spine is depicted as cyan spheres. Amino acid V57 is V170 in hPINK1, V170G in PD, A70 is A217/A217G. **(B)** The K72-E91 ionic interaction in PKA (equivalent to K219-E240 in hPINK1, E240 is E240K in PD). PKA is shown in cartoon representation. The αC helix and E91 are shown in green, and the β3 strand and K72 are shown in teal. Interactions between these residues and ATP (orange/cyan sticks) are shown in red. In both figures, PDB ID: 1ATP.

Gly386 (G386A) is part of the DFG motif, which makes up the N-terminal anchor of the kinase activation loop. This residue has been shown to undergo a dramatic rotation of its main chain upon a kinase adopting the inactive conformation (Kornev et al, 2006), with its dihedral phi-angle changing by approximately 140°. This rotation leads to a change in conformation of the nearby aspartic acid, preventing it from coordinating the ATP-stabilising Mg^{2+} ions, and breaks a hydrogen bond between this residue and the Gly386 main chain (Figure 4.22). In this way, the conformation of this glycine residue acts as a switch between the active and inactive conformations and only glycine is able to undergo

the extreme rotation necessary for this due to its lack of a side chain (Kornev et al, 2006). Gly386 is mutated to alanine in PD and leads to a loss of kinase activity. Despite the small size of the alanine side chain, it would not be able to undergo the required drastic conformational change and would prevent PINK1 from moving between the active and inactive conformations.

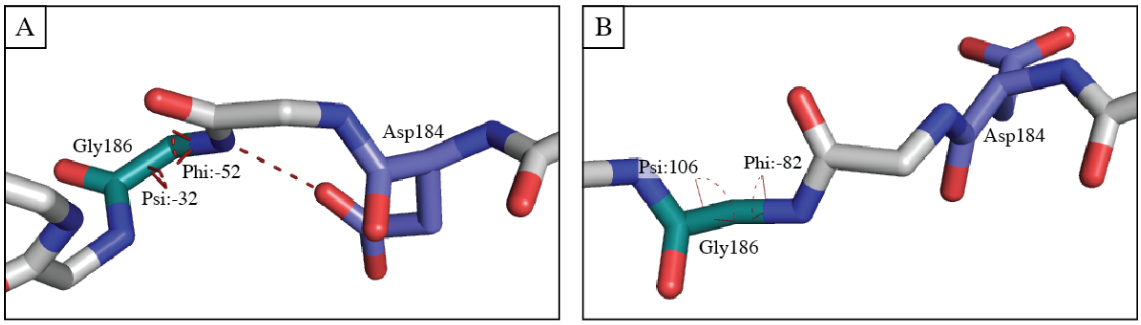

Figure 4.22: Conformation of the magnesium loop segment in both active and inactive PKA structures

(A) Active PKA segment is shown as sticks. G186 (G386 in hPINK1) forms a hydrogen bond (shown in red) via its main chain with D184 (384 in hPINK1). Phi and psi angles (shown in red) for G186 are -52 and -32 respectively. PDB ID: 1ATP **(B)** Upon assuming the inactive conformation, the main chain of G186 undergoes a dramatic twist. The phi and psi angles of this residue are now -87 and 106 respectively. The hydrogen bond between G186 and D184 is broken. PDB ID: 4DFY

Residue Glu417 (E417G) is predicted to form a salt bridge to another highly conserved residue, Arg497 (Arg280 in PKA), which helps stabilise the C-lobe of the kinase and which has been shown to be essential for maximal kinase activity (Figure 4.23A) (Yang et al, 2012). PD-linked mutation of this residue to glycine leads to a loss of this bond since glycine is not capable of forming the necessary ionic interaction and therefore a loss of PINK1 kinase activity.

Residues Trp437 (W437R) and Gly440 (G440E) are both found in the αF helix and their homologous residues in PKA, along with several other hydrophobic residues, form a tight interaction with residues from the αH helix, including Leu489 (L489P), also mutated in PD (Figure 4.23). This interaction between the αF and αH helix is critical for stabilising the

hydrophobic core of the protein, based around the αF helix. This helix is the nucleation site for the previously mentioned C-spine, and also for another similar hydrophobic network of residues that come together in a manner dependent on activation loop conformation, the R-spine (Kornev et al, 2008). Stability of the αF helix is therefore important for the subsequent ability of the kinase to assume the active conformation. Trp437 is a highly conserved residue that not only interacts with the αH helix, but also interacts with and stabilises the alanine and proline of the APE motif (Kornev et al, 2008). Trp437 is mutated to arginine in PD, changing a large hydrophobic residue to a positively charged one. Although the effect of this substitution on PINK1 activity is unknown, it seems likely that the substitution of an amino acid forming such critical interactions would lead to a loss of activity. Gly440 is strongly conserved throughout protein kinases and analysis of the structure of PKA (Zheng et al, 1993) shows that its tiny side chain allows the formation of a pocket for a nearby leucine residue (Kornev et al, 2008). Therefore, the PD-linked mutation of Gly440 to glutamic acid, a large, negatively charged residue would completely disrupt this hydrophobic arrangement and lead to the observed loss of kinase activity. Leu489 is found in the αH helix and helps form a hydrophobic shield surrounding the αF helix (Kornev et al, 2008). This residue is mutated to proline in PD and leads to a loss of kinase activity, presumably due to destabilization of the interface between the αF and αH helices.

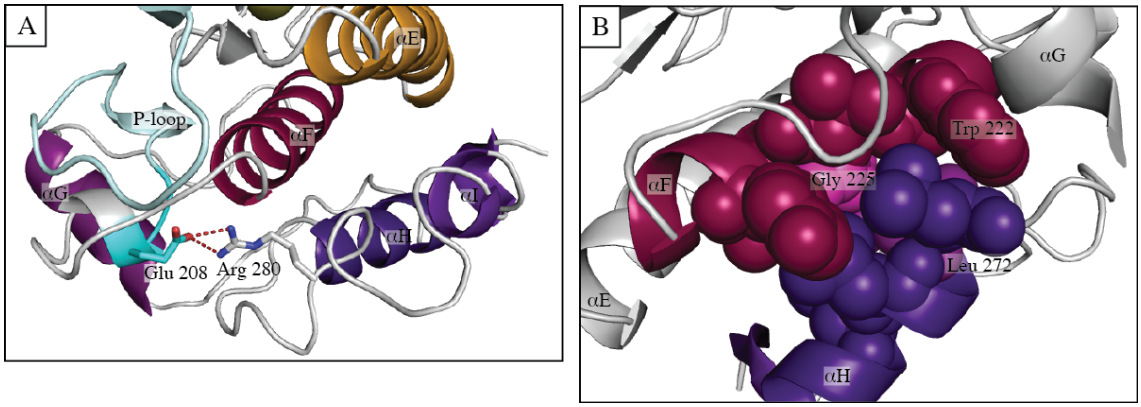

Figure 4.23: Depiction of the structure of PKA in the active conformation showing residues and motifs homologous to PD-mutated residues in hPINK1

(A) Stabilising interaction between E208 and R280 in PKA (E417 and R497 in hPINK1, E417G in PD). The structure of PKA is shown in cartoon representation. The APE motif is coloured cyan and E208 is shown in cyan sticks. R280 is shown in white sticks and the hydrogen bond between the two residues is shown in red. Secondary structure elements of the C-lobe are labeled and coloured as follows: αE helix: orange; P-loop/activation loop: pale cyan; αF helix: dark red; αG helix: violet; αH helix: purple; αI helix: indigo. **(B)** Stabilising interaction between αF and αH helices. The structure of PKA is shown in cartoon representation. Contributing residues from the αF and αH helices are coloured pink and purple respectively and shown as spheres. PKA equivalents of residues mutated in PINK1 are labeled as follows: W222, dark pink, is hPINK1 W437, W347R in PD; G225, light pink, is hPINK1 G440, G440E in PD; L272, partially hidden and light purple, is hPINK1 L489, L489P in PD. The lack of space for a larger side chain in the space occupied by G225 is visible. For both figures, PDB ID: 1ATP

4.5 Conclusions

After the discovery of PINK1 from the insect species *Tribolium castaneum* (TcPINK1) as a valid and well-characterised model for human PINK1 (hPINK1), it has been possible for the first time to obtain highly pure PINK1 protein and furthermore to conduct crystallisation screens with this protein. Several constructs were tested that yielded crystals growing in multiple conditions. The diffraction of these crystals was poor and despite extensive optimisation attempts, it was not possible to overcome this problem and as a result the structure of TcPINK1 has not yet been determined. The crystal structure of PINK1 would resolve many unanswered questions, such as the structure and topology of the unique PINK1 insertions and C-terminal domain and furthermore their functional role, which can sometimes be understood from the structure. In addition it would provide a conclusive explanation for the effect of PD-linked mutations.

However, there are some questions that it is possible to speculate upon even in the absence of a PINK1 crystal structure. There is a wealth of knowledge about the structure and function of protein kinases, from the role of individual amino acids and motifs to whole networks of residues and structural elements. This information can be transferred to even distantly related kinases such as PINK1 due to the high conservation of the protein kinase fold. Even in the absence of strong sequence similarity, many features are universally present in all kinases and much can be understood from analyzing these differences and similarities.

Chapter 5

5 Regulation of Parkin by PINK1 phosphorylation of the Ubl domain and ubiquitin

5.1 Introduction

Parkin is a ubiquitin E3 ligase which, like PINK1, was first linked to Parkinson's disease through genetic analysis of familial cases (Kitada et al, 1998). Moreover, Parkin mutations are numerically significant and represent the most common cause of autosomal recessive Parkinson's disease. Cell biological analyses have implicated Parkin along with PINK1 in the regulation of mitophagy, ensuring damaged mitochondria are removed from the cell (Matsuda et al, 2010; Narendra et al, 2008; Narendra et al, 2010; Okatsu et al, 2012). PINK1 is constitutively degraded under normal conditions and Parkin is kept in an autoinhibited, inactive state. However, when the mitochondrial membrane potential is lost, PINK1 becomes stabilised and this leads to recruitment of Parkin from the cytosol to the mitochondria, where it then becomes activated. Although the mechanism of Parkin recruitment is unknown, it has been shown that PINK1 regulates the activity of Parkin by phosphorylation, leading to its activation. PINK1 exerts a dual regulatory effect over Parkin activity. Firstly, it phosphorylates Parkin at residue Ser65 in its N-terminal Ubl (ubiquitin-like) domain (Kondapalli et al, 2012), and secondly it phosphorylates ubiquitin, also at Ser65 (Kane et al, 2014; Kazlauskaite et al, 2014b; Koyano et al, 2014). Examination of the crystal structure of ubiquitin (Vijay-Kumar et al, 1987) and the solution NMR structure of the isolated Ubl domain (Sakata et al, 2003) shows that Ser65 is located in the same position in these two proteins, which is not surprising since they both share the conserved ubiquitin fold (Appendix 12). The effect of both of these phosphorylation events *in vitro* is to activate Parkin, with each individual phosphorylation leading to a degree

of activation and maximal activation being achieved when both sites are phosphorylated (Kazlauskaite et al, 2014b; Ordureau et al, 2014).

The precise mechanism by which this activation occurs is unclear, however a small amount of information is available. Multiple crystal structures of Parkin have recently been determined, including several high-resolution truncated structures lacking the Ubl domain (Riley et al, 2013; Spratt et al, 2013; Trempe et al, 2013; Wauer & Komander, 2013) and a lower-resolution full-length structure (Trempe et al, 2013). From the examination of these structures, it has become apparent that multiple intramolecular interactions keep Parkin in a complex autoinhibited state (Figure 5.1). An interaction between the RING0 domain and the RING2 domain obscures the catalytic cysteine, Cys431, and an interaction between the Ubl domain, RING1 domain and the REP (regulatory element of Parkin) helix blocks what is predicted to be the E2 binding site (Trempe et al, 2013). In addition, modelling of a Parkin:E2~Ub complex showed that the active sites of the E2 (UBE2D2) and Parkin would be around 50 Å apart, with the active site of the E2 pointing away from the Parkin active site (Wauer & Komander, 2013). This data suggests that significant conformational rearrangements must occur to bring Parkin into a conformation that is catalytically competent; firstly making the E2 binding site accessible, followed by E2 binding and subsequently the E2 and E3 active sites moving in close enough proximity to allow ubiquitin transfer to occur.

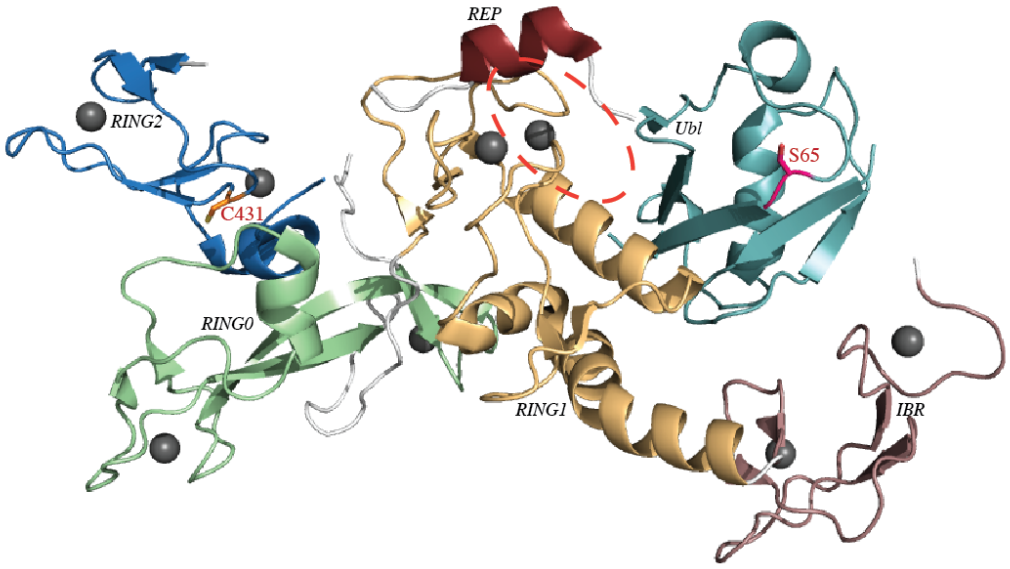

Figure 5.1: Crystal structure of autoinhibited full-length Parkin showing the location of Ser65, Cys431 and potential E2 binding site

Turquoise: Ubl domain; green: RING0; gold: RING1; pink: IBR; red: REP helix; blue: RING2. Ser65 is shown as pink sticks, Cys431 is shown as orange sticks. Zinc ions are shown as grey spheres. The predicted E2 binding region (Wauer & Komander, 2013) is shown with a red dotted circle. PDB ID: 4K95.

Since PINK1 phosphorylation of the Ubl domain and ubiquitin is sufficient to activate Parkin, these rearrangements must be mediated by these two phosphorylation events. An initial hypothesis proposed that opening of the Parkin structure was mediated by electrostatic repulsion between the PINK1-phosphorylated Ubl domain and the RING0 domain. However, examination of the full-length, low resolution Parkin structure shows that the PINK1 phosphorylation site, Ser65, is not found at the interface between the Ubl and the RING1 domain (Figure 5.1). This suggests that the initial hypothesis was incorrect and a more complex mechanism must be responsible. Further examination of the Parkin structure suggests how this might occur.

Three basic regions (referred to as pocket 1, 2 and 3) on the surface of Parkin that bind to negatively charged sulphate ions are visible in the crystal structure (Figure 5.2). Pocket 1 is specifically highlighted in one of the papers describing a truncated Parkin crystal structure,

where the authors suggest it might be responsible for recruitment of Parkin to the mitochondria via the binding of PINK1 autophosphorylation sites (Wauer & Komander, 2013). However, such pockets could also plausibly act as binding sites for the phosphorylated Ubl domain or phospho-ubiquitin. Binding of one of these phosphorylated ligands might serve as a mechanism by which the activating phosphorylation signal could be spread throughout the Parkin molecule and lead to the required conformational changes.

Pocket 1 consists of residues K161, R163 and K211, all of which are located in the RING0 domain. Interestingly, two PD-linked Parkin mutations, K161N and K211N, affect residues found in pocket 1 and have been shown to prevent the mitochondrial localisation of Parkin (Matsuda et al, 2010). This makes pocket 1 a likely candidate for a regulatory binding site. Pocket 2 consists of residues K151, H302, R305 and Q316. K151 is in the RING0 domain, the remaining residues are found in the RING1 domain, with pocket 2 being situated at an interface between these two domains. This makes pocket 2 interesting since any regulatory binding event here would involve both RING1, where the E2 binds, and RING0, which blocks the active site. Finally pocket 3 consists solely of residue R455 and forms only a superficial surface interaction with a sulphate ion in the crystal structure. For this reason, it is unlikely to act as a binding site for phospho-proteins. The amino acid residues making up each of these pockets are highly conserved between species, further indicating that they might be of functional relevance (Appendix 13).

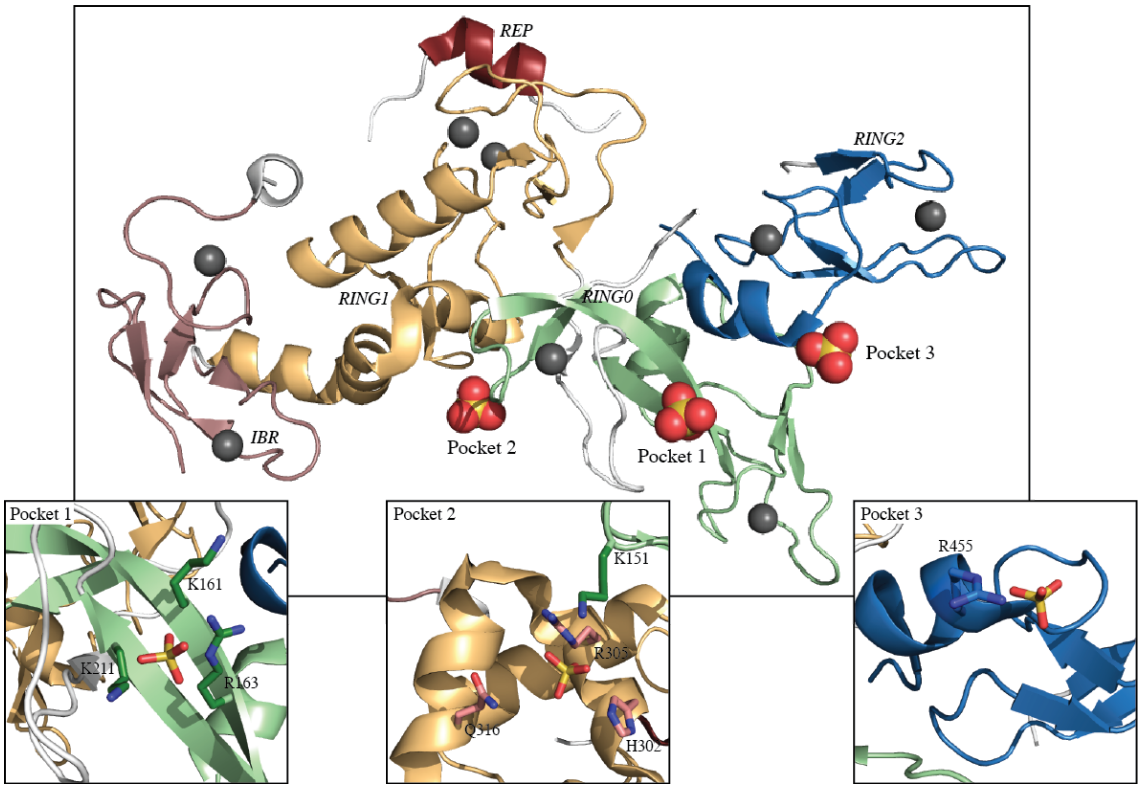

Figure 5.2: Crystal structure of ΔUbl Parkin showing potential phosphate binding pockets

Main panel shows the cartoon structure of ΔUbl Parkin and the location of bound sulphate ions. Green: RING0; gold: RING1; pink: IBR; red: REP helix; blue: RING2. Sulphate ions are shown as yellow/red spheres and zinc ions are shown as grey spheres. Inset panels show residues forming each of the putative phosphate-binding pockets. Colouring is the same as in the main panel. PDB ID: 4BM9.

In order to understand more about the regulation of Parkin by PINK1, it was decided to study the binding of the phospho-Ubl domain to Parkin. In order to do this, it was necessary to produce a supply of homogeneous Ser65-phosphorylated Ubl domain, which was attempted by two different methods.

5.2 Production of Ser65-phosphorylated Ubl domain

5.2.1 Anion exchange purification of Ser65-phosphorylated Ubl domain

The Ubl domain of Parkin (1-76) was overexpressed in *E. coli* with a His-SUMO tag and purified using nickel affinity chromatography and cation exchange. It was subsequently phosphorylated with MBP-TcPINK1 128-570. After phosphorylation, the Ubl domain was separated from MBP-TcPINK1 using a centrifugal concentrator. The resulting mixture of phospho and de-phospho Ubl domain was then further purified with high-resolution anion exchange chromatography, yielding several peaks with baseline separation, corresponding to the phospho and de-phospho Ubl domain and a contaminant. The purity of each peak was assessed by immunoblotting and SDS-PAGE analysis (Figure 5.3). Western blot analysis showed that both the first and second peaks contained phosphorylated Ubl domain.

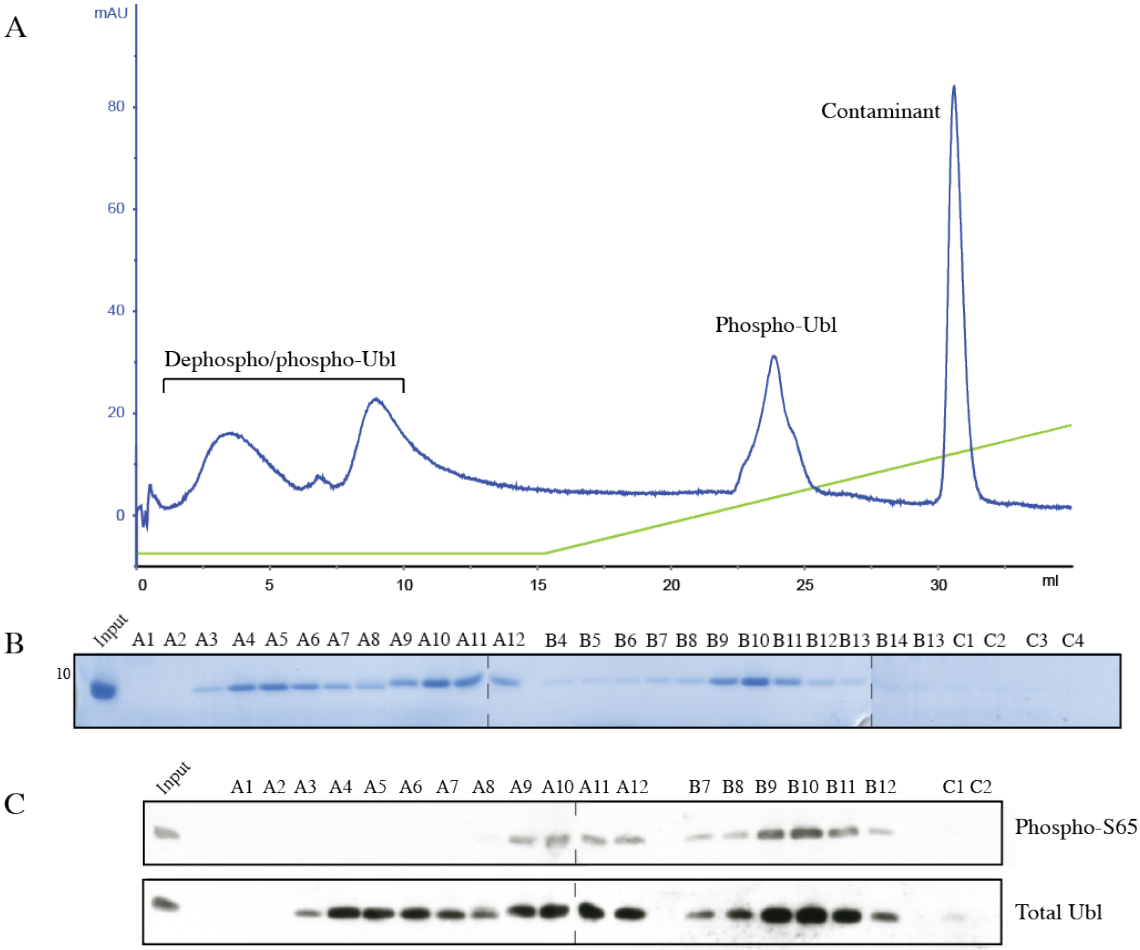

Figure 5.3: Ion exchange purification of *in vitro* Ser65-phosphorylated Ubl domain

(A) Chromatogram of ion exchange purification. Blue: UV_{280} absorbance; green: % buffer B. **(B)** SDS-PAGE analysis of fractions from ion exchange purification. **(C)** Western blotting of protein-containing fractions from (B). Top panel: phospho-Ser65 antibody. Bottom panel: total anti-Parkin antibody.

In order to determine what proportion of each peak was phosphorylated, MALDI mass spectrometry was carried out on samples from each of the peak fractions. This revealed that the input sample contained approximately a 1:1 ratio of phospho- to dephospho-Ubl. The first peak (fractions A3-A5, A9-A11) contained a mixture of phospho and dephospho-Ubl and the second peak contained only phospho-Ubl domain (Figure 5.4). A trace quantity of dephospho-Ubl domain was present in the most concentrated fraction (B10) from the second peak. This purification was repeated several times with similar results, showing that the purification of homogeneous phospho-Ubl domain is possible. However,

the yield was very low, with only around 200-500 µg of pure phosphorylated protein being obtained using starting material from a 12 L *E. coli* culture.

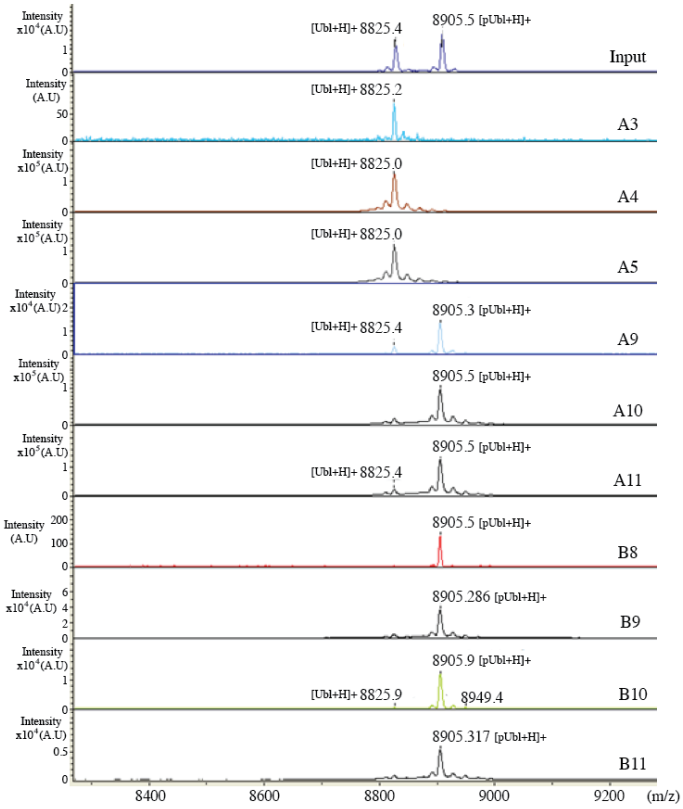

Figure 5.4: MALDI analysis of ion exchange fractions from Ser65-phosphorylated Ubl domain purification

Performed by Dr. Stella Ritorto. Input: Protein before high-resolution anion exchange purification. Fractions A3-A5, A9-A11: Peak 1; Fractions B8-B11: Peak 2.

5.2.2 Production of Ser65-phosphorylated Ubl domain using genetically encoded phosphoserine incorporation

In recent years it has become possible to genetically engineer organisms such as *E. coli* to allow them to utilise an expanded genetic code and subsequently to incorporate non-natural amino acids into proteins as they are synthesised by the ribosome (Chin, 2014). This technology has been applied to allow the insertion of phosphoserine (Sep) into a target protein, permitting the expression of phosphorylated proteins and the study of their properties (Park et al, 2011). This method provides several advantages compared to

previous approaches used to study the effects of phosphorylation. An upstream kinase to phosphorylate the target protein is not required and the introduction of phosphoserine accurately recapitulates the effects of biological phosphorylation, whereas the commonly used serine/threonine to glutamic acid phosphomimetic mutation often does not. Phosphoserine has been successfully inserted into GFP (green fluorescent protein), WNK4 (with no lysine 4) and MEK1 (mitogen activated ERK-activating kinase 1) (Heinemann et al, 2012; Park et al, 2011). In particular, it has been shown that MEK1 with Sep inserted at a physiological phosphorylation site is many times more active than both the wild type protein and the corresponding glutamic acid mutant, validating the utility of this approach (Park et al, 2011).

Sep insertion into recombinant proteins is achieved by repurposing the amber stop codon (TAG/UAG) to encode for the anticodon of an orthogonal tRNA conjugated to Sep ($tRNA^{Sep}$) that can then be used for protein synthesis (Figure 5.5). An orthogonal aminoacyl tRNA synthetase (SepRS) has been produced that allows the synthesis of $tRNA^{Sep}$ along with an EF-Tu (Elongation factor-Tu) that has been engineered to accept $tRNA^{Sep}$ (EF-Sep) and allow its incorporation into polypeptides (Park et al, 2011). Further improvements to this system resulted in the EcAR7 strain of *E. coli*, which has the gene encoding RF-1 (release factor-1) knocked out. RF-1 terminates polypeptide synthesis at amber stop codons (TAG) and its absence should increase the efficiency of Sep-containing protein synthesis. In addition, the terminating TAG codons of seven essential genes are reassigned to TAA to counteract the lethality associated with RF-1 knockout (Heinemann et al, 2012).

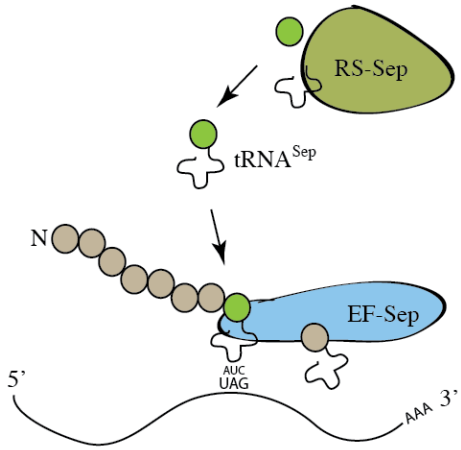

Figure 5.5: Schematic of Sep insertion into recombinant proteins

An orthogonal aminoacyl tRNA synthetase (RS-Sep, olive) synthesizes tRNA^{Sep} from the cellular pool of orthogonal tRNA (black clover-leaf shape) and Sep (green sphere). tRNA^{Sep} then pairs with the amber stop codon on an mRNA molecule and Sep is incorporated into the nascent polypeptide (grey spheres) by the ribosome (not pictured) and an elongation factor that has been modified to accept tRNA^{Sep} (EF-Sep, blue).

In collaboration with the laboratory of Dr. Jesse Rinehart (Yale University), who provided reagents, this technology was applied to the Ubl domain of Parkin to generate Ser65-phosphorylated Ubl domain (Sep65 Ubl, to distinguish from *in vitro*-phosphorylated Ubl domain). A GST-tagged Ubl domain construct (1-76) containing a TAG codon for residue 65 was transformed into EcAR7 cells along with a plasmid carrying the orthogonal tRNA, RS-Sep and EF-Sep. Recombinant GST-Sep65 Ubl domain was expressed and purified with glutathione resin. The GST tag was removed overnight with GST-PreScission protease (GST-PP) and the resulting cleaved protein was then eluted. This was done in parallel with the wild type GST-Ubl domain in order to compare the yield, purity and levels of Sep incorporation achieved. Both wild type and Sep65 Ubl domain were obtained, however they were contaminated with the cleaved GST tag and GST-PP (Figure 5.6).

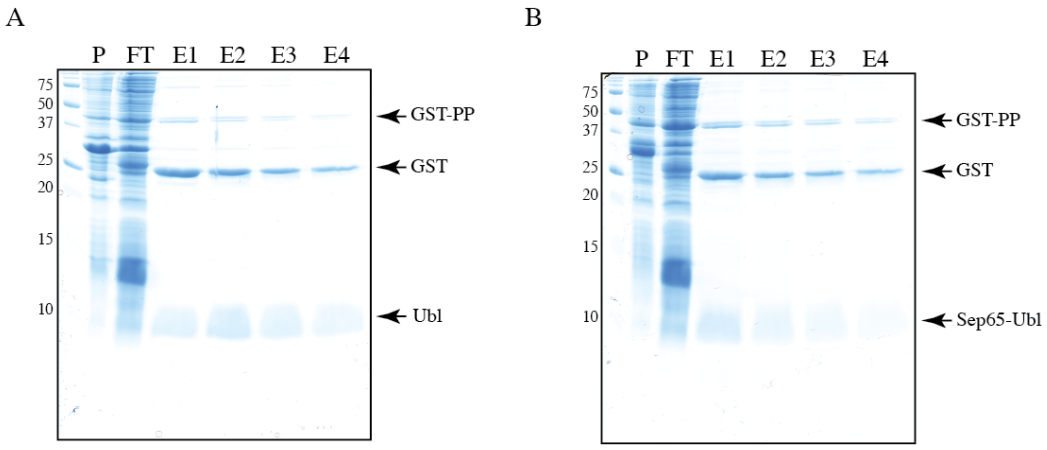

Figure 5.6: Recombinant expression of Ubl and Sep65 Ubl in EcAR7 cells

(A) Expression and purification of wild type Ubl domain. **(B)** Expression and purification of Sep65 Ubl domain. P: insoluble pellet fraction; FT: flowthrough not bound to glutathione resin; E1-4: eluted fractions 1-4; GST-PP: GST-PreScission protease.

In order to confirm the phosphorylation of the Sep65 Ubl domain, both the wild type and Sep65 Ubl domain proteins were analysed by LC-MS to determine their precise molecular weights (Figure 5.7). This analysis revealed that the wild type Ubl domain had the expected molecular weight of 9235 Da. However, the Sep65 Ubl sample contained a mixture of two different species. One of these was the Sep65 Ubl domain, with a molecular weight of 9315 Da. The other was Ubl domain in which the Sep incorporation site had been skipped by the translation machinery, producing a shorter protein lacking the phosphoserine with a molecular weight of 9148 Da. There was a significant quantity of the skipped Ubl domain present in the Sep65 Ubl sample, suggesting that this technology is not currently suitable for producing pure and homogeneously phosphorylated Ubl domain.

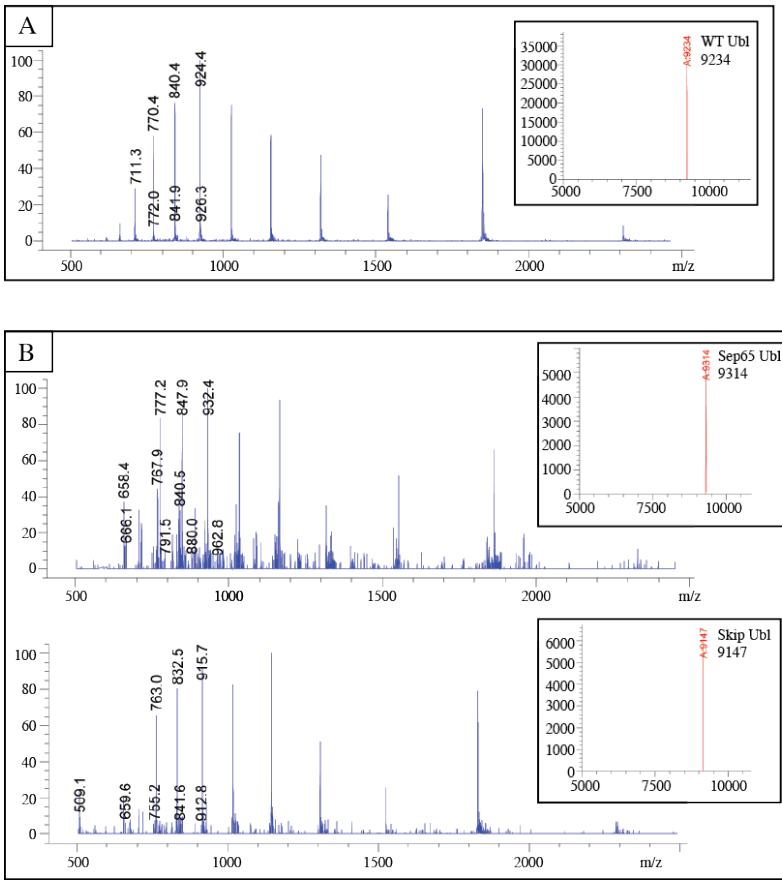

C

Protein	Observed mass (Da)	Expected mass (Da)
Ubl	9234	9235
Sep65 Ubl	9315	9315
65-skip Ubl	9148	9148

Figure 5.7: LC-MS analysis of wild type and Sep65 Ubl domain

(A) Mass spectra of wild type Ubl domain sample. Inset shows deconvoluted spectrum and observed molecular weight. **(B)** Mass spectra of Sep65 Ubl domain sample. Top panel corresponds to peak containing Sep65 Ubl domain. Deconvoluted spectrum and observed molecular weight shown in inset. Bottom panel corresponds to peak containing Ubl domain with 65 position skipped. Deconvoluted spectrum and observed molecular weight shown in inset. **(C)** Table showing observed and expected molecular weights of all Ubl species observed.

5.3 Analysis of binding of the phospho-Ubl domain to Parkin

5.3.1 Establishment of the AlphaScreen assay to study binding to ΔUbl Parkin

Ser65-phosphorylated Ubl domain that had been phosphorylated *in vitro* with TcPINK1 and purified by ion exchange (Section 5.2.1) was used in studies to determine whether the phospho-Ubl domain is capable of binding to the same site on Parkin occupied by the non-phosphorylated Ubl domain. In order to determine this, an AlphaScreen assay was established and employed (Figure 5.8). Dr. Jinwei Zhang performed all AlphaScreen experiments described in this thesis.

The methodology and applications of the AlphaScreen assay, including the measurement of protein-protein interactions, are reviewed in (Taouji et al, 2009). The AlphaScreen is a bead-based proximity assay whereby two tagged proteins, in this instance GST-Ubl (1-76) and ΔUbl Parkin-biotin (80-465), are incubated with each other and subsequently with two types of bead; the donor beads (streptavidin-coated) and the acceptor beads (glutathione-coated). If the two proteins interact, the two beads are brought into close proximity via binding between their coatings and the protein affinity tags. The donor bead can be excited with a wavelength of 680 nm, leading to the generation of singlet oxygen (an excited state of O_2). This can diffuse for up to 200 nm in solution and if the acceptor bead is within that radius (i.e. if the two proteins are interacting), then the acceptor bead will be stimulated to emit light at 520-620 nm. This assay can be further utilised to test the binding of an additional ligand to either component. For example, if untagged Ubl domain was added, it would compete out the GST-Ubl by binding to ΔUbl Parkin-Biotin, reducing the fluorescent signal. If a ligand is added and no binding occurs, no loss of fluorescent signal will be seen.

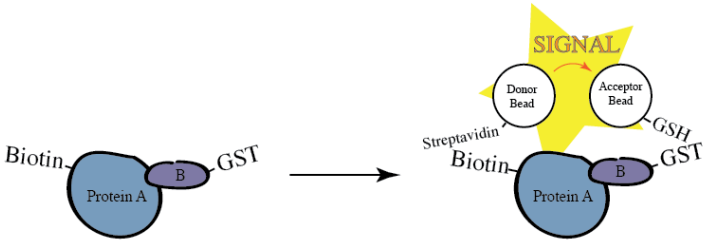

Figure 5.8: Schematic of AlphaScreen assay

Two tagged proteins (GST and biotin tags) are mixed together and are then incubated with glutathione-coated donor beads and streptavidin-coated acceptor beads. If the proteins interact, the donor and acceptor beads will be brought into close proximity and excitation of the donor bead will transfer to the acceptor bead, leading to a signal being emitted.

Before utilising the AlphaScreen to study the binding between Parkin and the phospho-Ubl domain, the validity and specificity of this assay was established. In order to determine that the assay was suitable for measuring interactions between Parkin and the Ubl domain, wild type GST-tagged Ubl domain and ΔUbl Parkin-biotin were incubated together at a constant concentration and the concentration of untagged wild type Ubl domain was increased. As expected, as the concentration of untagged Ubl domain added to the assay increased, the fluorescent signal measured was decreased, demonstrating that untagged Ubl domain is able to compete out the interaction between the GST-Ubl domain and ΔUbl Parkin-biotin (Figure 5.9A&C). To test the specificity of this assay, the same experiment was repeated but with the addition of an unrelated protein, SrtA (Sortase A), in the place of untagged Ubl. The addition of SrtA to the assay did not lead to any decrease in the fluorescent signal measured (Figure 5.9B). This indicates that SrtA is not able to displace the GST-Ubl domain from ΔUbl Parkin-biotin and therefore that any displacement seen in this assay is the result of a specific interaction between Parkin and the titrated protein.

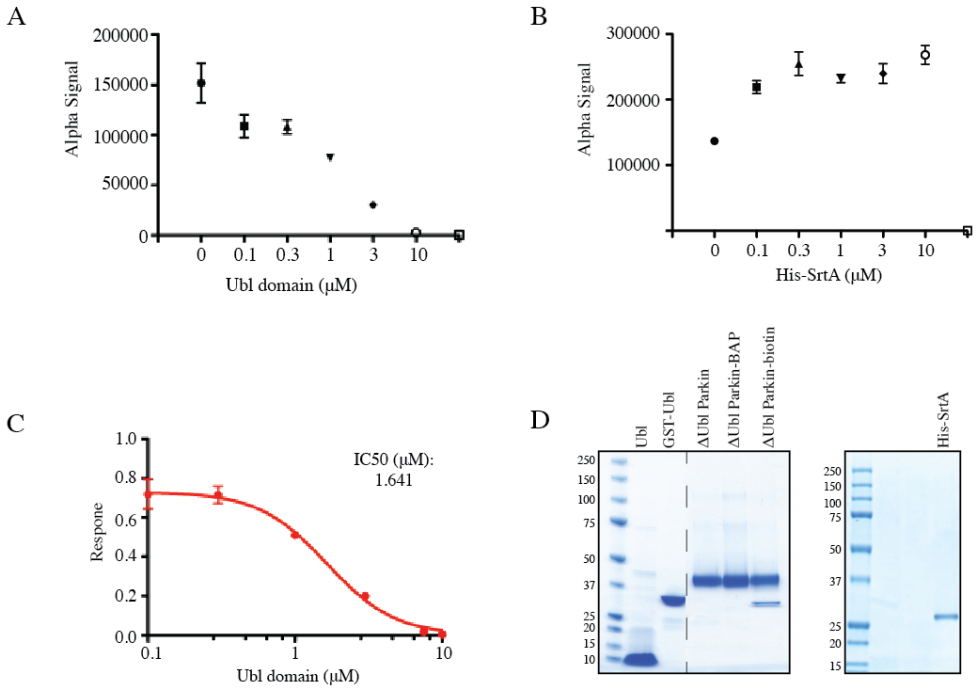

Figure 5.9: Establishment of AlphaScreen assay

Performed by Dr. Jinwei Zhang **(A)** Raw data showing fluorescent signal generated by interaction between GST-Ubl (0.3 μM) and ΔUbl Parkin-biotin (0.1 μM) as increasing concentrations of Ubl (0.1 – 10 μM) are added. **(B)** Raw data showing fluorescent signal generated by interaction between GST-Ubl (0.3 μM) and ΔUbl Parkin-biotin (0.1 μM) as increasing concentrations of His-SrtA (0.1 – 10 μM) are added. **(C)** Processed data showing kinetics of displacement of GST-Ubl by untagged Ubl domain, with an IC_{50} value of 1.64 μM. **(D)** SDS-PAGE showing proteins used in this study. BAP: biotin acceptor peptide.

5.3.2 Analysis of the binding of the phospho-Ubl domain to Parkin

Subsequently, the AlphaScreen assay was used to determine if the phospho-Ubl domain was able to displace the binding of the GST-Ubl domain from ΔUbl Parkin-biotin. Wild type untagged Ubl domain was used as a control, as this has been shown to displace the GST-tagged Ubl domain from ΔUbl Parkin (Figure 5.9). In addition, unphosphorylated Ubl domain from the first peak of the anion exchange purification (Figure 5.3) was included to confirm that this step had not altered the properties of the Ubl domain. The concentrations of ΔUbl Parkin-biotin and GST-Ubl were kept constant, the concentration of either wild type or phospho-Ubl was increased and the fluorescent signal was measured.

IC_{50} values for the wild type and phosphorylated Ubl domain were determined, indicating the concentration required to displace 50% of the GST-Ubl domain from ΔUbl Parkin. This experiment revealed that the wild type Ubl domain is able to displace GST-Ubl binding from ΔUbl Parkin and has an IC_{50} of 2.95 μM (Figure 5.10A&D). Likewise, the dephospho-Ubl from the anion exchange purification was able to displace GST-Ubl from ΔUbl Parkin with an IC_{50} value of 6.18 μM (Figure 5.10B&E), suggesting that the anion exchange procedure had not interfered with the integrity of the Ubl domain. In contrast, the Ser65-phosphorylated Ubl domain was completely unable to displace the GST-Ubl from ΔUbl Parkin (Figure 5.10C) and so an IC_{50} value could not be determined.

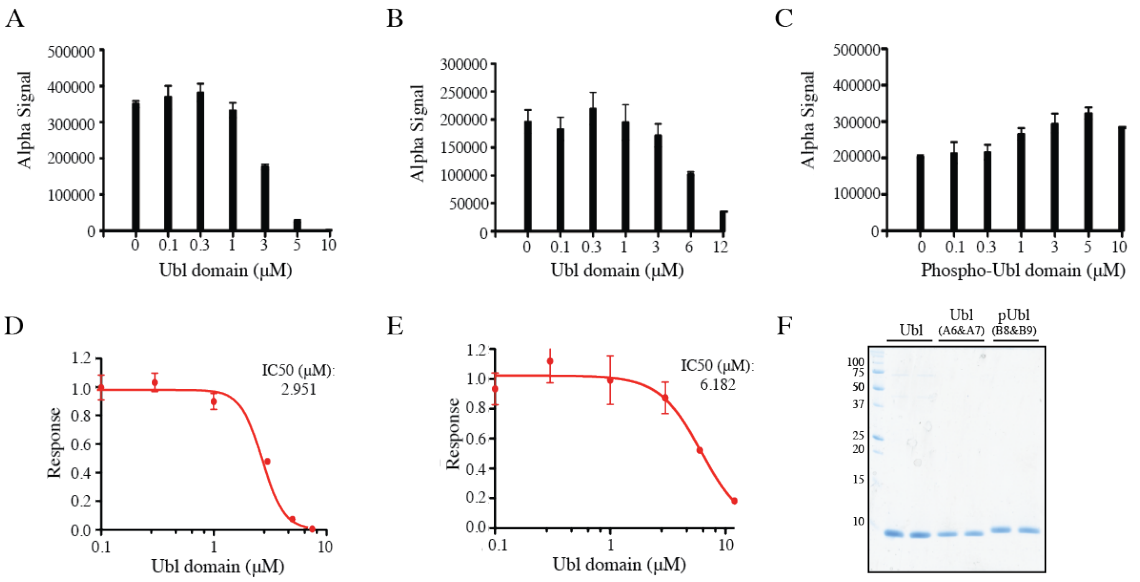

Figure 5.10: Measurement of interactions between ΔUbl Parkin and wild type and Ser65-phosphorylated Ubl domain

Performed by Dr. Jinwei Zhang **(A)** Raw data showing fluorescent signal generated by interaction between GST-Ubl (0.3 μM) and ΔUbl Parkin-biotin (0.1 μM) as increasing concentrations of Ubl (0.1 – 10 μM) are added. **(B)** Raw data showing fluorescent signal generated by interaction between GST-Ubl (0.3 μM) and ΔUbl Parkin-biotin (0.1 μM) as increasing concentrations of Ubl from pooled ion exchange fractions (A6 & A7) (0.1 – 12 μM) are added. **(C)** Raw data showing fluorescent signal generated by interaction between GST-Ubl (0.3 μM) and ΔUbl Parkin-biotin (0.1 μM) as increasing concentrations of Ser65 phospho-Ubl from pooled ion exchange fractions (B8 & B9) (0.1 – 10 μM) are added. **(D)** Processed data showing kinetics of displacement of GST-Ubl by untagged Ubl domain, with an IC_{50} value of 2.95 μM. **(E)** Processed data showing kinetics of displacement of GST-Ubl by untagged Ubl domain (fractions A6 & A7), with an IC_{50} value of 6.18 μM. **(F)** SDS-PAGE of Ubl proteins used in this experiment.

5.4 Discussion

It has been shown that PINK1 is able to activate the E3 ligase activity of Parkin in two ways: by phosphorylating Parkin in its N-terminal Ubl domain and by phosphorylating ubiquitin. Both of these PINK1 substrates are phosphorylated at residue Ser65 and both of these phosphorylation events are required to achieve maximum activation of Parkin. However, the molecular mechanisms by which these two phosphoproteins orchestrate Parkin activation were unclear. Studies with stoichiometrically phosphorylated Ubl domain (Figure 5.3) have demonstrated that phosphorylation of the Ubl domain by PINK1 appears to prevent its binding to Parkin at the site where the unphosphorylated Ubl domain normally binds (Figure 5.10), most likely the RING1 domain. Studies have shown that addition of the phospho-Ubl domain in *trans* is only able to activate ΔUbl Parkin, not the full-length enzyme (Kazlauskaite et al, 2014b). This suggests that the phospho-Ubl domain is only able to activate Parkin when the unphosphorylated Ubl domain is not bound to Parkin.

These studies, and the AlphaScreen studies described in this thesis (Figure 5.10), were conducted with phospho-Ubl domain added in *trans* to ΔUbl Parkin, whereas the Ubl domain in full-length Parkin is fused to the rest of the Parkin protein. An additional study utilising PINK1-phosphorylated Parkin and ubiquitin determined that, at least with respect to *in vitro* ubiquitin chain synthesis, phosphorylation of the Ubl domain in intact Parkin appears to be the primary Parkin-activating force (Ordureau et al, 2014). The rate constants of chain synthesis were 1.5- to 10-fold lower (depending on chain type) when full-length Parkin was activated only by phospho-ubiquitin compared to when it was activated by near-stoichiometric Ubl domain phosphorylation. Interestingly, it was also shown that phospho-Ubl domain addition in *trans* to ΔUbl Parkin led to weaker activation than the addition of phospho-ubiquitin, suggesting that it is important for the phospho-Ubl domain

to be contiguous with the rest of the Parkin molecule for it to exert its maximum activating effect (Ordureau et al, 2014). This can be explained by the fact that the Ubl domain is attached to the rest of Parkin by a flexible linker region and so upon its phosphorylation and dissociation from the RING1 domain, it is still tethered to Parkin, greatly increasing the effective local concentration and making any subsequent binding event more probable compared to when it is added in *trans*. It was not possible to detect binding of the phospho-Ubl to regions outside of the dephospho-Ubl binding site with the AlphaScreen methodology and so the binding and subsequent affinity of any interaction between the phospho-Ubl and Parkin is not known. In order to determine this, it would be necessary to perform further binding studies, such as isothermal calorimetry (ITC), between the phospho-Ubl and ΔUbl Parkin, which would mimic the situation in which the Ubl domain has already been displaced from its binding site on Parkin after PINK1 phosphorylation.

Molecular dynamics simulations carried out with a model of full-length phosphorylated Parkin have suggested that PINK1 phosphorylation of the Ubl domain acts as a trigger to begin several rearrangements that lead to Parkin assuming an active conformation (Caulfield et al, 2014). The authors of this paper suggest that firstly, the phospho-Ubl dissociates from RING1, followed by the REP helix moving away from the E2 site on RING1 and finally the RING0 domain moves away from RING2, exposing the catalytic cysteine. Interestingly, further simulations of an E2~Ub complex binding to this activated Parkin model shows that the bound E2 continues to slide across the surface of Parkin, bringing the conjugated ubiquitin molecule in close proximity to the active site cysteine (Caulfield et al, 2014). This simulation addresses the issue of the apparent great distance to be bridged between the E2 binding site and the active site in the autoinhibited Parkin structure (Wauer & Komander, 2013), however it does not take into account the additional activating effects of phospho-ubiquitin on Parkin (Kazlauskaite et al, 2014b; Ordureau et

al, 2014). Furthermore, studies on the binding of phospho-ubiquitin to Parkin and Ser65-phosphorylated Parkin have shown that Ser65 Ubl domain phosphorylation appears to increase the affinity of the interaction between phospho-ubiquitin and Parkin by approximately 21-fold; phospho-ubiquitin binds to Parkin with an affinity of 365 nM but to phospho-Parkin with an affinity of 17 nM, as determined by ITC studies (Ordureau et al, 2014).

Several unanswered questions remain. Firstly, what is the affinity of the interaction between the isolated phospho-Ubl domain and Parkin and what can be understood from this about the differing contributions of phospho-ubiquitin and the phospho-Ubl domain to Parkin activation? Secondly, where on Parkin do the phosphorylated Ubl domain and phospho-ubiquitin bind? The putative phosphate-binding pockets (Figure 5.2) make compelling candidates, however, there is currently no data to support this hypothesis. Finally, the precise molecular mechanisms by which phospho-ubiquitin and Ubl domain phosphorylation lead to the rearrangement of Parkin into an active conformation remain to be defined.

5.5 Conclusions:

For many years there has been accumulating evidence pointing towards a link between PINK1 and Parkin, beginning with the observed similarity between the respective patient phenotypes and continuing with the genetic link established by studies in *Drosophila*. Further pieces of this puzzle fell into place when it was discovered that PINK1 and Parkin act as a mitochondrial surveillance system, with PINK1 recruiting Parkin to damaged mitochondria and eventually with the discovery that PINK1 directly regulates Parkin activity by phosphorylation in its N-terminal Ubl domain. A further twist was added to this mechanism by the discovery that PINK1 also phosphorylates ubiquitin, which then acts in an allosteric fashion to control Parkin activity. This combination of Ubl domain phosphorylation and phosphorylated ubiquitin is known to be necessary for maximum Parkin activation, however the molecular mechanism of this activation remains unclear. The biophysical studies described in this chapter have provided initial insight, showing that phosphorylation of the Ubl domain displaces it from its binding site on Parkin. However, much work remains to be done to further unravel the precise events and molecular rearrangements that shift Parkin from its autoinhibited to fully active conformation.

Appendix

6 Appendix – List of supporting figures

Mutation	State in patient	Conservation in TcPINK1	Location in TcPINK1	PMID
G32R	HET (P)	✔ (G31)	MTS	18704525
P52L	HET (P)	✖ (K54)	MTS	19351622
L67F	HET (P)	✖ (R71)	MTS	18330912
R68P	HET (P)	✖ (I72)	MTS	15349860
A78V	HET (P)	✖ (T82)	Linker (MTS-TM)	18541801
C92F	CH	✖ (D101)	Linker (MTS-TM)	15349860
R98W	HET (P)	✖ (A107)	TM	18330912
I111S	HET (P)	✖ (L120)	Linker (TM-KD)	18330912
Q115L	HET (P&C)	✖ (E125)	Linker (TM-KD)	16009891
A124V	HET (C)	✖ (V129)	Linker (TM-KD)	18330912
C125G	CH	✔ (C130)	Linker (TM-KD)	16401616
Q126P	HOM	✖ (W131)	Linker (TM-KD)	18286320
T145M	HET (C)	✖ (R151)	Linker (TM-KD)	18330912
R147H	HET (P)	✖ (F152)	Linker (TM-KD)	15505171
L148W	HET (C)	✖ (E153)	Linker (TM-KD)	17344846
A168P	HOM	✖ (G174)	KD, I (Gly-rich loop)	15349860
V170G	HOM	✔ (V176)	KD, I	19500570
K186N	HET (C)	N/A	KD, Ins1	18330912
G193R	HET (P)	N/A	KD, Ins1	17960343
P196L	HET (P)	N/A	KD, Ins1	16009891
P196S	HET (C)	N/A	KD, Ins1	17344846

Figure 6.1 – continued on next page

Mutation	State in patient	Conservation in TcPINK1	Location in TcPINK1	PMID
R207Q	HET (P)	N/A	KD, Ins1	21925922
P209L	HET (C)	N/A	KD, Ins1	17344846
P209A	HET (P)	N/A	KD, Ins1	23261939
P215L	HET (C)	✔ (P192)	KD, II	17344846
A217D	HOM	✔ (A194)	KD, II	16966503
E231G	HET (P)	✖ (H208)	KD, III	15596610
N235I	HET (C)	✖ (K212)	KD, III	15596610
M237V	HET (P)	✔ (M214)	KD, III	18973254
E240K	CH	✔ (E217)	KD, III (E-K salt bridge)	15596610
A244G	CH	✔ (A221)	KD, III	18307263
R246Q	HET (P)	✖ (M223)	KD, IV	19889566
T257I	HET (P)*	✖ (E234)	KD, Ins2	18330912
R263G	HET (C)	✖ (N239)	KD, Ins2	15596610
L268V	HET (P)	✔ (L244)	KD, Ins2	16207217
H271Q	HOM	✔ (H247)	KD, Ins2	15349870
R276Q	HET (P)	✖ (A252)	KD, IV	18330912
R279H	HET (P)	✖ (S255)	KD, IV	15970950
A280T	HET (P)	✖ (V256)	KD, IV	16482571
P296L	HET (C)	✔ (P272)	KD, Ins3	18330912
P305A	HET (P)	✔ (P281)	KD, Ins3	20558144
G309D	HOM	✔ (G285)	KD, Ins3	15087508

Figure 6.1 – continued on next page

Mutation	State in patient	Conservation in TcPINK1	Location in TcPINK1	PMID
T313M	HOM	✖ (S289)	KD, V	17030667
V317I	HET (P)	✖ (L293)	KD, V	16969854
V317I	CH	✖ (L293)	KD, V	18307263
M318L	HET (P)	✔ (M294)	KD, V	15596610
P322L	HET (P)	✖ (D298)	KD, V	18330912
A339T	HET (P&C)	✖ (S314)	KD, VIA	15596610
A340T	HET (P&C)	✖ (L315)	KD, VIA	15596610
M341I	HET (C)	✖ (L316)	KD, VIA	17344864
M342V	HET (P)	✖ (L317)	KD, VIA	18541801
L347P	HOM	✔ (L322)	KD, VIA	15596610
D362H	HET (C)	✔ (D377)	KD, VIB	15596610
L369P	CH	✔ (L344)	KD, VIB	16401616
C377F	HET (C)	✖ (S352)	KD, VIB	17344846
A383T	HET (C)	✖ (S358)	KD, VII	16969854
F385L	HET (P)	✔ (F360)	KD, VII (DFG)	18704525
G386A	HOM	✔ (G361)	KD, VII (DFG)	16401616
C388R	HOM	✔ (C363)	KD, VII	15955953
G395V	HET (P)	✔ (G370)	KD, VII	18330912
P399L	HET (P) **	✔ (P374)	KD, VII/VIII	16632486
R407Q	HET (P) ***	✖ (K382)	KD, VIII	16257123
G409V	HOM	✔ (G384)	KD, VIII	16401616

Figure 6.1: Full list of reported PINK1 sequence variations

PINK1 mutations (numbering according to hPINK1) are listed along with mode of inheritance (HET: heterozygous; HOM: homozygous; CH: compound heterozygous), conservation in TcPINK1, location in TcPINK1 (MTS: mitochondrial targeting sequence; TM: transmembrane helix; KD: kinase domain, I-VII: conserved kinase subdomains) and any conserved kinase motif affected. PubMed ID (PMID) of the publication describing the identification of each variant is also listed. Green: HOM/CH, conserved in TcPINK1; orange: HOM/CH, not conserved in TcPINK1.

A

P	G	A	C	S	T	V	I	L	M	F	Y	W	H	K	R	Q	N	D	E	*
1.2	1.2	1	1	1.2	1.2	1	1	1	1	1.2	1.2	1	1	1.2	1	1	1.2	1.2	1.2	1
1.2	1.2	1	1	1.2	1.2	1	1	1	1	1.2	1.2	1	1	1.2	1	1	1.2	1.2	1.2	1
1	0.62	0.64	1	0.94	0.95	0.67	0.94	0.75	1.03	1.16	1.46	2.05	0.94	0.96	1.13	1.01	0.74	1.23	0.78	0
0.82	0.69	0.92	0.93	1.61	1.19	0.68	1.34	0.74	0.89	0.98	1.41	1.42	1.03	0.98	1.17	0.87	0.65	0.87	0.81	0
0.74	0.98	0.67	1.13	1.43	0.88	0.63	0.69	0.61	0.81	0.99	2.2	1.57	1.09	0.71	1.27	0.77	0.7	1.02	1.12	0
0.78	0.54	0.87	1.07	1.53	1.48	0.72	0.77	0.93	0.98	1.27	1.7	0.93	0.99	0.93	1.97	0.98	0.62	0.37	0.55	0
0.85	0.57	0.91	1.2	1.3	1.31	0.45	0.47	1.03	1.1	0.64	1.17	1.2	0.99	1.27	1.51	1.16	1.06	1.02	0.8	0
0.00	0.00	0.00	0.00	21.00	21.00	0.00	0.00	0.00	0.00	0.00	0.00	0.00	0.00	0.00	0.00	0.00	0.00	0.00	0.00	0.00
2.94	0.92	0.74	1.11	1.4	1.23	0.75	0.55	0.52	0.45	0.51	0.97	0.87	0.91	1.47	1.58	0.8	1.15	0.66	0.46	0
1.35	0.98	1	1.14	1.57	1.04	0.54	0.6	1.1	1.03	1.12	1.41	0.82	1	0.83	1.91	0.61	1.11	0.44	0.39	0
0.92	0.66	0.82	1.16	1.76	1.08	0.6	0.56	0.83	0.7	1.68	1.54	1.31	0.88	1.08	1.77	0.98	0.61	0.58	0.48	0
0.71	0.95	0.89	1.13	1.27	0.95	0.97	0.7	0.9	0.93	1.04	1.5	1.19	1.01	1.2	2.03	0.77	0.92	0.59	0.35	0
1.2	1.2	1	1	1.2	1.2	1	1	1	1	1.2	1.2	1	1	1.2	1	1	1.2	1.2	1.2	1
1.2	1.2	1	1	1.2	1.2	1	1	1	1	1.2	1.2	1	1	1.2	1	1	1.2	1.2	1.2	1
1.2	1.2	1	1	1.2	1.2	1	1	1	1	1.2	1.2	1	1	1.2	1	1	1.2	1.2	1.2	1.00

B

Score	ID	Protein	Position	Sequence	MW
0.2900	K1853_HUMAN	RecName: Full=Uncharacterized protein KIAA1853; AltName: Full=Medulloblastoma antigen MU-MB-2.76;	432	EKRSYSRSPSYSSKS	68713
0.2900	K1853_MOUSE	RecName: Full=Uncharacterized protein KIAA1853 homolog;	430	EKRSYSRSPSYSSKS	67980
0.3030	FA66E_HUMAN	RecName: Full=Putative protein FAM66E;	15	SQDRYRNTPSSRIFT	5233
0.3030	CAC1D_MOUSE	RecName: Full=Voltage-dependent L-type calcium channel subunit alpha-1D; AltName: Full=Voltage-gated calcium channel subunit alpha Cav1.3; AltName: Full=Calcium channel, L type, alpha-1 polypeptide isoform 2;	1923	TGYDSRRSPRRRLLP	247034
0.3046	PR38A_BOVIN	RecName: Full=Pre-mRNA-splicing factor 38A;	238	YRRSRSRSPRRRSRS	37513
0.3046	PR38A_HUMAN	RecName: Full=Pre-mRNA-splicing factor 38A;	238	YRRSRSRSPRRRSRS	37513
0.3046	PR38A_MACFA	RecName: Full=Pre-mRNA-splicing factor 38A;	238	YRRSRSRSPRRRSRS	37513
0.3046	PR38A_MOUSE	RecName: Full=Pre-mRNA-splicing factor 38A;	238	YRRSRSRSPRRRSRS	37476
0.3046	PR38A_PONAB	RecName: Full=Pre-mRNA-splicing factor 38A;	238	YRRSRSRSPRRRSRS	37513
0.3089	WDR25_HUMAN	RecName: Full=WD repeat-containing protein 25;	462	TVWPYRMSRRRRYEG	60197
0.3143	SRRM1_HUMAN	RecName: Full=Serine/arginine repetitive matrix protein 1; AltName: Full=Ser/Arg-related nuclear matrix protein; AltName: Full=SR-related nuclear matrix protein of 160 kDa; Short=SRm160;	310	RSRSRSYSPRRRPSP	102518
0.3143	SRRM1_MOUSE	RecName: Full=Serine/arginine repetitive matrix protein 1; AltName: Full=Plenty-of-prolines 101;	308	RSRSRSYSPRRRPSP	107084
0.3143	SRRM1_PONAB	RecName: Full=Serine/arginine repetitive matrix protein 1;	310	RSRSRSYSPRRRPSP	104084
0.3153	SFR2B_HUMAN	RecName: Full=Splicing factor, arginine/serine-rich 2B; AltName: Full=Pre-mRNA-splicing factor SRP46; Short=Splicing factor SRp46;	158	RGSRYSRSPYSRSPY	32347
0.3228	PRP4B_BOVIN	RecName: Full=Serine/threonine-protein kinase PRP4 homolog; EC=2.7.11.1; AltName: Full=PRP4 pre-mRNA-processing factor 4 homolog;	468	SPRRRSRSPRRRDRG	116775

Figure 6.2: PINKtide ScanSite matrix

(A) Weighted matrix for searching the ScanSite database determined from Figure 3.10 showing the preference for each amino acid at a given position within a substrate peptide. **(B)** Results from using ScanSite to search SwissProt for mammalian proteins matching the matrix shown in (A).

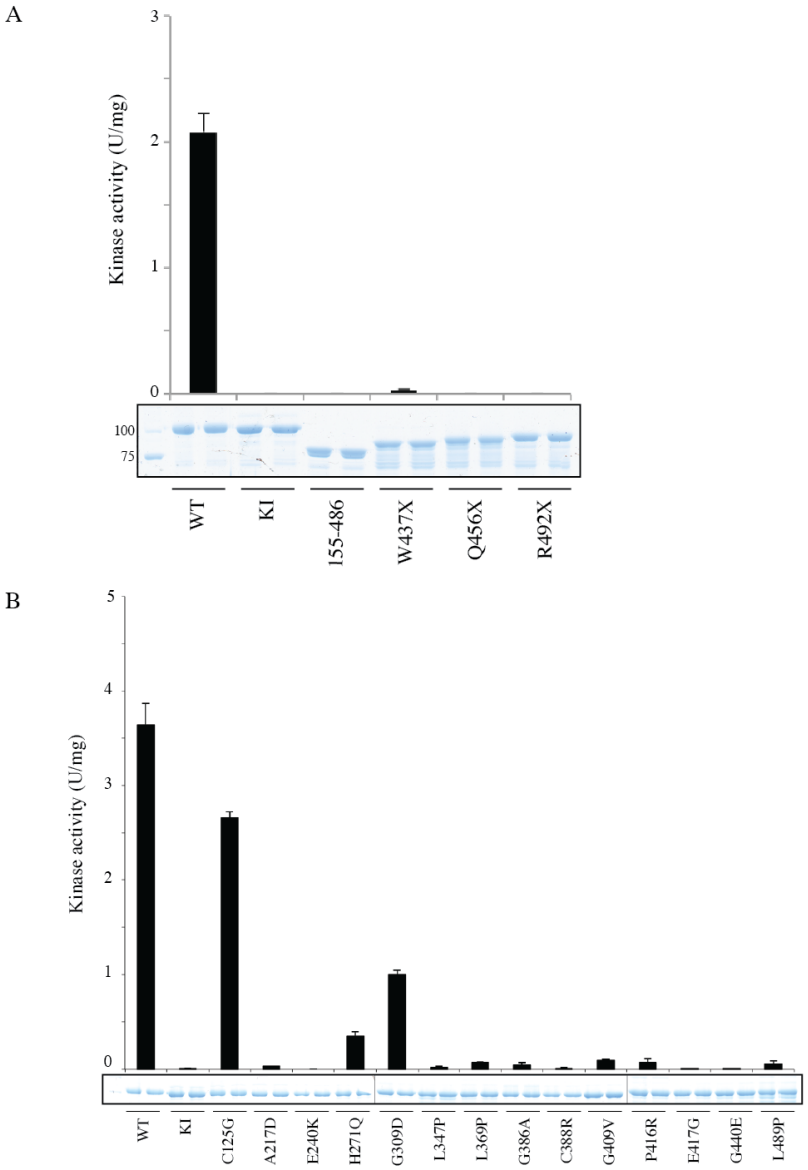

Figure 6.3: Effect of Parkinson's disease-linked mutations in TcPINK1 against myelin basic protein

(A) Full-length MBP-tagged TcPINK1 enzymes containing point mutations (1 μg) were incubated in presence of myelin basic protein (5 μg) and [γ^{32}P] ATP for 30 min. Reactions were terminated by spotting onto P81 paper, and quantified by scintillation counting. The results are presented as ± SD for three experiments undertaken in duplicate (upper panel). In the lower panel, representative Coomassie stained gels showing the relative amounts of PINK1 enzyme used for each assay are shown. **(B)** Full-length MBP-tagged TcPINK1 enzymes containing point mutations (1 μg) were incubated in presence of myelin basic protein (5 μg) and [γ^{32}P] ATP for 30 min. Reactions were terminated by spotting onto P81 paper, and quantified by scintillation counting. The results are presented as ± SD for three experiments undertaken in duplicate (upper panel). In the lower panel, representative Coomassie stained gels showing the relative amounts of PINK1 enzyme used for each assay are shown.

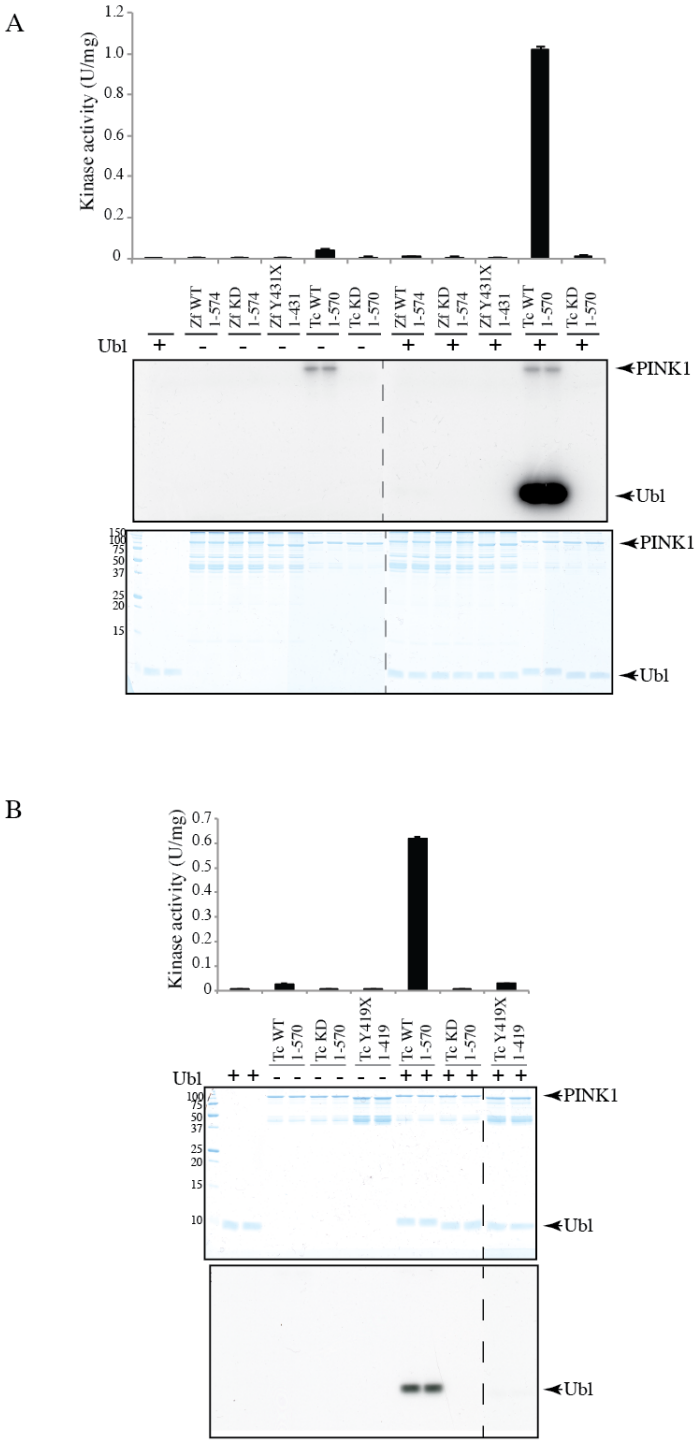

Figure 6.4 Activity of Zebrafish PINK1 and TcPINK1 Y419X mutant against Ubl domain

(A) Full-length MBP-tagged wild type, kinase inactive (D372A) ZfPINK1, Y431X mutant and TcPINK1 wild type and kinase inactive (D359A) (1µg) were incubated in the presence of [γ^{32}P] ATP and Ubl domain (2 µM) for 30 min at 30°C. Assays were terminated by addition of loading buffer and separated by SDS-PAGE. Proteins were detected by Coomassie staining (upper panel) and incorporation of [γ^{32}P] ATP was detected by autoradiography (lower panel). Fine dividing lines indicate that reactions were resolved on separate gels and grouped in the final figure. Phosphorylation was quantified by

scintillation counting of excised gel bands. **(B)** Full-length MBP-tagged wild type and kinase inactive (D359A) TcPINK1 and Y419X mutant (1μg) were incubated in the presence of [γ^{32}P] ATP and MBP (2 μM) for 30 min at 30°C. Assays were terminated by addition of loading buffer and separated by SDS-PAGE. Proteins were detected by Coomassie staining (upper panel) and incorporation of [γ^{32}P] ATP was detected by autoradiography (lower panel). Fine dividing lines indicate that reactions were resolved on separate gels and grouped in the final figure. Phosphorylation was quantified by scintillation counting of excised gel bands.

His-SUMO 138-570 D359A IEX:

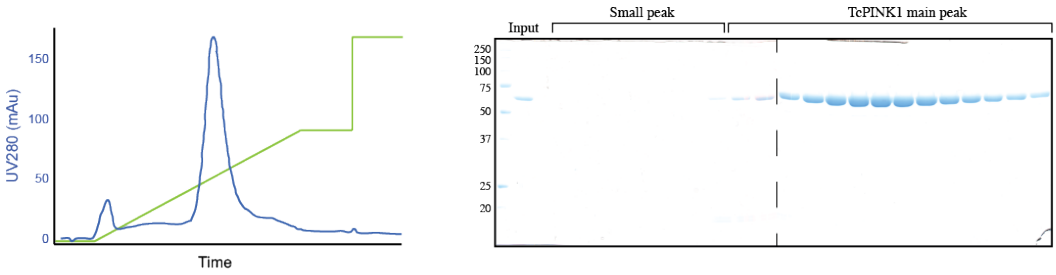

His-SUMO 147-570 D359A IEX:

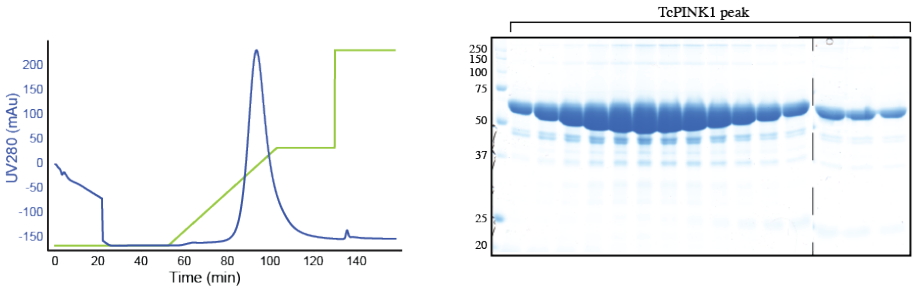

His-SUMO 148-570 D359A IEX:

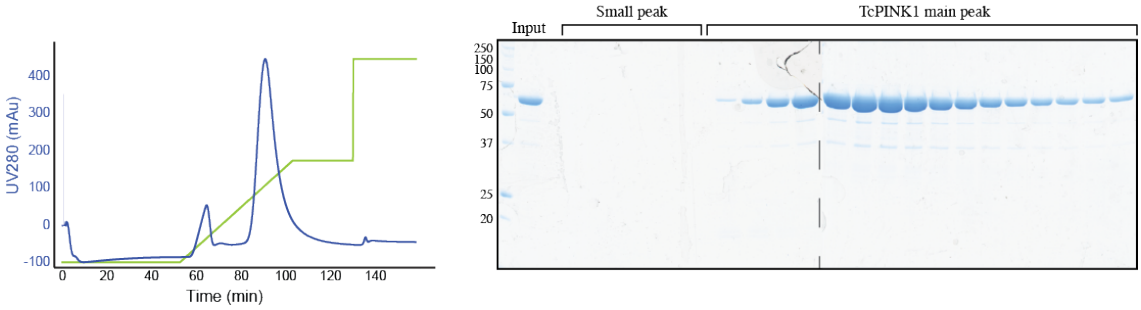

His-SUMO 152-570 D359A IEX:

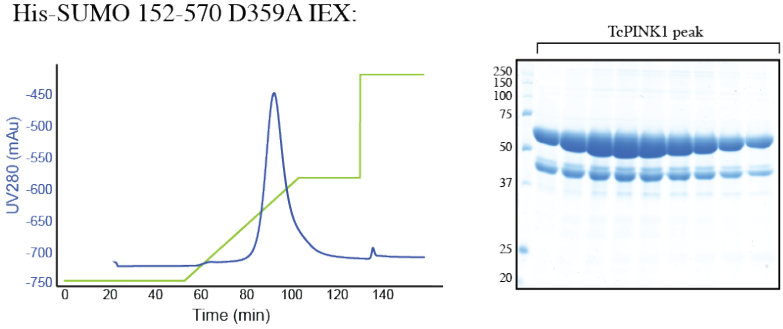

Figure 6.5 – continued on next page

His-SUMO 153-570 D359A IEX:

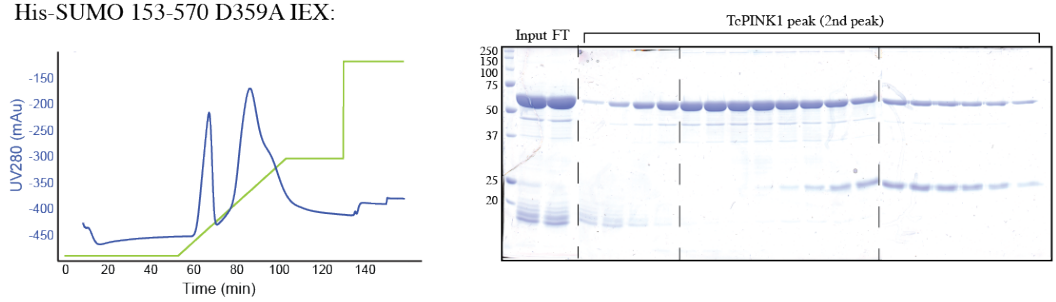

His-SUMO 156-570 D359A IEX and SENP1 cleavage:

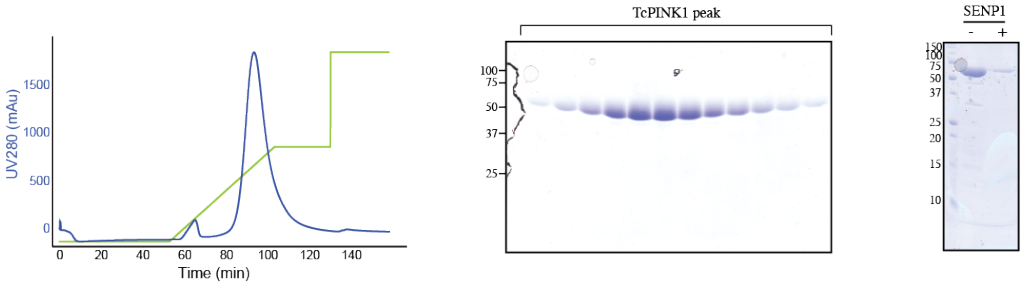

His-SUMO 157-570 D359A IEX:

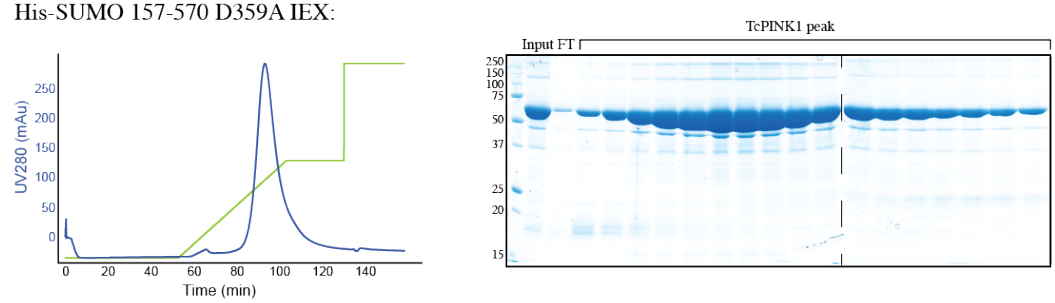

His-SUMO 160-570 D359A IEX:

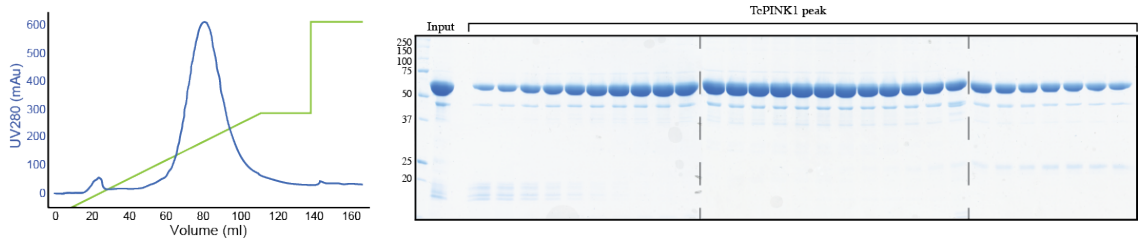

Figure 6.5 – continued on next page

His-SUMO 165-570 D359A IEX:

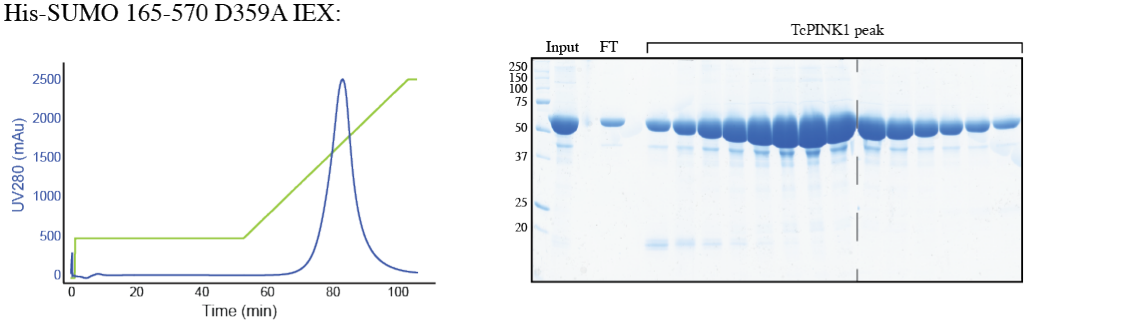

165-570 D359A GF:

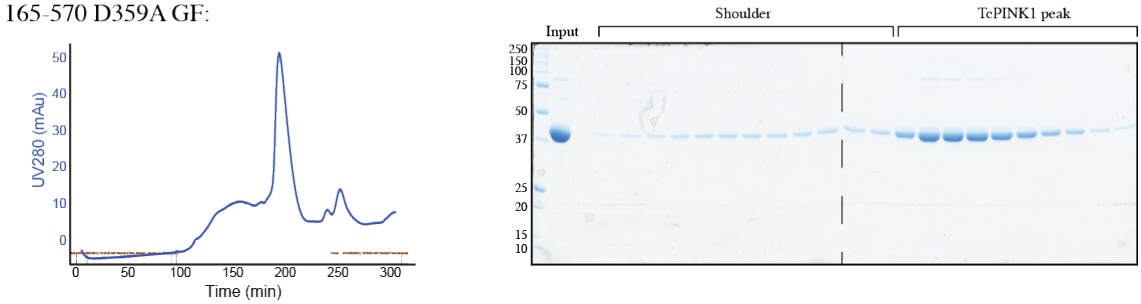

Figure 6.5: Purification of His-SUMO TcPINK1 constructs not used for crystallization trials

Anion exchange and gel filtration chromatograms and SDS-PAGE gels for the indicated constructs are shown. For chromatograms, blue: absorbance at 280 nm; green: % buffer B. For SDS-PAGE gels, Input: protein before purification; FT: flow through not bound to column; TcPINK1 peak: peak fractions.

Screen	Ligand?	Details
JCSG I/II	None, ADP	N/A
Proplex I/II	None	N/A
Index I/II	None, ADP, ATP, AMP-PNP	N/A
Membfac	None, ADP, AMP-PNP	N/A
Natrix	None, ADP, AMP-PNP	N/A
PEG/Ion	None, ADP	N/A
PACT Premier	None, ADP	N/A
MemStart/MemSys	None, ADP	N/A
MemPlus	None, ADP	N/A
Crystal Screen I/II	None, ADP	N/A
Protein Complex	None, ADP	N/A
Grid Screen	None, ADP, ATP, AMP-PNP	Hit from JCSG 2.18
Grid Screen	None, ADP, ATP, AMP-PNP	Hit from Natrix 37
Grid Screen	None, ADP, ATP, AMP-PNP	Hit from Natrix 38
Grid Screen	None, ADP, ATP, AMP-PNP	Hit from Membfac 26
Grid Screen	None, ADP, ATP, AMP-PNP	Hit from Membfac 28
Grid Screen	None, ADP, ATP, AMP-PNP	Hit from Membfac 43
Grid Screen	None, ADP, ATP, AMP-PNP	Hit from Membfac 45
Grid Screen	None, ADP, ATP, AMP-PNP	Hit from Membfac 19
Grid Screen	None, ADP, ATP, AMP-PNP	Hit from Crystal Screen 2.33
Additive Screen	None, ADP	On hit from grid screen around JCSG 2.18
Additive Screen	None, ADP	On hit from grid screen around Membfac 28

Figure 6.6 – continued on next page

Screen	Ligand?	Details
Additive Screen	None, ADP	On hit from grid screen around Natrix 38
Additive Screen	ATP, AMP-PNP	On hit (I) from grid screen around Membfac 26
Additive Screen	None, ADP	On hit (II) from grid screen around Membfac 26

Figure 6.6: List of crystallization screens set up for TcPINK1 155-570 (D359A)

The name/type of each screen is given along with ligands included and details in the case of grid screens and additive screens. This list is not exhaustive and screens may have been set up more than once, for example with variations in protein concentration.

Screen	Ligand?	Details
JCSG I/II	None, ADP	N/A
Crystal Screen I/II	None, ADP	N/A
Index I/II	None, ADP	N/A
Membfac	None, ADP	N/A
Natrix	None, ADP	N/A

Figure 6.7: List of crystallization screens set up for lysine methylated TcPINK1 155-570 (D359A)

The name/type of each screen is given along with ligands included and details in the case of grid screens and additive screens. This list is not exhaustive and screens may have been set up more than once, for example with variations in protein concentration.

Screen	Ligand?	Details
JCSG I/II	None, ADP, AMP-PNP	N/A
Crystal Screen I/II	None, AMP-PNP	N/A
Index I/II	None, AMP-PNP	N/A
Membfac	None, ADP, AMP-PNP	N/A
Natrix	None, ADP, AMP-PNP	N/A
Salt RX	None, AMP-PNP	N/A
Morpheus	None, ADP	N/A
MemStart/MemSys	None, ADP	N/A
MemPlus	None, ADP	N/A
PACT Premier	None, ADP	N/A
ProPlex I/II	None, ADP	N/A
Protein Complex	None, ADP	N/A
Grid Screen	None, ADP, ATP, AMP-PNP	Hit from JCSG 2.10
Grid Screen	None, ADP, ATP, AMP-PNP	Hit from JCSG 2.47
Grid Screen	None, ADP, ATP, AMP-PNP	Hit from Membfac 31
Grid Screen	None, ADP, ATP, AMP-PNP	Hit from Membfac 21
Grid Screen	None, ADP, ATP, AMP-PNP	Hit from Membfac 15
Grid Screen	None, ADP,	Hit from MemPlus A2
Grid Screen	None, ADP	Hit from MemPlus C4
Grid Screen	None, ADP,	Hit from MemPlus D6
Grid Screen	None, ADP	Hit from MemPlus B10
Grid Screen	None, ADP	His from MemStart/MemSys A2

Figure 6.8 – continued on next page

Screen	Ligand?	Details
Grid Screen	None, ADP	On hit from PACT G11
Grid Screen	None, ADP	On hit from Proplex F9
Additive Screen	None, ADP	On hit (I) from grid screen around Membfac 15
Additive Screen	None, AMP-PNP	On hit (II) from grid screen around Membfac 15

Figure 6.8: List of crystallization screens set up for TcPINK1 150-570 (D359A)

The name/type of each screen is given along with ligands included and details in the case of grid screens and additive screens. This list is not exhaustive and screens may have been set up more than once, for example with variations in protein concentration.

Screen	Ligand?	Details
JCSG I/II	None, ADP	N/A
Crystal Screen I/II	None, ADP	N/A
Index I/II	None, ADP	N/A
Membfac	None, ADP	N/A
Natrix	None, ADP	N/A
Salt RX	None, ADP	N/A
PACT Premier	None, ADP	N/A

Figure 6.9: List of crystallization screens set up for lysine methylated TcPINK1 150-570 (D359A)

The name/type of each screen is given along with ligands included and details in the case of grid screens and additive screens. This list is not exhaustive and screens may have been set up more than once, for example with variations in protein concentration.

Screen	Ligand?	Details
JCSG I/II	None, ADP	N/A
Crystal Screen I/II	None, ADP	N/A
Index I/II	None, ADP	N/A
Membfac	None, ADP	N/A
Natrix	None, ADP	N/A
Proplex I/II	None, ADP	N/A
PACT Premier	None, ADP	N/A
Grid Screen	None, ADP	On hit from Membfac 13
Grid Screen	None, ADP	On hit from JCSG 2.15
Grid Screen	None, ADP	On hit from CS 2.31
Grid Screen	None, ADP	On hit from Index 35

Figure 6.10: List of crystallization screens set up for TcPINK1 149-570 (D359A)

The name/type of each screen is given along with ligands included and details in the case of grid screens and additive screens.

Screen	Ligand?	Details
JCSG I/II	None, ADP	N/A
Crystal Screen I/II	None, ADP	N/A
Index I/II	None, ADP	N/A
Membfac	None, ADP	N/A
Natrix	None, ADP	N/A
Proplex I/II	None, ADP	N/A
PACT Premier	None, ADP	N/A
Grid Screen	None, ADP	On hit from Membfac 13
Grid Screen	None, ADP	On hit from JCSG 2.15
Grid Screen	None, ADP	On hit from CS 2.31
Grid Screen	None, ADP	On hit from Index 35

Figure 6.11: List of crystallization screens set up for TcPINK1 151-570 (D359A)

The name/type of each screen is given along with ligands included and details in the case of grid screens and additive screens.

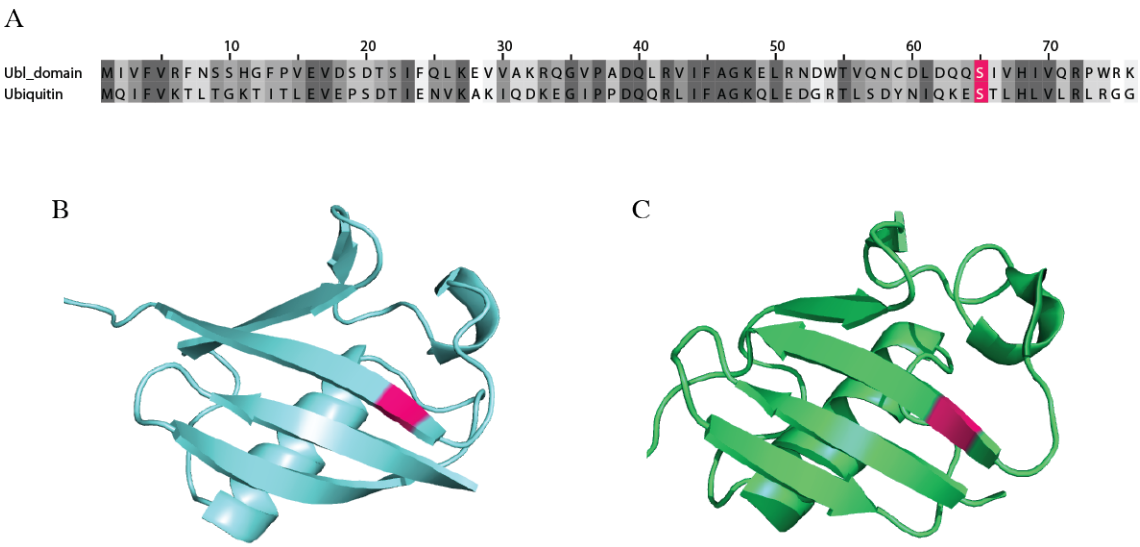

Figure 6.12: Sequence alignment and structure of Ubl domain and ubiquitin

(A) Sequence alignment of Ubl domain of Parkin and ubiquitin, with Ser65 highlighted in pink. **(B)** Crystal structure of ubiquitin with S65 highlighted in pink. PDB ID: 1UBQ. **(C)** Solution NMR structure of Ubl domain with S65 highlighted in pink. PDB ID: 1IYF.

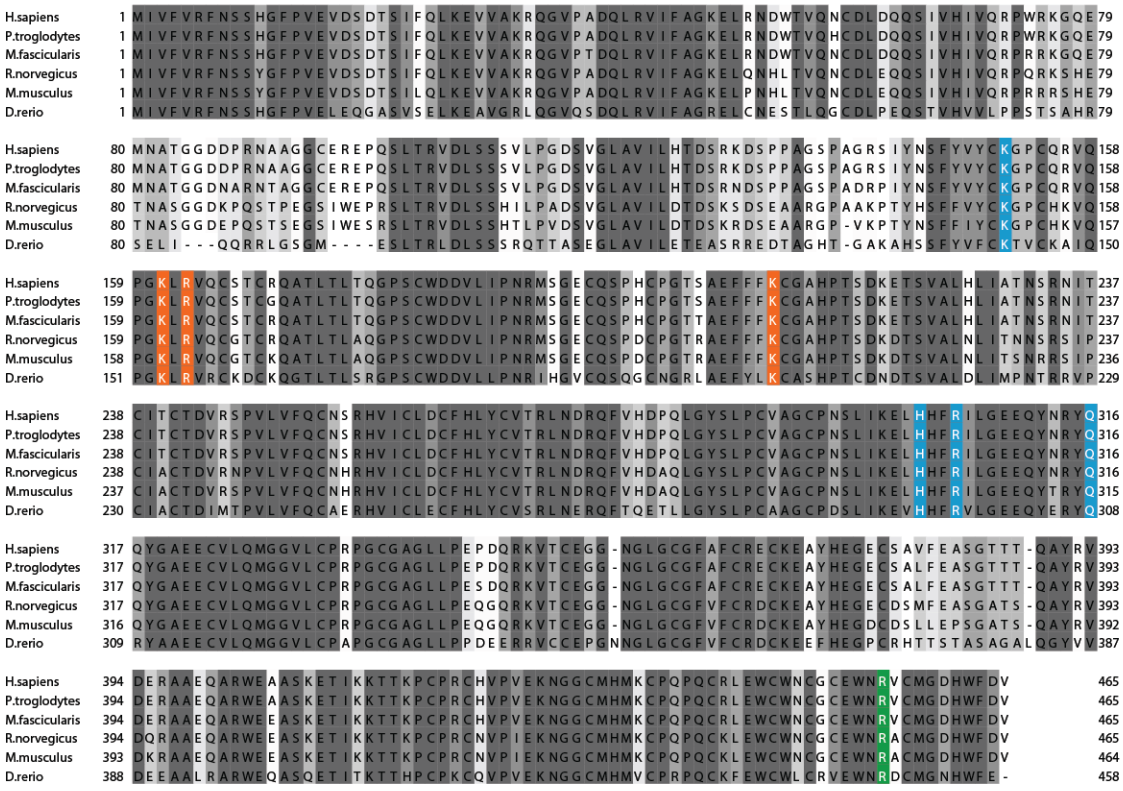

Figure 6.13: Multiple sequence alignment of Parkin

Multiple sequence alignment of human Parkin with sulphate-binding pockets highlighted. Orange: Pocket 1 (K161, R163, K211); blue: Pocket 2 (K151, H302, R305, Q316); green: Pocket 3 (R455).

Bibliography

7 Bibiliography

Aarsland D, Bronnick K, Ehrt U, De Deyn PP, Tekin S, Emre M, Cummings JL (2007) Neuropsychiatric symptoms in patients with Parkinson's disease and dementia: frequency, profile and associated care giver stress. *J Neurol Neurosurg Psychiatry* **78:** 36-42

Abramov AY, Gegg M, Grunewald A, Wood NW, Klein C, Schapira AH (2011) Bioenergetic consequences of PINK1 mutations in Parkinson disease. *PLoS One* **6:** e25622

Adams JA (2001) Kinetic and catalytic mechanisms of protein kinases. *Chem Rev* **101:** 2271-2290

Alessi DR, Caudwell FB, Andjelkovic M, Hemmings BA, Cohen P (1996) Molecular basis for the substrate specificity of protein kinase B; comparison with MAPKAP kinase-1 and p70 S6 kinase. *FEBS Lett* **399:** 333-338

Anderson KE, Coadwell J, Stephens LR, Hawkins PT (1998) Translocation of PDK-1 to the plasma membrane is important in allowing PDK-1 to activate protein kinase B. *Curr Biol* **8:** 684-691

Aranda S, Laguna A, de la Luna S (2011) DYRK family of protein kinases: evolutionary relationships, biochemical properties, and functional roles. *Faseb J* **25:** 449-462

Bartels T, Choi JG, Selkoe DJ (2011) alpha-Synuclein occurs physiologically as a helically folded tetramer that resists aggregation. *Nature* **477:** 107-110

Batkin M, Schvartz I, Shaltiel S (2000) Snapping of the carboxyl terminal tail of the catalytic subunit of PKA onto its core: characterization of the sites by mutagenesis. *Biochemistry* **39:** 5366-5373

Bax B, Carter PS, Lewis C, Guy AR, Bridges A, Tanner R, Pettman G, Mannix C, Culbert AA, Brown MJ, Smith DG, Reith AD (2001) The structure of phosphorylated GSK-3beta complexed with a peptide, FRATtide, that inhibits beta-catenin phosphorylation. *Structure* **9:** 1143-1152

Bayliss R, Sardon T, Vernos I, Conti E (2003) Structural basis of Aurora-A activation by TPX2 at the mitotic spindle. *Mol Cell* **12:** 851-862

Becker D, Richter J, Tocilescu MA, Przedborski S, Voos W (2012) Pink1 kinase and its membrane potential (Deltapsi)-dependent cleavage product both localize to outer mitochondrial membrane by unique targeting mode. *J Biol Chem* **287:** 22969-22987

Beilina A, Van Der Brug M, Ahmad R, Kesavapany S, Miller DW, Petsko GA, Cookson MR (2005) Mutations in PTEN-induced putative kinase 1 associated with recessive

parkinsonism have differential effects on protein stability. *Proc Natl Acad Sci U S A* **102:** 5703-5708

Beitz JM (2014) Parkinson's disease: a review. *Front Biosci (Schol Ed)* **6:** 65-74

Berardelli A, Rothwell JC, Thompson PD, Hallett M (2001) Pathophysiology of bradykinesia in Parkinson's disease. *Brain* **124:** 2131-2146

Bergman H, Deuschl G (2002) Pathophysiology of Parkinson's disease: from clinical neurology to basic neuroscience and back. *Mov Disord* **17 Suppl 3:** S28-40

Bernheimer H, Birkmayer W, Hornykiewicz O, Jellinger K, Seitelberger F (1973) Brain dopamine and the syndromes of Parkinson and Huntington. Clinical, morphological and neurochemical correlations. *J Neurol Sci* **20:** 415-455

Berwick DC, Hers I, Heesom KJ, Moule SK, Tavare JM (2002) The identification of ATP-citrate lyase as a protein kinase B (Akt) substrate in primary adipocytes. *J Biol Chem* **277:** 33895-33900

Billia F, Hauck L, Konecny F, Rao V, Shen J, Mak TW (2011) PTEN-inducible kinase 1 (PINK1)/Park6 is indispensable for normal heart function. *Proc Natl Acad Sci U S A* **108:** 9572-9577

Blackinton JG, Anvret A, Beilina A, Olson L, Cookson MR, Galter D (2007) Expression of PINK1 mRNA in human and rodent brain and in Parkinson's disease. *Brain Res* **1184:** 10-16

Bonifati V, Rizzu P, van Baren MJ, Schaap O, Breedveld GJ, Krieger E, Dekker MC, Squitieri F, Ibanez P, Joosse M, van Dongen JW, Vanacore N, van Swieten JC, Brice A, Meco G, van Duijn CM, Oostra BA, Heutink P (2003) Mutations in the DJ-1 gene associated with autosomal recessive early-onset parkinsonism. *Science* **299:** 256-259

Bradford MM (1976) A rapid and sensitive method for the quantitation of microgram quantities of protein utilizing the principle of protein-dye binding. *Anal Biochem* **72:** 248-254

Brown NR, Noble ME, Endicott JA, Johnson LN (1999) The structural basis for specificity of substrate and recruitment peptides for cyclin-dependent kinases. *Nat Cell Biol* **1:** 438-443

Bullock AN, Das S, Debreczeni JE, Rellos P, Fedorov O, Niesen FH, Guo K, Papagrigoriou E, Amos AL, Cho S, Turk BE, Ghosh G, Knapp S (2009) Kinase domain insertions define distinct roles of CLK kinases in SR protein phosphorylation. *Structure* **17:** 352-362

Burchell L, Chaugule VK, Walden H (2012) Small, N-terminal tags activate Parkin E3 ubiquitin ligase activity by disrupting its autoinhibited conformation. *PLoS One* **7:** e34748

Burnett G, Kennedy EP (1954) The enzymatic phosphorylation of proteins. *J Biol Chem* **211:** 969-980

Bussell R, Jr., Eliezer D (2001) Residual structure and dynamics in Parkinson's disease-associated mutants of alpha-synuclein. *J Biol Chem* **276:** 45996-46003

Capdeville R, Silberman S, Dimitrijevic S (2002) Imatinib: the first 3 years. *Eur J Cancer* **38 Suppl 5:** S77-82

Cardona F, Sanchez-Mut JV, Dopazo H, Perez-Tur J (2011) Phylogenetic and in silico structural analysis of the Parkinson disease-related kinase PINK1. *Hum Mutat* **32:** 369-378

Caulfield TR, Fiesel FC, Moussaud-Lamodiere EL, Dourado DF, Flores SC, Springer W (2014) Phosphorylation by PINK1 Releases the UBL Domain and Initializes the Conformational Opening of the E3 Ubiquitin Ligase Parkin. *PLoS Comput Biol* **10:** e1003935

Chan DC (2006) Mitochondrial fusion and fission in mammals. *Annu Rev Cell Dev Biol* **22:** 79-99

Chaugule VK, Burchell L, Barber KR, Sidhu A, Leslie SJ, Shaw GS, Walden H (2011) Autoregulation of Parkin activity through its ubiquitin-like domain. *Embo J* **30:** 2853-2867

Chin JW (2014) Expanding and reprogramming the genetic code of cells and animals. *Annu Rev Biochem* **83:** 379-408

Clark IE, Dodson MW, Jiang C, Cao JH, Huh JR, Seol JH, Yoo SJ, Hay BA, Guo M (2006) Drosophila pink1 is required for mitochondrial function and interacts genetically with parkin. *Nature* **441:** 1162-1166

Cohen P (2002) The origins of protein phosphorylation. *Nat Cell Biol* **4:** E127-130

Cotzias GC, Van Woert MH, Schiffer LM (1967) Aromatic amino acids and modification of parkinsonism. *N Engl J Med* **276:** 374-379

Cross DA, Alessi DR, Cohen P, Andjelkovich M, Hemmings BA (1995) Inhibition of glycogen synthase kinase-3 by insulin mediated by protein kinase B. *Nature* **378:** 785-789

Dar AC, Dever TE, Sicheri F (2005) Higher-order substrate recognition of eIF2alpha by the RNA-dependent protein kinase PKR. *Cell* **122:** 887-900

De Bondt HL, Rosenblatt J, Jancarik J, Jones HD, Morgan DO, Kim SH (1993) Crystal structure of cyclin-dependent kinase 2. *Nature* **363:** 595-602

de Lau LM, Breteler MM (2006) Epidemiology of Parkinson's disease. *Lancet Neurol* **5:** 525-535

Deas E, Plun-Favreau H, Gandhi S, Desmond H, Kjaer S, Loh SH, Renton AE, Harvey RJ, Whitworth AJ, Martins LM, Abramov AY, Wood NW (2011) PINK1 cleavage at position A103 by the mitochondrial protease PARL. *Hum Mol Genet* **20:** 867-879

Derewenda ZS (2004) Rational protein crystallization by mutational surface engineering. *Structure* **12:** 529-535

Duker AP, Espay AJ (2013) Surgical treatment of Parkinson disease: past, present, and future. *Neurol Clin* **31:** 799-808

Edgar RC (2004a) MUSCLE: a multiple sequence alignment method with reduced time and space complexity. *BMC Bioinformatics* **5:** 113

Edgar RC (2004b) MUSCLE: multiple sequence alignment with high accuracy and high throughput. *Nucleic Acids Res* **32:** 1792-1797

Ehringer H, Hornykiewicz O (1960) [Distribution of noradrenaline and dopamine (3-hydroxytyramine) in the human brain and their behavior in diseases of the extrapyramidal system]. *Klin Wochenschr* **38:** 1236-1239

Farriol-Mathis N, Garavelli JS, Boeckmann B, Duvaud S, Gasteiger E, Gateau A, Veuthey AL, Bairoch A (2004) Annotation of post-translational modifications in the Swiss-Prot knowledge base. *Proteomics* **4:** 1537-1550

Finley D (2009) Recognition and processing of ubiquitin-protein conjugates by the proteasome. *Annu Rev Biochem* **78:** 477-513

Frame S, Cohen P (2001) GSK3 takes centre stage more than 20 years after its discovery. *Biochem J* **359:** 1-16

Frame S, Cohen P, Biondi RM (2001) A common phosphate binding site explains the unique substrate specificity of GSK3 and its inactivation by phosphorylation. *Mol Cell* **7:** 1321-1327

Gandhi S, Wood-Kaczmar A, Yao Z, Plun-Favreau H, Deas E, Klupsch K, Downward J, Latchman DS, Tabrizi SJ, Wood NW, Duchen MR, Abramov AY (2009) PINK1-associated Parkinson's disease is caused by neuronal vulnerability to calcium-induced cell death. *Mol Cell* **33:** 627-638

Gautier CA, Kitada T, Shen J (2008) Loss of PINK1 causes mitochondrial functional defects and increased sensitivity to oxidative stress. *Proc Natl Acad Sci U S A* **105:** 11364-11369

Geisler S, Holmstrom KM, Skujat D, Fiesel FC, Rothfuss OC, Kahle PJ, Springer W (2010) PINK1/Parkin-mediated mitophagy is dependent on VDAC1 and p62/SQSTM1. *Nat Cell Biol* **12:** 119-131

Goldberg J, Nairn AC, Kuriyan J (1996) Structural basis for the autoinhibition of calcium/calmodulin-dependent protein kinase I. *Cell* **84:** 875-887

Goldschmidt L, Cooper DR, Derewenda ZS, Eisenberg D (2007) Toward rational protein crystallization: A Web server for the design of crystallizable protein variants. *Protein Sci* **16:** 1569-1576

Greene AW, Grenier K, Aguileta MA, Muise S, Farazifard R, Haque ME, McBride HM, Park DS, Fon EA (2012) Mitochondrial processing peptidase regulates PINK1 processing, import and Parkin recruitment. *EMBO Rep* **13:** 378-385

Greene JC, Whitworth AJ, Kuo I, Andrews LA, Feany MB, Pallanck LJ (2003) Mitochondrial pathology and apoptotic muscle degeneration in Drosophila parkin mutants. *Proc Natl Acad Sci U S A* **100:** 4078-4083

Hagelueken G, Huang H, Harlos K, Clarke BR, Whitfield C, Naismith JH (2012) Crystallization, dehydration and experimental phasing of WbdD, a bifunctional kinase and methyltransferase from Escherichia coli O9a. *Acta Crystallogr D Biol Crystallogr* **68:** 1371-1379

Hanks SK, Hunter T (1995) Protein kinases 6. The eukaryotic protein kinase superfamily: kinase (catalytic) domain structure and classification. *Faseb J* **9:** 576-596

Heinemann IU, Rovner AJ, Aerni HR, Rogulina S, Cheng L, Olds W, Fischer JT, Soll D, Isaacs FJ, Rinehart J (2012) Enhanced phosphoserine insertion during Escherichia coli protein synthesis via partial UAG codon reassignment and release factor 1 deletion. *FEBS Lett* **586:** 3716-3722

Heras B, Edeling MA, Byriel KA, Jones A, Raina S, Martin JL (2003) Dehydration converts DsbG crystal diffraction from low to high resolution. *Structure* **11:** 139-145

Hertz NT, Berthet A, Sos ML, Thorn KS, Burlingame AL, Nakamura K, Shokat KM (2013) A neo-substrate that amplifies catalytic activity of parkinson's-disease-related kinase PINK1. *Cell* **154:** 737-747

Hindle JV, Petrelli A, Clare L, Kalbe E (2013) Nonpharmacological enhancement of cognitive function in Parkinson's disease: a systematic review. *Mov Disord* **28:** 1034-1049

Hope H (1988) Cryocrystallography of biological macromolecules: a generally applicable method. *Acta Crystallogr B* **44 (Pt 1):** 22-26

Hughes AJ, Daniel SE, Blankson S, Lees AJ (1993) A clinicopathologic study of 100 cases of Parkinson's disease. *Arch Neurol* **50:** 140-148

Huse M, Kuriyan J (2002) The conformational plasticity of protein kinases. *Cell* **109:** 275-282

Hutti JE, Jarrell ET, Chang JD, Abbott DW, Storz P, Toker A, Cantley LC, Turk BE (2004) A rapid method for determining protein kinase phosphorylation specificity. *Nat Methods* **1:** 27-29

Jaleel M, Nichols RJ, Deak M, Campbell DG, Gillardon F, Knebel A, Alessi DR (2007) LRRK2 phosphorylates moesin at threonine-558: characterization of how Parkinson's disease mutants affect kinase activity. *Biochem J* **405:** 307-317

Jankovic J (2008) Parkinson's disease: clinical features and diagnosis. *J Neurol Neurosurg Psychiatry* **79:** 368-376

Jeffrey PD, Russo AA, Polyak K, Gibbs E, Hurwitz J, Massague J, Pavletich NP (1995) Mechanism of CDK activation revealed by the structure of a cyclinA-CDK2 complex. *Nature* **376:** 313-320

Jin SM, Lazarou M, Wang C, Kane LA, Narendra DP, Youle RJ (2010) Mitochondrial membrane potential regulates PINK1 import and proteolytic destabilization by PARL. *J Cell Biol* **191:** 933-942

Johnson LN, Lewis RJ (2001) Structural basis for control by phosphorylation. *Chem Rev* **101:** 2209-2242

Kahle PJ, Waak J, Gasser T (2009) DJ-1 and prevention of oxidative stress in Parkinson's disease and other age-related disorders. *Free Radic Biol Med* **47:** 1354-1361

Kallunki T, Su B, Tsigelny I, Sluss HK, Derijard B, Moore G, Davis R, Karin M (1994) JNK2 contains a specificity-determining region responsible for efficient c-Jun binding and phosphorylation. *Genes Dev* **8:** 2996-3007

Kane LA, Lazarou M, Fogel AI, Li Y, Yamano K, Sarraf SA, Banerjee S, Youle RJ (2014) PINK1 phosphorylates ubiquitin to activate Parkin E3 ubiquitin ligase activity. *J Cell Biol* **205:** 143-153

Katzenschlager R, Lees AJ (2002) Treatment of Parkinson's disease: levodopa as the first choice. *J Neurol* **249 Suppl 2:** II19-24

Kazlauskaite A, Kelly V, Johnson C, Baillie C, Hastie CJ, Peggie M, Macartney T, Woodroof HI, Alessi DR, Pedrioli PG, Muqit MM (2014a) Phosphorylation of Parkin at Serine65 is essential for activation: elaboration of a Miro1 substrate-based assay of Parkin E3 ligase activity. *Open Biol* **4:** 130213

Kazlauskaite A, Kondapalli C, Gourlay R, Campbell DG, Ritorto MS, Hofmann K, Alessi DR, Knebel A, Trost M, Muqit MM (2014b) Parkin is activated by PINK1-dependent phosphorylation of ubiquitin at Ser65. *Biochem J* **460:** 127-139

Kemp BE, Graves DJ, Benjamini E, Krebs EG (1977) Role of multiple basic residues in determining the substrate specificity of cyclic AMP-dependent protein kinase. *J Biol Chem* **252:** 4888-4894

Khoury GA, Baliban RC, Floudas CA (2011) Proteome-wide post-translational modification statistics: frequency analysis and curation of the swiss-prot database. *Sci Rep* **1**

Kim Y, Park J, Kim S, Song S, Kwon SK, Lee SH, Kitada T, Kim JM, Chung J (2008) PINK1 controls mitochondrial localization of Parkin through direct phosphorylation. *Biochem Biophys Res Commun* **377:** 975-980

Kitada T, Asakawa S, Hattori N, Matsumine H, Yamamura Y, Minoshima S, Yokochi M, Mizuno Y, Shimizu N (1998) Mutations in the parkin gene cause autosomal recessive juvenile parkinsonism. *Nature* **392:** 605-608

Kitada T, Pisani A, Porter DR, Yamaguchi H, Tscherter A, Martella G, Bonsi P, Zhang C, Pothos EN, Shen J (2007) Impaired dopamine release and synaptic plasticity in the striatum of PINK1-deficient mice. *Proc Natl Acad Sci U S A* **104:** 11441-11446

Klein C, Westenberger A (2012) Genetics of Parkinson's disease. *Cold Spring Harb Perspect Med* **2:** a008888

Komander D (2009) The emerging complexity of protein ubiquitination. *Biochem Soc Trans* **37:** 937-953

Komander D, Rape M (2012) The ubiquitin code. *Annu Rev Biochem* **81:** 203-229

Kondapalli C, Kazlauskaite A, Zhang N, Woodroof HI, Campbell DG, Gourlay R, Burchell L, Walden H, Macartney TJ, Deak M, Knebel A, Alessi DR, Muqit MM (2012) PINK1 is activated by mitochondrial membrane potential depolarization and stimulates Parkin E3 ligase activity by phosphorylating Serine 65. *Open Biol* **2:** 120080

Kornev AP, Haste NM, Taylor SS, Eyck LF (2006) Surface comparison of active and inactive protein kinases identifies a conserved activation mechanism. *Proc Natl Acad Sci U S A* **103:** 17783-17788

Kornev AP, Taylor SS, Ten Eyck LF (2008) A helix scaffold for the assembly of active protein kinases. *Proc Natl Acad Sci U S A* **105:** 14377-14382

Koyano F, Okatsu K, Kosako H, Tamura Y, Go E, Kimura M, Kimura Y, Tsuchiya H, Yoshihara H, Hirokawa T, Endo T, Fon EA, Trempe JF, Saeki Y, Tanaka K, Matsuda N (2014) Ubiquitin is phosphorylated by PINK1 to activate parkin. *Nature* **510:** 162-166

Krebs EG, Fischer EH (1956) The phosphorylase b to a converting enzyme of rabbit skeletal muscle. *Biochim Biophys Acta* **20:** 150-157

Kreegipuu A, Blom N, Brunak S (1999) PhosphoBase, a database of phosphorylation sites: release 2.0. *Nucleic Acids Res* **27:** 237-239

Langston JW, Ballard P, Tetrud JW, Irwin I (1983) Chronic Parkinsonism in humans due to a product of meperidine-analog synthesis. *Science* **219:** 979-980

Lazarou M, Jin SM, Kane LA, Youle RJ (2012) Role of PINK1 binding to the TOM complex and alternate intracellular membranes in recruitment and activation of the E3 ligase Parkin. *Dev Cell* **22:** 320-333

Lee CD, Sun HC, Hu SM, Chiu CF, Homhuan A, Liang SM, Leng CH, Wang TF (2008) An improved SUMO fusion protein system for effective production of native proteins. *Protein Sci* **17:** 1241-1248

Lin W, Kang UJ (2008) Characterization of PINK1 processing, stability, and subcellular localization. *J Neurochem* **106:** 464-474

Lucking CB, Durr A, Bonifati V, Vaughan J, De Michele G, Gasser T, Harhangi BS, Meco G, Denefle P, Wood NW, Agid Y, Brice A (2000) Association between early-onset Parkinson's disease and mutations in the parkin gene. *N Engl J Med* **342:** 1560-1567

Lutz AK, Exner N, Fett ME, Schlehe JS, Kloos K, Lammermann K, Brunner B, Kurz-Drexler A, Vogel F, Reichert AS, Bouman L, Vogt-Weisenhorn D, Wurst W, Tatzelt J, Haass C, Winklhofer KF (2009) Loss of parkin or PINK1 function increases Drp1-dependent mitochondrial fragmentation. *J Biol Chem* **284:** 22938-22951

Manning G, Whyte DB, Martinez R, Hunter T, Sudarsanam S (2002) The protein kinase complement of the human genome. *Science* **298:** 1912-1934

Matsuda N, Sato S, Shiba K, Okatsu K, Saisho K, Gautier CA, Sou YS, Saiki S, Kawajiri S, Sato F, Kimura M, Komatsu M, Hattori N, Tanaka K (2010) PINK1 stabilized by mitochondrial depolarization recruits Parkin to damaged mitochondria and activates latent Parkin for mitophagy. *J Cell Biol* **189:** 211-221

Mattson MP (2007) Calcium and neurodegeneration. *Aging Cell* **6:** 337-350

Metzger MB, Hristova VA, Weissman AM (2012) HECT and RING finger families of E3 ubiquitin ligases at a glance. *J Cell Sci* **125:** 531-537

Mills RD, Sim CH, Mok SS, Mulhern TD, Culvenor JG, Cheng HC (2008) Biochemical aspects of the neuroprotective mechanism of PTEN-induced kinase-1 (PINK1). *J Neurochem* **105:** 18-33

Morais VA, Haddad D, Craessaerts K, De Bock PJ, Swerts J, Vilain S, Aerts L, Overbergh L, Grunewald A, Seibler P, Klein C, Gevaert K, Verstreken P, De Strooper B (2014) PINK1 loss-of-function mutations affect mitochondrial complex I activity via NdufA10 ubiquinone uncoupling. *Science* **344:** 203-207

Morais VA, Verstreken P, Roethig A, Smet J, Snellinx A, Vanbrabant M, Haddad D, Frezza C, Mandemakers W, Vogt-Weisenhorn D, Van Coster R, Wurst W, Scorrano L, De Strooper B (2009) Parkinson's disease mutations in PINK1 result in decreased Complex I activity and deficient synaptic function. *EMBO Mol Med* **1:** 99-111

Morrison DK (2012) MAP kinase pathways. *Cold Spring Harb Perspect Biol* **4**

Muqit MM, Abou-Sleiman PM, Saurin AT, Harvey K, Gandhi S, Deas E, Eaton S, Payne Smith MD, Venner K, Matilla A, Healy DG, Gilks WP, Lees AJ, Holton J, Revesz T, Parker PJ, Harvey RJ, Wood NW, Latchman DS (2006) Altered cleavage and localization of PINK1 to aggresomes in the presence of proteasomal stress. *J Neurochem* **98:** 156-169

Najafov A, Shpiro N, Alessi DR (2012) Akt is efficiently activated by PIF-pocket- and PtdIns(3,4,5)P3-dependent mechanisms leading to resistance to PDK1 inhibitors. *Biochem J* **448:** 285-295

Narendra D, Tanaka A, Suen DF, Youle RJ (2008) Parkin is recruited selectively to impaired mitochondria and promotes their autophagy. *J Cell Biol* **183:** 795-803

Narendra DP, Jin SM, Tanaka A, Suen DF, Gautier CA, Shen J, Cookson MR, Youle RJ (2010) PINK1 is selectively stabilized on impaired mitochondria to activate Parkin. *PLoS Biol* **8:** e1000298

Niefind K, Guerra B, Pinna LA, Issinger OG, Schomburg D (1998) Crystal structure of the catalytic subunit of protein kinase CK2 from Zea mays at 2.1 A resolution. *Embo J* **17:** 2451-2462

Nolen B, Taylor S, Ghosh G (2004) Regulation of protein kinases; controlling activity through activation segment conformation. *Mol Cell* **15:** 661-675

Okatsu K, Oka T, Iguchi M, Imamura K, Kosako H, Tani N, Kimura M, Go E, Koyano F, Funayama M, Shiba-Fukushima K, Sato S, Shimizu H, Fukunaga Y, Taniguchi H, Komatsu M, Hattori N, Mihara K, Tanaka K, Matsuda N (2012) PINK1 autophosphorylation upon membrane potential dissipation is essential for Parkin recruitment to damaged mitochondria. *Nat Commun* **3:** 1016

Ordureau A, Sarraf SA, Duda DM, Heo JM, Jedrychowski MP, Sviderskiy VO, Olszewski JL, Koerber JT, Xie T, Beausoleil SA, Wells JA, Gygi SP, Schulman BA, Harper JW (2014) Quantitative Proteomics Reveal a Feedforward Mechanism for Mitochondrial PARKIN Translocation and Ubiquitin Chain Synthesis. *Mol Cell*

Paisan-Ruiz C, Jain S, Evans EW, Gilks WP, Simon J, van der Brug M, Lopez de Munain A, Aparicio S, Gil AM, Khan N, Johnson J, Martinez JR, Nicholl D, Carrera IM, Pena AS, de Silva R, Lees A, Marti-Masso JF, Perez-Tur J, Wood NW, Singleton AB (2004) Cloning of the gene containing mutations that cause PARK8-linked Parkinson's disease. *Neuron* **44:** 595-600

Park HS, Hohn MJ, Umehara T, Guo LT, Osborne EM, Benner J, Noren CJ, Rinehart J, Soll D (2011) Expanding the genetic code of Escherichia coli with phosphoserine. *Science* **333:** 1151-1154

Park J, Lee G, Chung J (2009) The PINK1-Parkin pathway is involved in the regulation of mitochondrial remodeling process. *Biochem Biophys Res Commun* **378:** 518-523

Park J, Lee SB, Lee S, Kim Y, Song S, Kim S, Bae E, Kim J, Shong M, Kim JM, Chung J (2006) Mitochondrial dysfunction in Drosophila PINK1 mutants is complemented by parkin. *Nature* **441:** 1157-1161

Patterson H, Nibbs R, McInnes I, Siebert S (2014) Protein kinase inhibitors in the treatment of inflammatory and autoimmune diseases. *Clin Exp Immunol* **176:** 1-10

Pearce LR, Komander D, Alessi DR (2010) The nuts and bolts of AGC protein kinases. *Nat Rev Mol Cell Biol* **11:** 9-22

Pelech SL (1995) Networking with proline-directed protein kinases implicated in tau phosphorylation. *Neurobiol Aging* **16:** 247-256; discussion 257-261

Petit A, Kawarai T, Paitel E, Sanjo N, Maj M, Scheid M, Chen F, Gu Y, Hasegawa H, Salehi-Rad S, Wang L, Rogaeva E, Fraser P, Robinson B, St George-Hyslop P, Tandon A (2005) Wild-type PINK1 prevents basal and induced neuronal apoptosis, a protective effect abrogated by Parkinson disease-related mutations. *J Biol Chem* **280:** 34025-34032

Plun-Favreau H, Klupsch K, Moisoi N, Gandhi S, Kjaer S, Frith D, Harvey K, Deas E, Harvey RJ, McDonald N, Wood NW, Martins LM, Downward J (2007) The mitochondrial protease HtrA2 is regulated by Parkinson's disease-associated kinase PINK1. *Nat Cell Biol* **9:** 1243-1252

Polymeropoulos MH, Lavedan C, Leroy E, Ide SE, Dehejia A, Dutra A, Pike B, Root H, Rubenstein J, Boyer R, Stenroos ES, Chandrasekharappa S, Athanassiadou A, Papapetropoulos T, Johnson WG, Lazzarini AM, Duvoisin RC, Di Iorio G, Golbe LI, Nussbaum RL (1997) Mutation in the alpha-synuclein gene identified in families with Parkinson's disease. *Science* **276:** 2045-2047

Ponsen MM, Stoffers D, Booij J, van Eck-Smit BL, Wolters E, Berendse HW (2004) Idiopathic hyposmia as a preclinical sign of Parkinson's disease. *Ann Neurol* **56:** 173-181

Poole AC, Thomas RE, Andrews LA, McBride HM, Whitworth AJ, Pallanck LJ (2008) The PINK1/Parkin pathway regulates mitochondrial morphology. *Proc Natl Acad Sci U S A* **105:** 1638-1643

Poole AC, Thomas RE, Yu S, Vincow ES, Pallanck L (2010) The mitochondrial fusion-promoting factor mitofusin is a substrate of the PINK1/parkin pathway. *PLoS One* **5:** e10054

Popovic D, Vucic D, Dikic I (2014) Ubiquitination in disease pathogenesis and treatment. *Nat Med* **20:** 1242-1253

Postuma RB, Gagnon JF, Montplaisir J (2013) Rapid eye movement sleep behavior disorder as a biomarker for neurodegeneration: the past 10 years. *Sleep Med* **14:** 763-767

Pridgeon JW, Olzmann JA, Chin LS, Li L (2007) PINK1 protects against oxidative stress by phosphorylating mitochondrial chaperone TRAP1. *PLoS Biol* **5:** e172

Puschmann A (2013) Monogenic Parkinson's disease and parkinsonism: clinical phenotypes and frequencies of known mutations. *Parkinsonism Relat Disord* **19:** 407-415

Rafie-Kolpin M, Chefalo PJ, Hussain Z, Hahn J, Uma S, Matts RL, Chen JJ (2000) Two heme-binding domains of heme-regulated eukaryotic initiation factor-2alpha kinase. N terminus and kinase insertion. *J Biol Chem* **275:** 5171-5178

Rascol O, Goetz C, Koller W, Poewe W, Sampaio C (2002) Treatment interventions for Parkinson's disease: an evidence based assessment. *Lancet* **359:** 1589-1598

Rascol O, Payoux P, Ory F, Ferreira JJ, Brefel-Courbon C, Montastruc JL (2003) Limitations of current Parkinson's disease therapy. *Ann Neurol* **53 Suppl 3:** S3-12; discussion S12-15

Reyes-Turcu FE, Ventii KH, Wilkinson KD (2009) Regulation and cellular roles of ubiquitin-specific deubiquitinating enzymes. *Annu Rev Biochem* **78:** 363-397

Rhodes G. (2006) Crystallography made crystal clear a guide for users of macromolecular models. Elsevier/Academic Press.

Riederer P, Wuketich S (1976) Time course of nigrostriatal degeneration in parkinson's disease. A detailed study of influential factors in human brain amine analysis. *J Neural Transm* **38:** 277-301

Riley BE, Lougheed JC, Callaway K, Velasquez M, Brecht E, Nguyen L, Shaler T, Walker D, Yang Y, Regnstrom K, Diep L, Zhang Z, Chiou S, Bova M, Artis DR, Yao N, Baker J, Yednock T, Johnston JA (2013) Structure and function of Parkin E3 ubiquitin ligase reveals aspects of RING and HECT ligases. *Nat Commun* **4:** 1982

Rosenberg OS, Deindl S, Sung RJ, Nairn AC, Kuriyan J (2005) Structure of the autoinhibited kinase domain of CaMKII and SAXS analysis of the holoenzyme. *Cell* **123:** 849-860

Russi S, Juers DH, Sanchez-Weatherby J, Pellegrini E, Mossou E, Forsyth VT, Huet J, Gobbo A, Felisaz F, Moya R, McSweeney SM, Cusack S, Cipriani F, Bowler MW (2011) Inducing phase changes in crystals of macromolecules: status and perspectives for controlled crystal dehydration. *J Struct Biol* **175:** 236-243

Sakata E, Yamaguchi Y, Kurimoto E, Kikuchi J, Yokoyama S, Yamada S, Kawahara H, Yokosawa H, Hattori N, Mizuno Y, Tanaka K, Kato K (2003) Parkin binds the Rpn10 subunit of 26S proteasomes through its ubiquitin-like domain. *EMBO Rep* **4:** 301-306

Samaranch L, Lorenzo-Betancor O, Arbelo JM, Ferrer I, Lorenzo E, Irigoyen J, Pastor MA, Marrero C, Isla C, Herrera-Henriquez J, Pastor P (2010) PINK1-linked parkinsonism is associated with Lewy body pathology. *Brain* **133:** 1128-1142

Sarraf SA, Raman M, Guarani-Pereira V, Sowa ME, Huttlin EL, Gygi SP, Harper JW (2013) Landscape of the PARKIN-dependent ubiquitylome in response to mitochondrial depolarization. *Nature* **496:** 372-376

Schapira AH, Cooper JM, Dexter D, Jenner P, Clark JB, Marsden CD (1989) Mitochondrial complex I deficiency in Parkinson's disease. *Lancet* **1:** 1269

Scheid MP, Marignani PA, Woodgett JR (2002) Multiple phosphoinositide 3-kinase-dependent steps in activation of protein kinase B. *Mol Cell Biol* **22:** 6247-6260

Sheridan DL, Kong Y, Parker SA, Dalby KN, Turk BE (2008) Substrate discrimination among mitogen-activated protein kinases through distinct docking sequence motifs. *J Biol Chem* **283:** 19511-19520

Silvestri L, Caputo V, Bellacchio E, Atorino L, Dallapiccola B, Valente EM, Casari G (2005) Mitochondrial import and enzymatic activity of PINK1 mutants associated to recessive parkinsonism. *Hum Mol Genet* **14:** 3477-3492

Sim CH, Gabriel K, Mills RD, Culvenor JG, Cheng HC (2012) Analysis of the regulatory and catalytic domains of PTEN-induced kinase-1 (PINK1). *Hum Mutat* **33:** 1408-1422

Sim CH, Lio DS, Mok SS, Masters CL, Hill AF, Culvenor JG, Cheng HC (2006) C-terminal truncation and Parkinson's disease-associated mutations down-regulate the protein serine/threonine kinase activity of PTEN-induced kinase-1. *Hum Mol Genet* **15:** 3251-3262

Song S, Jang S, Park J, Bang S, Choi S, Kwon KY, Zhuang X, Kim E, Chung J (2013) Characterization of PINK1 (PTEN-induced putative kinase 1) mutations associated with Parkinson disease in mammalian cells and Drosophila. *J Biol Chem* **288:** 5660-5672

Soundararajan M, Roos AK, Savitsky P, Filippakopoulos P, Kettenbach AN, Olsen JV, Gerber SA, Eswaran J, Knapp S, Elkins JM (2013) Structures of Down syndrome kinases, DYRKs, reveal mechanisms of kinase activation and substrate recognition. *Structure* **21:** 986-996

Spillantini MG, Crowther RA, Jakes R, Hasegawa M, Goedert M (1998) alpha-Synuclein in filamentous inclusions of Lewy bodies from Parkinson's disease and dementia with lewy bodies. *Proc Natl Acad Sci U S A* **95:** 6469-6473

Spillantini MG, Schmidt ML, Lee VM, Trojanowski JQ, Jakes R, Goedert M (1997) Alpha-synuclein in Lewy bodies. *Nature* **388:** 839-840

Spratt DE, Martinez-Torres RJ, Noh YJ, Mercier P, Manczyk N, Barber KR, Aguirre JD, Burchell L, Purkiss A, Walden H, Shaw GS (2013) A molecular explanation for the recessive nature of parkin-linked Parkinson's disease. *Nat Commun* **4:** 1983

Stavropoulos I, Khaldi N, Davey NE, O'Brien K, Martin F, Shields DC (2012) Protein disorder and short conserved motifs in disordered regions are enriched near the cytoplasmic side of single-pass transmembrane proteins. *PLoS One* **7:** e44389

Taouji S, Dahan S, Bosse R, Chevet E (2009) Current Screens Based on the AlphaScreen Technology for Deciphering Cell Signalling Pathways. *Curr Genomics* **10:** 93-101

ter Haar E, Coll JT, Austen DA, Hsiao HM, Swenson L, Jain J (2001) Structure of GSK3beta reveals a primed phosphorylation mechanism. *Nat Struct Biol* **8:** 593-596

Trempe JF, Sauve V, Grenier K, Seirafi M, Tang MY, Menade M, Al-Abdul-Wahid S, Krett J, Wong K, Kozlov G, Nagar B, Fon EA, Gehring K (2013) Structure of parkin reveals mechanisms for ubiquitin ligase activation. *Science* **340:** 1451-1455

Ubersax JA, Ferrell JE, Jr. (2007) Mechanisms of specificity in protein phosphorylation. *Nat Rev Mol Cell Biol* **8:** 530-541

Unoki M, Nakamura Y (2001) Growth-suppressive effects of BPOZ and EGR2, two genes involved in the PTEN signaling pathway. *Oncogene* **20:** 4457-4465

Valente EM, Abou-Sleiman PM, Caputo V, Muqit MM, Harvey K, Gispert S, Ali Z, Del Turco D, Bentivoglio AR, Healy DG, Albanese A, Nussbaum R, Gonzalez-Maldonado R, Deller T, Salvi S, Cortelli P, Gilks WP, Latchman DS, Harvey RJ, Dallapiccola B, Auburger G, Wood NW (2004) Hereditary early-onset Parkinson's disease caused by mutations in PINK1. *Science* **304:** 1158-1160

Vera L, Stura EA (2013) Strategies for Protein Cryocrystallography. *Crystal Growth & Design* **14:** 427-435

Vijay-Kumar S, Bugg CE, Cook WJ (1987) Structure of ubiquitin refined at 1.8 A resolution. *J Mol Biol* **194:** 531-544

Vos M, Esposito G, Edirisinghe JN, Vilain S, Haddad DM, Slabbaert JR, Van Meensel S, Schaap O, De Strooper B, Meganathan R, Morais VA, Verstreken P (2012) Vitamin K2 is a mitochondrial electron carrier that rescues pink1 deficiency. *Science* **336:** 1306-1310

Walden H, Martinez-Torres RJ (2012) Regulation of Parkin E3 ubiquitin ligase activity. *Cell Mol Life Sci* **69:** 3053-3067

Wales P, Pinho R, Lazaro DF, Outeiro TF (2013) Limelight on alpha-synuclein: pathological and mechanistic implications in neurodegeneration. *J Parkinsons Dis* **3:** 415-459

Walte A, Ruben K, Birner-Gruenberger R, Preisinger C, Bamberg-Lemper S, Hilz N, Bracher F, Becker W (2013) Mechanism of dual specificity kinase activity of DYRK1A. *Febs J* **280:** 4495-4511

Walter TS, Meier C, Assenberg R, Au KF, Ren J, Verma A, Nettleship JE, Owens RJ, Stuart DI, Grimes JM (2006) Lysine methylation as a routine rescue strategy for protein crystallization. *Structure* **14:** 1617-1622

Waterhouse AM, Procter JB, Martin DM, Clamp M, Barton GJ (2009) Jalview Version 2--a multiple sequence alignment editor and analysis workbench. *Bioinformatics* **25:** 1189-1191

Wauer T, Komander D (2013) Structure of the human Parkin ligase domain in an autoinhibited state. *Embo J* **32:** 2099-2112

Wenzel DM, Lissounov A, Brzovic PS, Klevit RE (2011) UBCH7 reactivity profile reveals parkin and HHARI to be RING/HECT hybrids. *Nature* **474:** 105-108

West AB, Moore DJ, Biskup S, Bugayenko A, Smith WW, Ross CA, Dawson VL, Dawson TM (2005) Parkinson's disease-associated mutations in leucine-rich repeat kinase 2 augment kinase activity. *Proc Natl Acad Sci U S A* **102:** 16842-16847

Wichmann T, DeLong MR, Guridi J, Obeso JA (2011) Milestones in research on the pathophysiology of Parkinson's disease. *Mov Disord* **26:** 1032-1041

Woods YL, Rena G, Morrice N, Barthel A, Becker W, Guo S, Unterman TG, Cohen P (2001) The kinase DYRK1A phosphorylates the transcription factor FKHR at Ser329 in vitro, a novel in vivo phosphorylation site. *Biochem J* **355:** 597-607

Yamano K, Youle RJ (2013) PINK1 is degraded through the N-end rule pathway. *Autophagy* **9:** 1758-1769

Yang J, Wu J, Steichen JM, Kornev AP, Deal MS, Li S, Sankaran B, Woods VL, Jr., Taylor SS (2012) A conserved Glu-Arg salt bridge connects coevolved motifs that define the eukaryotic protein kinase fold. *J Mol Biol* **415:** 666-679

Zeqiraj E, Filippi BM, Deak M, Alessi DR, van Aalten DM (2009) Structure of the LKB1-STRAD-MO25 complex reveals an allosteric mechanism of kinase activation. *Science* **326:** 1707-1711

Zhang J, Yang PL, Gray NS (2009) Targeting cancer with small molecule kinase inhibitors. *Nat Rev Cancer* **9:** 28-39

Zheng J, Trafny EA, Knighton DR, Xuong NH, Taylor SS, Ten Eyck LF, Sowadski JM (1993) 2.2 A refined crystal structure of the catalytic subunit of cAMP-dependent protein kinase complexed with MnATP and a peptide inhibitor. *Acta Crystallogr D Biol Crystallogr* **49:** 362-365

Zhou C, Huang Y, Shao Y, May J, Prou D, Perier C, Dauer W, Schon EA, Przedborski S (2008) The kinase domain of mitochondrial PINK1 faces the cytoplasm. *Proc Natl Acad Sci U S A* **105:** 12022-12027

Zimprich A, Biskup S, Leitner P, Lichtner P, Farrer M, Lincoln S, Kachergus J, Hulihan M, Uitti RJ, Calne DB, Stoessl AJ, Pfeiffer RF, Patenge N, Carbajal IC, Vieregge P, Asmus F, Muller-Myhsok B, Dickson DW, Meitinger T, Strom TM, Wszolek ZK, Gasser T (2004) Mutations in LRRK2 cause autosomal-dominant parkinsonism with pleomorphic pathology. *Neuron* **44:** 601-607

Ziviani E, Tao RN, Whitworth AJ (2010) Drosophila parkin requires PINK1 for mitochondrial translocation and ubiquitinates mitofusin. *Proc Natl Acad Sci U S A* **107:** 5018-5023